

Understanding the role of stress granules in the inner ear

Ana Cláudia Gasparinho Gonçalves

A thesis submitted for the degree of Doctor of Philosophy

UCL Ear Institute

University College London

December 2016

Declaration

I, Ana Cláudia Gasparinho Gonçalves, confirm that the work presented in this thesis is my own. Where information has been derived from other sources, I confirm that this has been indicated in the thesis.

Abstract

The human ear undergoes stress constantly. Exposure to noise, drugs or ageing contribute to the irreversible loss of hair cells, resulting in hearing loss. To understand why we go deaf, it is important to understand how the ear responds to stress. Stress granules (SGs) are aggregates of mRNA and proteins that are formed during stress. The SG-pathway has been implicated in the cochlea's response to aminoglycoside antibiotics, suggesting that SGs play an important role during ototoxicity. Dysregulation of SG-formation has also been linked to neurodegeneration, supporting the hypothesis that SGs play a critical role in cell survival.

Here, the formation and regulation of SGs have been investigated in an inner ear context using a combination of inner ear-derived UB/OC-2 cells, cochlear explants and the *in-vivo* mouse cochlea. Cells were labelled for two SG-proteins, TIA-1 and Caprin-1, and polyA⁺ mRNA was detected within SGs using RNA-immuno-FISH. A novel quantification method was developed to characterise in detail the number and size of SGs upon two stress paradigms, heat shock and arsenite. PolyA⁺ mRNA was observed to aggregate within SGs following different types of stress, suggesting that SGs are involved in post-transcriptional regulation of gene expression in the cochlea.

Experiments in cochlear explants suggest that pharmacological induction of SGs promotes outer hair cell survival during aminoglycoside exposure. In addition, SG-formation was observed in the *in-vivo* C57BL/6 cochlea during ageing, suggesting that SGs may be related to cochlear degeneration.

Hsp70, previously shown to promote hair cell survival following ototoxicity has been associated with SGs in other systems. Here, Hsp70 expression was evaluated in OC-2 cells following different stressors and evidence suggests it to be a key regulator of SGs.

Taken together, these data implicate the SG pathway with maintenance of auditory function as a potential therapeutic target for further investigation.

Acknowledgments

Firstly, I would like to thank my supervisors Dr. Jonathan Gale and Dr. Sally Dawson for all their help, enthusiasm, patience and words of advice and guidance. I will always be grateful for the opportunity to undertake my PhD in such a great lab.

I would also like to thank Dr. Lisa Nolan and Naila Haq, for the help during the first stages of this project and for sharing their knowledge (and many good moments!) with me.

In addition, I would also like to thank Action on Hearing Loss for funding this PhD studentship, as well as participation in a number of conferences.

In the lab, I must thank Camille Tardieu, George Stavrinou, Dr. Magdalena Zak, Miriam Gomez, Sara Weber, Silvia Prades and Dr. Zoe Mann. Thank you for listening to me, for all the advice and help and for all the great laughs that we shared. You will always have a special place in my heart! I would like to extend thanks to Dr. Katie Smith, Stephanie Juniat, Phoebe Murphy and Daniela Franchini for all the good moments that we have spent together!

A special thanks to my friends back in Portugal who have always been there for me.

Another special thanks to my uncle, the one and only, whose phone calls always come in the right time and always make me smile.

Most importantly, I must thank my parents and grandparents for everything. Thank you for supporting my studies, always believing in me, for never questioning my choices and for always being there for me.

O agradecimento mais importante tem de ser aos meus Pais e Avós, por tudo. Obrigada por terem sempre apoiado os meus estudos, por sempre acreditarem em mim, por nunca questionarem as minhas escolhas e por estarem sempre lá para mim.

Cláudia Gonçalves

December 2016

Table of contents

Declaration	2
Abstract	3
Acknowledgments.....	4
Table of contents	5
List of figures	8
List of tables	11
Abbreviations.....	12
1. Introduction	16
1.1. Hearing loss, hair cell loss and implications.....	16
1.2. The ear structure and function.....	19
1.3. Types of hearing loss	23
1.4. Cochlear stress	27
1.5. Stress pathways in the ear: Hsp70	30
1.6. Stress pathways in the ear: stress granules	33
1.7. The role of stress granules in cellular stress.....	35
1.8. Properties of SGs	37
1.9. Regulation of translation during stress.....	41
1.10. Dynamics of stress granule formation.....	48
1.11. Stress granules and other RNA granules.....	50
1.12. Stress granules and viral infection.....	53
1.13. Stress granules in neurodegenerative diseases	55
1.14. Pharmacological manipulation of stress granules.....	58
1.15. Aims of the project.....	63
2. Methods	65
2.1. The UB/OC-2 cell line.....	65
2.2. In-vitro culture of OC-2 cells	66
2.3. C57BL/6 mice.....	66
2.4. Mouse cochlear explants.....	67
2.5. Heat shock studies	67
2.6. Sodium arsenite studies	68
2.7. pp242 studies.....	68
2.8. ISRIB studies	69
2.9. Hydroxamate (-)-9 studies	69
2.10. Hsp70 protein overexpression	70
2.11. Cochleae neomycin studies.....	70

2.12.	Cochleae sisomicin studies	70
2.13.	Mouse cochleae cryosections.....	71
2.14.	RNA-immuno-Fluorescence in situ hybridisation	72
2.15.	RNA-FISH probes	73
2.16.	General immunofluorescence protocol	75
2.17.	Secondary antibody controls	76
2.18.	Colocalisation quantification	77
2.19.	Stress granule quantification	78
2.19.1.	Stress granule quantification in OC-2 cells	79
2.19.2.	Stress granule quantification in mouse cochlear explants.....	82
2.20.	Calculations of stress granule density	87
2.21.	Quantification of surviving hair cells	90
3.	Dynamics of SG assembly during stress in the OC-2 cell line.....	92
3.1.	Introduction	92
3.2.	Results	94
3.2.1.	Heat shock stress triggers SG formation in the OC-2 cell line.....	94
3.2.2.	Sodium arsenite stress triggers SG formation in the OC-2 cell line.....	100
3.2.3.	Pharmacological studies demonstrate that SG pathway can be manipulated in the OC-2 cell line	105
3.2.3.1.	pp242 reduces SG formation during heat shock treatment in the OC-2 cell line.....	105
3.2.3.2.	pp242 does not reduce SG formation during arsenite stress in the OC-2 cell line.....	111
3.2.3.3.	ISRIB significantly reduces SG formation in OC-2 cells.....	116
3.2.3.4.	Hydroxamate (-)-9 promotes SG formation in OC-2 cells	123
3.2.4.	Summary.....	130
3.3.	Discussion.....	134
4.	Characterising the role of SGs during cochlear stress	139
4.1.	Introduction	139
4.2.	Results	141
4.2.1.	Cochlear cells assemble SGs in response to stress	141
4.2.2.	Pharmacological manipulation of SGs in mouse cochlear explants	153
4.2.3.	Hydroxamate (-)-9 protects outer hair cells from aminoglycoside-induced cell death.....	167
4.2.3.1.	Neomycin-induced cochlear stress.....	167
4.2.3.2.	Sisomicin-induced cochlear stress	177
4.2.4.	Age-related changes in the in-vivo cochlea	185
4.3.	Discussion.....	189

5.	Investigating the role of Hsp70 in SG formation in the auditory system	197
5.1.	Introduction	197
5.2.	Results	199
5.2.1.	Hsp70 protein expression increases during heat shock recovery and is associated with SG absence.....	199
5.2.2.	Hsp70 gene expression increases after heat shock.....	204
5.2.3.	Arsenite stress does not trigger Hsp70 protein expression	205
5.2.4.	qPCR confirms reduced Hsp70 gene expression upon arsenite stress when compared to heat shock.....	207
5.2.5.	RNA-immuno-FISH confirms the exclusion of Hsp70 RNA from SGs during stress in the OC-2 cell line	208
5.2.6.	Hsp70 overexpression prior to heat shock stress impairs SG formation ...	210
5.2.7.	SG formation is unaffected by Hsp70 overexpression prior to arsenite stress	214
5.3.	Discussion.....	217
6.	General discussion.....	223
7.	References.....	242

List of figures

	Page
Figure 1.1 – Schematic representation of the human ear.....	18
Figure 1.2 – Cross-section of the organ of Corti.....	22
Figure 1.3 – Schematic representation of a hair cell.....	22
Figure 1.4 – Caprin-1 overexpression induces SG formation in OC-2 cells.....	34
Figure 1.5 - Schematics representing translation initiation in the absence or presence of stress.....	43
Figure 1.6 – Downstream effects of heat shock in cell signalling pathways.....	46
Figure 1.7 – Downstream effects of sodium arsenite in cell signalling pathways...	47
Figure 1.8 - Model for the cycling of mRNA between different cellular compartments.....	52
Figure 1.9 – Chemical structure of pp242.....	60
Figure 1.10 – Chemical structure of (A) silvestrol and (B) (±)-rocaglamide hydroxamate 3.....	61
Figure 1.11 – Chemical structure of hydroxamate derivatives 7, 8 and 9.....	62
Figure 1.12 – Chemical structure of ISRIB isosteromers, <i>trans</i> -ISRIB and <i>cis</i> -ISRIB.....	62
Figure 2.1 – Secondary antibody controls for Alexa Fluor 488 and 546 in OC-2 cells.....	76
Figure 2.2 – Secondary antibody control for Alexa Fluor 647 in OC-2 cells.....	76
Figure 2.3 – Secondary antibody controls for Alexa Fluor 488 and 546 in mouse cochlear explants.....	77
Figure 2.4 – Secondary antibody controls for Alexa Fluor 488 and 546 in <i>in-vivo</i> cryosections.....	77
Figure 2.5 – Example of raw images (pre-processed).....	80
Figure 2.6 – Example of processed images.....	80
Figure 2.7 – Caprin-1 and TIA-1 areas delineated (in yellow) to be considered for further analysis using SG counter plugin.....	81
Figure 2.8 – SG counter plugin main input window.....	81
Figure 2.9 – SG counter plugin outputs after analysis.....	82
Figure 2.10 – Example of raw images (pre-processed) for the inner hair cell region.....	84
Figure 2.11 – Example of processed images for the inner hair cell region.....	84
Figure 2.12 – TIA-1 area delineated in hair cells (in yellow) to be considered for further analysis using SG counter plugin.....	85
Figure 2.13 – SG counter plugin outputs after analysis for SGs in inner hair cells.....	85
Figure 2.14 – Example of processed images for the supporting cells region.....	86
Figure 2.15 – SG counter plugin outputs after analysis for SGs in supporting cells.....	87
Figure 2.16 – Hair cell dimension measurements.....	89
Figure 2.17 – Representation of the different regions considered for analysis of SG density in hair cells.....	90
Figure 2.18 – Examples of healthy and dead hair cells, based on MyosinVIIa and DAPI signals.....	91
Figure 3.1 – Caprin-1 and TIA-1 aggregate with polyA ⁺ mRNA at cytoplasmic SGs after heat shock stress.....	96
Figure 3.2 – Quantification of SGs using three different markers during heat shock study.....	98
Figure 3.3 – Frequency histogram showing the distribution in size of SGs using two different markers during heat shock study.....	99
Figure 3.4 - Caprin-1 and TIA-1 aggregate with polyA ⁺ mRNA at cytoplasmic SGs after sodium arsenite stress.....	101
Figure 3.5 – Quantification of SGs using three different markers during sodium arsenite stress study.....	103

Figure 3.6 – Frequency histogram showing the distribution in size of SGs using two different markers during arsenite stress study.....	104
Figure 3.7 - pp242 reduces the formation of Caprin-1 and TIA-1 positive SGs during heat shock stress.....	106
Figure 3.8 – Dose-dependent effect of pp242 on the number and size of SGs upon heat shock stress.....	108
Figure 3.9 – Frequency histogram showing the distribution in size of SGs with pp242 exposure during heat shock stress.....	109
Figure 3.10 – Time-dependent effect on the number of SGs formed upon pp242 incubation prior to heat shock stress.....	110
Figure 3.11 - pp242 fails to reduce the formation of Caprin-1 and TIA-1 positive SGs during arsenite stress.....	112
Figure 3.12 – Dose-dependent effect of pp242 on the number and size of SGs upon arsenite stress.....	114
Figure 3.13 – Frequency histogram showing the distribution in size of SGs with pp242 exposure during arsenite stress.....	115
Figure 3.14 – SG formation following heat shock and arsenite stress is reduced in the presence of ISRIB.....	117
Figure 3.15 – ISRIB effects on SG number and size upon heat shock stress.....	119
Figure 3.16 – ISRIB effects on the SG number and size upon arsenite stress.....	121
Figure 3.17 – Frequency histogram showing the distribution in size of SGs after heat shock and arsenite treatments alone and in the presence of ISRIB.....	122
Figure 3.18 - Hydroxamate (-)-9 treatment induces the formation of SGs.....	124
Figure 3.19 – PolyA ⁺ mRNA is a component of the SGs originated by hydroxamate (-)-9 incubation.....	125
Figure 3.20 – Dose-dependent effect of hydroxamate (-)-9 in the formation of SGs.....	127
Figure 3.21 – Frequency histogram showing the distribution in size of SGs according to different hydroxamate (-)-9 concentrations.....	128
Figure 3.22 – Average number of SGs generated after different incubation periods with 0.1 μM of hydroxamate (-)-9 in the OC-2 cell line.....	129
Figure 3.23 – Summary of the number of SGs generated by the different treatments in OC-2 cells.....	132
Figure 3.24 – Summary of the size of SGs generated by the different treatments in OC-2 cells.....	133
Figure 4.1 – Mouse hair cells assemble SGs in response to stress.....	143
Figure 4.2 – PolyA ⁺ mRNA aggregates with TIA-1 at SGs following stress in hair cells.....	144
Figure 4.3 – Mouse supporting cells assemble SGs in response to stress.....	145
Figure 4.4 – PolyA ⁺ mRNA aggregates with TIA-1 at SGs following stress in supporting cells.....	146
Figure 4.5 – Quantification of the number of SGs in hair cells.....	148
Figure 4.6 – Quantification of the size of SGs in hair cells.....	149
Figure 4.7 – Quantification of SGs in supporting cells.....	150
Figure 4.8 – Quantification of SGs following sodium arsenite stress in hair cells...	152
Figure 4.9 – SG formation can be manipulated in hair cells.....	155
Figure 4.10 – Distribution of polyA ⁺ mRNA and TIA-1 in hair cells following pharmacological manipulation of SG formation.....	156
Figure 4.11 – SG formation can be manipulated in supporting cells.....	157
Figure 4.12 – Distribution of polyA ⁺ mRNA and TIA-1 in supporting cells following pharmacological manipulation of SG formation.....	158
Figure 4.13 – Hydroxamate (-)-9 does not present adverse effects on the hair cell stereocilia bundles.....	159
Figure 4.14 – Quantification of SGs present after ISRIB and hydroxamate (-)-9 treatments in cochlear hair cells.....	161
Figure 4.15 – Quantification of SG size after ISRIB and hydroxamate (-)-9 treatments in cochlear hair cells.....	162
Figure 4.16 – Detailed quantification of SGs following hydroxamate (-)-9 treatment in hair cells.....	163
Figure 4.17 – Quantification of SGs present after ISRIB and hydroxamate (-)-9	164

treatments in supporting cells.....	
Figure 4.18 - Experimental paradigms to assess the effects of hydroxamate (-)-9 on the neomycin-induced toxicity.....	167
Figure 4.19 – Hydroxamate (-)-9 pre-treatment increases hair cell survival following neomycin-induced toxicity.....	169
Figure 4.20 – Hydroxamate (-)-9 pre-treatment protects inner hair cells from neomycin-induced hair cell death.....	171
Figure 4.21 – Surviving inner hair cells reveal SG formation.....	172
Figure 4.22 - Experimental paradigms to assess the effects of SG manipulation on the neomycin-induced toxicity.....	172
Figure 4.23 - Hydroxamate (-)-9 pre-treatment increases the number of outer hair cells after 48h recovery from neomycin-induced hair cell death.....	173
Figure 4.24 - Hydroxamate (-)-9 pre-treatment protects outer hair cells after 48h recovery from neomycin-induced hair cell death.....	176
Figure 4.25 – Sisomicin-treated mouse cochlear explants.....	178
Figure 4.26 – Dose-response curve representing different sisomicin concentrations and percentage of surviving cells.....	179
Figure 4.27 - Experimental paradigms to assess the effects of SG manipulation on the sisomicin-induced toxicity.....	180
Figure 4.28 - Hydroxamate (-)-9 pre-treatment significantly protects outer hair cells after 48h recovery from sisomicin-induced hair cell death.....	183
Figure 4.29 – Hydroxamate (-)-9 pre-treatment significantly protects outer hair cells after 48h recovery from sisomicin-induced hair cell death.....	184
Figure 4.30 – SG formation in the aged organ of Corti.....	186
Figure 4.31 – PolyA ⁺ mRNA aggregates with TIA-1 at SGs in the aged organ of Corti.....	187
Figure 4.32 – SG formation in the aged spiral ganglia.....	188
Figure 5.1 – Hsp70 protein expression increases during recovery from heat shock.....	200
Figure 5.2 - Hsp70 protein intensity is correlated with the absence of SGs.....	201
Figure 5.3 – Increased Hsp70 expression associates with SG disassembly during recovery from heat shock stress.....	202
Figure 5.4 – Increased Hsp70 expression is inversely correlated with the number of SGs during heat shock stress.....	203
Figure 5.5 – <i>Hsp70</i> gene expression significantly increases after heat shock stress.....	204
Figure 5.6 – Hsp70 protein expression does not increase during arsenite stress and subsequent recovery.....	206
Figure 5.7 - <i>Hsp70</i> gene expression is reduced as a consequence of arsenite exposure when compared to heat shock in the OC-2 cell line.....	207
Figure 5.8 – Hsp70 mRNA is excluded from SGs during stress in the OC-2 cell line.....	209
Figure 5.9 – Infection with Ad-Hsp70 does not generate SG formation in OC-2 cells.....	210
Figure 5.10 – Hsp70 overexpression inhibits SG formation under heat shock stress.....	212
Figure 5.11 – Overexpression of Hsp70 reduces the number of SGs formed upon heat shock stress.....	213
Figure 5.12 – Overexpression of Hsp70 does not impair arsenite-induced SG formation.....	215
Figure 5.13 – Overexpression of Hsp70 does not affect the number of SGs formed upon arsenite stress.....	216
Figure 6.1 – Proposed mechanism of cell signalling pathways activated upon heat shock in OC-2 cells.....	236
Figure 6.2 – Proposed mechanism of cell signalling pathways activated upon sodium arsenite in OC-2 cells.....	237
Figure 6.3 – Proposed differential pathways activated upon heat shock and arsenite stress in OC-2 cells.....	238

List of tables

	Page
Table 1.1 – Grades of hearing impairment.....	23
Table 1.2 – Examples of SG components.....	40
Table 2.1 – Probes used to detect PTGES3 and Hsp70 RNAs.....	74
Table 2.2 – Measurements of inner hair cells (IHC) height, radius and nucleus radius.....	88
Table 2.3 – Measurements of outer hair cells (OHC) height, radius and nucleus radius.....	88

Abbreviations

°C – Celsius degrees

γIF – Gamma interferon

4E-BP1 – eIF4E binding protein 1

ABR – Auditory brainstem response

Ad-Hsp70 – Adenovirus-induced Hsp70 protein

AKT – Protein kinase B

ALS – Amyotrophic lateral sclerosis

ATF4 – Activating transcription factor 4

ATP – Adenosine triphosphate

Bcl-2 – B-cell lymphoma 2

BSA – Bovine serum albumin

Caprin-1 – Cytoplasmic activation/proliferation-associated protein-1

CO₂ – Carbon dioxide

DAPI – 4',6-diamidino-2-phenylindole

dB – Decibels

DMEM - Dulbecco's modified Eagle's medium

DNA – Deoxyribonucleic acid

E – Embryonic day

EDTA – Ethylenediamine tetraacetic acid

eEF – Eukaryotic elongation factor

eIF – Eukaryotic initiation factor

FBS – Fetal bovine serum

FM1-43 – N-(3-Triethylammoniumpropyl)-4-(4-(Dibutylamino) Styryl) Pyridinium Dibromide

FTLD – Frontotemporal lobar degeneration

FISH – Fluorescence *in situ* hybridisation

FUS – Fused in sarcoma protein

G3BP1 - Ras GTPase-activating protein-binding protein 1

GCN2 – General control nonderepressible

GDP – Guanosine diphosphate

GFP – Green fluorescent protein

GJB2 – Gap junction beta 2
GJB6 – Gap junction beta 6
GTP – Guanosine-5'-triphosphate
GSK3 – Glycogen synthase kinase 3
h - hour
H₂O₂ – Hydrogen peroxide
HIV-1 – Human immunodeficiency virus type-1
HRI – Heme-regulated inhibitor
HSF1 – Heat shock factor 1
Hsp – Heat shock protein
HTLV-1 – Human T cell leukaemia virus type-1
h - height
Hz – Hertz
IHC – Inner hair cell
ISRIB – Integrated stress response inhibitor
JNK – c-Jun N-terminal kinases
MAPK – Mitogen-activated protein kinases
MEFs – Murine embryonic fibroblasts
Met^t-RNA – Translation initiation codon (3'-UAC-5' anticodon)
mg – Milligrams
mL – Millilitres
mM – Milimolar
MOI – Multiplicity of infection
mRNA – Messenger ribonucleic acid
mRNPs – Messenger ribonucleoprotein particles
mTORC – Mammalian target of rapamycin complex
MT-RNR1 – Mitochondrially Encoded 12S RNA
MT-TS1 – Mitochondrially encoded tRNA serine 1
MyoVIIa – MyosinVIIa
NF-κB – Nuclear factor kappa-light-chain-enhancer of activated B cells
nM - Nanomolar
OC-2 cells – Organ of Corti 2 cells

OHC – Outer hair cell
P – Post-natal day
PABP1 – Poly(A) binding protein 1
PBS – Phosphate buffered saline
PERK – Protein kinase RNA-like endoplasmic reticulum kinase
PFA – Paraformaldehyde
PFU – Plaque forming units
PI-3K – Phosphatidylinositol-3 kinase
PKA – Protein kinase A
PKR – Protein kinase R
PolyA⁺ mRNA – Polyadenylated messenger RNA
PRD – Prion-related domain
PRPS1 – Phosphoribosylpyrophosphate protein
r – radius
r – Pearson correlation coefficient
RGG – Glycine-arginine-rich motif
RIP-seq – RNA immno precipitation sequencing
RNA – Ribonucleic acid
ROS – Reactive oxygen species
rRNA – Ribosomal RNA
S – Ribosomal subunit
SG – Stress granule
SLC26A4 – Solute carrier family 26 member 4
TDP43 – Tar DNA-binding protein 43
TIA-1 – T-cell intracellular antigen
TIAR – T-cell intracellular antigen protein
TNF – Tumour necrosis factor
tRNA – Transfer RNA
UB/OC-2 cells – University of Bristol / Organ of Corti 2 cells
µm – Micrometre
µM – Micromolar
UV – Ultraviolet

V – Volume

VCP – Valosin-containing protein

WHO – World health organisation

1. Introduction

1.1. Hearing loss, hair cell loss and implications

Hearing loss is the most common disability affecting human senses and is characterised by a partial or total inability to hear. Hearing loss presents a major impact throughout different stages of human life: in children, hearing impairment often leads to poor language acquisition, academic underachievement, lack of social engagement and decreased self-esteem, which can in turn reflect in fewer employment opportunities and personal achievements later in life. In adults, hearing loss often leads to limited access to services, unemployment, exclusion from communication and social activities and, consequently, social isolation and depression (Davis et al. 1986; Dalton et al. 2003).

According to the World Health Organisation (WHO), 360 million people worldwide suffer from moderate to profound hearing loss (WHO, 2012)¹. Epidemiologic studies indicate that, of this, 328 million are adults and more than a half of this number corresponds to people of 65 years or above (WHO, 2012)¹.

In mammals, the hearing organ is the cochlea, a spiral-shaped fluid-filled bony structure, broader at the base and narrower at the apex (Fig.1.1) (Fettiplace & Hackney 2006). The core sensory component of the cochlea is the organ of Corti that comprises the hair cells and supporting cells. Hair cells are the sensory receptors for hearing in the cochlea and for balance in the utricle, part of the vestibular system (Furness 2015). Through detection of sound stimuli, amplification and conversion to electrical signals, hair cells are responsible for the hearing process (Fettiplace & Hackney 2006; Furness 2015).

In mammals, hair cell loss is directly linked to hearing loss and deafness, since regeneration of hair cells does not occur in the mammalian ear (Martini 2007; Furness 2015). On the contrary, other vertebrates such as birds have the ability to replace lost hair cells, by neighbouring supporting cell division or transdifferentiation (Martini 2007; Furness 2015). Hence, the lack of a regeneration process in mammals results in permanent and irreversible effects associated with hair cell loss and, consequently, hearing loss (Martini 2007).

¹ World Health Organisation – WHO global estimates on prevalence of hearing loss
Available at http://www.who.int/pbd/deafness/WHO_GE_HL.pdf?ua=1 – Accessed on 25th October 2016

Different factors can contribute to the degeneration and loss of hair cells, including genetic predisposition, noise exposure, administration of ototoxic drugs and ageing. All these factors are thought to play a significant role in the development of hearing loss and, given the increase in human life expectancy, it is predictable that the total number of individuals affected by some form of hearing loss will rise (WHO, 2015)². In addition, hearing loss has been associated with the development of dementia, probably due to social isolation and/or the fact that hearing loss and progressive dementia may share a common neuropathologic degenerative process (Uhlmann et al. 1989; Ives et al. 1995; Lin et al. 2011). Considering all this, it is important to understand how and why hair cells are lost and what are the molecular pathways underlying the hair cell's response to insults. The development of preventative or therapeutic strategies to avoid hair cell damage may help to decrease the number of individuals affected by hearing loss and to lessen the effects of hearing loss in people's lives.

This thesis aims at contributing to a better understanding of how the inner ear responds to stress conditions. The stress granule (SG) pathway has been recently implicated in the cochlea's response to stress (Towers et al. 2011) and it is likely that SGs are involved in cell survival (Kedersha et al. 1999; Kedersha et al. 2002; Kedersha et al. 2005). However, the mechanisms by which hair cells assemble SGs or the function of SGs in the inner ear is yet poorly understood. Consequently, this thesis describes the first studies in the hearing system involving characterisation of SG formation, pharmacological manipulation of this pathway and assessments of the effects of SG manipulation on the hair cell survival following cochlear stress.

² World Health Organisation – Deafness and Hearing Loss
Available at <http://www.who.int/mediacentre/factsheets/fs300/en/> - Accessed on 25th October 2016

Figure 1.1 – Schematic representation of the human ear. The three main sections of the human ear are shown: outer, middle and inner ear. The outer ear contains the ear canal. The eardrum separates the outer ear from the middle ear. The middle ear, located between the outer and the inner ear, contains three ossicles named malleus, incus and stapes (not shown) and the tympanic cavity. The eustachian tube in the middle ear joins the tympanic cavity with the nasal cavity. The inner ear comprises the cochlea and the vestibular system. The auditory nerve transmits the neuronal impulses resulted from sound stimuli from the cochlea to the brain. Reproduced from “National Institutes of Health” *MedlinePlus*³.

³ – National Institutes of Health – *MedlinePlus*
Available at <https://medlineplus.gov/magazine/issues/spring15/articles/spring15pg9.html> - Accessed on 22nd October 2016.

1.2. The ear structure and function

The human ear is divided into three main sections: the outer, middle and inner ear. The range of audible sound for humans is approximately 20 Hz to 20000 Hz. The outer and middle ears mainly function to amplify the sound signal, whereas the inner ear transduces mechanical vibration into neuronal impulses (Alberti 2001).

The pinna, part of the outer ear, is a cartilaginous external part which protrudes from the skull and functions to collect and direct the sound into the ear canal. The outer ear canal is approximately 4 centimetres long and consists of an outer and inner part: the outer part contains hairy skin with sweat glands and oily sebaceous glands which form ear wax, an essential barrier and disinfectant that helps to protect the ear. The inner part consists of thin skin and is responsible for the direction of the sound to the tympanic membrane or eardrum (Fig.1.1). The tympanic membrane separates the outer ear from the middle ear and is the first part of the sound transducing mechanism. The sound conducted through vibrations of the tympanic membrane at the end of the external ear canal is then transmitted to the three ossicles in the middle ear (malleus, incus and stapes) (Alberti 2001).

The middle ear lies between the tympanic membrane and the inner ear (cochlea). The middle ear is filled with air and connects to the back of the nose through the eustachian tube (Fig.1.1). The eustachian tube arises at the front end of the middle ear and consists of a bony structure when close to the ear that thins towards the back end of the nose, the nasopharynx. As mentioned, the sound-induced vibrations of the tympanic membrane are conducted through vibrations of the three ossicles into the oval window of the cochlea (Alberti 2001). The oval window vibrations are transformed into oscillatory changes in the pressure within the fluid-filled cochlea (Hudspeth 2014).

The cochlea (Fig.1.1) corresponds to the auditory portion of the inner ear and is a spiral-shaped structure in the bony labyrinth that, in humans, consists of two and a half turns around its central axis, the modiolus. The human cochlea contains approximately 16000 hair cells that are responsible for the transduction of the vibrations into nervous impulses. The bony labyrinth also contains the vestibular organs, responsible for motion and linear acceleration detection. The utricle and saccule sense linear accelerations, whereas the three semi-circular canals detect rotational movements (angular acceleration) (Alberti 2001; Beisel et al. 2005).

The oval window vibrations in the cochlea (caused by vibrations of the three ossicles of the middle ear, as mentioned) generate a change in the pressure

between the fluid-filled compartments that causes a travelling wave on the basilar membrane. The transduction of sound frequencies is tonotopically distributed along the cochlear duct: high frequency sounds are transduced at the base of the cochlea, whereas low frequency sounds are transduced at the apex of the cochlea (Russell & Sellick 1978).

Three fluid-filled compartments are present within the cochlea: scala vestibuli, scala tympani and scala media (Hudspeth 2014). Both scala vestibuli (connected to the oval window) and scala tympani (connected to the round window) are filled with perilymph, an extracellular fluid similar to the one found surrounding most cells. The scala media is filled with endolymph, a fluid rich in K^+ secreted by the cells of the stria vascularis. The process of generating the unusual ionic composition of the endolymph also generates a potential of approximately +80mV in the scala media respectively to the other compartments. Consequently, the main driving force for sensory transduction is the endocochlear potential, generated by the stria vascularis (Hudspeth 2014; Raphael & Altschuler 2003).

In the cochlea, two types of cells that lie on top of the basilar membrane are highly specialised in the conversion of the mechanical sound pressure to neuronal impulses: outer and inner hair cells (Fig.1.2). The outer hair cells occur in three rows and are responsible for mediating the cochlear active process, providing a motor function that enhances and modulates the function of inner hair cells (Hudspeth 2014; Raphael & Altschuler 2003). Mammalian outer hair cells are generally cylindrical, with a spherical nucleus located in the basal area of the cell (Fig.1.2). At the base, outer hair cells are surrounded by Deiter's cells. The apical domain of outer hair cells contains the stereocilia, in a staircase arrangement known as hair bundle (Osborne et al. 1984).

Inner hair cells, occurring in a single row, act by detecting basilar membrane motion and transmitting the afferent information to the brain through the spiral ganglia (Fig.1.2) (Hudspeth 2014). They are generally pear-shaped and present a spherical nucleus located in the centre of the cell. At their basal poles, bathed in perilymph, inner hair cells contact with supporting cells and neuronal terminals. The apical surface of inner hair cells contact with the endolymph of the scala media (Raphael & Altschuler 2003).

Located on the apical surface of sensory hair cells, stereocilia are cellular projections mostly comprised of F-actin (Fig.1.2). Their size decreases in a gradient towards the base of the cochlea, with the tallest stereocilia found at the cochlear

apex (Peng et al. 2011; Raphael & Altschuler 2003). The stereocilia movements control the opening of the transduction ion channels in the hair cells (Pickles et al. 1984). The flux of K^+ and Ca^{2+} ions generates a transduction current that, ultimately, leads to the release of neurotransmitter from the hair cell base to the brain (Fig.1.3) (Raphael & Altschuler 2003). Type I afferent neurons innervate the inner hair cells and are responsible for the transmission of the neuronal impulses from the cochlea to the brain. On the contrary, efferent neurons transmit information from the brain to the cochlea (Fig.1.3) (Alberti 2001). Lying on top of the outer hair cells stereocilia is the tectorial membrane (Fig.1.2), a strip of extracellular matrix composed of collagen (Richardson et al. 2008). The tectorial membrane plays an important mechanical role in hearing by ensuring the balance between the coupling and fine frequency resolution along the cochlea (Lukashkin et al. 2010).

Between the hair cells reside the supporting cells, which maintain an environment in the cochlear epithelium that allows hair cells to function (Raphael & Altschuler 2003). At least five types of supporting cells reside in the cochlear epithelium and from the outer edge to the inner edge of the cochlea they are: Hensen's, Deiters', pillar, inner phalangeal and border cells (Raphael & Altschuler 2003). Supporting cells are crucial for K^+ recycling via K^+/Cl^- co-transporters and gap junctions. Supporting cells are thought to function as mediators of hair cell development, function, death and phagocytosis, thus being essential for normal hearing (Wangemann 2006; Raphael & Altschuler 2003; Monzack & Cunningham 2013). In addition, supporting cells contribute to hair cell regeneration in non-mammalian vertebrates. In these, supporting cells can actively repair lost hair cells, either by mitotic division, in which supporting cells divide to generate novel hair cells, or transdifferentiation, in which supporting cells undergo a transformation process to become hair cells (Monzack & Cunningham 2013).

Figure 1.2 – Cross-section of the organ of Corti. The apical surface of the inner hair cells (IHC) and outer hair cells (OHC) is bathed in the K^+ rich endolymph, whereas the basolateral surface of both IHC and OHC is bathed in the Na^+ rich perilymph. Hair bundles or stereocilia are present at the apical surface of hair cells. Overlying the sensory hair cells is the tectorial membrane. The basilar membrane separates the scala media from the scala tympani. The auditory nerve and spiral ganglia transmit the neuronal impulses from the cochlea to the brain. Image reproduced from (Peng et al. 2011).

Figure 1.3 – Schematic representation of a hair cell. Outer hair cells present a cylindrical-like shape with a spherical nucleus towards the base of the cell (as represented in the figure), whereas inner hair cells present a pear-like shape with a more central nucleus. The stereocilia are located on the apical surface of the hair cells, bathing on the endolymph. On the basal surface of the cells, synaptic vesicles release the neurotransmitters from the hair cells to the brain via the afferent neurons. The efferent neurons carry information from the brain to the cochlea. The basolateral area of hair cells where the nerve fibres reside is bathed in perilymph⁴.

⁴ Available at - <http://www.open.edu/openlearn/ocw/mod/oucontent/view.php?id=2577&printable=1> - Accessed on the 11th November 2016.

1.3. Types of hearing loss

Hearing loss is the most common sensory impairment worldwide. According to the WHO, over 5% of the world's population presents disabling hearing loss, which corresponds to approximately 328 million adults and 32 million children. With regard to the elderly, epidemiologic studies suggest that approximately one-third of the population over 65 years old is affected by disabling hearing loss, with a greatest prevalence in South Asia, Asia Pacific and sub-Saharan Africa (WHO, 2015)⁵. Disabling hearing loss refers to hearing loss greater than 30 decibels (dB) in the better ear in children and a hearing loss greater than 40 dB in the better ear in adults.

The severity of hearing loss is characterised as follows by the hearing thresholds in dB over the frequencies of 500 Hz, 1000 Hz, 2000 Hz and 4000 Hz in the better ear (Table 1.1):

Table 1.1 – Grades of hearing impairment. Adapted from (WHO, 2008)⁶.

Grade of impairment	Correspondent audiometric ISO value (better ear)	Performance
0 – No impairment	25 dB or better	No or very slightly hearing problems. Able to hear whispers.
1 – Slight impairment	26-40 dB or better	Able to hear and repeat words spoken in normal voice at 1 meter.
2 – Moderate impairment	41-60 dB or better	Able to hear and repeat words spoken in raised voice at 1 meter.
3 – Severe impairment	61-80 dB or better	Able to hear some words when shouted into better ear.
4 – Profound impairment including deafness	81dB or greater	Unable to hear and understand even a shouter voice.

⁵ World Health Organisation – Deafness and Hearing Loss
Available at <http://www.who.int/mediacentre/factsheets/fs300/en/> - Accessed on 25th October 2016

⁶ WHO – Grades of hearing impairment. Available at
http://www.who.int/pbd/deafness/hearing_impairment_grades/en/ - Accessed on 11th November 2016

Hearing loss can result from abnormalities of the external ear canal and/or the ossicles of the middle ear and thus being designated as conductive, from malfunctions of the inner ear, designated as sensorineural, or it can result from a combination of both. Hearing loss can occur as a consequence of genetic inheritance or acquired causes. Approximately 1 in every 1000 infants is born with hearing impairment and, of these, one half is likely to be due to genetic factors (Morton 1991; Van Camp et al. 1997). Hereditary hearing loss is classified as non-syndromic, when hearing impairment is the only clinically relevant feature, or syndromic, when hearing impairment is associated with malformations of the external ear or other organs (e.g. eyes, skin or thyroid) (Martini 2007). Non-syndromic hearing loss accounts for approximately 70% of hereditary hearing loss and is classified according to the different types of inheritance pattern: autosomal recessive (~80% of the cases), autosomal dominant (~20%), X-linked (~1%) and mitochondrial (<1%) (Martini 2007).

The locus DFNB1 (autosomal recessive non-syndromic deafness) accounts for approximately 50% of congenital recessive non-syndromic hearing loss worldwide (Smith & Jones 1993). Mutations in *GJB2* gene, coding for connexin 26 protein, are present in high prevalence in populations such as Ashkenazi Jewish, Caucasian and Japanese (Kenneson et al. 2002). The DFNA3 locus (autosomal dominant non-syndromic deafness), for instance, carries dominant mutations in genes such as *GJB2* and *GJB6*, the latter coding for connexin 30 (Smith et al. 1993). Despite being present in other tissues, connexins are highly expressed in the organ of Corti and vestibular system. They are thought to provide a rapid removal of ions away from the region of the sensory cells during transduction to ensure sensitivity (Forge et al. 1999). Genes such as *POU3F4* and *PRPS1*, coding for a transcription factor protein and phosphoribosylpyrophosphate protein, respectively, are responsible for X-linked deafness, which affects approximately one in every 50000 new-born males (Russell et al. 1995; Liu et al. 2016). Mitochondrial inheritance of hearing loss is mostly due to mutations in *MT-RNR1* or *MT-TS1* genes. Mutations in *MT-RNR1* have been associated with predisposition to aminoglycoside antibiotic ototoxicity and/or late-onset sensorineural hearing loss (Pandya 1993). Hearing loss caused by aminoglycoside ototoxicity occurs within a few days to weeks after administration of antibiotics such as gentamicin, tobramycin, kanamycin, streptomycin, neomycin or sisomicin. Besides the hearing loss phenotype, mutations in *MT-TS1* gene have also been reported to cause palmoplantar keratoderma (Pandya 1993).

Syndromic forms of hearing impairment account for the remaining 30% of hereditary hearing loss. *SLC26A4* gene, coding for Pendrin protein, is responsible for Pendred syndrome, the most common syndromic form of hearing loss, that includes a combination of goitre (thyroid abnormality) and severe sensorineural hearing loss (Coyle et al. 1996). Other syndromic conditions of hearing loss include Wolfram syndrome, in which hearing loss is found in combination with diabetes mellitus and optic atrophy, and Usher syndrome, in which retinitis pigmentosa is also present (Weil et al. 1995; Bessalova et al. 2001).

Acquired hearing loss refers to acquired causes that may lead to hearing loss at any age, without congenital interference. In children, acquired hearing loss often results from prenatal infections such as toxoplasmosis, rubella, cytomegalovirus and herpes, or postnatal infections caused by bacterial meningitis or *Escherichia coli*, *Listeria monocytogenes*, *Streptococcus agalactiae*, and *Enterobacter cloacae*. In adults, on the contrary, despite the contribution of infectious diseases, acquired hearing loss is frequently associated with noise exposure, trauma, iatrogenic effects of certain drugs or related to ageing (Kochhar et al. 2007; Martini 2007).

Noise-induced hearing loss is responsible for more than one third of the cases of acquired hearing loss in developed countries. Excessive noise exposure is responsible for a greater acceleration of hearing impairment in the ageing population sooner than would occur from the ageing process itself (WHO, 1997)⁷. Acoustic trauma, depending on the intensity of the noise, can cause anatomic changes in the ear such as disruption of stereocilia, complete damage of the organ of Corti or rupture of intracochlear membranes (Bodmer 2008). Acoustic trauma is also suggested to promote significant changes in the cochlear blood flow, that include vascular permeability, capillary vasoconstriction and blood stagnation in the stria capillaries, thus resulting in cochlear anoxia (Poirrier et al. 2010).

Age-related hearing loss or presbycusis associates with acquired forms of hearing impairment and is characterised by diminished hearing and speech comprehension in noisy environments, slow processing of acoustic information and impaired localisation of sound. Presbycusis refers to hearing loss in the elderly individuals, representing the multifactorial insults to the auditory system of a lifetime. Ageing and noise exposure have been suggested as the most common insults that can contribute to the degeneration of the auditory system, along with genetic

⁷ World Health Organisation - Prevention of noise-induced hearing loss, 1997
Available at <http://www.who.int/pbd/deafness/en/noise.pdf> - Accessed on 11th November 2016.

susceptibility and exposure to ototoxic agents (Gates & Mills 2005). Based on histopathological studies of temporal bones of ageing individuals, four different types of presbycusis have been proposed: sensory, neural, metabolic and mechanical (Schuknecht 1964). Sensory presbycusis is caused by atrophy of the organ of Corti and the auditory nerve in the basal end of the cochlea, consistent with high frequency hearing loss. The neural type is characterised by the loss of neurons in the auditory pathways that is suggested to occur later in life and is consistent with loss in speech discrimination. Metabolic presbycusis refers to a slow and progressive sensorineural type of hearing loss that is caused by atrophy of the stria vascularis, which reflects in a loss across all frequencies. Mechanical presbycusis was suggested to be a result of stiffness of the basilar membrane or other mechanical disorder and its functional manifestation corresponds to a descending audiometric curve (Schuknecht 1964). Since multiple environmental and genetic factors can be involved in the onset and progression of age-related hearing loss, most cases are of mixed pathology and affect different cell types.

Aminoglycosides are a class of antibiotics widely used for the treatment of infections caused by gram-negative bacteria, such as *Escherichia coli*, *Mycobacterium tuberculosis* and *Pseudomonas* (Forge & Schacht 2000). Despite their high efficacy in controlling infections, aminoglycoside exposure is often associated with a pattern of permanent, bilateral high frequency hearing loss (Guthrie 2008). Examples of aminoglycoside antibiotics include neomycin, sisomicin, streptomycin and gentamicin. They are produced by soil actinomycetes and present low-molecular weight of approximately 300 to 600 daltons (Forge & Schacht 2000; Guthrie 2008). Aminoglycosides share a similar chemical structure, generally comprised of three rings: cyclitols (a saturated six-carbon ring) and five or six-membered sugars linked via glycosidic bonds (Forge & Schacht 2000). The presence of amino groups attached to the various rings of the structure and the hydroxyl groups confer the chemical properties to the aminoglycosides, such as high water solubility and a basic character (Forge & Schacht 2000). Aminoglycosides antibiotics are not toxic *per se*, requiring the redox-capacity of a transition metal ion in order to become ototoxic (Forge & Schacht 2000; Guthrie 2008). It is thought that the formation of free radicals once inside the hair cells is a hallmark of the aminoglycoside toxicity that requires the presence of iron salts (Forge & Schacht 2000; Huth et al. 2011). Mutations in the mitochondrial DNA were found to play a role in the aminoglycoside-triggered hair cell death (Guthrie 2008). A single nucleotide change in the mitochondrial DNA that codes for the 12S *rRNA* gene reveals increased

susceptibility to aminoglycoside toxicity. This alteration turns the *12S rRNA* gene conformation similar to the bacterial ribosomal gene, thus enhancing aminoglycoside binding and its toxic effects in the ear (Guthrie 2008; Huth et al. 2011). Another ototoxic drug commonly used is cisplatin, a very efficient chemotherapy agent used for the treatment of several types of cancer, such as head, neck, lung, cervical, prostate and melanoma (Schacht et al. 2013). Cisplatin side effects typically include nephrotoxicity and in the inner ear, hair cell damage (Schacht et al. 2013). Cisplatin mostly damages outer hair cells at the base of the cochlea, the stereocilia, stria vascularis and spiral ganglion neurons (Comis et al. 1986; Huang et al. 2000; Poirrier et al. 2010).

In summary, hearing loss, within its various types, is the most common sensory pathology that presents highly complex and multifactorial causes. The WHO estimates that approximately 60% of the childhood hearing loss cases could be prevented through preventative measures and appropriate therapeutic interventions (WHO, 2016)⁸. As regarding the adult age-related hearing loss cases, it is likely that a lifetime of noise exposure, along with deterioration of the cochlear structures that comes with ageing, play an important role and synergise to promote the decline of the hearing function. Preventative measures, such as avoiding exposure to excessive noise, could help to avoid damage and deterioration of hearing. In addition, more research is needed to identify the molecular pathways underlying hair cell damage and loss following noise exposure or during ageing, for instance. Identification of key players in hair cell's response to damage may help to identify novel therapeutic targets aimed at preserving the hearing function.

1.4. Cochlear stress

As previously mentioned, the hearing process occurs in a series of events, from the amplification and direction of sound in the outer and middle ear to the transduction into neuronal impulses that are conducted from the inner ear to the brain. The mechanisms of sound detection, amplification and processing rely on a well-coordinated series of events that are likely to be a cause of intrinsic stress within the cochlea. Amplification of sound, maturation of the high specialised hair cells, vibrations of basilar membrane, different ionic composition amongst distinct

⁸ World Health Organisation – Childhood Hearing Loss, 2016
Available at http://www.who.int/pbd/deafness/world-hearing-day/WHD2016_Brochure_EN_2.pdf -
Accessed on 11th November 2016

compartments and the high specialised movements of stereocilia that control the opening of the transduction channels are examples of the constant stress environment that is present within the inner ear. The maintenance of such delicate and well-coordinated processes ensures a correct detection and perception of the sound stimuli. However, dysregulation of any of these processes can contribute to damage and degeneration of the highly specialised hair cells, thus leading to hearing loss. As mentioned above, the loss of cochlear hair cells in mammals is an irreversible process due to the lack of regenerative capacity of these cells, leading to the development of hearing loss and deafness (Martini 2007). Many causes can contribute to the degeneration of hair cells, including genetic predisposition, noise exposure and the administration of certain drugs. Such causes often generate changes in the cellular homeostasis and trigger the activation of stress-induced pathways (Altschuler et al. 2002).

Many lines of evidence suggest the involvement of oxidative stress in hair cell damage and loss, as a consequence of noise exposure, ototoxic drugs or ageing (Lopez-Gonzalez et al. 1999; Staecker et al. 2001; Henderson et al. 2006). Indeed, oxidative stress caused by formation of reactive oxygen species (ROS) has been pointed out as one of the main associations with age-related hearing loss (Ohlemiller et al. 1999). Decreasing in glutathione and antioxidant enzymes have been observed in the organ of Corti and spiral ganglion neurons of the aged cochlea (Poirrier et al. 2010). In support of a ROS theory for hearing loss, mice strains lacking antioxidant enzymes present enhanced propensity to age-related hair cells loss and/or susceptibility to noise-induced hearing loss (McFadden et al. 1999; Ohlemiller et al. 2000).

Acoustic trauma, depending on the intensity of the noise, can cause structural changes in the ear such as disruption of stereocilia, complete damage of the organ of Corti or rupture of intracochlear membranes (Borg & Engström 1983; Hua Hu & Henderson 1997; Ohlemiller et al. 1999; Hu et al. 2002; Bodmer 2008). Noise exposure also induces excessive glutamate at the synapse between the inner hair cells and the afferent neurons, which contributes to neurodegeneration (Moser & Starr 2016). Pro-apoptotic stress pathways, such as JNK, p38MAPK, release of mitochondrial cytochrome c and caspase activation were also suggested to be involved in hair cell death following noise exposure (Nicotera et al. 2003; Murai et al. 2008; Meltser et al. 2009; Tabuchi et al. 2010).

Aminoglycoside antibiotics present high ototoxic effects, as previously mentioned, likely to be caused by the formation of ROS. Aminoglycosides are not toxic *per se*, requiring the redox-capacity of a transition metal once inside the hair cells (Forge & Schacht 2000; Guthrie 2008). For instance, when gentamicin combines with iron salts, the gentamicin-iron complex promotes iron-catalysed oxidations that directly promote the formation of ROS (Huth et al. 2011). Since this process requires electrons, unsaturated fatty acids such as arachidonic acid are likely to act as electron donors and, in return, these are oxidised to lipid peroxides (Forge & Schacht 2000; Huth et al. 2011). Lipid peroxides can, in turn, generate a chain reaction of peroxidation and ROS can undergo a Fenton-type reaction to hydroxyl radical (Forge & Schacht 2000; Huth et al. 2011):



Since arachidonic acid is essential for the integrity of the cellular membranes, ROS formation can affect membrane fluidity and permeability (Huth et al. 2011). Through lipid peroxidation, ROS toxicity in the hair cells includes disruption of enzymes, ion channels and receptors (Huth et al. 2011). Although ROS are components of the normal cellular metabolism and activation of antioxidants such as glutathione normally impedes ROS lethal accumulation, it is thought that the ROS generated following aminoglycoside exposure largely exceed the capacity of the cells to repair their toxic effects, thus leading to apoptotic cell death (Forge & Schacht 2000; Huth et al. 2011). Following aminoglycoside exposure, pro-apoptotic mediators such as JNK, c-Jun, c-FOS, Bcl-2 and caspases, for instance, have been shown to be activated and directly involved in aminoglycoside-triggered hair cell death (Cheng 2005; Huth et al. 2011). Despite the large activation of pro-apoptotic cascades following aminoglycoside administration, hair cells have also been reported to die by activation of caspase-independent apoptotic pathways, such as necrosis (Jiang et al. 2006).

Cisplatin, a drug used against different types of cancer, has also been shown to be highly ototoxic and to generate the formation of ROS once inside the hair cells. Increased ROS content was suggested to trigger mitochondrial release of cytochrome c, thus activating pro-apoptotic pathways, such as caspase-3 and caspase-9 (Poirrier et al. 2010). Cisplatin has also been shown to disrupt microtubules and cytoskeleton (Schacht et al. 2013). In addition, it is thought that its ability to bind glutathione and other sulfhydryl-containing molecules can contribute

to an impairment of cellular detoxification mechanisms, thus leading to ototoxicity and cell death (Schacht et al. 2013).

Given the broad contribution of many factors leading to the damage and loss of hair cells, a large body of research has been focused in the study of the stress pathways involved in cochlear stress, aimed at identifying possible strategies for otoprotection. Antioxidants, inhibitors of pro-apoptotic stress pathways and neurotransmission blockers have been widely tested during cochlear stress in order to assess their effects on the hair cell protection. Despite the success of some of these studies *in-vitro*, *in-vivo* experiments are needed to assess the systemic effects of such treatments, given the ultimate objective of application in humans. In addition, it is not clear to date which molecular pathways are involved in the hair cell's protection following different types of ototoxic insult. A better understanding of these pathways is likely to provide novel insight into the mechanisms that regulate hair cell survival during stress and, consequently, the identification of novel therapeutic targets for the protection of hair cells from damage.

1.5. Stress pathways in the ear: Hsp70

The heat shock response is a conserved stress defence mechanism common to bacteria, animals and plants. Although originally discovered as a consequence of elevated temperature (Ritossa 1962), the heat shock response has been shown to be activated by a wide variety of stresses, such as oxidative stress, ischemia and transition metal ions (Gabai & Sherman 2002; Shamovsky & Nudler 2008). In the inner ear, heat shock has been shown to promote cell survival upon different types of insult, such as cisplatin and aminoglycoside exposure, excessive noise and ischemia (Dechesne et al. 1992; Myers et al. 1992; Thompson & Neely 1992; Oh et al. 2000).

The induction of the heat shock response in eukaryotes is controlled by the transcription factor heat shock factor 1 (HSF1). Aside from being constitutively expressed during physiological conditions, HSF1 is dramatically activated upon stress exposure (Sarge et al. 1993; Richter et al. 2010). In its physiological state, HSF1 is generally found as a monomer complexed with the heat shock proteins (Hsp) 70 and 90. Upon stress exposure, HSF1 is transported to the nucleus, hyperphosphorylated and starts the transcription of *Hsp70* gene (Shamovsky & Gershon 2004; Shamovsky & Nudler 2008; Richter et al. 2010; Silver & Noble

2012). Due to its peripheral nuclear localisation, the *Hsp70* gene transcription is optimised during stress (Kurshakova et al. 2007).

Hsp70 is a 70-kDa class of molecular chaperone proteins that assist a wide range of folding processes under physiological and stress conditions. For instance, Hsp70 assists in the folding of *de novo* proteins, stabilisation of polypeptides and re-folding following denaturation (Mayer & Bukau 2005; Shaner & Morano 2007; Richter et al. 2010). The broad activity of Hsp70 is due to the recognition of a short degenerate motif in the substrates that consists of five residues enriched in hydrophobic amino acids flanked by regions enriched in positively charged amino acids (Mayer 2013).

Early since its discovery, the heat shock response and especially, Hsp70, have been associated with cellular protection. The hypothesis that Hsp70 may be protective during stress has been sustained by the facts that Hsp70 is constitutively expressed during physiological conditions and, following stress exposure, its expression dramatically increases (Baler 1996; Gabai & Sherman 2002; Mayer & Bukau 2005). This suggests that, although Hsp70 may be normally required by the cells to ensure their regular physiology, its presence may be critical during stress.

Hsp70 has been directly associated with hearing protection following noise exposure, since increasing in body temperature (e.g. heat shock) and consequent activation of Hsp70 have been shown to be protective against noise-induced hearing loss (Yoshida et al. 1999). Moreover, mice deficient in Hsp70, *Hsf1*^{-/-}, demonstrate increased susceptibility to noise-induced hearing loss (Sugahara et al. 2003; Fairfield et al. 2005), indicating the importance of this protein in cell protection and hearing preservation during stress conditions.

In mouse utricles, pre-treatment with heat shock and individual Hsp proteins, including Hsp70, protected hair cells from cisplatin- and aminoglycoside-induced hair cell death (Cunningham & Brandon 2006; Baker et al. 2015). Moreover, *in-vivo* data indicates that in mice overexpressing Hsp70 protein, cochlear hair cells are protected against aminoglycoside-induced death (Taleb et al. 2009). This corroborates previous studies in which deficiency in Hsp70 has been suggested to worsen hair cell death and hearing loss following noise exposure (Sugahara et al. 2003; Fairfield et al. 2005). Altogether, these results suggest that Hsp70 protein is particularly important in hair cell survival and hearing maintenance following different types of insult.

More recently, it has been shown that the Hsp70 protective effects observed following aminoglycoside exposure in mouse utricles are due to the synthesis of

Hsp70 by supporting cells and not hair cells (May et al. 2013). In that study it was shown that utricle hair cells do not produce Hsp70 following heat shock exposure and it was suggested that supporting cells actively synthesise Hsp70 to protect hair cells from aminoglycoside-induced death (May et al. 2013). The presence of Hsp70 was found to be critical for hair cell survival not only in utricles exposed to heat shock but also in co-cultured utricles that have not been subjected to heat shock stress (May et al. 2013). In agreement with this, removal of Hsp70 from the culture media abolished the protective effects of the co-culture (May et al. 2013). Despite the findings that Hsp70 is secreted by supporting cells to protect hair cells following aminoglycoside-induced cell death, internalisation of Hsp70 by hair cells was not reported, suggesting that Hsp70 may act at the hair cell's surface, probably through a specific receptor (May et al. 2013). The existence of a putative Hsp70 receptor in hair cells capable of triggering downstream protective cellular pathways when activated suggests that, not only a specific cell-to-cell communication mechanism involving Hsp70 in the inner ear exists, but also that Hsp70 may be critical for hair cell survival following stress conditions, either acting alone or by molecular interactions with other stress-responsive pathways once inside the hair cells. Consistent with this hypothesis, Hsp70 has been shown to inhibit apoptosis at various points in the cell death pathway following heat shock stress in other types of cells. In PEER and F3 cell lines, Hsp70 was shown to inhibit the activation of SAPK/JNK and caspase-3 pro-apoptotic factors (Mosser et al. 1997). Moreover, release of cytochrome c was inhibited from mitochondria in Hsp70-expressing PEER cells as a result of heat shock exposure (Mosser et al. 2000).

Hsp70 has also been shown to be involved in regulation of inflammation. In HEK293T cells, Hsp70 degraded p65, a critical component of the NF- κ B signalling, thus inhibiting inflammation (Tanaka et al. 2014). In mice, Hsp70 was also shown to attenuate the toxic effects caused by tumour necrosis factor-triggered inflammation (Van Molle et al. 2002).

A number of studies have also associated Hsp70 with neuroprotection and animal models for neurodegenerative diseases have been studied for Hsp70 effects on the progression of the pathologies. For instance, administration of Hsp70 has been shown to inhibit motor and sensory neuron degeneration in mice *in-vivo* (Tidwell et al. 2004). A different study in mouse models has found that Hsp70 protects *in-vivo* astrocytes from oxidative stress and transgenic hippocampal neurons from glutamate toxicity (Lee et al. 2001).

Hsp70 has been shown to play an important role by contributing to the inhibition of neurodegeneration during Parkinson's or Alzheimer's disease (Ahn & Jeon 2006; Aridon et al. 2011; Bobkova et al. 2014; Yurinskaya et al. 2015). In mouse models for amyotrophic lateral sclerosis (ALS), Hsp70 has also been shown to delay the progression of the disease (Gifondorwa et al. 2007). Administration of arimoclomol, a co-inducer of heat shock proteins, promoted muscle function and motoneuron survival (Kieran et al. 2004; Kalmar et al. 2014). In addition, induction of Hsp70 through arimoclomol ameliorated the symptoms in mice models of retinitis pigmentosa, by protecting the structure of the photoreceptors and reducing the aggregation of rhodopsin (Parfitt et al. 2014).

Altogether, these evidences indicate that Hsp70 is likely to be one of the cellular key players in promotion of cell survival upon different insults, constituting a realistic target for development of novel therapies aimed at preserving cell survival. In the ear, despite its involvement in hair cell survival and hearing preservation during stress, the involvement of Hsp70 with other stress-activated pathways is yet poorly understood.

1.6. Stress pathways in the ear: stress granules

The first evidence of SG formation in the ear was reported in 2004, in a study of the chick basilar papilla exposed to aminoglycoside treatment (Mangiardi et al. 2004). The authors reported the presence of T-cell intracellular antigen related protein (TIAR)-positive granules in the cytoplasm of chicken hair cells subjected to gentamicin treatment and proposed that the granules may regulate part of the hair cell response to the aminoglycoside treatment in the avian model (Mangiardi et al. 2004).

More recently, in 2011, our laboratory published the first report of SG formation in the mammalian inner ear (Towers et al. 2011). Mammalian cochlear hair cells assembled SGs in response to neomycin treatment, suggesting that the SG pathway might be involved in the cochlea's response to stress (Towers et al. 2011). In this study, *Cytoplasmic activation/proliferation-associated protein-1 (Caprin-1)* gene was found to be a target of *POU4F3* (Towers et al. 2011). *POU4F3* is a transcription factor involved in inner ear development, essential for correct hair cell maturation and development (Xiang et al. 1997; Xiang et al. 1998). In addition, mutations in *POU4F3* have been associated with dominant non-syndromic hearing

loss in humans (Weiss et al. 2003; Collin et al. 2008). *Caprin-1* was identified as a target gene of *POU4F3* after a subtractive hybridisation screen in OC-2 cells, in which a reduction in *POU4F3* levels was associated with an increase in *Caprin-1* expression. Functional studies revealed that exogenous overexpression of *Caprin-1* in OC-2 cells induced the formation of cytoplasmic *Caprin-1*-positive SGs (Fig.1.4), suggesting that exogenous induction of *Caprin-1* is sufficient to induce SG formation (Towers et al. 2011).

Figure 1.4 – *Caprin-1* overexpression induces SG formation in OC-2 cells. Overexpression of *Caprin-1*-GFP resulted in SG formation, as confirmed by colocalisation with T-cell intracellular antigen (TIA-1) protein in the merged image. White arrowheads point to SGs. Scale bar= 20µm. Image adapted from (Towers et al. 2011).

Caprin-1 expression was also confirmed to be present in cochlear cells after gene expression analysis and at the protein level after immunohistochemistry (Towers et al. 2011). To confirm whether mouse cochlear hair cells have the potential to form SGs following ototoxic insult, mouse cochlear explants were then subjected to neomycin treatment and *Caprin-1* protein expression was evaluated. Following aminoglycoside-treatment, *Caprin-1* was observed to colocalise with TIA-1 protein, a known SG marker, in discrete cytoplasmic SGs in hair cells, thus confirming that the SG pathway is activated in mammalian hair cells following ototoxic stress (Towers et al. 2011). A working model was then proposed for these interactions, suggesting that hair cell damage (triggered by aminoglycoside, for instance), modifies *POU4F3* activity, thus resulting in an increase of *Caprin-1* expression and, consequently, SG formation.

Data from our laboratory also points to the existence of *in-vivo* SGs in the early-onset age-related hearing loss C57BL/6 mouse model. Presence of SGs *in-vivo* was detected in the cochlea and spiral ganglion using various SG-markers (e.g. TIA-1, *Caprin-1*, eIF4G, eIF3, G3BP1, eIF2 α and RACK1) and seems to clearly associate with increasing age (Emily Towers and Naila Haq, *unpublished*). C57BL/6 mice exposed to noise-induced damage also revealed to form *in-vivo* SGs in hair cells and spiral ganglion neurons (Lisa Nolan and Naila Haq, *unpublished*).

Together, these data suggest that the SG pathway is activated upon different cochlear stressors and is associated with hearing decline. However, despite suggesting that SG are highly implicated in the cochlea's response to stress, it is still unclear from these data which role SGs play in the inner ear as a response to stress.

1.7. The role of stress granules in cellular stress

In the presence of environmental stress (e.g. heat, hyper-osmolarity, oxidative conditions, hypoxia, UV radiation, among others) cells must adapt their gene expression and protein production in order to respond to the stress, repair the stress-induced damage and survive. This response involves a global translational silencing, characterised by a selective shutting down in the protein synthesis, towards the conservation of anabolic energy for the repair of stress-induced damage (Anderson & Kedersha 2002; Thomas et al. 2011). As a consequence of the stress-induced translational silencing, polysomes disassemble allowing translating ribosomes to “run off” the transcripts. This process generates circular polyadenylated messenger ribonucleoprotein particles (mRNPs) that can aggregate at SGs or processing bodies (Anderson & Kedersha 2009). These subsequent interactions will control the fate of mRNAs: mRNAs sequestered by processing bodies are likely to undergo degradation, whereas mRNAs aggregated at SGs will be selectively “triaged” from translation according to their function (Kedersha et al. 2005; Anderson & Kedersha 2006).

During stress conditions, the translation rate of “housekeeping” transcripts is reduced. Conversely, an associated relative increase in the translation of stress-responsive genes is observed (Kedersha & Anderson 2002). Such post-transcriptional modifications of gene expression are mainly controlled by the formation of cytoplasmic SGs (Anderson & Kedersha 2002; Anderson & Kedersha 2009).

SGs were first reported in 1983 as heat shock granules in cultures from Peruvian tomato cells (Nover et al. 1983). Five years later, it was shown that SGs are also generated in mammalian cells in response to heat shock treatment (Arrigo 1988). SGs are not found under physiological conditions (i.e. in normal unstressed cells) but are assembled as a response to stress. SGs are discrete, non-membranous cytoplasmic structures at which specific proteins bind to mRNA molecules during

the selective reduction of translation observed under stress conditions (Scharf et al. 1998; Nover et al. 1989; Kedersha & Anderson 2002).

SGs are described as fibrillo-granular structures of a moderate electron density with irregular outlines, not delineated by a membrane, with size ranging from 0.1 to several micrometres (Souquere et al. 2009). They are usually not in close association with any particular cellular organelle or the plasma membrane, which suggests that they are free, self-assembling structures (Kedersha et al. 1999; Souquere et al. 2009).

Through dynamic sequestration of mRNA molecules by specific RNA-binding proteins, SGs are thought to be preferred sites for mRNA storage and sorting during stress (Kedersha et al. 2000; Kedersha et al. 2002; Kedersha & Anderson 2002). The mRNA selection process is highly selective, since functional interactions of mRNAs with RNA-binding proteins at SGs may determine whether these molecules are translated during stress, stored at SGs to re-enter translation later on, or destroyed (Anderson & Kedersha 2009).

By acting at a post-transcriptional level, SGs can directly and quickly regulate how cells respond to stress, limiting the pool of available mRNAs for translation (Kedersha et al. 1999; Anderson & Kedersha 2008). Since the type of stress generates differential responses in different types of cells, SGs are not likely to target the same mRNA molecules upon stress, but to sequester specific transcripts depending on the biological context (i.e. type of stress and cell type) (Kedersha et al. 2002; Anderson & Kedersha 2008).

As transient structures, SGs were shown to disassemble when cells recover after sub-lethal stress, evidencing their ability to vanish when environmental conditions allow (Kedersha et al. 2000; Kedersha & Anderson 2002).

In summary, the SG pathway seems to be highly involved in regulation of cell survival. Through triage of specific mRNA molecules to be translated during stress, dynamic association with processing bodies and polysomes and direct regulation of the transcriptome expression, SGs seem to play a key role during transient stress conditions. Furthermore, the fact that SGs are not found during regular physiological conditions (i.e. in unstressed cells) supports the hypothesis that SG may be key players during cellular stress. Given that the SG pathway seems to be highly involved in controlling the cell's response to stress, it is likely that these structures are crucial to promote cell survival during stress.

1.8. Properties of SGs

Given the implication of SGs in the cellular response during stress conditions, a large body of research has been focusing in determining the key molecules involved in regulation of SG formation. Several initiation factors, deubiquitinating enzymes, RNA helicases, RNA-editing enzymes and translational silencers, amongst others, have been shown to be components of SGs, evidencing the important role of these structures in the control of post-transcriptional gene expression under stress conditions (Kedersha & Anderson 2002; Low et al. 2005; Brehm et al. 2007; Ohn et al. 2008; Kedersha et al. 2013). The presence of signalling molecules and pro-apoptotic factors have provided additional evidence that the post-transcriptional control of gene expression by SGs also involves cell survival decisions during stress (Kedersha et al. 1999; Kedersha et al. 2002; Tourrière et al. 2003; Kim et al. 2005; Ohn et al. 2008; Papadopoulou et al. 2013). In addition, impairment of SG formation showed to promote cell death during stress (Buchan & Parker 2009; Ghisolfi et al. 2012; Arimoto-Matsuzaki et al. 2016), consistent with the hypothesis that SGs may act as protective structures during transient stress. Moreover, evidence suggests that SGs are required to allow optimal translation of stress-responsive mRNAs, which might be dependent on the type of cell and nature of the stress applied (Kedersha & Anderson 2002; Kedersha et al. 2002; Buchan & Parker 2009). Interestingly, also RNA-editing enzymes were shown to be located to SGs, suggesting that SGs can alter RNA sequences through post-transcriptional modification of mRNA transcripts (Gallois-Montbrun et al. 2007; George et al. 2016). Association of SGs with microtubules was also reported, suggesting that SGs can be transported to specific sites in the cytoplasm and regulate the fate of RNA molecules and protein translation locally (Nadezhdina et al. 2010).

Knockdown of specific initiation factors and overexpression of translational silencing RNA-binding proteins can promote SGs assembly (Kedersha et al. 2000; Kedersha et al. 2002; Li et al. 2010; Kraft et al. 2008; Towers et al. 2011). On the other hand, knockdown of translational silencing proteins or inactivation of mammalian target of rapamycin complex (mTORC) pathway have been shown to impair SGs assembly (Kedersha et al. 1999; Ghisolfi et al. 2012; Fournier et al. 2013).

TIA-1 and TIAR are two proteins involved in many aspects of cellular metabolism, including mRNA splicing, translation, decay and cell survival. These proteins were reported to act downstream of the stress-induced phosphorylation of eIF2 α to promote the recruitment of untranslated mRNA molecules to SGs (Kedersha et al.

1999). TIA-1 and TIAR are composed of three amino-terminal RNA recognition motifs and one carboxy-terminal glutamine-rich motif structurally related to a prion protein, designated prion-related domain (PRD) (Gilks et al. 2004). The PRD was found to be required for SGs assembly, since it is responsible for the formation of protein aggregates at which the abortive initiation complexes are directed to form SGs (Gilks et al. 2004).

Caprin-1 is a ubiquitously expressed, well-conserved cytoplasmic phosphoprotein. Caprin-1 expression increases during cell cycle progression and decreases when proliferation ceases and cells differentiate (Grill et al. 2004; Gong et al. 2013). Caprin-1 was found to localise at mRNPs associated with polysomes and mRNAs (Angenstein et al. 2005). The ability of Caprin-1 to bind mRNA was proven to be dependent on its glycine-arginine-rich (RGG) motifs (Thandapani et al. 2013) and the propensity of these fragments to induce eIF2 α phosphorylation correlates with its capability to selectively bind mRNA (Solomon et al. 2007). Caprin-1 was also reported to be involved in proliferation and invasion of breast cancer cells (Gong et al. 2013). *Caprin-1*^{-/-} mice demonstrate reduction in the dendritic localisation of RNAs, as well as impairment of synapse formation, suggesting that Caprin-1 may be essential for the maintenance of the dendritic properties and for a correct dendritic localisation of RNAs (Shiina et al. 2010).

Caprin-1 was recently suggested to mediate SG assembly through interactions with GTPase-activating protein-binding protein 1 and 2 (G3BP) (Kedersha et al. 2016). In this interaction model it was suggested that, when G3BP is present in excess, either because of overexpression or because of an elevated number of stalled preinitiation complexes, stalled preinitiation complexes and G3BP oligomers may interact with SG components, such as Caprin-1 or TIA-1 to triage specific transcripts (Kedersha et al. 2016).

The first example of *ex-vivo* assembly of SGs in primary cells that have not been subjected to exogenous stress involved G3BP1. SG formation was detected in differentiating erythroid cells and it was proposed that SG-mediated reprogramming of globin metabolism may play a key role in globin production during erythroid differentiation (Ghisolfi et al. 2012). G3BP1 was found to regulate the expression of α -globin transcripts as well as the survival of differentiating erythroid progenitor cells. Knockdown of G3BP1 inhibited both spontaneous and arsenite-induced assembly of SGs in cultured primary human bone marrow CD34⁺ progenitor cells (Ghisolfi et al. 2012). Impairment of SGs formation upon G3BP knockdown did not

prevent erythroid differentiation despite α -globin downregulation but did, however, increase apoptotic cell death, thus contributing to the evidence that SGs promote cell survival (Ghisolfi et al. 2012).

TIA-1, Caprin-1, G3BP1 and other RNA-binding proteins generally contain two conserved domains, glycine rich domains and RNA recognition motifs. The glycine rich domain is hydrophobic and is responsible for the reversible aggregation of these proteins. The glycine domains in some RNA-binding proteins share homology with the yeast prion protein Sup35, such as the case of TIA-1 (Wolozin 2012). The RNA recognition motifs have large specificity and differ according to the transcripts that they can bind (Wolozin 2012).

Much of our understanding of the role and mechanisms involved in SG formation comes from experiments performed in cell lines or utilising *in-vitro* models (Kedersha et al. 2000; Zurla et al. 2011; Buchan & Parker 2009). To date, evidence of the role of SGs in regulating the *in-vivo* response to stress is limited. *In-vitro* experiments have used pharmacological and molecular manipulation to delineate the key players, but whilst these experiments have been essential to our understanding of SGs, it is likely that the response of cells to intrinsic stress has some significant differences to those *in-vitro*. In addition, despite the strong association of SGs with pro-survival functions, such as mentioned above, it is not clear to date what is the exact function of SGs. For instance, recent research has implicated SGs in neurodegeneration, as it will be discussed in section 1.13. Additional functional studies *in-vivo* are needed to address this question. Modulation of SG formation *in-vivo*, either by overexpression or inhibition of known SG components or chemical manipulation of SG formation is likely to provide additional information as to which mechanisms underlie regulation of SGs and what is their implication in cell survival decisions.

A summary with examples of SG components is shown in Table 1.2.

Table 1.2 – Examples of SG components.

Component	Function	Reference
40S ribosomal subunit	Translation	(Kedersha & Anderson 2002)
ADAR	RNA editing	(Weissbach & Scadden 2012)
AGO2	RNA silencing	(Leung et al. 2006)
APOBEC3G	Antiviral response	(Kozak et al. 2006; Gallois-Montbrun et al. 2007)
Ataxin-2	Translation	(Kaehler et al. 2012)
BRF1,2	mRNA decay and SG-processing bodies interaction	(Kedersha et al. 2005)
Caprin-1	Cell cycle	(Solomon et al. 2007)
CCAR-1	Apoptosis / microtubule formation	(Kolobova et al. 2009)
CPEB	mRNA repression	(Wilczynska et al. 2005)
DDX3	RNA helicase	(Chalupníková et al. 2008)
Dhh1	Translation repressor	(Parker & Sheth 2007)
DIS1	Unknown	(Ogawa et al. 2005)
eIF2 α	Translation initiation	(Kedersha & Anderson 2002)
eIF3	Translation initiation	(Kedersha et al. 2005)
eIF4A	Translation initiation	(Low et al. 2005)
eIF4B	Translation initiation	(Low et al. 2005)
eIF4E	Translation initiation	(Kedersha et al. 2005)
eIF4G	Translation initiation	(Kedersha et al. 2005)
FAST	Translation	(Kedersha et al. 2005)
FMRP	Translation	(Antar et al. 2005)
FBP	mRNA degradation	(Rothé et al. 2006)
FUS	Transcription control	(Lagier-Tourenne & Cleveland 2009)
FXR1	Translation	(Antar et al. 2005)
G3BP	Ras signalling	(Tourrière et al. 2003)
HDAC6	Transcriptional regulation	(Kwon et al. 2007)
hnRNP A1	mRNA metabolism	(Guil et al. 2006)
hnRNP A2	mRNA metabolism	(McDonald et al. 2011)
Huntingtin	unclear	(Ratovitski et al. 2012)
HuR	mRNA stabilization	(Papadopoulou et al. 2013)
KSRP	mRNA degradation	(Rothé et al. 2006)
Importin- α 1,4 and 5 Importin- β 1	Protein import	(Mahboubi et al. 2013)
IP5K	Signalling	(Brehm et al. 2007)
LINE1 (ORF1p)	Transposon	(Goodier et al. 2007)
Lin28	Development	(Balzer & Moss 2007)
MLN51	Splicing	(Baguet et al. 2007)
Ngr1	Translation repression	(Buchan 2008)
PABP-1	Translation	(Kedersha et al. 1999b)
RCK (p54)	Translation repressor	(Parker & Sheth 2007)
Plakophilin	Adhesion	(Hofmann et al. 2012)

Table 1.2 - continuation

PMR1	mRNA degradation	(Yang et al. 2006)
PolyA ⁺ mRNA	To be translated	(Kedersha et al. 1999b)
Prohibitin-2	Apoptosis	(Ohn et al. 2008)
PRTB	Translation	(Kim et al. 2008)
Pub1	Translation repression	(Buchan 2008)
Pumilio 2	mRNA silencing	(Vessey et al. 2006)
RACK1	Protein transport, stabilization, apoptosis	(Arimoto et al. 2008)
Rap 55	mRNA silencing	(Yang et al. 2006)
Rpb4	Transcription	(Lotan et al. 2005)
Scd6	mRNA silencing	(Yang et al. 2006)
SRC3	Transcription	(Anderson & Kedersha 2007)
Staufen	mRNA silencing	(Thomas et al. 2009)
SMN	RNP assembly	(Hua & Zhou 2004)
Tau	Stabilise microtubules	(Vanderweyde et al. 2012)
TDP-43	Transcription and splicing regulator	(McDonald et al. 2011)
TLS	Transcription control	(Lagier-Tourenne & Cleveland 2009)
TIA-1, TIAR	mRNA silencing	(Kedersha et al. 1999)
TRAF2	Signalling	(Kim et al. 2005)
TTP	mRNA silencing	(Stoecklin et al. 2004)
TUDOR-SN	RNA editing	(Weissbach & Scadden 2012)
USP10	Protein degradation	(Ohn et al. 2008)
Xrn1	Exonuclease	(Parker & Sheth 2007)
YB-1	Transcription factor	(Yang & Bloch 2007)
ZBP1	Localisation	(Stohr et al. 2006)

1.9. Regulation of translation during stress

The general shutting down of protein synthesis observed during stress conditions is initiated by the phosphorylation of the alpha sub-unit of the eukaryotic initiation factor 2 (eIF2 α), a crucial molecule of the eIF2 complex that enables the loading of the initiator tRNA (Met-tRNA_i^{Met}) onto the 40S ribosomal subunit (Hershey 1989). Phosphorylation of eIF2 α was first reported in rabbit reticulocyte lysates deprived of hemin (Farrell 1978). The absence of hemin results in the activation of the heme-regulated inhibitor (HRI), a highly specific eIF2 α kinase (Hershey 1991). The HRI kinase belongs to a family of serine/threonine kinases that function as “sensors” of environmental stress and act through phosphorylation of eIF2 α (Anderson & Kedersha 2002).

Five kinases have been identified that monitor environmental stress and directly modulate the translation machinery: protein kinase R (PKR), a double-stranded RNA-dependent protein kinase that is activated when the cells are exposed to viral infection, heat and UV radiation (Williams 2001); protein kinase RNA-like endoplasmic reticulum kinase (PERK) is a component of the endoplasmic reticulum that is activated when unfolded proteins accumulate in that structure (Williams 2001; Dever 2002; Anderson & Kedersha 2002); general control nonderepressible (GCN2) is a protein that controls amino acid levels and reacts to the amino acid absence (Kimball et al. 2003); HRI, as mentioned above, is activated in the absence of hemin and its function is related to the balanced synthesis of globin chains and heme during erythrocyte maturation (Han et al. 2001; Lu et al. 2001); Z-DNA kinase is an enzyme involved in the host antiviral response (Anderson & Kedersha 2008).

As a consequence of the phosphorylation mechanism of eIF2 α , the eIF2 ternary complex is transformed into a competitive inhibitor of eIF2B, a GTP/GDP exchange factor that converts the inactive ternary complex, GDP-associated, to active ternary complex, GTP-associated (Fig.1.5) (Hershey 1991). It was determined that, since eIF2B is present in cells at a low level, only about 30% of the phosphorylated eIF2 α is sufficient to inhibit all of the eIF2B (Duncan & Hershey 1987). As a result, the phosphorylation of eIF2 α inhibits protein translation by reducing the availability of eIF2-GTP-tRNA_i^{Met} ternary complex and, subsequently, leads to the accumulation of non-functional translation initiation complexes, which aggregate at SGs (Fig.1.5) (Hershey 1989; Thomas et al. 2011).

Several studies point the phosphorylation of eIF2 α as a key event for the assembly of SGs. A phosphomimetic eIF2 α mutant induced the assembly of SGs in the absence of any stressor agent, whereas a non-phosphorylatable eIF2 α mutant was found to prevent the assembly of SGs even in the presence of arsenite stress (Kedersha et al. 1999). Other studies corroborated these results finding that wild-type murine embryonic fibroblasts (MEF) assembled SGs in response to arsenite, heat shock or energy deprivation, whereas eIF2 α ^{-/-} MEFs incubated in the same conditions failed to assemble SGs (McEwen et al. 2005). Although phosphorylation of eIF2 α has been pointed out as a crucial step for SG formation, it was found that energy depletion can induce SGs without increasing eIF2 α phosphorylation (Kedersha et al. 2002).

Figure 1.5 - Schematics representing translation initiation in the absence or presence of stress. During physiological conditions in the absence of stress, eIF2B charges eIF2-GTP-tRNA^{Met} ternary complex by exchanging GDP for GTP. In the presence of eIF2-GTP-tRNA^{Met} ternary complex, 48S preinitiation complexes assemble at the 5'-cap of mRNA transcripts for scanning. When the anticodon of tRNA^{Met} recognises the initiation codon AUG, early initiation factors displace from the 60S ribosomal subunit and, as additional ribosomes join the transcripts, mRNA is converted into a polysome and translation takes place. In the presence of stress, phosphorylation of eIF2 α converts eIF2 into a competitive antagonist of eIF2B, depleting the formation of eIF2-GTP-tRNA^{Met} ternary complexes. SG proteins, such as TIA-1, join the deficient 48S complex and promote the translational silence of mRNA transcripts. Aggregation of additional RNA-binding proteins with stalled 48S preinitiation complexes forms SGs. Figure reproduced from (Anderson & Kedersha 2002).

Energy starvation and reduced ATP/GTP levels were shown to influence the regular translation mechanisms (in addition to ternary complex formation) such as amino acyl-tRNA charging, eIF4A, eIF1A, and the translation termination events. Nevertheless, the strong link between SGs assembly and phosphorylation of eIF2 α suggests that reduced levels of GTP could result in reduced levels of the eIF2-GTP-tRNA^{iMet} ternary complex and, the absence of ternary complex might trigger SG formation, rather than increased phospho-eIF2 α by itself (Kedersha & Anderson 2002; Kedersha et al. 2002).

As mentioned before, a number of kinases monitor environmental stress and affect the eIF2 α phosphorylation, thus modulating stress-induced changes in mRNA translation (Anderson & Kedersha 2008). These kinases generally respond to type I stresses, such as heat shock, cold shock, arsenite and hypoxia (Arimoto et al. 2008). Type I stressor agents induce post-transcriptional changes of gene expression and normally suppress apoptosis through the formation of SGs (when the stress is applied at a sub-lethal dose) (Arimoto et al. 2008). Type II stressor agents, such as X-rays, hydrogen peroxide and genotoxic drugs, directly induce apoptosis via p38 and JNK MAPK pathways without triggering SG formation (Arimoto et al. 2008).

Heat shock and sodium arsenite are examples of type I stresses. Heat shock consists in exposing cells or organisms to higher temperatures than their normal physiological temperature, affecting the cellular organisation at different levels: fragmentation of Golgi apparatus and endoplasmic reticulum, disruption of cytoskeleton, misfolding / aggregation of proteins and reduction in the number of mitochondria, amongst others (Vogel et al. 1995; Latchman 2004; Richter et al. 2010). Sodium arsenite, another example of a type I stress, is a potent oxidative stressor responsible for cardiovascular and neurological diseases that can be inhaled or absorbed through skin contact (Snow 1992; Abernathy et al. 1999). Sodium arsenite effects include inhibition of cell cycle progression, chromosomes modifications, loss of actin filaments and microtubules and increased glutathione levels (Li & Chou 1992; Jha et al. 1992).

Whereas heat shock has been shown to mainly activate PERK (Fig.1.6) (Xu et al. 2011), sodium arsenite specifically activates HRI kinase (Fig.1.7) (Lu et al. 2001; McEwen et al. 2005).

Activation of PERK or HRI leads ultimately to phosphorylation of eIF2 α , thus reducing the availability of eIF2-GTP-tRNA^{iMet} ternary complex and, subsequently,

leading to the accumulation of non-functional translation initiation complexes, which aggregate at SGs (Figs.1.6 and 1.7) (Hershey 1989; Thomas et al. 2011).

Heat shock also activates protein kinase A (PKA) and phosphatidylinositol-3 kinase / protein kinase B (PI-3K/AKT) pathways (Fig.1.6) (Choi et al. 1991; Cross et al. 1995; Pap & Cooper 1998; Hers et al. 2011; Moore et al. 2013). Downstream targets of PI-3K pathway include the activation of Akt, when PI-3K is activated, and consequent inhibition of glycogen synthase kinase 3 (GSK3), thus de-repressing HSF1 (Cross et al. 1995; Pap & Cooper 1998; Wang et al. 2003; Wang et al. 2004; Hers et al. 2011; Chou et al. 2012; Moore et al. 2013). Activation of PKA also contributes to inhibit GSK3 (Fang et al. 2000).

Heat shock and sodium arsenite also activate p38-MAP and c-Jun pathways (Figs.1.6 and 1.7) (Waskiewicz & Cooper 1995; Yaglom et al. 1999). These have been implicated in anti-inflammatory responses, as well as pro-apoptotic events (Coulthard et al. 2009; Bogoyevitch et al. 2010). The pro-survival JAK-STAT pathway, responsible for cellular proliferation, differentiation, immune response and pro-apoptotic events has also been shown to be specifically inhibited under sodium arsenite stress (Fig.1.7) (Huang et al. 2007; Ivanov et al. 2013).

The schematics below show the cellular kinases activated upon heat shock and sodium arsenite stresses and the downstream cellular events triggered by these stresses.

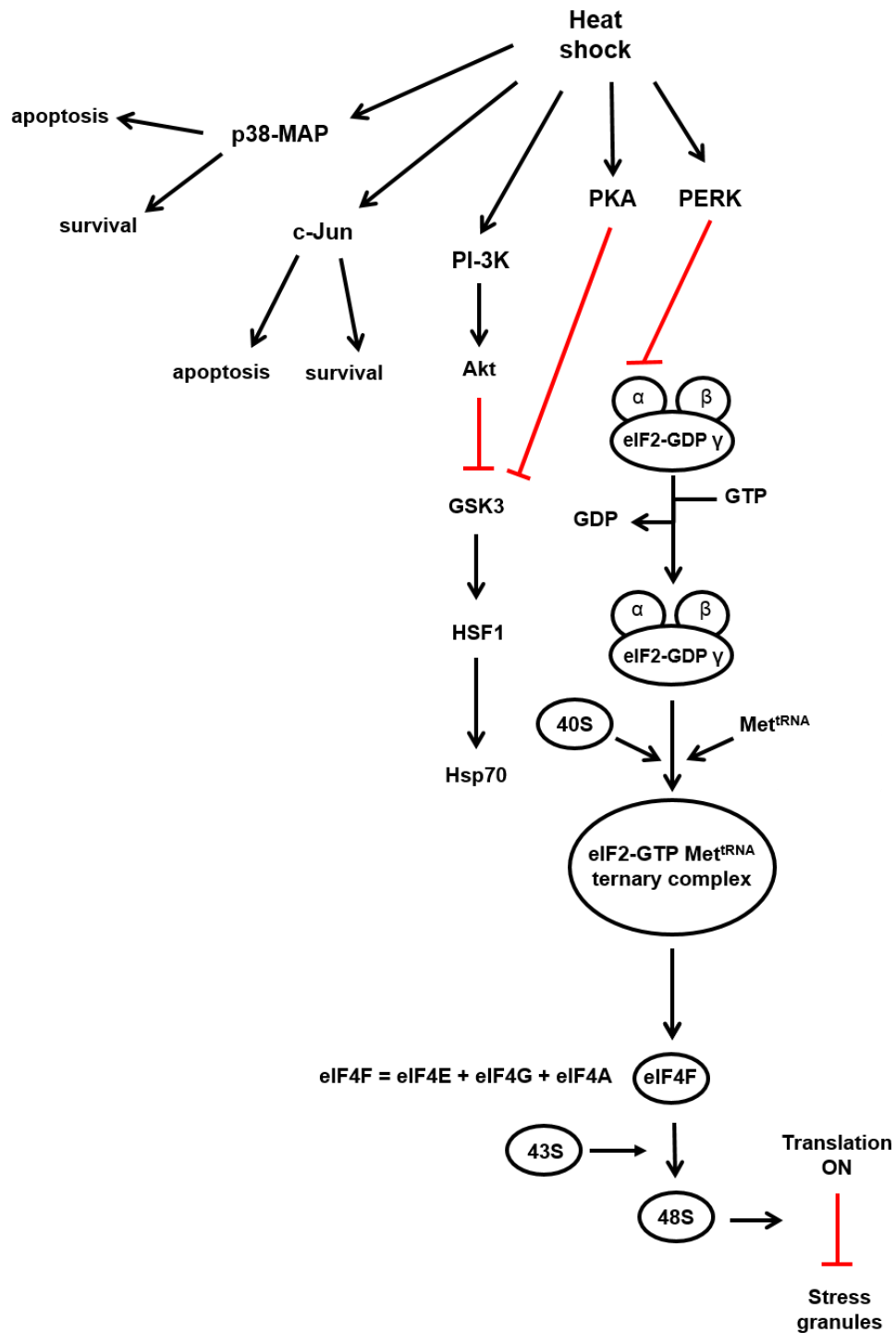


Figure 1.6 – Downstream effects of heat shock in cell signalling pathways. Stress-sensor kinase PERK is activated under heat shock conditions, leading to direct phosphorylation of eIF2 α . Phosphorylation of eIF2 α triggers a series of downstream events that include reduction on the availability of eIF2-GTP-tRNA^{Met} ternary complex, resulting ultimately on SG formation. PKA activation directly inhibits GSK3, de-repressing HSF1 and promoting Hsp70 expression. Heat shock also activates PI-3K kinase, which also contributes to repression of GSK, through Akt activation. The p38-MAP and c-Jun kinases involved in cell survival decisions are also activated upon heat shock exposure. Black arrows represent activation pathways and red symbols inhibition pathways.

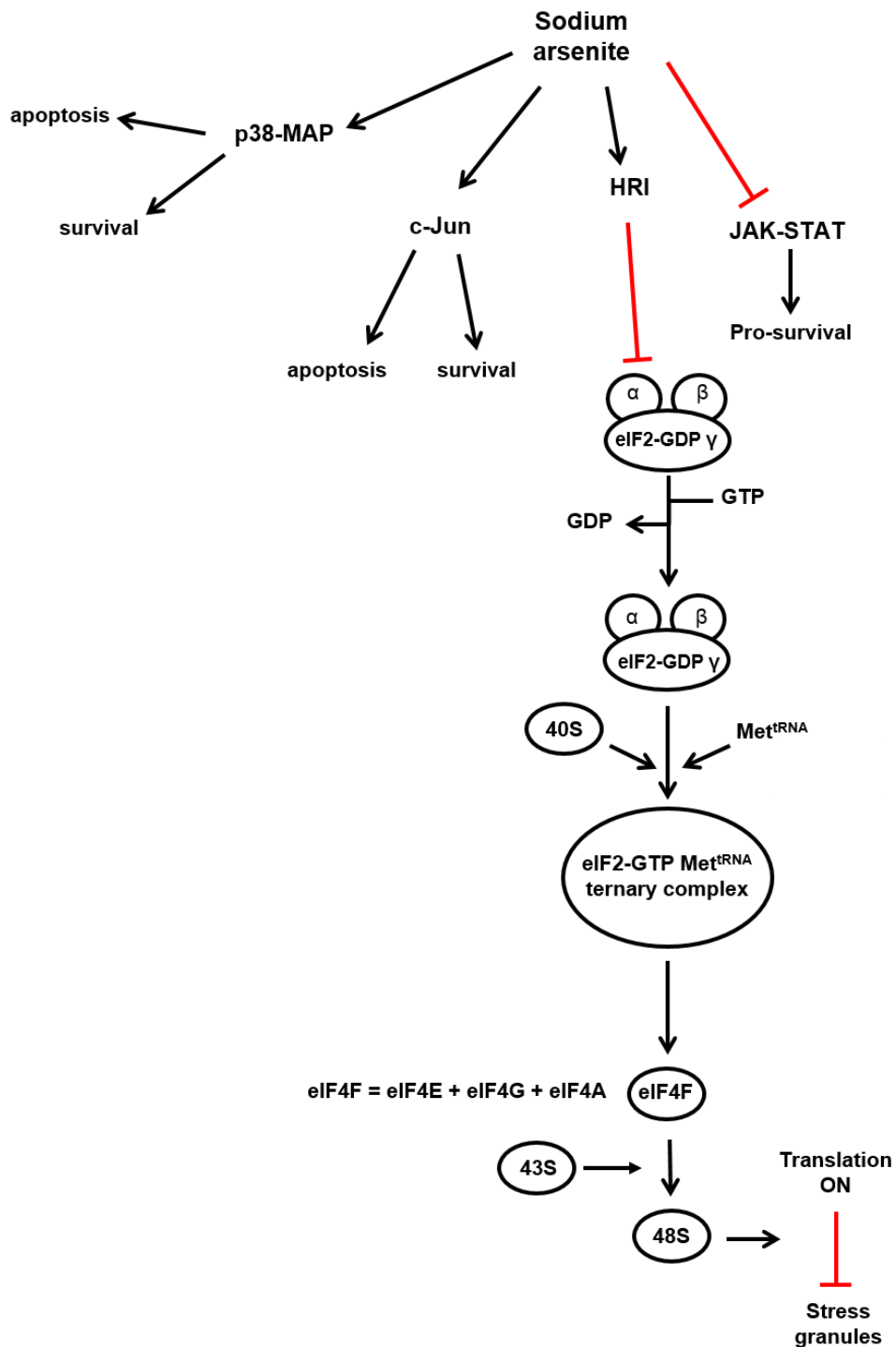


Figure 1.7 – Downstream effects of sodium arsenite in cell signalling pathways. Stress-sensor kinase HRI is activated under arsenite conditions, leading to direct phosphorylation of eIF2 α . Phosphorylation of eIF2 α triggers a series of downstream events that include reduction on the availability of eIF2-GTP-tRNA^{Met} ternary complex, resulting ultimately on SG formation. Arsenite inhibits PI-3K activation, thus contributing to Akt activation. The p38-MAP and c-Jun kinases involved in cell survival decisions are also activated upon arsenite exposure. The pro-survival JAK-STAT signalling pathway is inhibited following arsenite stress. Black arrows represent activation pathways and red symbols inhibition pathways.

1.10. Dynamics of stress granule formation

For SGs to assemble some conditions are required such as stalled ribosomes, polysome disassembly and mRNP aggregation, in a series of reversible steps.

The first stage of SG assembly is generally initiated by phosphorylation or drug inactivation of eIF2 α , resulting in the abortion of translation initiation complexes, with the affected transcripts being converted into 48S mRNPs as translation initiation is interrupted and ribosomes “run off” (Kedersha et al. 1999).

Stage two is characterised by the presence of 48S free mRNPs which are essential substrates for SG assembly. In this step, the accumulation of RNA-binding proteins accompanies the increase of inter-molecular interactions with RNA molecules (Fujimura et al. 2009). TIA-1, TIAR, TTP, BRF1, FMRP, FXR1, CPEB, G3BP and SMN proteins are examples of SG constituents that generally aggregate at this stage (Anderson & Kedersha 2008).

Stage three of SG assembly is designated secondary aggregation and involves the binding of mRNA transcripts to multiple proteins that develop homotypic and heterotypic interactions, thus promoting secondary aggregation of mRNPs and generating SGs visible by light microscopy (Kedersha et al. 2000).

The fourth stage of SG assembly comprises the recruitment of proteins that although they lack interaction with mRNAs, are integrated at SGs through protein-protein interactions. These are thought to be implicated in the regulation of other aspects of cellular metabolism, such as signalling pathways (Anderson & Kedersha 2008). A recent study suggested that SGs may contain cores surrounded by a dynamic “shell” (Jain et al. 2016). The central cores are likely to be relatively stable and are mainly formed by polyA⁺ mRNA, G3BP1 and PABP1 proteins (Jain et al. 2016; Wheeler 2016). The “shell” was hypothesised to be a dynamic structure that contributes to the formation of the core and promotes weak protein-protein interactions (Jain et al. 2016; Wheeler 2016).

The fifth step consists of the sorting of specific mRNA molecules, a process that has been called “molecular triage”. Here, mRNAs are triaged by RNA-binding proteins according to their function and their fate is determined through interactions with polysomes (promoting translation during stress), processing bodies (resulting in RNA decay) or storage in SGs to re-enter translation at later stages (Kedersha et al. 2000; Anderson & Kedersha 2002; Anderson & Kedersha 2006).

Once the stress is over, SGs start to disassemble (Anderson & Kedersha 2008). A recent study suggested that disassembly of SGs occurs in a series of steps in which RNAs are actively excluded from SGs, leading to structural instability. Larger SGs seem to break into smaller core structures that are then disassembled with the advanced recovery (Wheeler 2016).

A number of studies have associated both autophagy and the participation of chaperones with the disassembly/clearance of SGs. In yeast, both SGs and processing bodies were shown to be targeted to the vacuole by autophagy (Buchan et al. 2013). The ubiquitin-selective chaperone valosin-containing protein (VCP) was identified as a key player during SG disassembly (Buchan et al. 2013). Mutations in VCP have been associated with neurodegenerative diseases such as ALS and frontotemporal lobar degeneration (FTLD), which are also characterised by pathological accumulation of SG-marker proteins (Buchan et al. 2013). In HeLa cells, depletion of VCP results in the accumulation of defective ribosomal products in the proximity of SGs, which may contribute to the persistency of SGs (Seguin et al. 2014).

Mutations disrupting autophagy lead to the accumulation of SGs in yeast, thus contributing to the evidence that autophagy participates in the disassembly of SGs (Buchan et al. 2013).

The chaperone protein Hsp70 (section 1.5) has also been shown to play a role in SG clearance (Walters et al. 2015). Yeast strains defective in Hsp70 showed impaired SG disassembly (Walters et al. 2015). In addition, yeast strains lacking Hsp40 also showed defects in SGs disassembly during recovery. These observations suggest that both Hsp40 and Hsp70 may work together to alter the conformation and/or interactions of specific SG proteins and, therefore, influence their disassembly (Walters et al. 2015). Moreover, yeast strains defective in Hsp40 were not able to restore translation during stress recovery (Walters et al. 2015). The authors hypothesise that Hsp40 can restore translation either by participating in the disassembly of mRNPs that are stored at SGs, and/or restoring the correct function of a defective translation initiation factor during recovery, ultimately leading to the clearance of SGs (Walters et al. 2015).

In a separate study, Hsp70 complexed with BAG3 and Hspb8, was shown to participate in SG disassembly in HeLa cells (Ganassi et al. 2016). BAG3, a nucleotide-exchange factor and Hspb8, a small heat shock protein, were found to associate with Hsp70 in the degradation of ubiquitinated and misfolded proteins

(Ganassi et al. 2016). When the chaperone function of this Hspb8-BAG3-Hsp70 complex is impaired, defective ribosomal products accumulate in SGs. Additionally, this complex was shown to participate in the disassembly of the majority of SGs in HeLa cells following stress (Ganassi et al. 2016).

In HeLa cells, inhibition of autophagy and lysosome function impaired the dynamics of SG formation and disassembly, suggesting that these are critical for a correct SG growth and clearance (Seguin et al. 2014). However, in another study, the majority of SGs in HeLa cells were found to disassemble in a chaperone-mediated way, whereas only a minor fraction of SGs were cleared by autophagy (Ganassi et al. 2016).

While contrasting data point to different key players in SG disassembly, it is not clear yet which mechanisms regulate the clearance of SGs when stress is over. This question is particularly important when considering the implication of persistent SGs in neurodegenerative diseases (as it will be discussed in section 1.13). A better understanding of which mechanisms underlie disassembly of SGs may provide key evidence as to which pathways are prone to dysregulation in neurodegenerative diseases and, consequently, may identify novel therapeutic targets.

1.11. Stress granules and other RNA granules

Over 100 genes have been identified involving modulation of SGs and/or processing bodies in yeast, exposing a previously unknown dense network of physical and genetic interactions controlling mRNP granule dynamics (Buchan et al. 2013).

Processing bodies are cytoplasmic RNA granules containing components of the mRNA decay machinery, the nonsense-mediated decay pathway and the RNA-induced silencing complex (Anderson & Kedersha 2006; Parker & Sheth 2007). Although processing bodies contain exclusive components not shared with SGs such as DCP1a/2 and GW182, they can also share many proteins with SGs, such as FAST, XRN1, eIF4E, TTP, BRF1 and BRF2 (Kedersha et al. 2005). Unlike SGs, processing bodies are present during physiological conditions (i.e. in unstressed cells) and do not require the presence of a stressor agent or eIF2 α phosphorylation to assemble. While SGs contain translation initiation factors from stalled 48S pre-initiation complexes, such as eIF3, eIF4A, eIF4G, processing bodies

are defined by components of the mRNA decay machinery, such as DCP1a/2 (Kedersha et al. 2005; Kedersha & Anderson 2007).

RAP55, Ge-1 and GW182 are processing bodies components that are essential for their integrity, since depletion of these factors leads to the loss of processing bodies (Eulalio 2007). Since Ge-1 or GW182 orthologues were not found in the *Saccharomyces cerevisiae* yeast, it was suggested that processing bodies may present increased complexity in higher eukaryotes, as regards their composition and function (Eulalio 2007). It is suggested that, during the evolutionary process, processing bodies might have acquired additional components in multicellular organisms, such as components for RNA-silencing that are not found in *Saccharomyces cerevisiae*, and that the constitutive and stress functions of processing bodies might have segregated into distinct structures, such as SGs (Eulalio 2007).

SG assembly is thought to be dependent of processing body formation, whereas processing bodies can form independently of SGs (Buchan 2008). The formation of both SGs and processing bodies is based on two principles: they require non-translated RNA for their assembly and individual mRNPs brought together by dimerization or aggregation (Buchan et al. 2013). Moreover, it was suggested that the formation of a processing bodies-mRNP aggregate may be the key first step in deciding the fate of mRNAs after exit from polysomes during stress conditions (Buchan 2008).

One hypothesis to explain the role of processing bodies in promoting SGs formation is that mRNAs exiting translation first interact with processing bodies and then, subsequently, transit to SGs before re-entering translation (Buchan 2008). This hypothesis may explain why SGs form in proximity to processing bodies and why processing bodies would enhance the formation of SGs (Buchan 2008). In support of this, some studies demonstrate that SGs can interact with processing bodies and are likely to exchange mRNPs between them (Kedersha et al. 2005; Anderson & Kedersha 2006; Hoyle et al. 2007; Buchan 2008).

A working model illustrated in Figure 1.8 was proposed for the movements of cytoplasmic mRNAs between the nucleus, polysomes, processing bodies and SGs (Parker & Sheth 2007). In this model, mRNAs present in polysomes can undergo repeated rounds of translation initiation, elongation and termination to produce polypeptides (Fig.1.8). In order to answer to possible defects in translation initiation/termination, or through specific recruitment, mRNAs found in polysomes do

interact with components of the general repression/decay machinery and cease translation, thereby forming an mRNP that can assemble into processing bodies (Parker & Sheth 2007). The mRNAs associated with the repression/decay complex can be decapped and degraded, remain in the processing bodies state for mRNA storage, or exit the processing bodies for re-entry into translation (Fig.1.8). During the translational silencing period, some mRNAs may associate with factors promoting their accumulation in SGs, potentially enhancing their re-entry into translation (Parker & Sheth 2007).

Figure 1.8 - Model for the cycling of mRNA between different cellular compartments.
Reproduced from (Parker & Sheth 2007).

1.12. Stress granules and viral infection

Viral infection is dependent on the host translational machinery (Legros et al. 2011; Katoh et al. 2013). Part of the cellular response to viral infection comprises the activation of the stress-sensor kinase PKR, thus triggering phosphorylation of eIF2 α and, consequently, SG formation (Miller 2011). Since stress-induced translational arrest plays an important role in host antiviral defence, it is not surprising that many viruses have developed strategies to interfere with host SG machinery.

The Japanese Encephalitis Virus (JEV) core protein was found to inhibit SG formation in Huh7 cells, by recruiting several SG associated proteins, including G3BP and USP10, through interaction with Caprin-1 (Katoh et al. 2013). Moreover, a mutant JEV carrying a core protein unable of binding to Caprin-1 displayed reduced propagation *in-vitro* and lower pathogenicity in mice than the wild-type JEV, suggesting that inhibition of SGs formation by the core protein is critical to antagonize host defence (Katoh et al. 2013).

Human T cell leukaemia virus type-1 (HTLV-1) is the causative agent of a rapidly fatal leukaemia and of a neurological degenerative disease (Proietti et al. 2005). Amongst the several regulatory proteins encoded by this virus, the Tax oncoprotein has been characterised as crucial in viral transcription, persistence and pathogenesis (Legros et al. 2011). It was demonstrated in HeLa cells that, in response to various stress stimuli, Tax travels from the nucleus to the cytoplasm and impairs SG assembly, through direct interaction with HDAC6, an essential component of SGs that regulates its formation and contributes to the control of RNA metabolism and translation (Kwon et al. 2007; Legros et al. 2011). It was then proposed that inhibition of both SG formation and correct cellular stress response by Tax may be pivotal to HTLV-1 leukaemogenesis (Legros et al. 2011).

A study investigating SG dynamics upon human immunodeficiency virus type-1 (HIV-1) infection revealed that this virus can specifically disrupt SG assembly, by inhibiting incorporation of cytoplasmic HuR, hnRNPA1, hnRNPA2 and TIAR to SGs (Valiente-Echeverría et al. 2014). Using HEK293T cells, the Gag viral protein was found to block not only SG assembly, even in the presence of overexpressed G3BP1 and TIAR, but also to dismantle already formed G3BP-positive SGs (Valiente-Echeverría et al. 2014). A working model was proposed in which the interaction between Gag and the eEF2 actively blocks SG assembly in the early stages and, later on, another interaction involving Gag and G3BP1 dismantles already formed SGs. This process should confer advantage to the virus replication,

since the viral mRNA translation continues to occur without any damage (Valiente-Echeverría et al. 2014).

Recently, it has been shown that Ebola virus sequesters SG components into the viral inclusions, thus blocking SG formation (Nelson et al. 2016). Although Ebola actively sequesters SG proteins within its viral inclusions, SG assembly does not occur within the inclusions (Nelson et al. 2016). VP35, a viral protein responsible for evasion strategies, was hypothesised to be involved in the inhibition of SG formation within the viral inclusions. This inhibition of SG assembly occurs as a consequence of VP35 blockage of PKR activation and disruption of eIF2 α phosphorylation (Nelson et al. 2016).

Although the examples described above are related to the inhibition of SGs during viral infection, the opposite situation, i.e., SG formation induced by viral infection, has also been observed. A study involving Reovirus revealed that P58^{1PK}, an inhibitor of the eIF2 α kinases PKR and PERK, was down-regulated in DU145 cells infected with Reovirus (Smith et al. 2006). Although eIF2 α phosphorylation is a cellular response that typically restricts viral growth, it was found that Reovirus replication is more efficient in the presence of eIF2 α kinases and when eIF2 α is phosphorylated at serine 51. Knowing that eIF2 α phosphorylation promotes the translation of activating transcription factor 4 (ATF4), a transcription factor that regulates cellular recovery from stress, Reovirus replication was tested in cells depleted for ATF4 (Smith et al. 2006). It was reported that the viral replication was compromised, suggesting that one or more ATF4 target gene products facilitate Reovirus infection (Smith et al. 2006). Based on these results, it was hypothesised that eIF2 α phosphorylation and, consequently, SG formation, might facilitate Reovirus replication in two ways — first, by inducing an ATF4-dependent gene expression program, and second, by creating an environment that places abundant Reovirus transcripts at a competitive advantage for limited components of the translational machinery (Smith et al. 2006).

Despite being a relatively young field, interesting viral strategies have already been reported in the modulation of SG formation during infection. Given the implication of SGs in cell survival, a better understanding of how virus modulate SG formation or how SGs can control viral infection, either through promotion or inhibition, may help in the development of therapies to control infections.

1.13. Stress granules in neurodegenerative diseases

Since its discovery, SGs have been widely associated with cytoprotective functions during transient stress. As described before, numerous reports have suggested that SGs function as temporary structures formed during cellular stress that contain regulated aggregation of RNA-binding proteins, translation initiation factors, ribosomal subunits and pro-apoptotic molecules, amongst others (Kedersha et al. 1999; Kedersha et al. 2002; Tourrière et al. 2003; Kim et al. 2005; Ohn et al. 2008; Papadopoulou et al. 2013). Evidence suggests that the main function of SGs is to provide a rapid, stress-specific sorting of RNA molecules to be translated during transient cellular stress. Dynamic association of SGs with other cellular RNA structures, such as processing bodies and polysomes, has supported this hypothesis (Kedersha et al. 2000; Kedersha & Anderson 2002; Anderson & Kedersha 2006). Despite some of the key constituents of SGs are RNA-binding proteins with prion-like domains in their structure, regular function of SGs dictates that they rapidly disassemble once the stress is removed (Kedersha et al. 1999). However, since RNA-binding proteins are associated with cell growth, proliferation and may regulate many age-related processes, dysfunction of these proteins is likely to trigger the loss of physiologic function and the onset of diseases associated with advancing age (Vanderweyde et al. 2013).

The discovery of mutations in RNA-binding proteins linked to persistent inclusions in neurodegenerative diseases has partially changed the notion of SGs as protective structures (Aulas et al. 2012; Aulas et al. 2015). In fact, persistent, irreversible protein aggregation has been linked to different neurodegenerative diseases, such as Alzheimer's, Huntington's, and ALS (Aulas et al. 2012; Ratovitski et al. 2012; Vanderweyde et al. 2012; Bentmann 2013; Ash et al. 2014).

A recent "liquid-liquid phase separation" model suggests that RNA granules, including SGs, comprise immiscible liquid droplets, held apart from the cytosol by transitory multiple low-affinity interactions between low complexed / intrinsically disordered proteins and RNA (Kedersha et al. 2016). Whereas in most of the cases RNA granules exhibit a dynamic behaviour compatible with this model, others may display anomalous transition to more static and solid-like state, such as observed in pathological aggregates characteristic of neurodegenerative diseases (Kedersha et al. 2016).

A number of SG-proteins have been reported to aggregate within pathological inclusions observed during neurodegeneration. Although it is not clear to date which

factors contribute to the dysregulation of SG compounds, one hypothesis for protein aggregation during neurodegeneration has been proposed (Jarrett & Lansbury 1993; Dobson 2003; Wolozin 2012). Proteins are suggested to be present in a cell as monomers and, some of these, through still unknown means, misfold randomly. The misfolded proteins would then undergo oligomerisation and aggregation to form fibrils. The authors propose that any of these events occurs with a specific biological function and the rate of aggregation and fibril formation is likely to be dependent on the amount of monomeric proteins present at early stages (Wolozin 2012; Jarrett & Lansbury 1993; Dobson 2003).

As mentioned before, many of the RNA-binding proteins found to aggregate at SGs have been associated with pathological conditions. For instance, TIA-1, TTP and G3BP1 were found to colocalise with TDP-43 in ALS; TIA-1 was found to be present at tau aggregates in Alzheimer's disease and Caprin-1 and G3BP1 were found to associate with pathological lesions in Huntington's disease (Ratovitski et al. 2012; Vanderweyde et al. 2012; Ash et al. 2014).

ALS pathogenesis can be caused by mutations in different genes, in which are included the *FUS* gene, encoding FUS protein and *TARDBP* gene, encoding for TDP-43, a known SG-associated protein that contributes to SGs formation and maintenance (McDonald et al. 2011; Aulas et al. 2012). Reduction in the functional levels of TDP-43 has been linked to dysregulation of SG dynamics, leading to a continued translation inhibition and, consequently, increased cellular vulnerability (Aulas et al. 2012). TIA-1 positive structures were found to colocalise with TDP-43 in motor neurons from a sporadic case of ALS (Volkening et al. 2009). On the other hand, observation of control neurons showed very few TIA-1 structures and did not reveal any colocalisation of these with TDP-43 (Volkening et al. 2009). Furthermore, it has been shown in *Drosophila* brain that TDP-43-associated neurodegeneration induces chronic eIF2 α phosphorylation, a crucial mechanism for SG formation (Kim et al. 2014). Analysis of sections of *post-mortem* human brain and spinal cord tissue from an ALS case also revealed the presence of FUS inclusions positive for the SG-associated proteins PABP-1 and eIF4G, suggesting that SGs are part of the characteristic inclusion bodies formed during ALS pathogenesis (Dormann et al. 2010).

In Huntington's disease, SG-markers such as TIA-1, Caprin-1 and G3BP have been observed in aggregates of the mutated huntingtin protein (Ratovitski et al. 2012). Huntingtin protein was shown to play an important role in the regulation and translation of RNA molecules during environmental stress and the presence of the

mutated huntingtin, through interaction with Caprin-1 and G3BP, was suggested to affect the correct response under stress conditions (Ratovitski et al. 2012).

A role for SGs in tauopathies has also been hypothesised since it was found that colocalisation of tau protein with TIA-1-positive SGs is dependent on the disease severity, as colocalisation increases with both the SG size and disease progression (Vanderweyde et al. 2012). Moreover, analysis of *post-mortem* human brain tissue of individuals suffering from Alzheimer's disease revealed the same pattern affecting the human brain, with larger tau inclusions being more likely to colocalise with SG markers than smaller tau aggregates. SGs were also found during the analysis of older control brain tissue, but their size was smaller when compared to the Alzheimer's disease features and their presence was not associated with tau (Vanderweyde et al. 2012). SG formation was reported to stimulate the formation of tau inclusions and, intriguingly, tau was suggested to stimulate SG formation (Vanderweyde et al. 2012).

It has been proposed that the transient SG formation normally observed during stress is needed for an appropriate cellular response, whereas the hyperactive response to the presence of chronic stress during neurodegenerative diseases results in formation of persistent and deleterious SGs (Ash et al. 2014). It is suggested that these deleterious SGs might sequester non-essential mRNA molecules that are not necessary in a short term, but are required for the normal neuronal function in a longer term (Ash et al. 2014). The aggregation of determined proteins at SGs seems to trigger the development of some pathological conditions and the specific nature of chronic diseases seems to prevent SGs disassembly which directly relates with the disease's progression (Ash et al. 2014).

Defects identified in mRNA translation pathways and protein synthesis were proved to be implicated in the pathogenesis of metabolic disorders such as type 2 diabetes. Wolcott-Rallison syndrome, a monogenic form of diabetes, is caused by mutations in PERK, one of the key regulators of eIF2 α phosphorylation and consequently, SG formation (Delépine et al. 2000; Adeli 2011). Similarly to this, some RNA-binding proteins have been shown to play a crucial role in cancer, since mRNA regulation constitutes an effective and rapid mechanism to alter gene expression (Wurth 2012). For example, eIF4E, a component of SGs, were found to be overexpressed in multiple cancer types, including prostate and breast cancer (Coleman et al. 2009; Graff et al. 2009; Hsieh & Ruggero 2010). Increased expression of eIF4E was associated with increasing grade of disease and also poor prognosis in both types of cancer (Coleman et al. 2009; Graff et al. 2009). HuR is an RNA-binding protein

known to be involved with the mRNA nuclear export and stability, previously found to aggregate at SGs (Papadopoulou et al. 2013). The cytoplasmic expression of this protein was associated with a poor patient outcome in lung cancer and also with severe pathological features (Wang et al. 2011). In a mouse model of Creutzfeldt Jacob disease, reduction of eIF2 α phosphorylation promoted protein synthesis, thus inhibiting SG formation and reducing the prion-induced neurodegeneration (Moreno et al. 2012). On the contrary, increased levels of eIF2 α phosphorylation were associated with prion-related neurodegeneration (Moreno et al. 2012).

While the association with dysregulation of SG dynamics and neurodegeneration becomes more apparent, some questions remain to be investigated. For instance, it is not clear yet which mechanisms trigger the transition from temporary to persistent structures. In addition, it is not clear exactly how translation repression, likely to be associated with SG formation, affects and contributes to the pathophysiology of neurodegeneration. Future research involving modulation of key players, such as SG proteins and eIF2 α phosphorylation in *in-vivo* mouse models of neurodegenerative pathologies may help not only to understand exactly how dysfunction of these structures affects neurodegeneration but also to develop novel strategies for pharmacotherapy of neurodegenerative diseases.

1.14. Pharmacological manipulation of stress granules

As previously mentioned, SG formation is directly associated with inhibition of protein synthesis, generally initiated by phosphorylation of eIF2 α (Kedersha et al. 1999). Five different kinases (PERK, HRI, GCN2, PKR and Z-DNA) serve as sensors of stress and, through the activation of stress signalling cascades, control the levels of eIF2 α phosphorylation (Anderson & Kedersha 2002).

The discovery of eIF2 α phosphorylation and inhibition of protein translation as key mechanisms to trigger SG assembly lead to the hypothesis that SG formation could be modulated through chemical manipulation of that pathway. In fact, a number of compounds that interfere with protein translation have been shown to regulate SG formation. Cycloheximide or emetine are examples of drugs that inhibit protein synthesis, thus promoting the assembly of SGs (Kedersha et al. 2000; Kramer et al. 2008). Salubrinal, an activator of PERK, promotes inhibition of eIF2 α dephosphorylation, contributing to the reduction of protein translation and,

consequently, to promote SG formation (Long et al. 2005; Schewe & Aguirre-Ghiso 2009; Gao et al. 2013). On the other hand, GSK2606414, an inhibitor of PERK, decreases SG assembly during stress conditions, by reducing eIF2 α phosphorylation (Kim et al. 2014).

In spite of the clear association between eIF2 α phosphorylation and SG formation, other chemical compounds have been reported to induce SG formation independently of eIF2 α phosphorylation. Puromycin, for instance, promotes SG assembly through destabilisation of polysomes (Kedersha et al. 2000; Kramer et al. 2008; Unsworth et al. 2010). Pateamine A and hippuristanol target eIF4A at the translation initiation step, thus preventing the formation of 48S preinitiation complexes and inhibiting protein translation (Bordeleau et al. 2005; Dang et al. 2006). In this case, stalled 48S preinitiation complexes provide the mRNA substrate from which SGs are formed (Kedersha & Anderson 2007).

Three chemical compounds have been chosen to manipulate SG formation during the work presented in this thesis (presented in Chapters 3 and 4): pp242, integrated stress response inhibitor (ISRIB) and hydroxamate (-)-9.

The mTORC pathway regulates cell metabolism, growth, proliferation and survival (Laplane & Sabatini 2009). This pathway is activated during different cellular events, such as tumour formation, angiogenesis, adipogenesis and T-lymphocyte activation. Dysregulation of mTORC pathway has been observed in cancer and type 2 diabetes, for instance (Laplane & Sabatini 2009). pp242 (Fig.1.9) is a pyrazolopyrimidine that specifically inhibits members of the PI-3K family, including mTORC 1 and 2 (Apsel et al. 2008; Feldman et al. 2009). *In-vitro* effects of pp242 include growth suppression of leukaemia, myeloma, gastric and bladder cancer cell lines (Hoang et al. 2012; Ono et al. 2013; Xing et al. 2014; Zhang et al. 2016). Inhibition of mTORC pathway by pp242 has also been associated with lysosomal activation in autophagy and mitophagy in transformed cells (Zhou et al. 2013; Gordeev et al. 2015).

The mTORC pathway is involved in SG formation through eIF4E binding protein 1 (4E-BP1) phosphorylation (Fournier et al. 2013). 4E-BP1 is a repressor of mRNA translation and, when phosphorylated by hormones or growth factors, is inactivated, thus promoting protein synthesis (Gingras et al. 1999). When the mTORC pathway is disrupted, the specific binding of hypophosphorylated 4E-BP1 to eIF4E inhibits its association with eIF4G1, impairing the formation of mTORC-dependent translation initiation complexes. mTORC1 inactivation by pp242 specifically inhibits SG

formation through favouring the interaction of eIF4E with its hypophosphorylated 4E-BP1 inhibitory factor (Fournier et al. 2013). Targeting mTORC-induced eIF4E-eIF4G1 association by the pp242-mediated hypophosphorylation of 4E-BP1 was shown to disrupt SG formation in HeLa cells (Fournier et al. 2013). Consequently, pp242 was used in this work to inhibit SG formation.

Figure 1.9 – Chemical structure of pp242. Adapted from (Apsel et al. 2008).

Hydroxamate (-)-9 (a kind gift of Dr Jerry Pelletier, McGill University, Quebec) is a chemical analogue of silvestrol, a rocaglate derivative from the tree *Aglaia silvestris* (Hwang et al. 2004; Rodrigo et al. 2012). Silvestrol has been shown to present high antiproliferative activity against different types of *in-vitro* cancer cell lines (e.g. lung, breast and prostate) (Rodrigo et al. 2012). Silvestrol acts by stimulating non-productive binding of eIF4A I and II to RNA, sequestering it from the eIF4F complex. eIF4A I and II are two RNA helicases required for the loading of the mRNA onto the 40S ribosome during the translation initiation. By disrupting the normal function of these helicases, silvestrol was found to inhibit translation initiation (Bordeleau et al. 2008). Efforts have been made to synthetically obtain silvestrol (Rodrigo et al. 2012). Due to the difficulty of joining the cyclopenta[*b*]benzofuran and dioxanyl fragments in its structure, Porco's group has attempted to prepare cyclopenta[*b*]benzofuran analogues lacking the dioxanyl moiety present in silvestrol (Rodrigo et al. 2012). From these, (±)-rocaglamide hydroxamate 3 was found to present eukaryotic translation inhibition activity, similar as silvestrol (Fig.1.10) (Rodrigo et al. 2012). Based on the hydroxamate 3 structure, hydroxamates 7-9

were synthesised with varying substitution of the N- and O- positions of the hydroxamate (Fig.1.11) (Rodrigo et al. 2012).

Figure 1.10 – Chemical structure of (A) silvestrol and (B) (±)-rocaglamide hydroxamate 3.
Adapted from (Rodrigo et al. 2012).

Hydroxamate (-)-9 and silvestrol reveal similar potencies towards the inhibition of translation in *ex-vivo* BJAB lymphoma cells, ranging from an IC_{50} of approximately 20nM when cells are exposed to hydroxamate (-)-9 for 1h to an IC_{50} of approximately 0.5nM when cells are exposed to compound for 72h. The IC_{50} for inducing cell death in BJAB cells was determined to be approximately 1.5nM following 72h exposure, indicating that the observed effects on the inhibition of the protein synthesis are not secondary consequences of cell death (Rodrigo et al. 2012). The solubility of hydroxamate (-)-9 is high at three physiologically relevant pH levels (>150mg/mL at pH 5.0, 6.2 and 7.4). The compound exhibits moderate to high permeability, is significantly bound by human plasma proteins (82-84% bound after 4h exposure), reveals excellent stability (100% remaining after 3h) in human plasma and exhibits significant hepatic stability in the presence of human and murine liver microsomes (>95% of compound remaining after 1h exposure), suggesting that hydroxamate (-)-9 should exhibit significant metabolic stability *in-vivo* (Rodrigo et al. 2012).

Since hydroxamate (-)-9 impairs translation initiation (Bordeleau et al. 2008), it was used in this work to promote SG formation.

Figure 1.11 – Chemical structure of hydroxamate derivatives 7, 8 and 9. Using hydroxamate 3 as a lead structure, Rodrigo and colleagues synthesised hydroxamates 7–9 with varying substitution of the N- and O positions of the hydroxamate. Adapted from (Rodrigo et al. 2012).

ISRIB (integrated stress response inhibitor) was identified in a large screening of small molecules that block PERK signalling and inhibit the integrated stress response (Sidrauski et al. 2013). ISRIB is a symmetric bis-glycolamide that contains a central bi-substituted cyclohexane and can exist as two diastereomers, *cis* and *trans* (Fig.1.12) (Sidrauski et al. 2013). When tested to evaluate reduction of protein synthesis, *trans*-ISRIB proved to be 100-fold more potent (IC_{50} = 5nM) than *cis*-ISRIB (IC_{50} = 600nM). Given the stereospecificity of the compound, the *trans*-isomer of ISRIB was chosen to be used (Sidrauski et al. 2013).

Figure 1.12 – Chemical structure of ISRIB isosteromers, *trans*-ISRIB and *cis*-ISRIB. Adapted from (Sidrauski et al. 2013).

The cellular target of ISRIB was recently shown be eIF2B (Sidrauski, et al. 2015; Halliday et al. 2015). Through activation of eIF2B, ISRIB specifically reverts the effects of eIF2 α phosphorylation during stress (Sidrauski, et al. 2015; Sidrauski, et al. 2015; Sekine et al. 2015). Additionally, ISRIB was shown to block SG formation dependent of eIF2 α phosphorylation (Sidrauski, et al. 2015). Since ISRIB renders cells insensitive to the effects of eIF2 α phosphorylation, the number of SGs generated by eIF2 α phosphorylation was reduced in U2OS cells treated with ISRIB (Sidrauski et al. 2015). Consistent with this, ISRIB failed to block the generation of

SGs resulting from disruption of eIF4A (following treatment with pateamine A), demonstrating its specificity to eIF2 α (Sidrauski et al. 2015).

Based on the observations that eIF2 α ^{+S51A} heterozygous mice display enhanced memory and that induction of eIF2 α kinase PKR in brain cells impairs memory, Sidrauski and colleagues tested the effects of ISRIB in memory (Sidrauski et al. 2013). By decreasing eIF2 α phosphorylation and promoting protein translation, ISRIB enhanced long-term memory in mice (Sidrauski et al. 2013). ISRIB displayed a half-life in plasma of 8h and showed to quickly cross the blood-brain barrier, since after a single intraperitoneal injection, ISRIB was detected in the brain of mice at high concentrations (Sidrauski et al. 2013).

In a subsequent study from another laboratory, ISRIB presented neuroprotective effects in prion-diseased mice (Halliday et al. 2015). In fact, ISRIB showed to efficiently restore protein translation in brains of prion-diseased mice without pancreatic toxicity (Halliday et al. 2015). Herein, ISRIB was used to inhibit SG formation.

1.15. Aims of the project

The inner ear is likely to be continuously exposed to stress, whether from noise exposure, chemicals, or ageing, amongst others, which contribute to the degradation of hair cells. The loss of mammalian hair cells is irreversible, thus resulting in hearing loss and deafness (Forge & Schacht 2000; Perez & Bao 2011; Huth et al. 2011; Schacht et al. 2013). In order to understand why hair cell loss occurs as a consequence of stress, it is crucial to understand how the inner ear responds to stress and which cellular pathways are activated during damage. Ultimately, the development of therapeutic strategies to protect hair cells from damage may help in the prevention of hearing loss.

A recent study from our laboratory has implicated SGs in the cochlea's response to stress, as hair cells were found to form SGs in response to ototoxic damage (Towers et al. 2011). Consequently, it is important to further characterise the formation and regulation of these structures during cochlear stress.

The overall aim of this PhD project is therefore to understand the role of SGs in cochlear stress, with the long term aim of providing novel targets for therapies

designed to protect hair cells during stress exposure. To achieve the overall aim, two research questions were formulated:

1. Does SG manipulation in the cochlea affect hair cell survival upon ototoxic stress?

Initially, a number of distinct assays were performed to characterise in detail the nature and components of SG formation. These were at first developed in an inner ear-derived cell line (OC-2) and then performed in mouse cochlear explants to further characterise and quantify the hair cell response in terms of SG formation. Upon understanding the dynamics of the SG response to individual stressors, different pharmacological compounds that inhibit or promote SG formation were tested. Initial screens for the different compounds were performed in the OC-2 cell line in order to obtain optimum experimental conditions, prior to the use of *ex-vivo* mouse cochlear explants. Those pharmacological tools were used to promote/inhibit SG formation prior to/ during exposure to cochlear stress and their effect assessed by measurements of hair cell survival.

2. What is the relationship between Hsp70 expression and SG formation?

During the course of this work, some observations have indicated an apparent association between the expression of Hsp70 and the absence of SGs. Although data from other laboratories corroborate these observations (Cherkasov et al. 2013; Walters et al. 2015), this association is yet poorly understood. To further characterise the relationship between Hsp70 and SG formation, Hsp70 gene and protein expression was studied during SG assays using individual stressors in OC-2 cells. The cellular location of Hsp70 single RNA was assessed using a RNA-immuno-FISH approach and related to SG distribution. Overexpression of Hsp70 was performed and its effect was evaluated on SG formation upon different stressors.

2. Methods

2.1. The UB/OC-2 cell line

UB/OC-2 inner ear cell line (University of Bristol / Organ of Corti-2; herein referred as OC-2) (Rivolta et al. 1998) was used in this study to investigate SG assembly and disassembly and to develop and optimise new assays prior to animal use.

The H-2Kb-*tsA58* transgenic mouse was used by Rivolta and colleagues to isolate inner ear-derived cell lines (Rivolta et al. 1998). This mouse strain carries a conditionally expressed, temperature-sensitive immortalising gene (*T-Ag*) from the SV40 virus. This immortalising gene perpetuates cell division and prevents terminal differentiation (Rivolta et al. 1998). Since cochlear hair cells have their final mitotic division prior to differentiation at embryonic day (E) 14, Rivolta and colleagues selected the sensory epithelial cells at E13 and used different hair cell markers to identify hair cells *in-vitro*: (1) Brn3.1, a transcription factor expressed specifically in hair cells essential for their differentiation; (2) $\alpha 9$ AChR, $\alpha 9$ subunit of the nicotinic acetylcholine receptor, an isoform characteristic of hair cells; (3) Fimbrin, an actin cross-linking protein that is present in the stereocilia of hair cells; (4) MyosinVI and VIIa, since MyosinVI is generally located in the cuticular plate and, to a lesser extent, in the hair cell body (and absent from stereocilia) and MyosinVIIa is distributed across the whole cell body and stereocilia (Rivolta et al. 1998).

At E13, cells were then selected by epithelial morphology and for the expression of mRNA for $\alpha 9$ AChR and two cell lines were derived: UB/OC-1 and UB/OC-2. These cell lines proliferate at 33°C under gamma-interferon (γ IF), the permissive conditions of the expression of the immortalising gene *T-Ag* (Rivolta et al. 1998). When temperature is changed to 39°C and, in the absence of γ IF, *T-Ag* expression is downregulated, cell proliferation decreases and the cells form a regular, confluent, epithelial-like monolayer (Rivolta et al. 1998).

At 33°C, OC-1 cells reveal lower expression of hair cell markers such as Brn3.1, $\alpha 9$ AChR and MyosinVIIa, when compared to OC-2, suggesting that OC-2 cells were probably immortalised at an earlier differentiation stage. Since OC-2 cells express Brn3.1 at 33°C, these cells were identified as committed hair cell precursors. On the other hand, given the lower expression of Brn3.1 in OC-1 cells, these were suggested to have the ability to potentially differentiate into both supporting cells or hair cells (Rivolta et al. 1998).

Since their isolation, OC-1 and OC-2 cell lines have been broadly used in auditory research (Jagger et al. 2000; Clough et al. 2004; Mukherjea et al. 2008; Brunetta et al. 2012; Riccardi et al. 2016). Considering that one of the main objectives of this work is to assess the effect of SG formation on hair cell survival and the fact that OC-2 cells express hair cell markers, such as α 9AChR, Fimbrin, Brn3.1 and MyosinVIIa (Rivolta et al. 1998), the OC-2 cell line was chosen to perform the initial experiments of this thesis.

2.2. *In-vitro* culture of OC-2 cells

OC-2 cells were cultured at 33°C under 5% CO₂ atmosphere in Dulbecco's modified Eagle's medium (DMEM) supplemented with 10% fetal bovine serum (FBS) and 50 units/mL γ IF. The cell culture media conditions described in this thesis will be the same as these, otherwise indicated. Cell passaging was carried out when cells were about 90% confluent using pre-warmed trypsin for 3 minutes at 33°C until the cells became detached from the flask.

For seeding purposes, cells were counted using a haemocytometer and split into 35mm x 10mm petri dishes containing coverslips at a seeding density of 2×10^5 cells per dish.

2.3. C57BL/6 mice

Mouse cochlear explants and *in-vivo* cryosections used in this thesis were obtained from C57BL/6 mice. The hearing onset in this strain occurs at post-natal day (P) 12-13, probably due to the combined action of the maturation of the middle and inner ear (Shnerson & Pujol 1981). C57BL/6 mice show sensory hair cell loss degeneration relatively early: by 3 months of age, 75% of outer hair cells and 55% of inner hair cells are lost in the base of the cochlea (Spongr et al. 1997). By 26 months of age, C57BL/6 mice reveal more than 80% of the outer hair cells lost throughout the whole cochlea, whereas inner hair cell loss ranges from 100% at the base of the cochlea to approximately 20% in the apex (Spongr et al. 1997).

The C57BL/6 mice strain develops high frequency sensorineural hearing loss around 6-8 months of age, consistent with the hair cell loss described above. By 18-24 months of age, these mice are almost completely deaf, including for low

frequency sounds, compatible with hair cell loss throughout the entire cochlea (Spongr et al. 1997).

2.4. Mouse cochlear explants

Experiments were carried out using cochlear tissue isolated from post-natal (P) day 3 from C57BL/6 mice, killed according to Schedule 1 procedures as described in the United Kingdom (Scientific Procedures) Act of 1986. After cervical dislocation and decapitation, heads were cut in half and the brain was removed. Under a dissecting microscope, the bulla was isolated and placed into M199 medium (Sigma). Using fine forceps, the cartilaginous bulla was carefully removed. Holding the cochlea by the hook region, the neuronal tissue was removed from the centre of the cochlea and the stria vascularis was carefully peeled away from the base to the apex region, leaving the organ of Corti isolated. The hook and apical regions were cut using iridectomy scissors. The middle of the basal end of the cochlear coils was cultured in CellTak-coated glass-bottomed dishes. Glass-bottomed dishes (MatTek) were coated with CellTak (BD Biosciences) at a dilution of 0.05x (of a 0.9 mg/mL stock) in 0.1M of sodium bicarbonate at least half an hour before culturing. Before plating, glass-bottomed dishes were washed three times with DMEM F-12 (Sigma) containing 1% FBS (Sigma), pre-incubated at 37°C.

Mouse cochlear explants were cultured in DMEM F-12 medium supplemented with 1% FBS and 0.001% ciprofloxacin at 37°C under 5% CO₂ atmosphere, for 18-20h, before any treatments were applied.

2.5. Heat shock studies

OC-2 cells were incubated at 43°C under 5% CO₂ atmosphere for 1h in pre-warmed DMEM. When recovery periods were applied, cells were transferred to a 33°C 5% CO₂ incubator after the heat shock, for 1h, 2h or 4h. At the end of each time point, cells were fixed using 4% paraformaldehyde (PFA) in phosphate buffered saline (PBS) for 15 minutes at room temperature and then rinsed three times with PBS for 15 minutes. Cells were kept in PBS at 4°C until further analysis.

Mouse cochlear explants were incubated at 43°C for 1h with pre-warmed DMEM F-12 medium supplemented with 1% FBS. The samples were fixed using 4% PFA in

PBS for 30 minutes at room temperature and rinsed three times with PBS for 45 minutes. Samples were kept in PBS at 4°C until further analysis.

2.6. Sodium arsenite studies

For arsenite-induced stress, OC-2 cells were incubated at 33°C under 5% CO₂ atmosphere for 1h with 0.5mM sodium arsenite in DMEM. When recovery periods were applied, the medium containing sodium arsenite was removed, cells were rinsed and incubated with new arsenite-free medium at 33°C 5% CO₂ for 1h, 2h or 4h. At the end of each time point, cells were fixed using 4% PFA in PBS for 15 minutes at room temperature and then rinsed three times with PBS for 15 minutes. Cells were kept in PBS at 4°C until further analysis.

Mouse cochlear explants were incubated at 37°C for 1h with 0.5mM sodium arsenite in DMEM F-12 medium supplemented with 1% FBS. The samples were fixed using 4% PFA in PBS for 30 minutes at room temperature and rinsed three times with PBS for 45 minutes. Samples were kept in PBS at 4°C until further analysis.

2.7. pp242 studies

pp242 (5mg powder, Selleckchem) was diluted in DMSO to a 1mM stock solution and kept at -20°C. Fresh working solutions were made up through further serial dilution of the compound in DMEM media before each experiment.

OC-2 cells were pre-incubated with different concentrations of pp242 (25nM, 250nM, 2500nM and 5000nM) in DMEM for 24h at 33°C 5% CO₂ before heat shock exposure (43°C) or sodium arsenite (0.5mM, 33°C) for 1h. Different times of incubation were also studied, with OC-2 cells being pre-incubated for 6h, 12h and 24h with 2500nM of pp242 at 33°C 5% CO₂ atmosphere before heat shock stress at 43°C 5% CO₂ for 1h in DMEM. At the end of each pre-incubation period, the medium was removed, cells rinsed and new pre-warmed medium containing new pp242 solution was added, before heat shock exposure. Cells were fixed using 4% PFA in PBS for 15 minutes at room temperature and then rinsed three times with PBS for 45 minutes. Cells were kept in PBS at 4°C until further analysis.

2.8. ISRIB studies

ISRIB (5mg powder, Sigma) was diluted in DMSO to a 1mM stock solution and kept at 4°C. Fresh working solutions were made up through further serial dilution of the compound in DMEM media before each experiment.

OC-2 cells were exposed to either heat shock (43°C) or sodium arsenite (0.5mM, 33°C) for 1h in 5% CO₂ atmosphere in the presence of 200nM of ISRIB in DMEM. Cells were fixed using 4% PFA in PBS for 15 minutes at room temperature and then rinsed three times with PBS for 45 minutes. Cells were kept in PBS at 4°C until further analysis.

Mouse cochlear explants were incubated at 37°C 5% CO₂ for 1h with 0.5mM sodium arsenite in DMEM F-12 in the presence of ISRIB at 200nM. The samples were fixed using 4% PFA in PBS for 30 minutes at room temperature and rinsed three times with PBS for 45 minutes. Samples were kept in PBS at 4°C until further analysis.

2.9. Hydroxamate (-)-9 studies

Hydroxamate (-)-9 compound was a kind gift from Dr. Jerry Pelletier, McGill University, Montreal, Quebec. Hydroxamate (-)-9 stock solution (1mM in DMSO) was kept at -80°C and fresh working solutions were made up through further serial dilution of the compound in DMEM media before each experiment.

Unstressed OC-2 cells were exposed to different hydroxamate (-)-9 concentrations (1nM, 10nM, 100nM and 1000nM) at 33°C under 5% CO₂ atmosphere for 8h in DMEM. Different times of incubation were also studied, with OC-2 cells being incubated for 2h, 4h, 8h and 24h with 100nM of hydroxamate (-)-9 at 33°C 5% CO₂ atmosphere in DMEM. At the end of each experiment cells were fixed using 4% PFA in PBS for 15 minutes at room temperature and then rinsed three times with PBS for 45 minutes. Cells were kept in PBS at 4°C until further analysis.

Mouse cochlear explants were incubated at 37°C 5% CO₂ for 8h with 100nM of hydroxamate (-)-9 in DMEM F-12 medium supplemented with 1% FBS. The tissue was fixed using 4% PFA in PBS for 30 minutes at room temperature and rinsed three times with PBS for 45 minutes. Samples were kept in PBS at 4°C until further analysis.

2.10. Hsp70 protein overexpression

Recombinant adenovirus type 5 (dE1/E3) overexpressing Hsp70 (Ad-Hsp70) was a kind gift from Dr. Lisa Cunningham, National Institutes of Health, USA.

The virus was used to infect OC-2 cells prior to heat shock / sodium arsenite exposure. OC-2 cells were incubated during 24h at 37°C 5% CO₂ with different multiplicities of infection (MOI) of Ad-Hsp70 (0, 250, 500 or 1000) followed by 1h heat shock at 43°C or 1h 0.5mM sodium arsenite at 33°C under 5% CO₂ atmosphere. The final MOI used in the studies here presented was 500. The virus was used at stock titre of 2x10⁵. The Ad-Hsp70 virus was directly added to the cell growth media and the quantity of virus to add was determined using the following formulas:

Formula 1: (cells seeding concentration)(desired MOI)= Plaque forming units (PFU) desired*

Formula 2: (PFU desired)/virus titre = amount of virus to add according to determined MOI

2.11. Cochleae neomycin studies

Neomycin 1mM working solutions were obtained by diluting neomycin sulphate powder (Sigma) in DMEM F-12. Neomycin solutions were always equilibrated at 37°C 5% CO₂ for 20 minutes prior to the experiments. In some experiments, cultures were exposed to 6h 1mM neomycin and fixed immediately. Other experiments involved a recovery period in neomycin-free culture medium (as above indicated) for 48h after 6h 1mM neomycin exposure. The cochlear cultures were always fixed at room temperature at the end of the experiments, for 30 minutes, in 4% PFA and then washed three times for 45 minutes with PBS. Samples were kept in PBS at 4°C until further analysis. Neomycin-treated samples were imaged post-fixation using a Zeiss 510 NLO multi-photon upright confocal system.

2.12. Cochleae sisomicin studies

Sisomicin working solutions (10µM, 100µM, 200µM and 500µM) were obtained by diluting sisomicin sulphate salt (Sigma) in culture medium DMEM F-12. Sisomicin solutions were obtained by serial dilution and always equilibrated at 37°C 5% CO₂ for 20 minutes prior to the experiments. Sisomicin was added to the cultures for 1h and samples fixed after 48h recovery period in a sisomicin-free medium. The

cochlear cultures were fixed for 30 minutes in 4% PFA and washed three times for 45 minutes with PBS. Samples were kept in PBS at 4°C until further analysis.

Sisomicin-treated samples were either live imaged using a Zeiss Axiovert 200 spinning disc microscope or imaged post-fixation using a Zeiss 510 NLO multi-photon upright confocal system. For the living samples imaged using spinning disc microscopy, the explants were incubated with FM1-43 (Thermofisher) to visualise hair cells as indicated in (Gale et al. 2001). FM1-43 100µg was freshly diluted in DMEM F-12 medium in the dark to a final concentration of 3.3µM. FM1-43 was added to the samples during 30 seconds. Samples were then washed immediately three times (10 seconds each) and then for 15 minutes using DMEM F12. FM1-43 was detected using a 488nm laser excitation.

2.13. Mouse cochleae cryosections

Adult C57BL/6 mice were killed according to Schedule 1 procedures as described in the United Kingdom (Scientific Procedures) Act of 1986. After being euthanized with rising concentrations of CO₂, cervical dislocation was performed to confirm the death. Animals were decapitated and the heads were bisected. The brain was then removed and the bony cochlea was isolated by hand. Under a dissecting microscope, the cochlea was cleaned from surrounding tissue using fine forceps, the stapes bone was removed and two holes were made using a surgical needle: one on top of the apical region and the other at the basal end to allow the complete fluid penetration inside the cochlea. All the cochleae were fixed for 1h using 4% PFA in a rotator at room temperature. The cochleae were then washed three times with PBS for 45 minutes in a rotator. Decalcification of the bony cochleae was performed using 10% EDTA in a rotator at 4°C during 14-20h. Sufficient decalcification was confirmed by gently pressing the cochlea with forceps under a microscope. The cochleae were washed for three times with PBS for 45 minutes in a rotator at 4°C. Sucrose treatments were then applied as follows: 10% sucrose for 3h, 20% sucrose for 14h and 30% sucrose for 3h, all in PBS at 4°C in a rotator. The cochleae were then transferred into a cryomold containing 1% agarose in 18% sucrose in PBS at approximately 37°C. Each cochlea was placed into the cryomold under a dissecting microscope with the round window facing downwards and the modiolus parallel to the base. The agarose preparation was allowed to cool down for 30 minutes at 4°C. The excess of agarose was cut before the cochlea

preparation being transferred to a cryosection stub containing OCT medium. The preparation was frozen by manually rotating the stub using surgical forceps in liquid nitrogen.

The cryostat chamber was set to -25°C and the preparations were allowed to equilibrate the temperature with the cryostat for 30 minutes. Cryosections were cut at 12µm and mounted in SuperFrost Plus slides (Thermofisher). Sections were stored at -20°C until further manipulation.

2.14. RNA-immuno-Fluorescence *in situ* hybridisation

RNA-immuno-Fluorescence *in situ* hybridisation (RNA-immuno-FISH) was used in order to detect polyA⁺ mRNA at the same time as TIA-1 and Caprin-1 proteins by antibodies. This technique was performed immediately after any experiments, in order to avoid mRNA degradation. The protocol described below was based on (Kedersha et al. 1999; Brown & Buckle 2010).

OC-2 cells and mouse cochlear explants were fixed in 4% PFA in PBS for 15 and 30 minutes, respectively, and washed three times with PBS for 45 minutes. *In-vivo* cryosections were defrosted at room temperature and washed with PBS for 30 minutes. All samples were then permeabilised with -20°C methanol for 10 minutes and rinsed twice with 2x saline-sodium citrate buffer (SSC) (3M NaCl, 0.3M sodium citrate, pH 7) at room temperature. Hybridisation was performed at 43°C for 14-16 hours in the dark using a humid chamber in RNA hybridisation mixture containing 25% (v/v) formamide, 200ng/µL salmon sperm DNA, 5x Denhardt's solution, 50mM sodium phosphate pH 7, 1mM EDTA, 2x SSC and 200ng/µL of Cy3-labelled polydT-5' probe to detect polyA⁺ mRNA (Eurofins) or 100ng/µL of PTGES3 / Hsp70 probes (Stellaris, Biosearch technologies, section 2.15) to detect single RNA molecules. After hybridisation, samples were rinsed twice with 2xSSC for 5 minutes and three times with PBS for 15 minutes. Primary antibody detection was performed in blocking solution containing 0,5% Triton-X, 0.001% bovine serum albumin (BSA), 1% serum and 25U/mL RNAsin for 16h at 4°C in the dark for mouse cochlear explants or for 1h at 25°C in the dark for OC-2 cells and *in-vivo* cryosections. Antibodies were against the following proteins: TIA-1 (goat antibody; Santa Cruz Biotechnology; 1:300), Caprin-1 (rabbit antibody; Proteintech Europe; 1:500) and MyosinVIIa (rabbit antibody; Thermofisher; 1:500 / mouse antibody; Hybridoma bank; 1:500). Primary antibody was removed and cells were rinsed three times in

PBS for 15 minutes. Cells were incubated with the secondary antibody, donkey anti-(goat IgG) conjugated to Alexa Fluor 488 (Santa Cruz Biotechnology); donkey anti-(rabbit IgG) conjugated to Alexa Fluor 546 (Invitrogen); donkey anti-(mouse IgG) conjugated to Alexa Fluor 640 (Invitrogen); goat anti-(rabbit IgG) conjugated to Alexa Fluor 647 (Invitrogen) and DAPI (1mM), to assess chromatin structure, all 1:1000 concentration, in blocking solution containing 0.5% Triton-X, 0.001% BSA and 1% serum for 1h at 25°C in the dark, for OC-2 cells and *in-vivo* cryosections, and for 2h at 25°C in the dark, for cochlear explants. Samples were then rinsed in 2xSSC three times for 15 minutes. Coverslips containing OC-2 cells and *in-vivo* cryosections were mounted in slides using Fluoromount-G and kept at 4°C in the dark. Cochlear explants were kept in PBS at 4°C in the dark. OC-2 cells and *in-vivo* cryosections were imaged using a Zeiss 510 META inverted confocal microscope. Mouse cochlear explants were imaged using a Zeiss 510 NLO multi-photon upright confocal system.

2.15. RNA-FISH probes

Probes for detection of PTGES3 and Hsp70 RNAs were purchased from Stellaris, Biosearch technologies. Considering the *Mus musculus* cDNA sequence for each of the target RNAs, a set of probes was designed, using the Stellaris probe designer software. Each probe varied between 18-22nt. Minimum spacing between probes was determined as 0-2nt. Priority was given to probes designed with the highest stringency level to improve probe specificity and to probes binding to the translated sequence (although some UTRs have been included to increase the number of probes). Specific target binding for each individual probe was confirmed using Ensembl BLAST and probes revealing unspecific binding were discarded.

In Table 2.1 are listed the probes used to detect PTGES3 and Hsp70 RNAs, respectively.

Table 2.1 – Probes used to detect PTGES3 and Hsp70 RNAs.

Probe sequence (5'-3')	
PTGES3	Hsp70
ggctggtgacgcagcaaaat	accagatttggttctgagta
ttaggaaaagggcgcgag	ctctgcttcttctctc
tcaacccgggagagaaggaa	tgatgctccgggaaagtt
cagagggccagacaaacggg	tggtcgttggcgatgatctc
aatccaggcgatgacaacag	ttcgcgtcgaacacggtgtt
ctgcagaagttatcttct	agatctctccgggaagaac
tatctgcttagagctatc	atctctcatctctcgtcag
aactgggttagaggaggcaa	cgctgagagtcgtgaagta
acataatcaacccttagtga	atgatccgcagcacgtttag
ttaaactgccccacacaatg	aggtcgaagatgagcacggt
tcatgcataaggatactgcc	tcaggatggacacgtcgaac
cagttgcctaggatcaactg	tcgaagatgccgtcgtcgat
aattattgtccgagctgct	ctgagcacagctcttcaaac
agctgagagcttctcaatg	ttgaagaagtctgcagcag
tgttccgctcctttaa	ttgatgctctgttcaggctc
cagtttaaggtattagccaa	gagtagggtggaaggctc
tctgaaagaatggcagggt	tcgtacacctggatcagcac
acacctgaacactgacaagt	atgtcgaaggctcacctcgat
taagttaggcatccactag	tgacgttcaggatgccgttg
taccaagtgataggcttca	cagcaccttctctgtcag
atgtaaagcttaaggcca	catatctgtctcctagccag
tcttctcctccatgctaag	ataatgacagtctcaaggc
gtacatactcaagcaaca	tctaggacttgattgcagga
gccatactgactgtgcaaat	gataaagcccacgtgcaata
gtatttaacattgtccactc	gacacactgcagtgtaaat
tctccaacagttattaga	ggggcagtgtgaattgaag
cattccagtaaggggtaaat	aaagaactcaacagtctcct
acaggaccagtccaatctt	gtatcaacaatgtggcccag
tacagcaagcctcttgttc	tctgaaggacccgacacaag
tttacagggttcctgtgac	agtctccgctgtcagtaac
agctcccatttacagacac	ttaaagcaaggagaagcagc
tcacaacactgtctggctg	gtgcaaccacctgcaagat
	caacctggaacaagtctta
	ctgaacacatgctgggtgctg
	gttcaggatggtgtgtaaa
	tgaccggtaaaaattgacc
	gcacaagacctggcaagtga
	actgtcatacacagcaactc
	aatgttagtcaagcgtagcc
	caatgcaatgtccctgtgag
	atcttctcacacaagcaga

2.16. General immunofluorescence protocol

OC-2 cells were labelled for Caprin-1 (rabbit antibody; Proteintech Europe; 1:500), TIA-1 (goat antibody; Santa Cruz Biotechnology; 1:300) and Hsp70 (mouse antibody; Assaydesigns; 1:500). Blocking was performed for 30 minutes in solution containing 0.5% Triton-X, 0.001% BSA and 1% serum at 25°C. Primary antibody detection was performed in blocking solution containing 0.5% Triton-X, 0.001% BSA and 1% serum for 1h at 25°C. After primary antibody removal, cells were washed three times for 15 minutes with PBS. Secondary antibodies (donkey anti-(goat Ig) conjugated to Alexa Fluor 488 (Santa Cruz Biotechnology); (donkey anti-(rabbit Ig) conjugated to Alexa Fluor 546 (Invitrogen); and donkey anti-(mouse Ig) conjugated to Alexa Fluor 640 (Invitrogen)), all 1:1000 concentration, and DAPI (chromatin labelling, 1mM, 1:1000 concentration) were applied in a solution containing 0.5% Triton-X, 0.001% BSA and 1% serum for 1h at 25°C in the dark. Coverslips were washed three times for 15 minutes with PBS and mounted in microscope slides using Fluoromount-G. Slides were kept at 4°C in the dark. OC-2 cells were imaged using a Zeiss 510 META inverted confocal system.

Mouse cochlear explants were labelled for MyosinVIIa (rabbit antibody; Thermofisher; 1:500) and TIA-1 (goat antibody; Santa Cruz Biotechnology; 1:300). Blocking was performed for 1h in solution containing 0.5% Triton-X, 0.001% BSA and 1% serum at 25°C. Primary antibody detection was performed in blocking solution containing 0.5% Triton-X, 0.001% BSA and 1% serum for 16h at 4°C. After primary antibody removal, samples were washed three times for 45 minutes with PBS. Secondary antibodies (donkey anti-(goat IgG) conjugated to Alexa Fluor 488 (Santa Cruz Biotechnology) and donkey anti-(rabbit IgG) conjugated to Alexa Fluor 546 (Invitrogen)) and were applied in a solution containing 0.5% Triton-X, 0.001% BSA and 1% serum, along with Phalloidin 647 and DAPI (1mM) all 1:1000 concentration for 2h at 25°C in the dark. Samples were washed three times for 45 minutes with PBS in the dark. Mouse cochlear explants were kept in PBS at 4°C in the dark. Mouse cochlear explants were imaged using a Zeiss 510 NLO multi-photon upright confocal system.

2.17. Secondary antibody controls

To confirm that the antibody labelling observed was due only to the binding of secondary antibody to the primary antibody and not to nonspecific binding of the secondary antibody, controls were always performed in which no primary antibody was used. Example images of secondary antibodies control are shown below for OC-2 cells (Figs.2.1 and 2.2), mouse cochlear explants (Fig.2.3) and *in-vivo* cryosections (Fig.2.4).

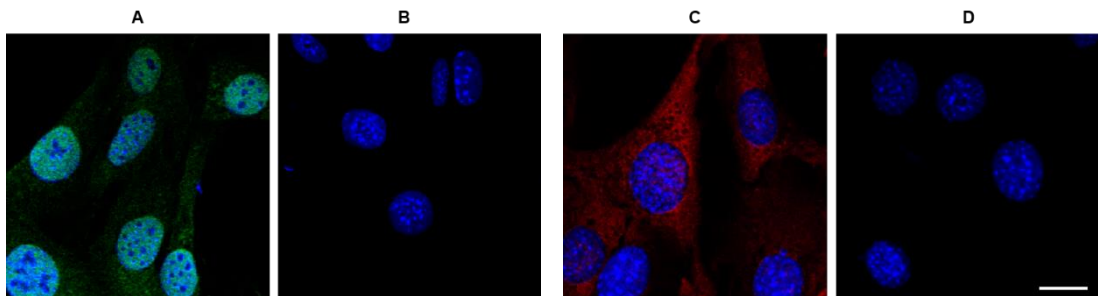


Figure 2.1 – Secondary antibody controls for Alexa Fluor 488 and 546 in OC-2 cells. (A) Donkey anti-(goat IgG) conjugated to Alexa Fluor 488 (SantaCruz Biotechnology) against TIA-1. (B) Donkey anti-(goat IgG) conjugated to Alexa Fluor 488 (SantaCruz Biotechnology) alone (without primary antibody). (C) Donkey anti-(rabbit IgG) conjugated to Alexa Fluor 546 (Invitrogen) against Caprin-1. (D) Donkey anti-(rabbit IgG) conjugated to Alexa Fluor 546 (Invitrogen) alone (without primary antibody). DAPI was used to label chromatin. Scale bar= 10 μ m.

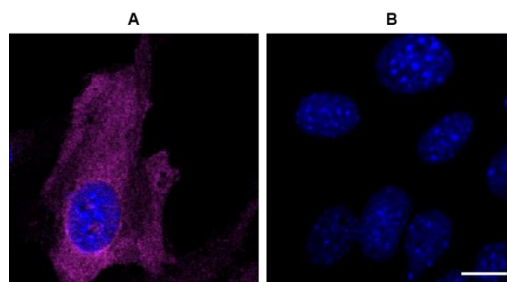


Figure 2.2 – Secondary antibody control for Alexa Fluor 647 in OC-2 cells. (A) Donkey anti-(mouse IgG) conjugated to Alexa Fluor 647 (Invitrogen) against Hsp70. (B) Donkey anti-(mouse IgG) conjugated to Alexa Fluor 647 (Invitrogen) alone (without primary antibody). DAPI was used to label chromatin. Scale bar= 10 μ m.

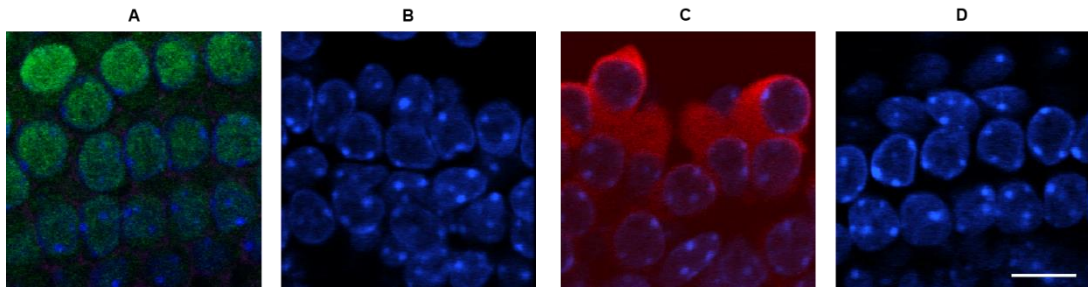


Figure 2.3 – Secondary antibody controls for Alexa Fluor 488 and 546 in mouse cochlear explants. (A) Donkey anti-(goat IgG) conjugated to Alexa Fluor 488 (SantaCruz Biotechnology) against TIA-1. (B) Donkey anti-(goat IgG) conjugated to Alexa Fluor 488 (SantaCruz Biotechnology) alone (no primary antibody). (C) Donkey anti-(rabbit IgG) conjugated to Alexa Fluor 546 (Invitrogen) against MyosinVIIa. (D) Donkey anti-(rabbit IgG) conjugated to Alexa Fluor 546 (Invitrogen) alone (no primary antibody). DAPI was used to label chromatin. Scale bar= 10 μ m.

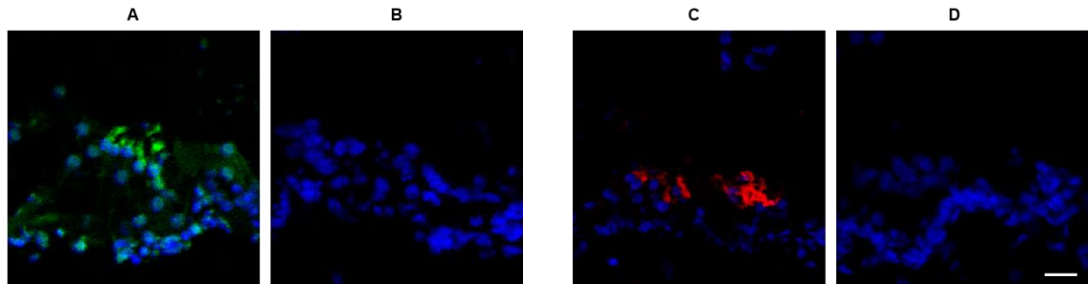


Figure 2.4 – Secondary antibody controls for Alexa Fluor 488 and 546 in *in-vivo* cryosections. (A) Donkey anti-(goat IgG) conjugated to Alexa Fluor 488 (SantaCruz Biotechnology) against TIA-1. (B) Donkey anti-(goat IgG) conjugated to Alexa Fluor 488 (SantaCruz Biotechnology) alone (no primary antibody). (C) Donkey anti-(rabbit IgG) conjugated to Alexa Fluor 546 (Invitrogen) against MyosinVIIa. (D) Donkey anti-(rabbit IgG) conjugated to Alexa Fluor 546 (Invitrogen) alone (no primary antibody). DAPI was used to label chromatin. Scale bar= 25 μ m.

2.18. Colocalisation quantification

Colocalisation analysis between polyA⁺ mRNA and Caprin-1 or TIA-1 SG-marker proteins was performed using “Coloc 2” plugin in Fiji software. Pearson’s correlation coefficient (r) was determined using the following formula:

$$r = \frac{\sum_i (Ch1_i - Ch1_{aver}) * (Ch2_i - Ch2_{aver})}{\sqrt{\sum_i (Ch1_i - Ch1_{aver})^2 * \sum_i (Ch2_i - Ch2_{aver})^2}}$$

in which Ch_i is the intensity of the fluorophore in individual pixels and Ch_{aver} is the arithmetic mean, considering two fluorophores, 1 and 2.

Pearson's r values range from -1, when two fluorescence intensities are perfectly, but inversely, related to one another, to 1, when two fluorescence intensities are perfectly, linearly related (Dunn 2011). Since Pearson's r subtracts the mean intensity from each pixel's intensity value, it is independent of both signal and background levels. By measuring the pixel-by-pixel covariance in the signal levels of two fluorophores, Pearson's r can calculate the linear dependence between two variables without any form of pre-processing, decreasing user bias (Dunn 2011).

2.19. Stress granule quantification

A plugin for the Fiji Image analysis package designated "SG counter" was used to determine the number and size of polyA⁺ mRNA, Caprin-1 and TIA-1-positive SGs. The SG counter plugin was created by Ann Sablina from Lomonosov Moscow State University, Russia. The plugin works based on the principle of thresholding the difference between the brightness of neighbouring pixels. It recognizes accentuated differences in the pixel brightness as a rapid change in the intensity for the smoothing process. During the smoothing process, SG outlines are determined by the difference in the brightness (taking into account a previous selected threshold) and subtracted from the original image. The final output comprises all the SGs identified by the software, based on the dimensions, number of smoothes, threshold and minimum particle circularity set before by the user. For TIA-1 analysis, when comparing the final plugin output and directly observing the unprocessed images, I noticed initially that the software was considering some nucleus TIA-1 staining as SGs. TIA-1 normally presents a nuclear pattern that is kept in the presence of stress when it migrates to the cytoplasm to aggregate at SGs and, because the automated SG counter plugin does not exclude the nucleus area for its analysis, TIA-1 nuclear staining was considered as SGs in the final output. To solve this issue, the DAPI image was used to create a binary mask image to remove all the pixel values from the nucleus region from TIA-1 signal (manual processing described below in sections 2.19.1 and 2.19.2).

For the Caprin-1 protein expression analysis another issue has arisen during the counting process. Caprin-1 presents mostly a cytoplasmic distribution, where it is normally expressed and is absent from the nucleus. Due to the fact that Caprin-1 presents such marked cytoplasmic brightness under control conditions, the SG

counter plugin was not always exactly accurate measuring the difference in the brightness between neighbouring pixels. Occasionally, it selected Caprin-1 bright pixels as SGs that were not visibly aggregated at SGs. This error was determined to be less than 10%, by manually counting the amount of SGs from a range of different images. All the images in this work were analysed using the same settings, so comparisons can be performed between images, since the same error is kept across all the analysis in the same extent.

2.19.1. Stress granule quantification in OC-2 cells

Using Fiji software, multi-TIFF Zeiss LSM files were split into the different channels (Caprin-1, TIA-1 and DAPI) (Fig.2.5). The nuclear DAPI signal was first considered for processing: after thresholding the image (using Fiji default threshold), a binary image was generated from the thresholded image, in which the DAPI nuclear signal had a value of 0 (zero) and background 1 (Fig.2.6). TIA-1 images were also submitted to a thresholding process and the resulting image was multiplied by the DAPI binary image on a pixel by pixel basis, to generate a TIA-1 image in which the nuclear signal was effectively removed (Fig.2.6). The subsequent final image was used to quantify SG formation (number and size) using SG counter (Fig.2.7). Even though Caprin-1 does not generally present nuclear staining, the same process was applied to exclude any possibility that the plugin would count nuclear Caprin-1 positive-SGs. To run the SG counter plugin, the threshold was set to 5000 and minimum particle size to 3 pixels, after manual identification and quantification of the amount of SGs from a range of different images. These settings were kept consistent across all the images analysed. All the remaining settings were kept by default (Fig.2.8). The output generated by the SG counter plugin described the number of SGs counted, their individual area, minimum and maximum intensity and pixel coordinates (Fig.2.9).

The number of SGs quantified is shown across this thesis as number of SGs per cell and size of SGs (μm^2) \pm the standard error of the mean.

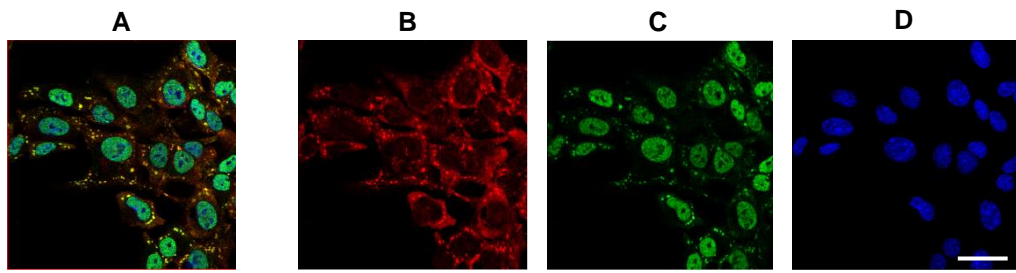


Figure 2.5 – Example of raw images (pre-processed). (A) Merged image of B, C and D. (B) Caprin-1 signal. (C) TIA-1 signal. (D) DAPI signal. OC-2 cells are shown. Scale bar= 25 μ m.

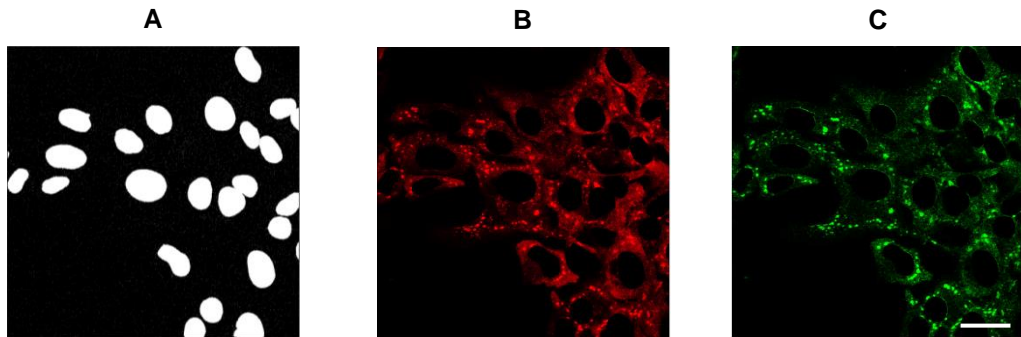


Figure 2.6 – Example of processed images. (A) DAPI image after thresholding and binary processing. (B) Caprin-1 signal after nucleus subtraction. (C) TIA-1 signal after nucleus subtraction. White areas in (A) correspond to the nuclear signal (value 0) and black areas correspond to background (value 1). (B) and (C) correspond to the result of multiplication on a pixel by pixel basis between Caprin-1 or TIA-1 (showed in B and C in Fig.2.5, respectively) by DAPI binary image. The result images contain the Caprin-1 and TIA-1 signal correspondent to the background areas of DAPI binary image, whereas the nuclear signal (white areas in DAPI binary) was reduced to zero. Scale bar= 25 μ m.

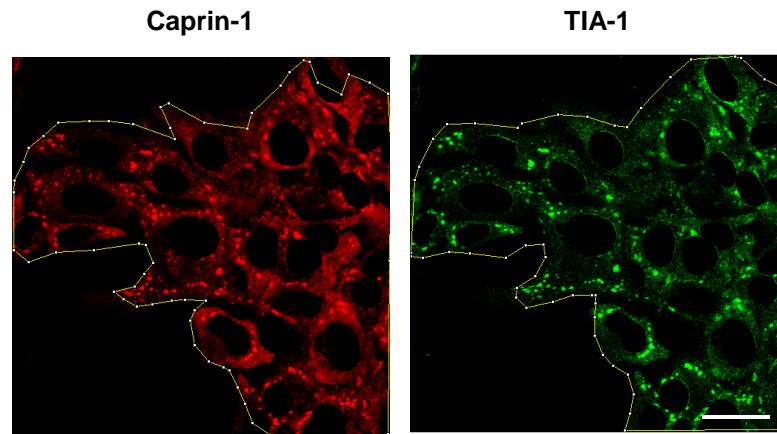


Figure 2.7 – Caprin-1 and TIA-1 areas delineated (in yellow) to be considered for further analysis using SG counter plugin. Scale bar= 25 μ m.

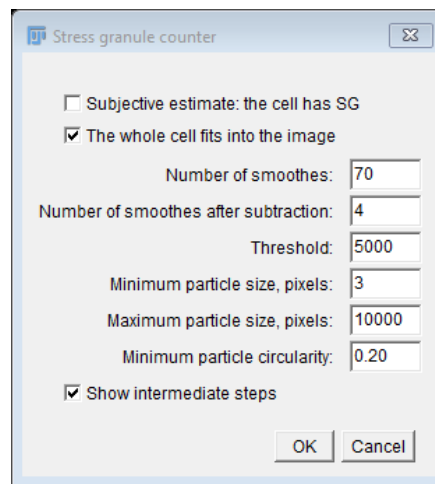


Figure 2.8 – SG counter plugin main input window. Threshold was set as 5000 and minimum particle size (in pixels) was set as 3, for all images. The remaining settings were kept by default: number of smoothes 70, number of smoothes after subtraction 4, maximum particle size 10000 and minimum particle circularity 0.2.

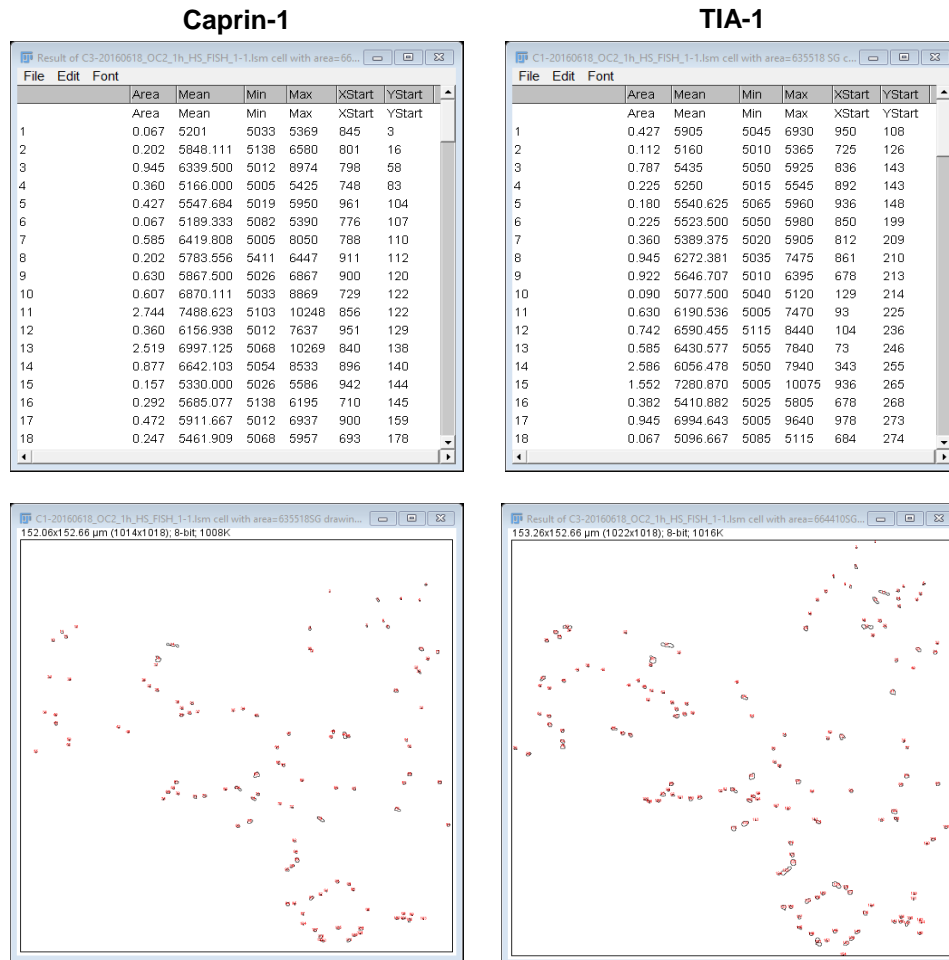


Figure 2.9 – SG counter plugin outputs after analysis. The SGs identified by the plugin are listed (top panels) and information regarding area, mean intensity signal, minimum signal, maximum signal and X/Y coordinates is shown for each individual granule. A correspondent map showing the location of the SGs quantified by the plugin is generated (bottom panels).

2.19.2. Stress granule quantification in mouse cochlear explants

SG quantification in mouse cochlear explants was also performed using the same SG counter plugin. Considering the multicellular composition of the cochlear explants and the three-dimensional structure, the previous protocol described in section 2.19.1 for SG quantification in OC-2 cells was adapted in order to quantify SGs in hair cells and supporting cells.

After splitting the images into different channels (Fig.2.10), the MyosinVIIa channel was used to isolate hair cells from supporting cells. To quantify SGs in hair cells, a MyosinVIIa binary image was created in which MyosinVIIa had value 1 and background 0 to isolate hair cells from the background (Fig.2.11). On the contrary,

when SG were quantified in supporting cells, the MyosinVIIa binary image had value 0 to MyosinVIIa signal (to eliminate the hair cell signal) and background 1 (Fig.2.14).

As described above, DAPI signal was used to extract the nuclear region. MyosinVIIa binary images were multiplied by a binary DAPI image (DAPI signal correspondent to 0 and background 1), generating a binary image with either hair cell cytoplasmic signal or supporting cell cytoplasmic signal (Figs.2.11 and 2.14). Next, the binary image with cytoplasmic signal (hair cells or supporting cells) was multiplied by TIA-1 immunofluorescent signal, generating a final image with TIA-1 signal only in the cytoplasm of hair cells or supporting cells (Figs.2.11 and 2.14). As before, TIA-1 signal was delineated for hair cells and supporting cells (Figs.2.12 and 2.14) and the analysis performed keeping the same settings previously described (Figs.2.13 and 2.15).

The images represented below show examples of SG quantification across the inner hair cell region (for inner hair cells and surrounding supporting cells), using a maximum intensity projection of the whole inner hair cell area, for the purposes of demonstration of the technique. Considering the 3D structure of the epithelium and to avoid overlapping of individual SGs when projecting in a larger scale, SG quantification was performed for maximum intensity projection images every $3\mu\text{m}$ (3 image slices of $1\mu\text{m}$ each) and the resulting number of SGs was summed the whole cells.

The number of SGs quantified is shown across this thesis as number of SGs per unit volume (μm^3) and size of SGs (μm^2) \pm the standard error of the mean.

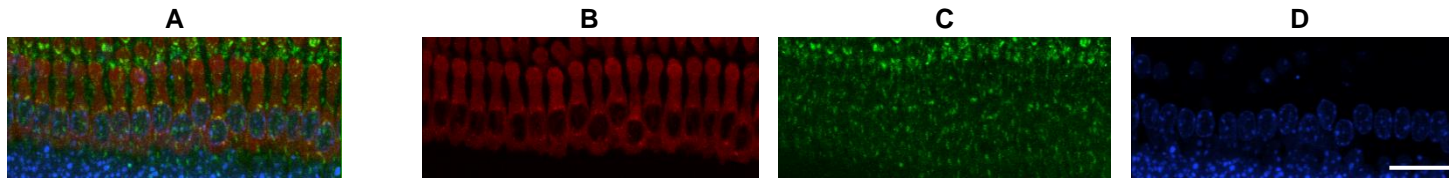


Figure 2.10 – Example of raw images (pre-processed) for the inner hair cell region. (A) Merged image of B, C and D. (B) MyosinVIIa signal. (C) TIA-1 signal. (D) DAPI signal. Scale bar= 25 μ m.

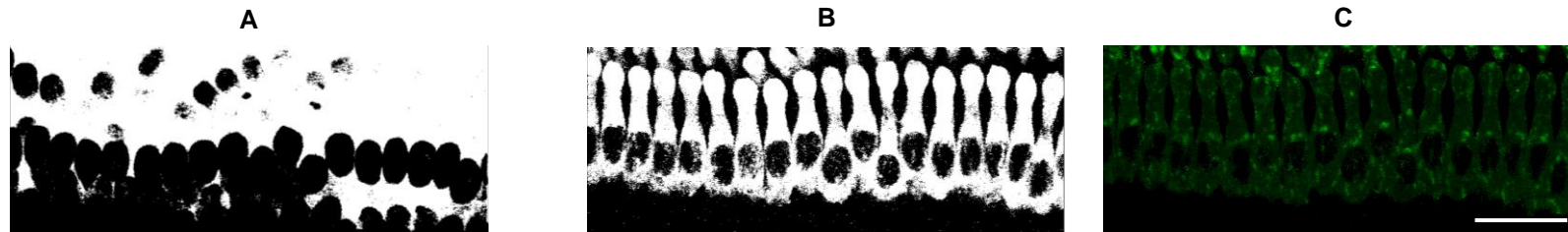


Figure 2.11 – Example of processed images for the inner hair cell region. (A) DAPI image after thresholding and binary processing. (B) MyosinVIIa signal image is shown after thresholding and binary processing. MyosinVIIa was here used to with value 1 (white areas) to isolate the hair cells, whereas the background (in black) has value 0. (C) Result from multiplication of TIA-1 signal alone (as in Fig.2.10 C) by the binary image for myosinVIIa and DAPI (i.e. TIA-1 signal in the cytoplasm of hair cells only). Scale bar= 25 μ m.

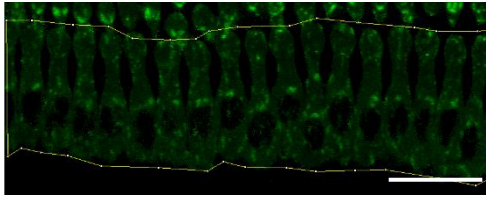


Figure 2.12 – TIA-1 area delineated in hair cells (in yellow) to be considered for further analysis using SG counter plugin. Scale bar= 25µm.

Results						
File	Edit	Font	Results			
	Area	Mean	Min	Max	XStart	YStart
127	0.903	2324.976	2008	2708	746	258
128	0.948	2730.140	2048	3436	673	260
129	0.022	2008.000	2008	2008	625	268
130	0.507	2255.478	2004	2572	839	272
131	0.198	2212.000	2072	2420	379	273
132	0.198	2052.889	2004	2092	808	276
133	0.771	2706.057	2004	3576	851	291

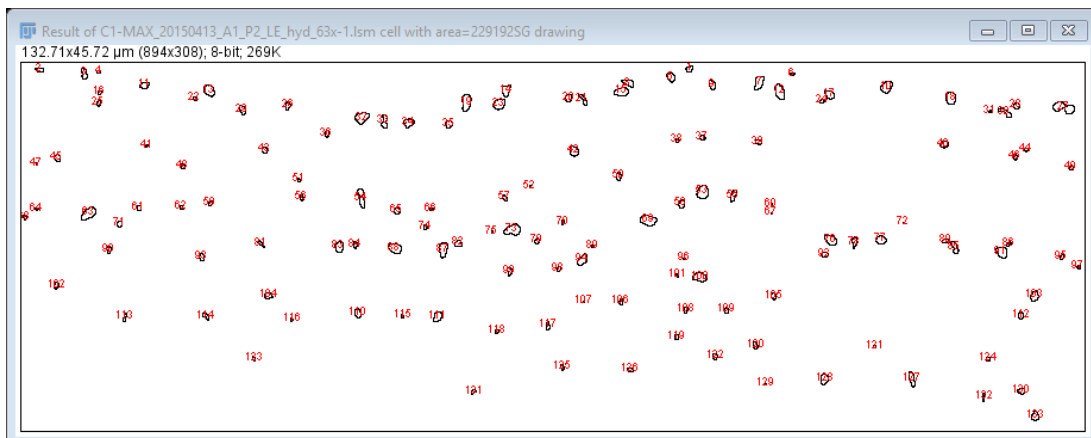


Figure 2.13 – SG counter plugin outputs after analysis for SGs in inner hair cells. The SGs identified by the plugin are listed (top panels) and information regarding area, mean intensity signal, minimum signal, maximum signal and X/Y coordinates is shown for each individual granule. A correspondent map showing the location of the SGs quantified in inner hair cells by the plugin is generated (bottom panels).

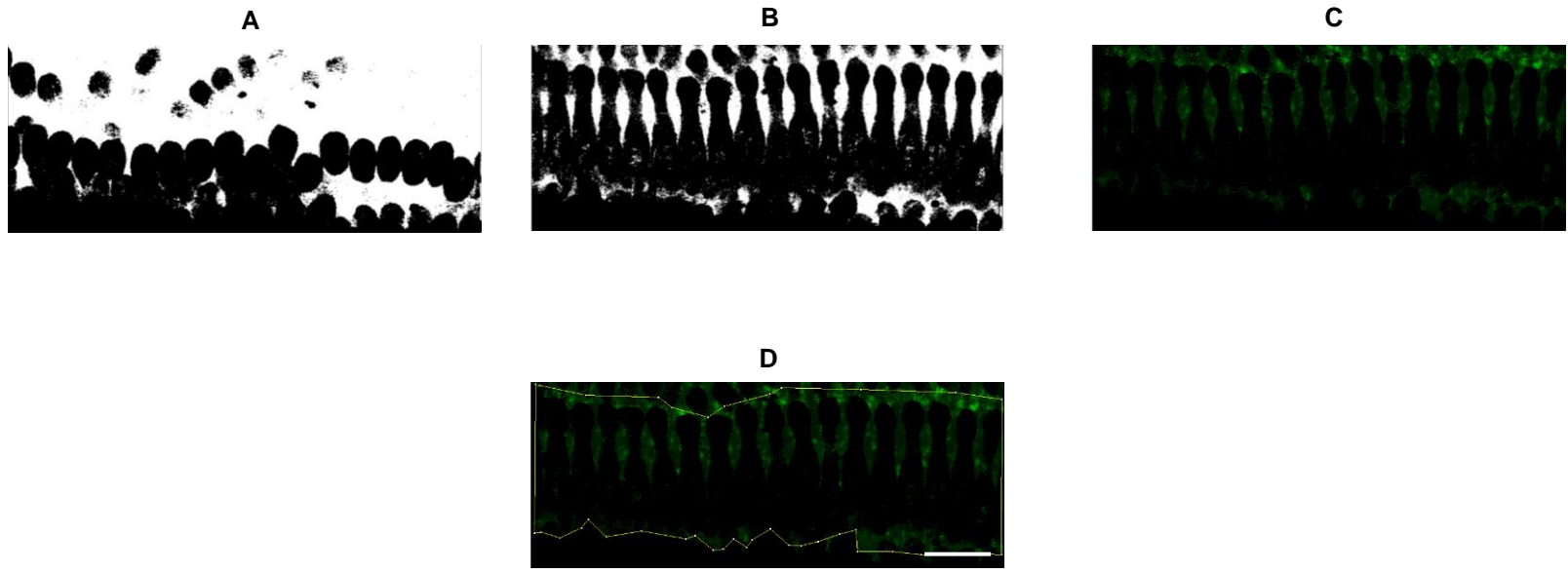


Figure 2.14 – Example of processed images for the supporting cells region. (A) DAPI image after thresholding and binary processing. (B) MyosinVIIa signal image is shown after thresholding and binary processing. MyosinVIIa was here used to with value 1 (white areas) to isolate the supporting cells from the hair cells, whereas the background (corresponding to the hair cell region, in black) has value 0. (C) Result from multiplication of TIA-1 signal alone (as in Fig.2.10 C) by the binary image for MyosinVIIa and DAPI (i.e. TIA-1 signal in the cytoplasm of hair cells only). (D) TIA-1 area delineated in supporting cells (in yellow) to be considered for further analysis using SG counter plugin. Scale bar= 25 μ m.

	Area	Mean	Min	Max	XStart	YStart
183	0.044	2028.000	2010	2046	719	304
184	0.044	2046.000	2028	2064	827	304
185	0.903	2253.073	2004	2580	755	307
186	0.022	2028.000	2028	2028	804	307
187	0.242	2183.455	2028	2334	791	310
188	0.331	2216.000	2016	2478	617	312
189	1.542	3067.029	2010	4830	844	312

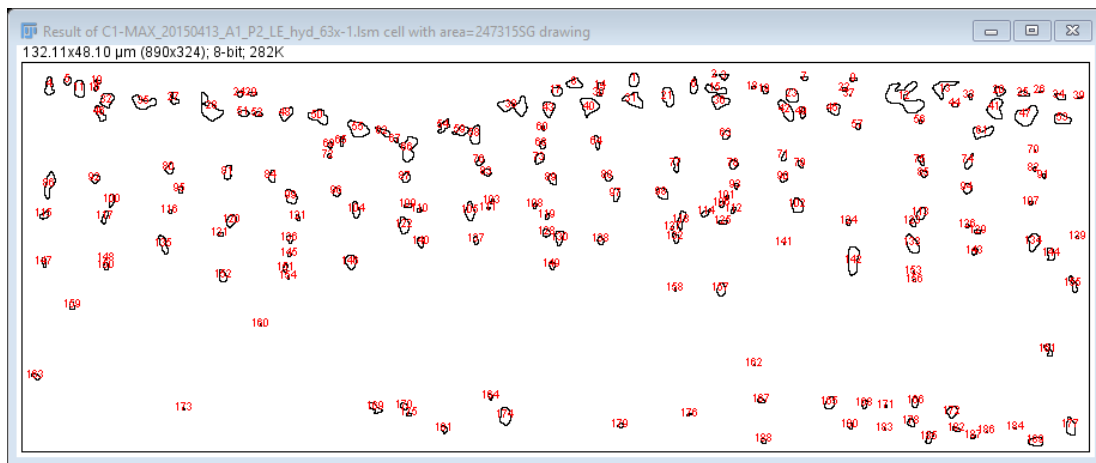


Figure 2.15 – SG counter plugin outputs after analysis for SGs in supporting cells. The SGs identified by the plugin are listed (top panels) and information regarding area, mean intensity signal, minimum signal, maximum signal and X/Y coordinates is shown for each individual granule. A correspondent map showing the location of the SGs quantified in supporting cells by the plugin is generated (bottom panels).

2.20. Calculations of stress granule density

Due to the multicellular and three-dimensional structure of the organ of Corti, SG quantification could not be precisely determined per cell, as it was performed before for OC-2 cells (single layer, without overlapping cells). Considering this, SG formation was estimated per cellular volume of hair cells and supporting cells. For this, hair cell volumes were approximated, by considering the similarity of the hair cell structure with a cylinder. Using Fiji (software), 24 hair cells were analysed (12

inner and 12 outer hair cells across 4 different images) and their average height (h), radius and nucleus radius were measured (Tables 2.2 and 2.3).

Table 2.2 – Measurements of inner hair cells (IHC) height, radius and nucleus radius.

	Height IHC	Radius IHC	Radius nucleus IHC
	16.9	4.2	3.8
	17.0	4.3	4.0
	17.5	3.8	3.6
	16.7	4.5	3.8
	17.6	4.2	3.5
	17.4	4.0	3.8
	17.0	4.3	3.3
	16.5	4.1	3.5
	17.0	4.6	3.6
	16.9	4.1	3.8
	17.0	4.0	3.8
	17.4	4.4	3.9
Average	17.1	4.2	3.7
1SD	0.3	0.2	0.2
Error	1.8%	4.7%	5.4%

Table 2.3 – Measurements of outer hair cells (OHC) height, radius and nucleus radius.

	Height OHC	Radius OHC	Radius nucleus OHC
1st row	17	4.3	3.4
	17.8	4.6	3.6
	17	3.9	3.6
2nd row	17.5	4.3	3.7
	17	4.2	4.3
	17	4	4
3rd row	17.7	3.9	3.9
	16.9	4.2	3.4
	16.9	4.4	3.3
	17.4	4.6	3.8
	16.9	4.3	3.6
	16.9	4.5	3.8
Average 1st row	17.3	4.25	3.5
Average 2nd row	17.1	4.0	3.9
Average 3rd row	17.0	4.4	3.6
Total average	17.2	4.2	3.7
1SD	0.3	0.2	0.2
Error	1.7%	4.7%	5.4%

Considering that the nuclear structure can be approximated to a sphere and that the hair cell structure can be approximated to a cylinder, the volumes of nucleus (V_n) and hair cells (V_c) were calculated by approximation using the following formulas:

$$V_n = \frac{4}{3} \pi r_n^3$$

$$V_c = \pi r^2 h$$

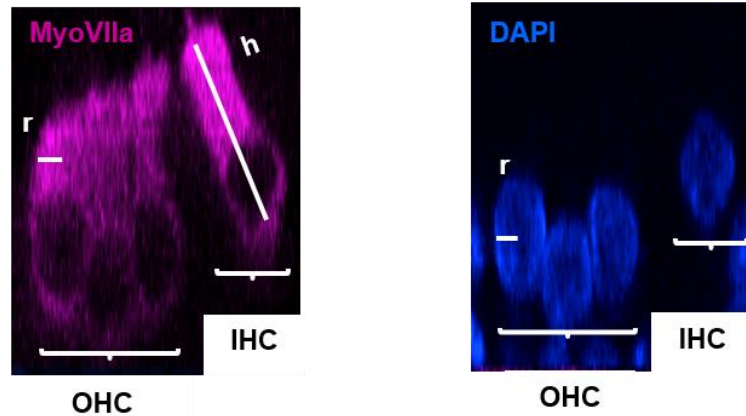


Figure 2.16 – Hair cell dimension measurements. Measurements included height (h), cell radius (r, in MyosinVIIa image) and nucleus radius (r, in DAPI image). Hair cells height and radius were obtained using MyosinVIIa signal and nucleus radius were obtained using DAPI signal, both in Fiji software.

Considering the polarised nature of hair cells, I hypothesised that there could be differential SG formation in different areas of the cells. For this, hair cells were divided into three distinct regions: basal, middle and luminal (Fig.2.17) and SG quantification assessed for the three different areas. The volume of luminal surface (V_L) corresponds to approximately $\frac{1}{3}$ of the whole hair cell volume, whereas the middle (V_M) and basal (V_B) surface's volumes correspond to approximately $\frac{1}{3}$ of the hair cell minus $\frac{1}{3}$ of the nucleus volume and $\frac{1}{3}$ of the hair cell volume minus $\frac{2}{3}$ of the nucleus volume, respectively, given the presence of the nucleus in those regions (Fig.2.17). In agreement with this, the cytoplasmic volume for each different region was calculated as follows:

$$V_L = \frac{1}{3} (\pi r^2 h) - 0$$

$$V_M = \frac{1}{3} (\pi r^2 h) - \frac{1}{3} (\frac{4}{3} \pi r^3)$$

$$V_B = \frac{1}{3} (\pi r^2 h) - \frac{2}{3} (\frac{4}{3} \pi r^3)$$

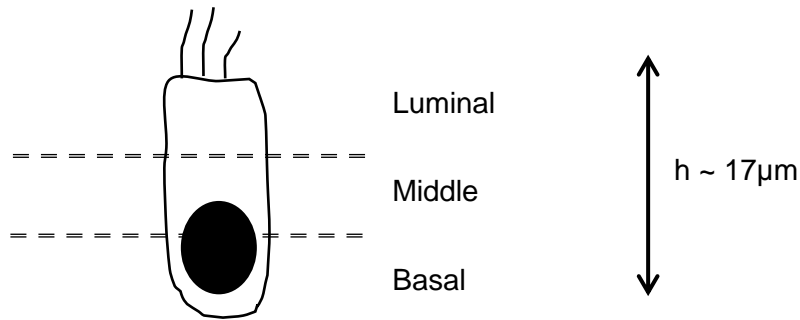


Figure 2.17 – Representation of the different regions considered for analysis of SG density in hair cells.

To determine the density of SGs per hair cell region, the SGs previously quantified by the SG counter plugin were then multiplied by the correspondent cytoplasmic volumes and obtained as approximated number of SGs per μm^3 of hair cell region.

Ideally, assessments of SG formation would be performed individually for each different supporting cell type but, due to the multicellular structure of the organ of Corti, the borders between the different supporting cells could not be distinguished across the different cells. Thus, to calculate the density of SGs in supporting cells, two different regions were considered in the organ of Corti: the lesser and greater epithelial ridges. This involved the supporting cells surrounding the inner hair cells and outer hair cells, derived from developmental stages as described in (Kelley 2007). The lesser epithelial ridge comprises the outer sulcus cells, whereas the greater epithelial ridge comprises the inner phalangeal cells and border cells (Kelley 2007).

2.21. Quantification of surviving hair cells

Quantification of surviving hair cells was based on two markers: MyosinVIIa and DAPI. Hair cells were considered healthy / surviving when presenting regular MyosinVIIa protein distribution throughout the cell's body and absent from the nucleus. Healthy cells were confirmed by regular DAPI staining without visible chromatin condensation (Fig.2.18). When cells presented irregular MyosinVIIa distribution (e.g. not distributed across the whole cell body or revealing nuclear presence) and / or irregular DAPI staining (e.g. chromatin condensation and nuclear shrinkage), cells were not considered as healthy, thus being counted as dead cells.

Figure 2.18 shows examples of healthy and dead cells for the purpose of quantification.

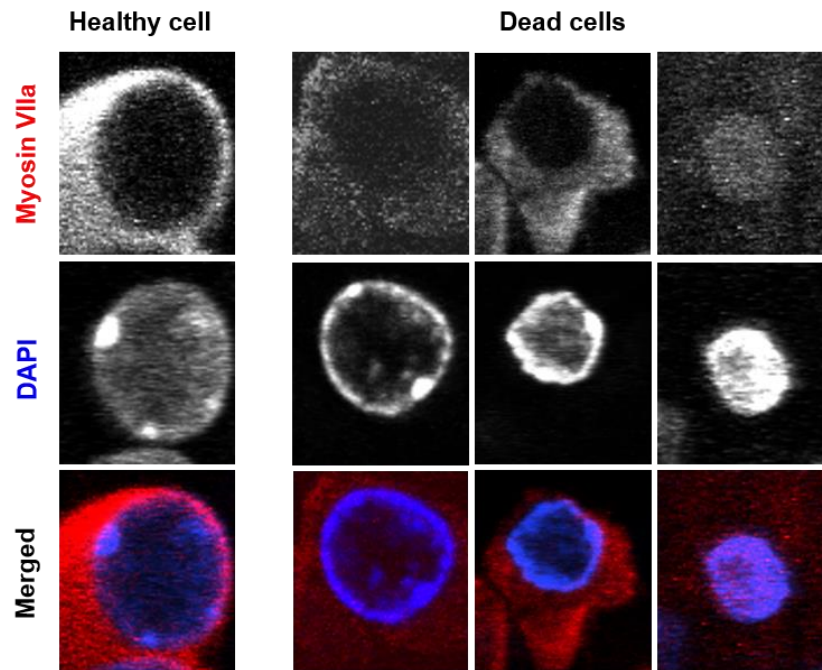


Figure 2.18 – Examples of healthy and dead hair cells, based on MyosinVIIa and DAPI signals.

3. Dynamics of SG assembly during stress in the OC-2 cell line

3.1. Introduction

Since their first description in tomato cells as heat granules (Nover et al. 1983), SGs have been the focus of intense research. Many studies have linked SGs to sites of dynamic shuttling of RNA molecules, thus contributing to RNA sorting and cell survival decisions during acute cellular stress (Kedersha et al. 1999; Kedersha et al. 2002; Kedersha et al. 2005). Electron microscopy examination has shown that SGs are non-membrane bound structures, averaging between 1-2 μm^2 (Souquere et al. 2009). Evidence suggests that SGs form rapidly after exposure to stress and disassemble once the stress has finished over a period of approximately 3 hours (Kedersha et al. 2002; Souquere et al. 2009). A number of stress sensor kinases that phosphorylate the regulatory serine of eIF2 α in response to different types of stress have been described (Chen & London 1995; Harding et al. 2000; Williams 2001; Dever 2002). Phosphorylation of eIF2 α has been indicated as a key event in triggering SG formation through disruption of the translation initiation complexes (Kedersha et al. 1999). PolyA⁺ mRNA, RNA-binding proteins, transcription factors and apoptosis molecules, amongst others, have been determined to be components of SGs, thus contributing to the evidence that SGs play an important role in cell survival decisions (Kedersha et al. 1999; Kedersha et al. 2002; Tourrière et al. 2003; Kim et al. 2005; Ohn et al. 2008; Papadopoulou et al. 2013). Along with this, impairment of SG formation has been shown to decrease cell survival during stress conditions (Buchan & Parker 2009), corroborating the hypothesis that SGs present cytoprotective effects. However, dysregulation of SG formation has been recently linked to neurodegeneration (Aulas et al. 2012; Ash et al. 2014). SG-marker proteins such as TIA-1, G3BP1 and TDP-43 were associated with protein aggregates present in Alzheimer's, Huntington's and ALS diseases, for instance. Malfunction of SGs is hypothesised to provide an ideal environment for the formation of pathological inclusions that along with repression of translation and/or trapping of essential RNA-binding proteins, contribute to the onset of several neurodegenerative proteinopathies (Aulas et al. 2012; Ratovitski et al. 2012; Vanderweyde et al. 2012; Ash et al. 2014; Bentmann 2013).

A number of different stresses have been associated with hair cell loss, including ageing, noise trauma and aminoglycoside exposure (Forge & Schacht 2000; Chen & Fechter 2003; Perez & Bao 2011; Huth et al. 2011). The damage and loss of mammalian hair cells is directly related with hearing impairment, since there is no natural regenerative mechanism to replace lost hair cells and, consequently, restore hearing (Martini 2007). Therefore, the development of preventative strategies to avoid hair cell damage and loss during stress may constitute a significant pathway towards prevention of hearing loss.

Previous work from our laboratory has shown that neonatal mouse cochlear explants assemble SGs as a consequence of aminoglycoside exposure (Towers et al. 2011), thus implicating SGs in the cochlea's response to stress. Despite these observations, detailed characterisation and quantification of SGs in the auditory system has not been described yet. This chapter and the initial studies of this thesis provide a detailed description of SG assembly in response to two different stressors, heat shock and sodium arsenite in an inner ear-derived cell line. The investigation is subsequently extended into pharmacological manipulation of SG formation.

3.2. Results

3.2.1. Heat shock stress triggers SG formation in the OC-2 cell line

The mammalian organ of Corti represents a challenge in hearing research: hair cells are present at a relatively low number, do not regenerate after embryonic development, are difficult to access (embedded within the temporal bone of the skull) and do not proliferate (Martini 2007). Considering these experimental constraints, the OC-2 cell line (Rivolta et al. 1998) was chosen to develop the initial studies of this project (see section 2.1 in methods).

Although OC-2 cells present experimental limitations when compared to the multicellular structure of the inner ear (e.g. lack of other cell markers, absence of differentiation) they are established as a suitable inner ear-derived cell line to develop assays and have been used in a number of different studies (Jagger et al. 2000; Clough et al. 2004; Brunetta et al. 2012).

SGs constitute a relatively recent field of study and their role in the inner ear is yet poorly understood. Since their first description in mammalian cells, TIA-1 protein has been widely used as a marker of SGs. Additionally, detection of polyA⁺ mRNA is crucial to further confirm the RNA/protein nature of SGs (Kedersha et al. 1999; Kedersha et al. 2000). Recently, Caprin-1 was reported to associate with SGs in cochlear hair cells (Towers et al. 2011), thus constituting an important additional marker for SGs in an inner ear context. Considering this, TIA-1 and Caprin-1 proteins were chosen to label SGs in this work, along with the detection of polyA⁺ mRNA.

Herein, OC-2 cells were used to study and assess SG formation and regulation in an inner ear context. In order to characterise the SG response of the auditory system, the first aim was to develop a robust assay to identify polyA⁺ mRNA simultaneously with TIA-1 and Caprin-1 proteins in OC-2 cells.

Heat shock was one of the stressor agents used in this study (see introduction section 1.9), since it is a well-known stressor that has been shown to trigger SG formation in different cell lines, such as DU145 or HeLa cells (Kedersha et al. 1999; Kedersha & Anderson 2002). Consequently, the heat shock paradigm used in this work to stress OC-2 cells was adapted from experimental conditions published elsewhere (Kedersha et al. 1999). OC-2 cells were firstly subjected to 43°C for 1h and then allowed to recover for 1h, 2h and 4h at 33°C, the normal culture temperature for OC-2 cells (see methods section 2.5).

RNA-Fluorescence *in situ* hybridisation (FISH) was combined with immunocytochemistry followed by confocal imaging for the first time in the OC-2 cell line (see methods section 2.14), enabling the detection of polyA⁺ mRNA simultaneously with SG-marker proteins Caprin-1 and TIA-1.

In control untreated cells (cultured at 33°C), polyA⁺ mRNA was distributed throughout the nucleus and the cytoplasm (Fig.3.1, panel B). Since the labelling of polyA⁺ mRNA detects the mature RNA molecules that have been polyadenylated and are consequently ready for translation, polyA⁺ mRNA was expected to localise in both nucleus, where the polyadenylation mechanism occurs, and in the cytoplasm where translation takes place. These data are consistent with previous observations in other cell lines, such as DU145 and U2OS (Kedersha et al. 1999; Zurla et al. 2011). TIA-1 protein was also found to distribute throughout the nucleus and the cytoplasm in untreated cells (Fig.3.1, panel C), whereas Caprin-1 was found widely distributed across the cytoplasm (Fig.3.1, panel A). The distribution of both Caprin-1 and TIA-1 proteins in untreated OC-2 cells is in agreement with previous studies in other cell lines (e.g. DU145, HeLa, 3T3, Sa-OS2) (Kedersha et al. 1999; Solomon et al. 2007; Sabile et al. 2013).

After 1h heat shock stress, SG formation was observed by the cytoplasmic aggregation of polyA⁺ mRNA with the SG-marker proteins Caprin-1 and TIA-1 (Fig.3.1, white arrows). These resembled the SGs reported by other authors, in terms of cytoplasmic distribution and components (Kedersha et al. 1999; Aulas et al. 2015). PolyA⁺ mRNA was identified for the first time, in an inner ear-derived cell line, as a component of Caprin-1 and TIA-1 positive SGs (Fig.3.1, panels E-G and merged panel H), thus confirming the RNA-containing nature of the SGs previously reported to occur in the OC-2 cell line (Towers et al. 2011). Although distributed across the cytoplasm, some SGs of small size were found to be present around the perinuclear region after heat shock treatment (Fig.3.1, yellow arrowheads).

When OC-2 cells were allowed to recover over a period of 4h, less SG aggregates were observed in the cytoplasm of the cells (Fig.3.1, panels I-T). Interestingly, the SGs found after 1h and 2h recovery were located near the nucleus (Fig.3.1, panels I-L and M-P). After 4h recovery from heat shock, polyA⁺ mRNA presented a similar distribution to untreated cells, without visible cytoplasmic aggregation (Fig.3.1, panel R). Correspondingly, by 4h of recovery, the distribution of Caprin-1 and TIA-1 SG-marker proteins resembled that of untreated cells: Caprin-1 mostly distributed

across the cytoplasm without granular aggregation and TIA-1 distributed across the nucleus and the cytoplasm (Fig.3.1, panels Q and S, respectively).

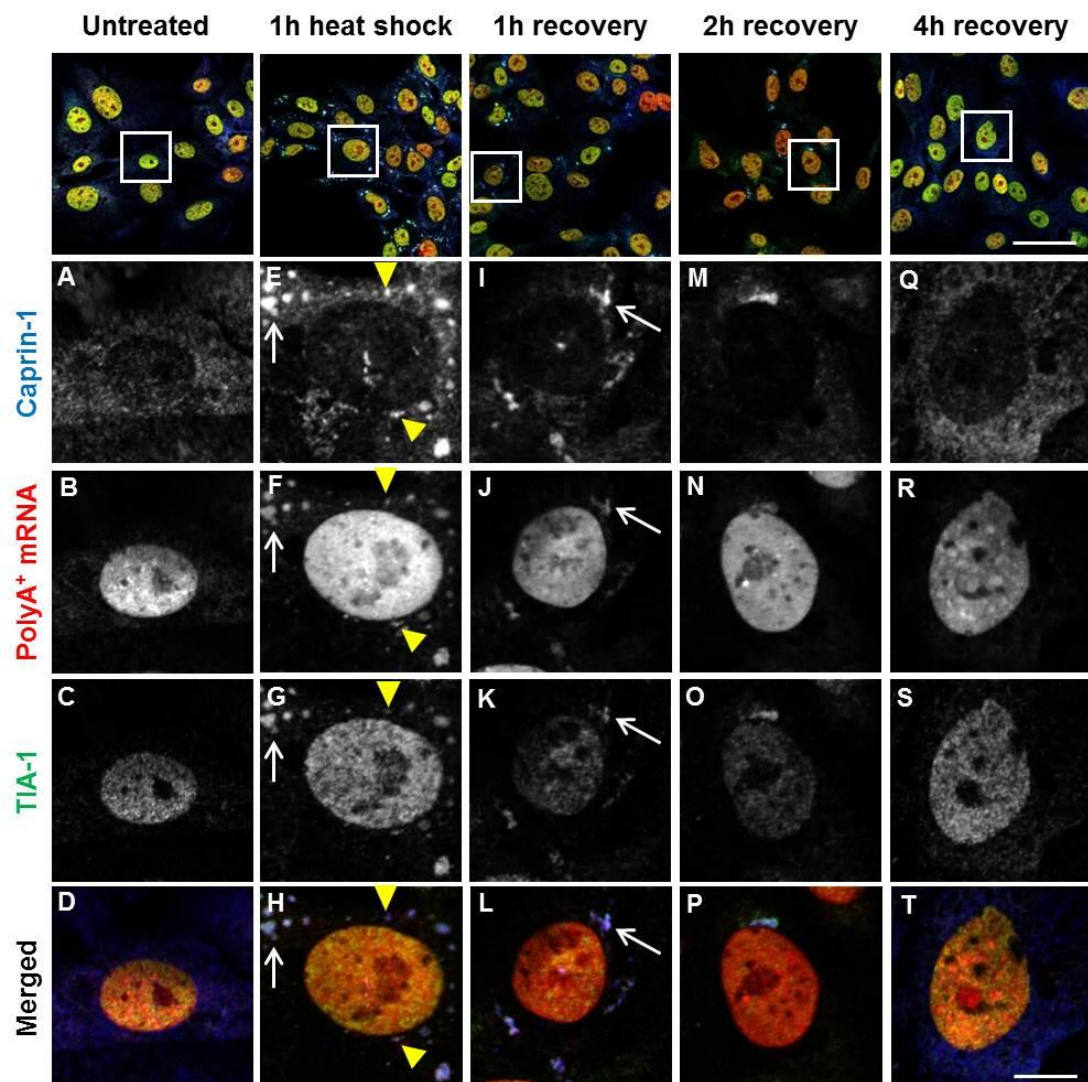


Figure 3.1 – Caprin-1 and TIA-1 aggregate with polyA⁺ mRNA at cytoplasmic SGs after heat shock stress. OC-2 cells were treated with heat shock for 1h at 43°C and allowed to recover at 33°C for 1h, 2h and 4h. Caprin-1/TIA-1 protein distribution is shown across different time-points during the heat shock stress study. PolyA⁺ mRNA was detected using a Cy3-labelled probe. White arrows point to SGs. Yellow arrowheads point to perinuclear SGs. Scale bar= 50 μm for top panel and 10 μm for boxed images.

Although some studies have attempted to quantify the percentage of cells containing SGs in different systems upon stress (Buchan et al. 2013; Arimoto-Matsuzaki et al. 2016), there is no standard quantification protocol available so far in the SG field. Here, a protocol aimed at quantifying the number and size of SGs was

developed for the first time (see methods section 2.19.1), enabling a comprehensive description of the SGs formed upon stress. Objective quantification of the SGs size, distribution and frequency also allows comparisons with that reported by other authors and to further understand how different stressors regulate SG formation in different cell types. In addition, a comprehensive quantification of SGs is here presented for the first time during post-stress recovery, to further understand how different stressors influence SG disassembly, in terms of SG number, size and frequency.

Quantification of the number of SGs corroborates RNA-immuno-FISH data and confirms that OC-2 cells assemble SGs in response to heat shock stress (Fig.3.2 A). In fact, upon heat shock, on average 3.1 ± 0.02 polyA⁺ mRNA aggregates were found to be present in the cytoplasm of each cell (Fig.3.2 A). Consistently, 3.3 ± 0.11 Caprin-1 and 2.6 ± 0.22 TIA-1 positive SGs were formed per cell after 1h heat shock stress (Fig.3.2 A). When compared to untreated control samples, the SGs quantified after 1h heat shock were statistically significant (Fig.3.2 A). Following heat shock stress, Pearson's correlation coefficient between polyA⁺ mRNA and Caprin-1 was determined as $r = 0.98$, as given by colocalisation analysis and an r of 0.97 for polyA⁺ mRNA and TIA-1.

Quantification confirmed the progressive reduction in SGs during the recovery period when compared to 1h heat shock (Fig.3.2 A). At 4h recovery from heat shock stress, the number of SGs were significantly reduced when compared to the number of SGs found after 1h heat shock (Fig.3.2 A), indicating that SGs disassembled during the 4h recovery period, reducing to 92% for polyA⁺ mRNA, 89% for Caprin-1 and 94% for TIA-1 positive SGs when compared to the number of granules formed after 1h heat shock (Fig.3.2 A). Moreover, when compared to the untreated condition, the amount of SGs quantified at 4h recovery was not statistically significant at $p < 0.05$ (one-way ANOVA, post-hoc Tukey test) (Fig.3.2 A), indicating a full recovery.

Across the time-points tested, quantification of the size of SGs did not reveal any statistical significant differences among polyA⁺ mRNA, Caprin-1 and TIA-1 positive SGs (Fig.3.2 B). PolyA⁺ mRNA aggregates averaged $1.5 \pm 1 \mu\text{m}^2$, whereas Caprin-1 averaged $1.6 \pm 0.5 \mu\text{m}^2$ and TIA-1 positive SGs averaged $1.4 \pm 0.6 \mu\text{m}^2$ after 1h of heat shock (Fig.3.2 B).

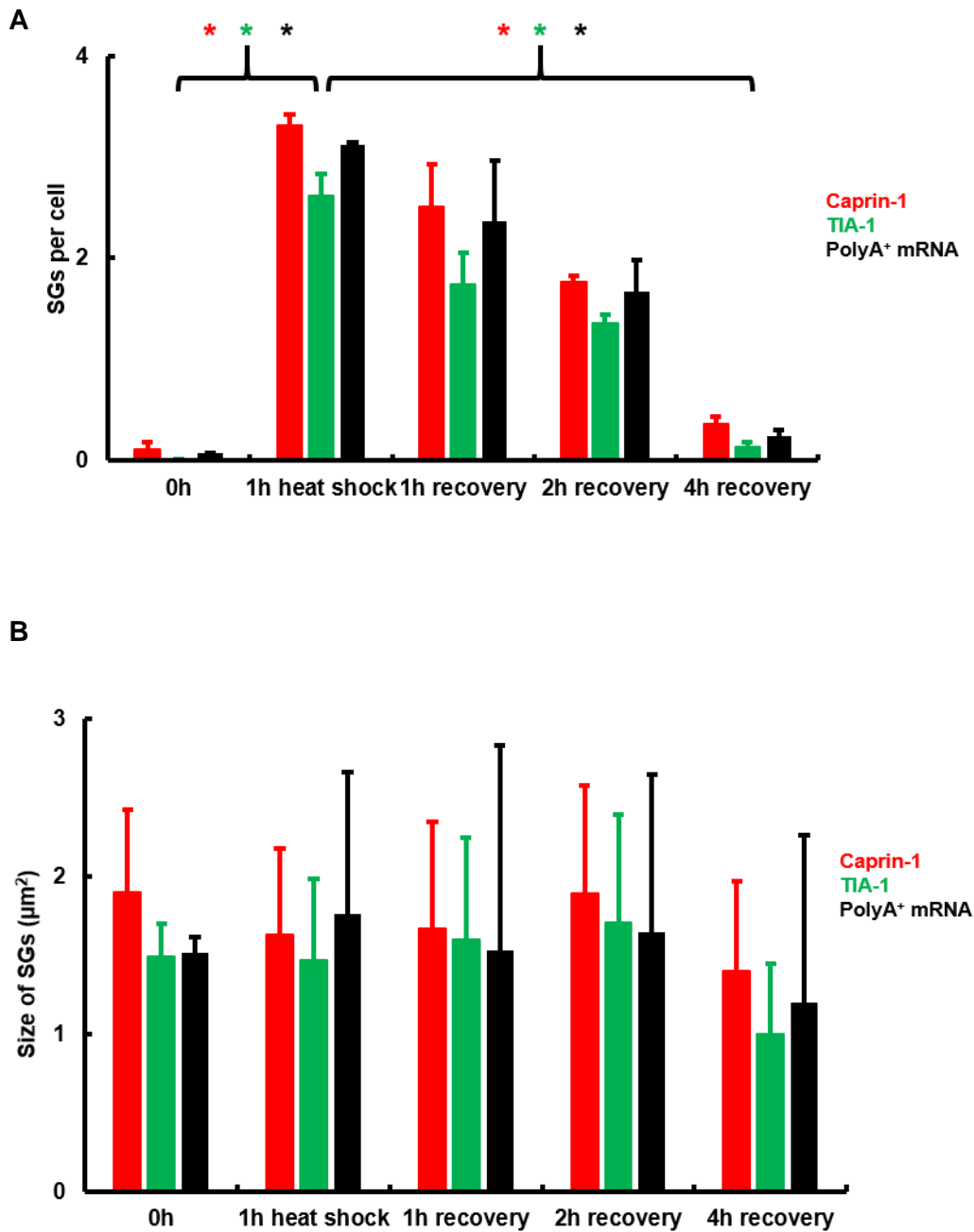


Figure 3.2 – Quantification of SGs using three different markers during heat shock study. (A) Average number of SGs per cell. (B) Average size of SGs (μm^2). OC-2 cells were submitted to heat shock stress for 1h at 43°C and allowed to recover for 1h, 2h and 4h at 33°C. Untreated condition is marked as 0h. Red bars represent Caprin-1, green bars represent TIA-1 and black bars represent polyA⁺ mRNA. Data were obtained from 3 separate experiments with triplicates and represent the average of the 9 samples. * $p < 0.05$, one-way ANOVA, post-hoc Tukey test. Error bars represent SEM.

The distribution of SG sizes was fairly uniform across the different time-points tested and followed a normal distribution skewed to the SGs of smaller size: Caprin-1-positive SGs presented the same pattern as TIA-1-positive SGs across the whole experiment, revealing more granules of smaller size (between $0.2 \mu\text{m}^2$ and $2 \mu\text{m}^2$) and less granules of larger size (from $2 \mu\text{m}^2$ up to $11 \mu\text{m}^2$) (Fig.3.3).

The cell density on the coverslips was consistent throughout all the time-points tested and cells did not present features comparable with increased cellular death.

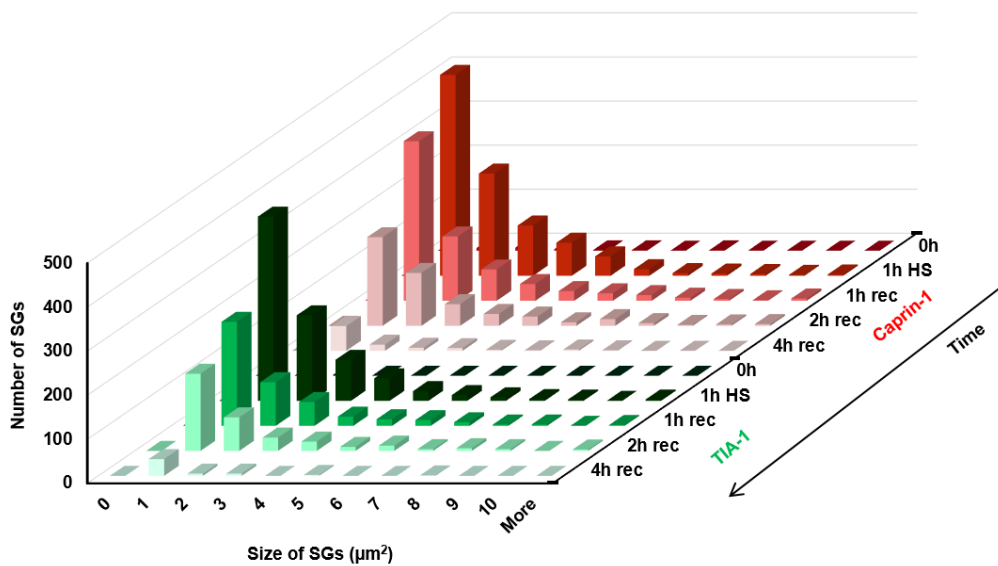


Figure 3.3 – Frequency histogram showing the distribution in size of SGs using two different markers during heat shock study. Values correspond to the total number of SGs observed before heat shock (0h, 33°C), after 1h heat shock (1h HS) at 43°C and different recovery (rec) periods (1h, 2h and 4h at 33°C). The y-axis represents the frequency of SGs, the x-axis indicates the size of SGs (from 0-10 μm^2 and more) and the z-axis indicates the time-points considered in this study, repeated for both Caprin-1 and TIA-1. The values represented here are the total frequency of SGs obtained from 9 samples.

3.2.2. Sodium arsenite stress triggers SG formation in the OC-2 cell line

Sodium arsenite was an additional stressor used to study the nature and components of SG formation and regulation in the OC-2 cell line. Sodium arsenite activates different cellular stress sensor kinases from heat shock (see introduction section 1.9) and has been extensively reported by other authors to induce SG formation (Kedersha et al. 2002; Kubacka et al. 2013; Aulas et al. 2015; Ohshima et al. 2015).

As in the previous section (3.2.1), the same methodology to detect and quantify SGs was used here.

OC-2 cells were incubated with 0.5mM of sodium arsenite for 1h, based on previous experimental conditions published elsewhere (Kedersha et al. 1999; Kedersha et al. 2000). As before, cells were allowed to recover for 1h, 2h and 4h in an arsenite-free medium.

As described before, in control untreated cells, Caprin-1 was found to be widely distributed in the cytoplasm (Fig.3.4, panel A), whereas polyA⁺ mRNA and TIA-1 were distributed throughout the nucleus and the cytoplasm (Fig.3.4, panels B and C, respectively).

After arsenite stress, Caprin-1 and TIA-1 proteins aggregated with polyA⁺ mRNA at SGs in the cytoplasm (Fig.3.4, panels E-H, white arrows). This is in agreement with previous results with heat shock stress (i.e. SG formation and components, Fig.3.1) and shows for the first time aggregation of polyA⁺ mRNA with Caprin-1 and TIA-1 proteins following arsenite treatment in the OC-2 cell line. The presence of small SGs in the perinuclear area following arsenite stress (Fig.3.4, panels E-H, yellow arrowheads) is also consistent with previous observations after heat shock (Fig.3.1).

When arsenite-treated cells were allowed to recover, SGs gradually disassembled (Fig.3.4, panels I-T), as observed by the distribution of polyA⁺ mRNA, Caprin-1 and TIA-1 that, at 4h recovery, resembled that of untreated samples. The reduction in the number of SGs during the recovery period is consistent with previous observations with heat shock (Fig.3.1) and is in agreement with others (Kedersha et al. 1999).

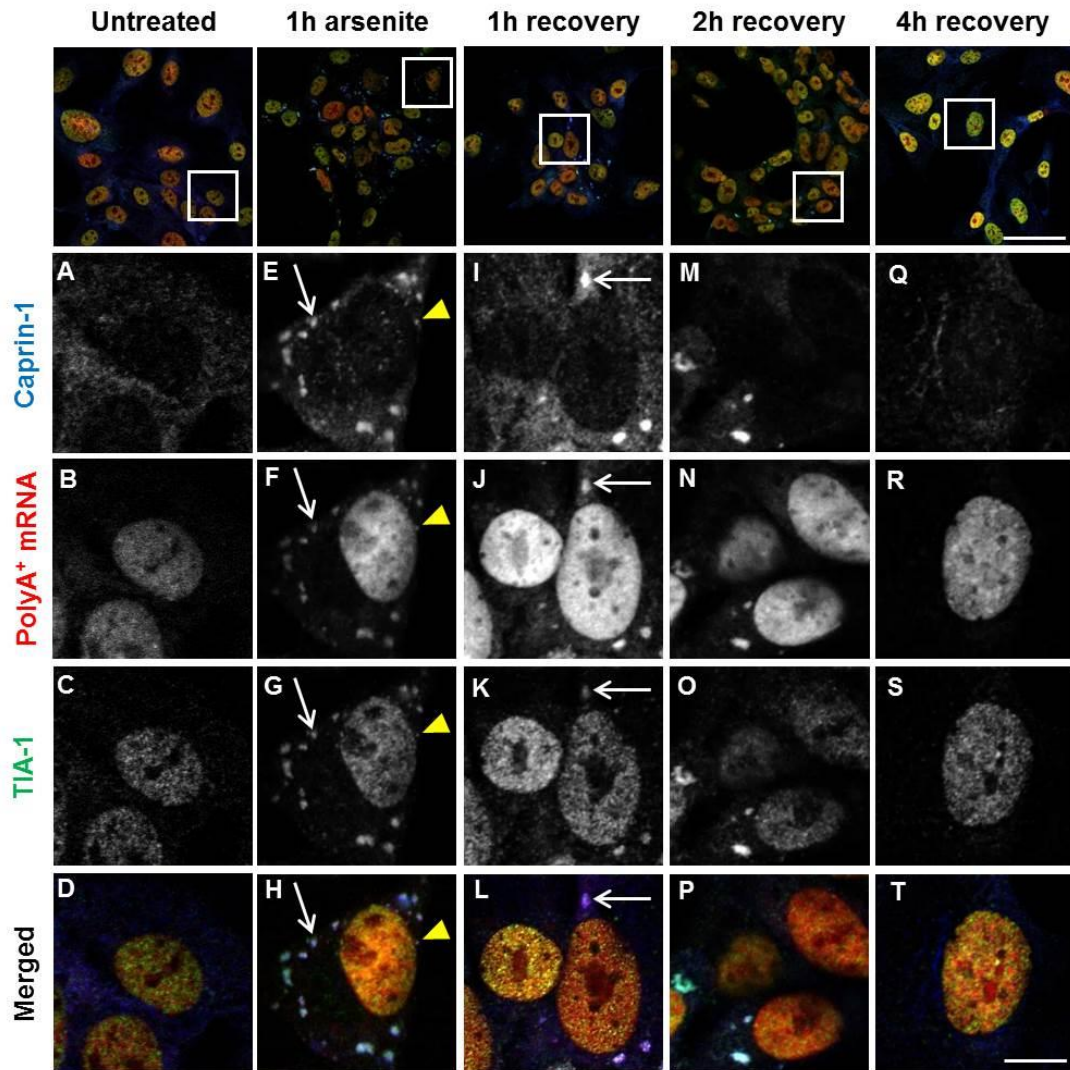


Figure 3.4 - Caprin-1 and TIA-1 aggregate with polyA⁺ mRNA at cytoplasmic SGs after sodium arsenite stress. OC-2 cells were treated with 0.5mM of sodium arsenite for 1h and allowed to recover in an arsenite-free medium for 1h, 2h and 4h. Caprin-1/TIA-1 protein distribution is shown across different time-points during arsenite stress study. PolyA⁺ mRNA was detected using a Cy3-labelled probe. White arrows point to SGs and yellow arrowheads point to perinuclear SGs. Scale bar= 50 μ m for top panel and 10 μ m for boxed images.

After 1h arsenite stress exposure, an average of 8.9 ± 1.1 polyA⁺ mRNA SGs were found in the cytoplasm of the cells (Fig.3.5 A). On average, 10.4 ± 0.9 Caprin-1-positive and 8.0 ± 0.9 TIA-1-positive SGs were present per cell (Fig.3.5 A). These values were statistically significant when compared to the untreated condition (Fig.3.5 A) and corroborate the observations following RNA-immuno-FISH (Fig.3.4). The Pearson's correlation coefficient between polyA⁺ mRNA and Caprin-1 was determined as $r = 0.99$, similar to the correlation between polyA⁺ mRNA and TIA-1, $r = 0.99$, indicating colocalisation of all three markers.

When OC-2 cells were allowed to recover in an arsenite-free medium, the number of SGs decreased as a function of the recovery time (Fig.3.5 A). At the end of the 4h recovery, the number of SGs was significantly different from the number found after 1h arsenite stress (Fig.3.5 A), corresponding to a reduction of 98% for polyA⁺ mRNA and TIA-1 and 96% for Caprin-1 positive SGs. When compared to untreated conditions, the number of SGs found after 4h recovery from arsenite stress did not statistically differ at $p < 0.05$ (one-way ANOVA, post-hoc Tukey test) (Fig.3.5 A).

Together, these results indicate that when cells are allowed to recover from arsenite stress, the number of SGs decreases as a function of the recovery period and, at 4h after arsenite treatment, the recovery is complete.

PolyA⁺ mRNA aggregates averaged $1.7 \pm 0.8 \mu\text{m}^2$ during arsenite stress study (Fig.3.5 B), whereas Caprin-1 and TIA-1 positive SGs averaged $2 \pm 0.5 \mu\text{m}^2$ (Fig.3.5 B). The size of SGs did not statistically differ during the time points tested and presented the same distribution skewed to smaller granules, as observed for the heat shock experiment (Fig.3.6).

The total number of cells considered in this experiment was consistent throughout all the time points tested and, at these conditions, increased cellular death was not reported.

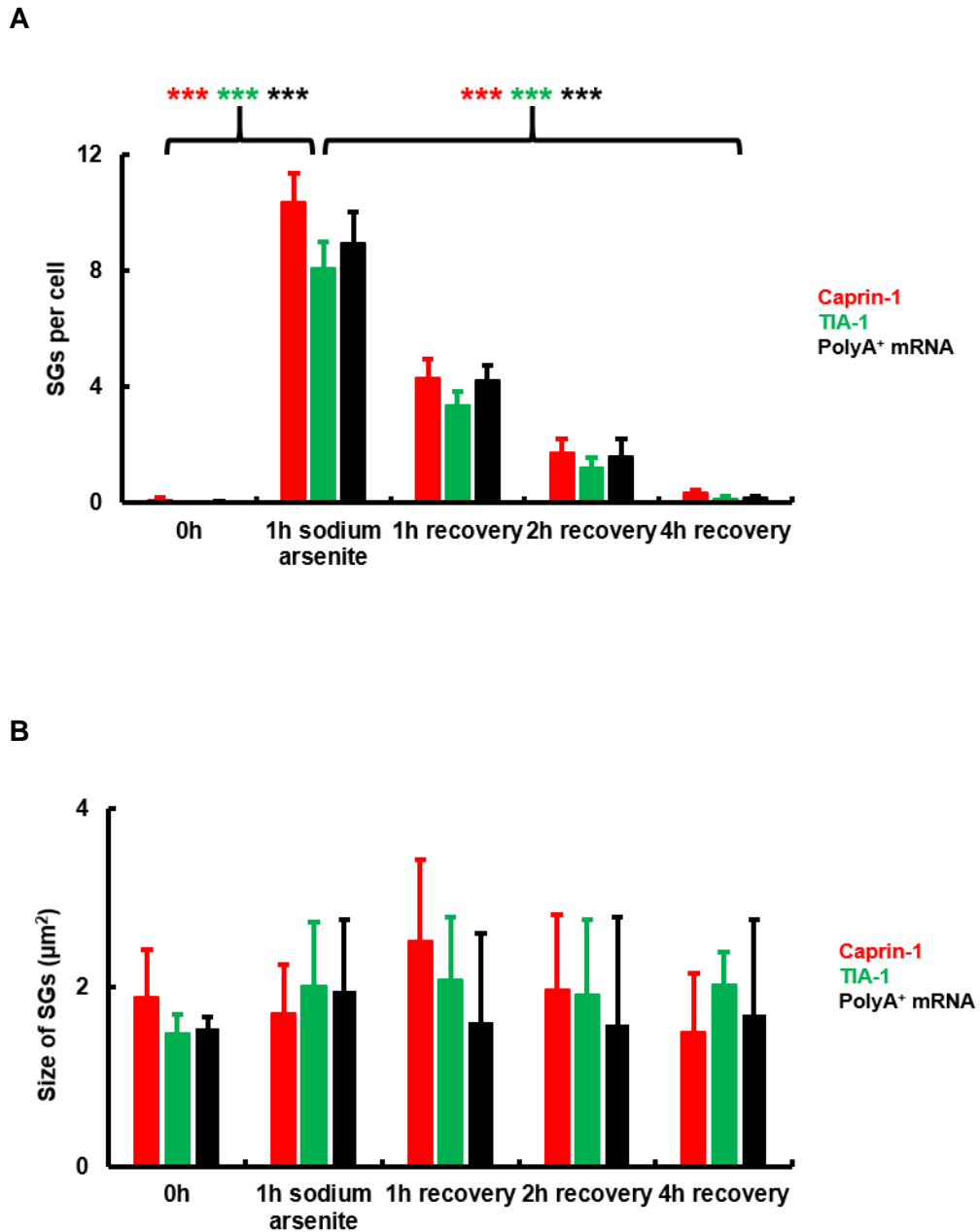


Figure 3.5 – Quantification of SGs using three different markers during sodium arsenite stress study. (A) Average number of SGs per cell. (B) Average size of SGs (μm^2). OC-2 cells were submitted to 0.5mM sodium arsenite for 1h and allowed to recover for 1h, 2h and 4h in an arsenite-free medium. Red bars represent Caprin-1, green bars represent TIA-1 and black bars represent polyA⁺ mRNA. Untreated condition is marked as 0h. Data were obtained from 3 separate experiments with triplicates and represent the average of the 9 samples. *** $p < 0.001$, one-way ANOVA, post-hoc Tukey test. Error bars represent SEM.

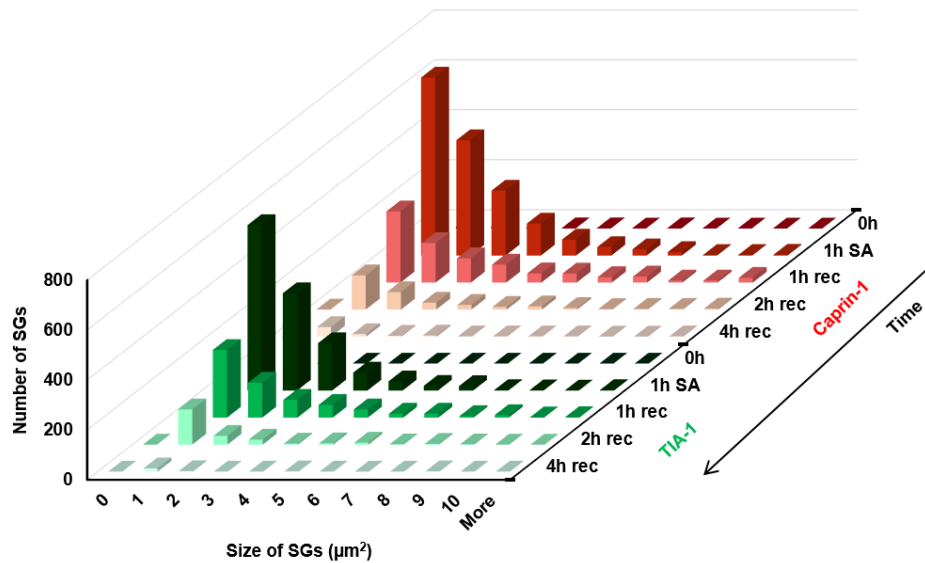


Figure 3.6 – Frequency histogram showing the distribution in size of SGs using two different markers during arsenite stress study. Values correspond to the total number of SGs observed before sodium arsenite stress (0h, untreated), after 1h 0.5mM sodium arsenite (1h SA) and after different recovery (rec) periods (1h, 2h and 4h in an arsenite-free medium). The y-axis represents the frequency of SGs, the x-axis indicates the size of SGs (from 0-10 μm^2 and more) and the z-axis indicates the time-points considered in this study, repeated for both Caprin-1 and TIA-1. The values represented here are the total frequency of SGs obtained from 9 samples.

All together, these experiments demonstrate that OC-2 cells respond to both heat shock and arsenite stresses by assembling SGs (Figs. 3.1 and 3.4, respectively). The development of robust assays to detect and quantify SGs (RNA-immuno-FISH and quantification) enabled confirmation of the RNA-containing nature of SGs formed in these cells and the number and size of SGs formed under different conditions. Additionally, recovery experiments showed that heat shock- and arsenite-triggered SGs disassemble over a recovery period of 4h, indicating that these stressors present reversible effects on the SG formation in the OC-2 cell line.

3.2.3. Pharmacological studies demonstrate that SG pathway can be manipulated in the OC-2 cell line

Several lines of evidence suggest that SGs are protective structures that promote cell survival during transient cellular stress (Kedersha et al. 1999; Kedersha et al. 2002; Buchan & Parker 2009; Arimoto-Matsuzaki et al. 2016). In the previous section, the successful assays developed to detect and quantify SGs demonstrated that OC-2 cells have the potential to assemble SGs as a response to stress and disassemble SGs when the stressors are removed (Figs.3.1 and 3.4). Next, different pharmacological compounds that modulate the assembly or inhibition of SGs were screened in the OC-2 cell line, considering the objective of future application in *ex-vivo* mouse cochlear explants. Ultimately, the hypothesis to explore is whether manipulating SG formation / disassembly prior to acute ototoxic stress can affect hair cell survival.

3.2.3.1. pp242 reduces SG formation during heat shock treatment in the OC-2 cell line

pp242 is a pyrazolopyrimidine that specifically inhibits members of the PI-3K family, mTORC 1 and 2 (Apsel et al. 2008; Feldman et al. 2009). The mTOR pathway is necessary for SG formation through 4E-BP1 phosphorylation (Fournier et al. 2013). When the mTOR pathway is disrupted, the specific binding of hypophosphorylated 4E-BP1 to eIF4E inhibits its association with eIF4G1, impairing the formation of mTORC1-dependent translation initiation complexes. mTORC1 inactivation by pp242 specifically inhibits SG formation through favouring the interaction of eIF4E with its hypophosphorylated 4E-BP1 inhibitory factor (Fournier et al. 2013). Targeting mTORC1-induced eIF4E-eIF4G1 association by the pp242-mediated hypophosphorylation of 4E-BP1 was shown to disrupt SG formation in HeLa cells (Fournier et al. 2013). Here, I tested whether pp242 could inhibit SG formation in the OC-2 cell line.

To assess whether SG formation could be pharmacologically inhibited in OC-2 cells, a range of different pp242 concentrations (0.025 μ M, 0.25 μ M, 2.5 μ M and 5 μ M) were applied for 24h prior to standard heat shock exposure. A DMSO control (at the highest DMSO concentration, 0.02%) was also tested. The pp242 concentrations chosen were based on previous studies (Feldman et al. 2009).

Immunocytochemistry followed by confocal imaging was used to detect Caprin-1 and TIA-1 SG-marker proteins. Quantification of SGs was performed as previously reported (section 2.19.1 in methods).

Heat shock treatment resulted in SG formation, as it can be seen by the cytoplasmic aggregation of Caprin-1 and TIA-1 in vehicle-treated controls (Fig.3.7, DMSO panel, white arrows). This is consistent with previous observations during heat shock experiments (section 3.2.1). When pp242 was used prior to heat shock stress and, as pp242 concentration was increased, the distribution of SG-marker proteins resembled that of unstressed cells more closely: Caprin-1 distributed across the cytoplasm and TIA-1 residing throughout the nucleus and cytoplasm (Fig.3.7, yellow arrows), indicating an effect of pp242 in preventing the aggregation of these proteins upon heat shock stress.

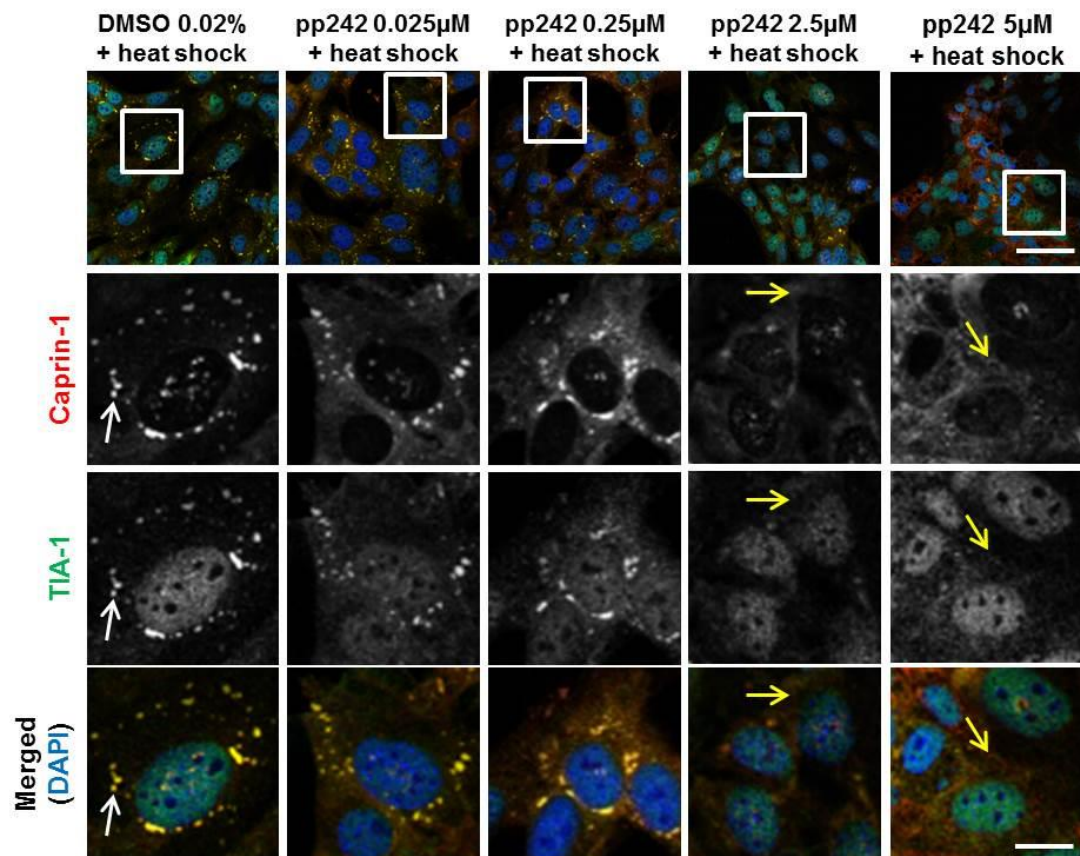


Figure 3.7 - pp242 reduces the formation of Caprin-1 and TIA-1 positive SGs during heat shock stress. OC-2 cells were pre-incubated with a range of pp242 concentrations (0.025, 0.25, 2.5 and 5µM) for 24h at 33°C prior to 1h exposure to heat shock stress at 43°C. Caprin-1/TIA-1 staining is shown for the DMSO control and the different pp242 concentrations tested. Chromatin structure was assessed using DAPI. White arrows point to SG formation and yellow arrows point to the effects of pp242 on the reduction of SGs. Scale bar= 25 µm for top panel and 10 µm for boxed images.

Quantification revealed that pre-incubation with pp242 before heat shock treatment significantly reduced the number of SGs formed, when compared to vehicle-treated controls (Fig.3.8 A). A reduction in SG formation was observed for all the pp242 concentrations used, when compared to the DMSO control, although this reduction was statistically significant at $p < 0.05$ (one-way ANOVA, post-hoc Tukey test) when using 0.25 μM and above for both Caprin-1 and TIA-1 positive SGs (Fig.3.8 A). At 2.5 μM , application of pp242 for 24 hours prior to heat shock reduced the average number of Caprin-1 and TIA-1 positive SGs per cell to 72 and 74% of control values, respectively (Fig.3.8 A). The average size of SGs was found not to significantly differ across the different pp242 concentrations tested (Fig.3.8 B) and the regular skewed distribution of more small granules and fewer large granules, as observed before for heat shock and sodium arsenite (sections 3.2.1 and 3.2.2, respectively), was observed across all the concentrations (Fig.3.9). This indicates that, at 2.5 μM and above, pp242 reduces the number of SGs formed upon heat shock stress in OC-2 cells without affecting the size of SGs.

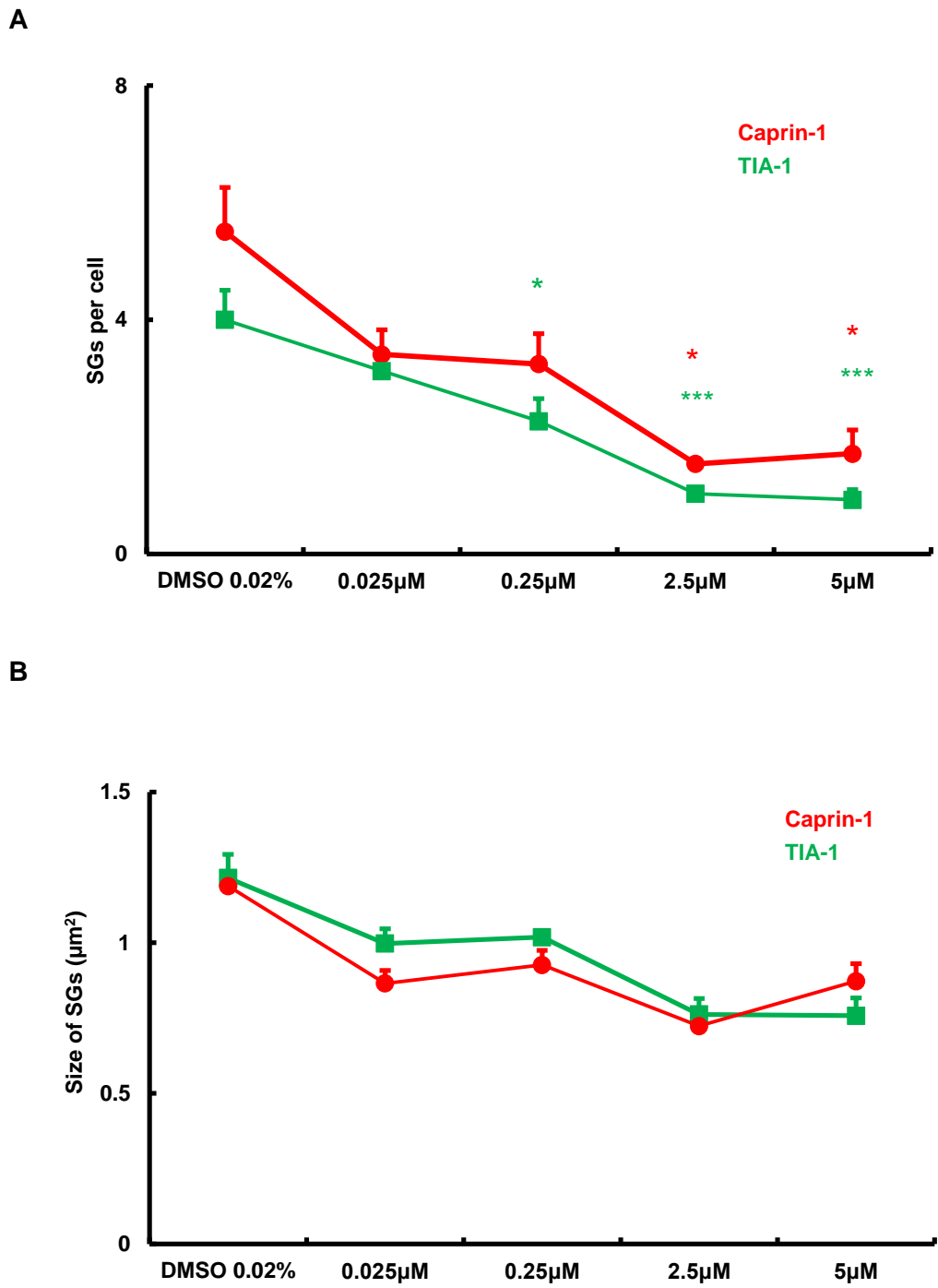


Figure 3.8 – Dose-dependent effect of pp242 on the number and size of SGs upon heat shock stress. OC-2 cells were incubated at 33°C for 24h with different concentrations of pp242 and DMSO as a control prior to heat shock exposure for 1h at 43°C. (A) Average number of SGs per cell. (B) Average size of SGs (μm^2). The values here represented were obtained from 3 separate experiments with triplicates and represent the average of the 9 samples. * $p < 0.05$; *** $p < 0.001$, one-way ANOVA, post-hoc Tukey test. Error bars represent SEM.

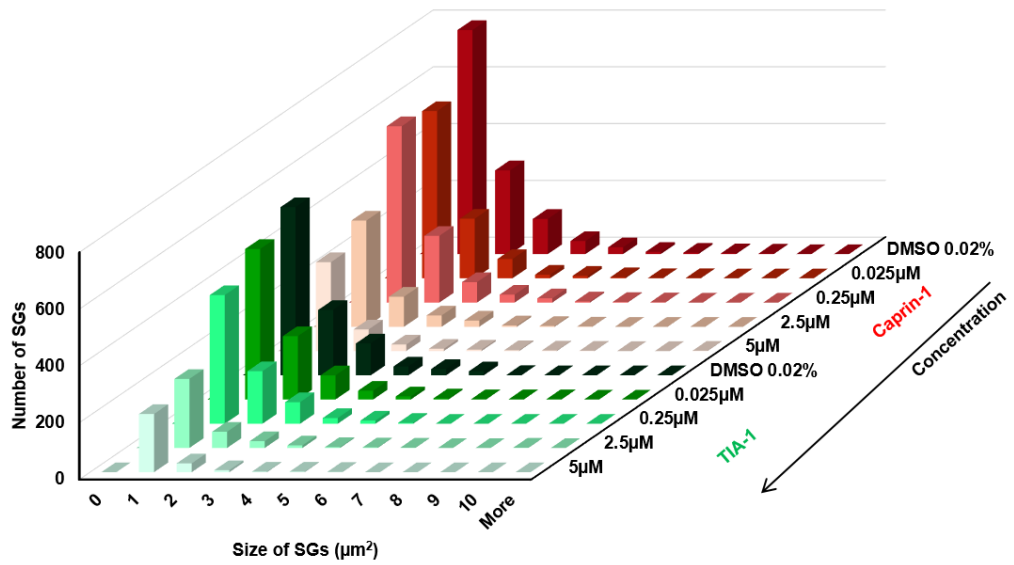


Figure 3.9 – Frequency histogram showing the distribution in size of SGs with pp242 exposure during heat shock stress. OC-2 cells were incubated with different concentrations of pp242 and DMSO as a control for 24h prior to heat shock treatment. The y-axis represents the frequency of SGs, the x-axis indicates the size of SGs (from 0-10 μm^2 and more) and the z-axis indicates the pp242 concentrations used in this study, repeated for both Caprin-1 and TIA-1. The values represented here are the total frequency of SGs obtained from 9 samples.

In order to minimise the exposure of cells to the compound, the effect of shortening pp242 pre-incubation time was tested.

OC-2 cells were pre-incubated with 2.5 μ M pp242 for 6h, 12h and 24h prior to 1h heat shock exposure. In comparison to vehicle-treated controls, the maximal pp242 effect on the SG reduction was observed with 24h pre-incubation, despite a reduction in the average number of Caprin-1 and TIA-1 positive SGs could be observed at all incubations times tested (Fig.3.10).

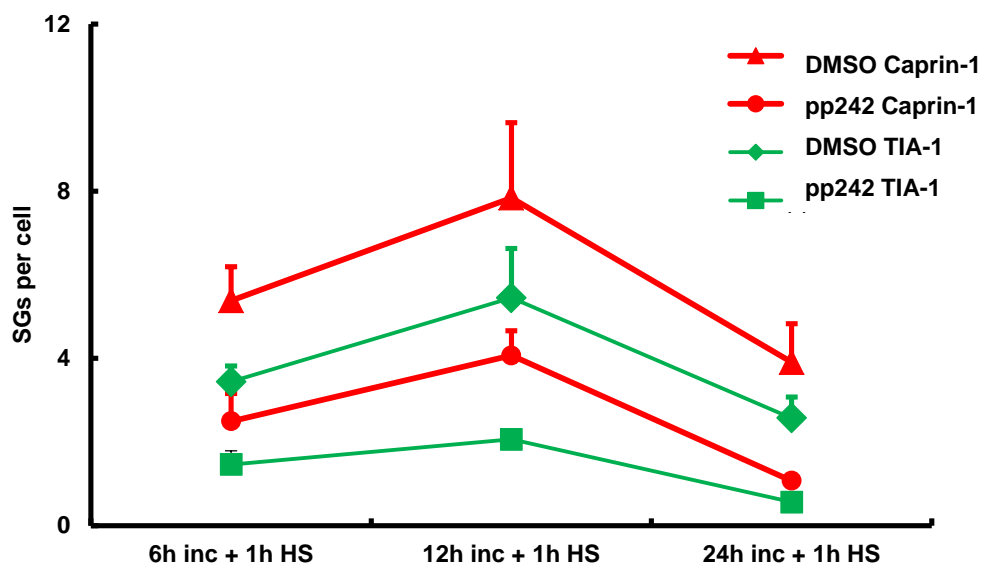


Figure 3.10 – Time-dependent effect on the number of SGs formed upon pp242 incubation prior to heat shock stress. OC-2 cells were incubated (inc) with 2.5 μ M of pp242 at 33°C during 6, 12h or 24h prior to the exposure to heat shock (HS) stress for 1h at 43°C. Triangles in red and diamonds in green represent the measurements for the Caprin-1 and TIA-1 DMSO 0.01% controls, respectively. Circles in red and squares in green represent the measurements for the Caprin-1 and TIA-1 for the 2.5 μ M pp242 treated samples, respectively. The values shown were obtained from 3 separate triplicate experiments and represent the average of 9 samples. One-way ANOVA followed by post-hoc Tukey test analysis was performed and no differences were found. Error bars represent SEM.

3.2.3.2. pp242 does not reduce SG formation during arsenite stress in the OC-2 cell line

Following the results achieved with heat shock treatment, the effects of pp242 on the SG inhibition were also tested using sodium arsenite as a stressor agent. Considering that arsenite was found to induce more SGs than heat shock (see section 3.2.2) and that the lowest pp242 concentrations tested prior to heat shock incubation (0.025 μ M and 0.25 μ M) did not inhibit SG formation (section 3.2.3.1), those concentrations were not included here. Consequently, pp242 concentrations were increased to test its effects on the SG inhibition upon arsenite treatment. OC-2 cells were incubated with 2.5 μ M, 5 μ M and 10 μ M of pp242 for 24h (along with a 0.04% DMSO control) prior to 0.5mM sodium arsenite exposure for 1h.

As before, immunocytochemistry followed by confocal imaging was used to detect SG-marker proteins Caprin-1 and TIA-1. Semi-automated quantification of SGs was performed as previously reported (see section 2.19.1 methods).

Vehicle-treated samples exposed to 1h 0.5mM arsenite stress revealed SG formation, as assessed by the distribution of SG-marker proteins Caprin-1 and TIA-1 (Fig.3.11, DMSO panel, white arrows). Pre-incubation with pp242 did not seem to affect the distribution of Caprin-1 and TIA-1 following arsenite stress, since these two proteins were found to aggregate at cytoplasmic SGs, regardless of increases in pp242 concentration (Fig.3.11, yellow arrows).

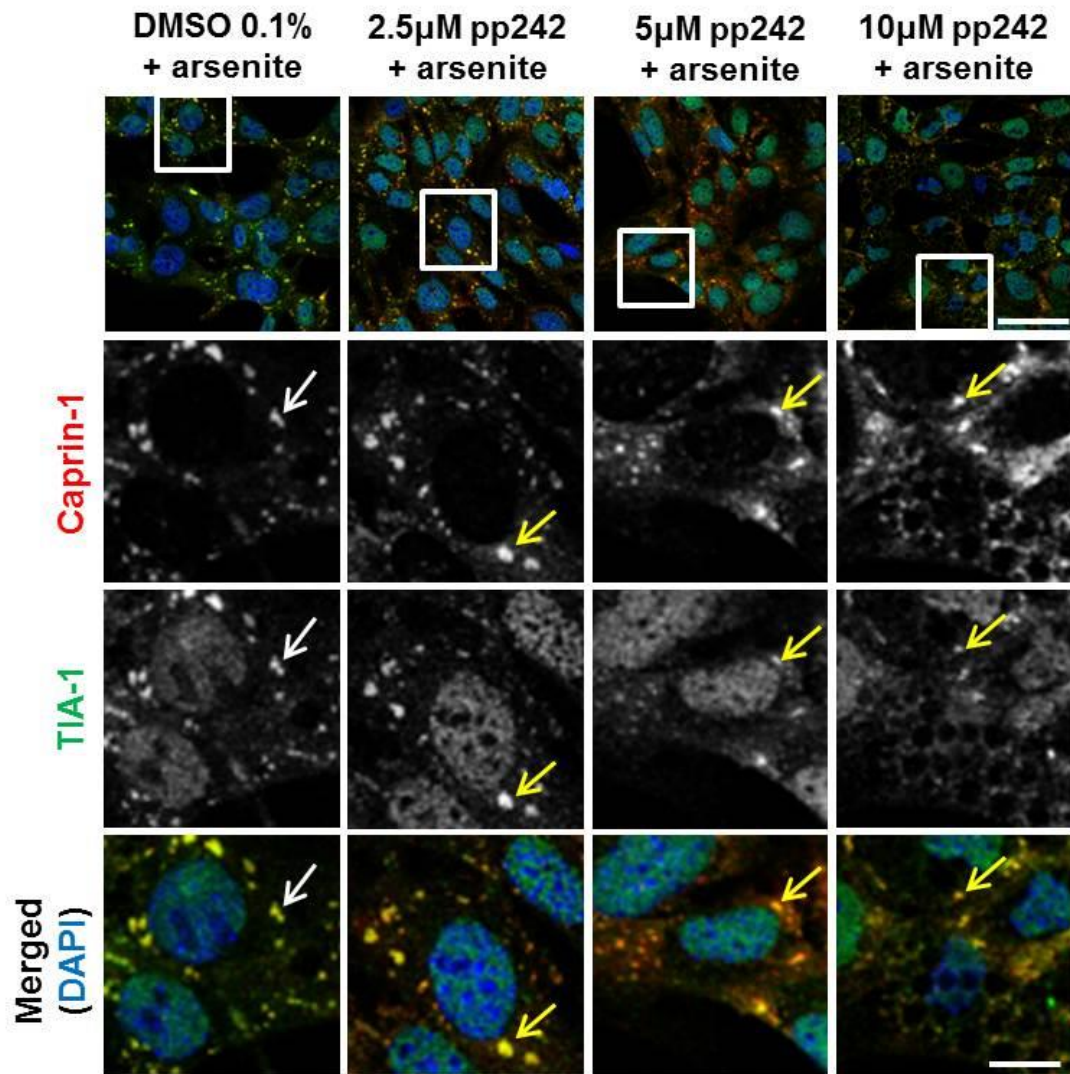


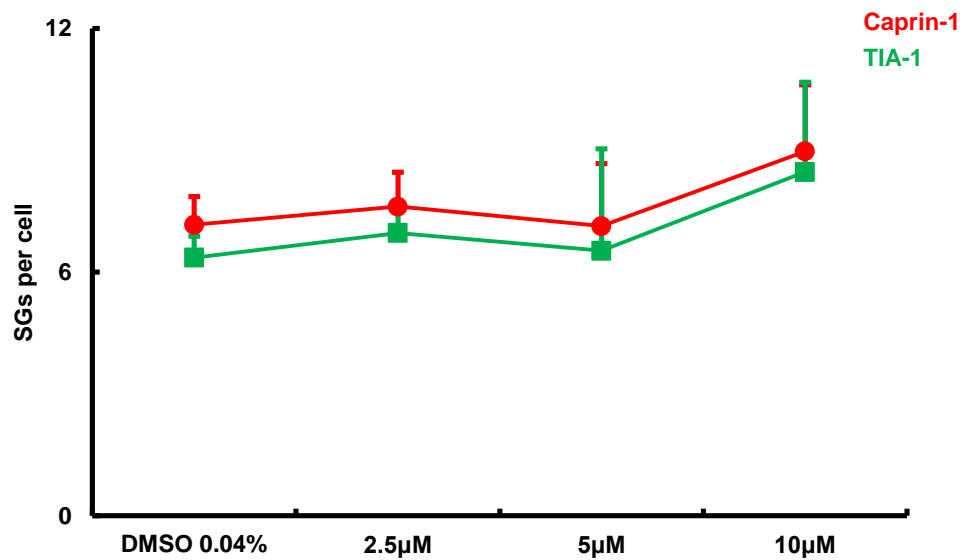
Figure 3.11 - pp242 fails to reduce the formation of Caprin-1 and TIA-1 positive SGs during arsenite stress. OC-2 cells were pre-incubated with a range of pp242 concentrations (2.5, 5 and 10 μ M) for 24h prior to 1h exposure to arsenite stress at 33°C. Caprin-1/TIA-1 staining is shown for the DMSO control and the different pp242 concentrations tested. Chromatin structure was assessed using DAPI staining. Inset in merged image for 10 μ M concentration shows a zoomed in area evidencing the cytoplasmic “vacuoles” formed under the usage of this pp242 concentration. White arrows point to SG formation following arsenite stress. Yellow arrows point to the presence of SGs during pp242 treatment. Scale bar= 25 μ m for top panel and 10 μ m for boxed images.

Pre-incubation for 24h with pp242 at the highest concentration failed to reduce SG formation during arsenite treatment, as none of the concentrations tested showed a decrease on the SG numbers when compared to vehicle-treated controls (Fig.3.12 A). The different pp242 concentrations tested prior to arsenite exposure did not significantly inhibit SG formation, since after 1h arsenite there was an average of 7 ± 2 SGs per cell formed when 2.5 and $5\mu\text{M}$ of pp242 was used, similar to what was observed with DMSO controls (Fig.3.12 A). On average, 8 ± 2 SGs per cell were observed with the highest pp242 concentration tested, $10\mu\text{M}$, reaching higher numbers than the DMSO control (Fig.3.12 A).

It is worth noting that when OC-2 cells were incubated for 24h with the highest pp242 concentration tested, $10\mu\text{M}$, the cells did present some cytoplasmic “vacuoles” (Fig.3.11, inset in merged image for $10\mu\text{M}$ concentration), which suggested that this level of concentration might be toxic to the cells. This phenomenon was observed before by other authors (Francipane & Lagasse 2013).

The average size of SGs did not statistically differ with the increased pp242 concentrations used (Fig.3.12 B). SGs generated in DMSO controls averaged approximately $1 \pm 0.4 \mu\text{m}^2$ in size following arsenite stress and in the presence of pp242 the SGs generated averaged $0.7 \pm 0.3 \mu\text{m}^2$ in size (Fig.3.12 B).

A



B

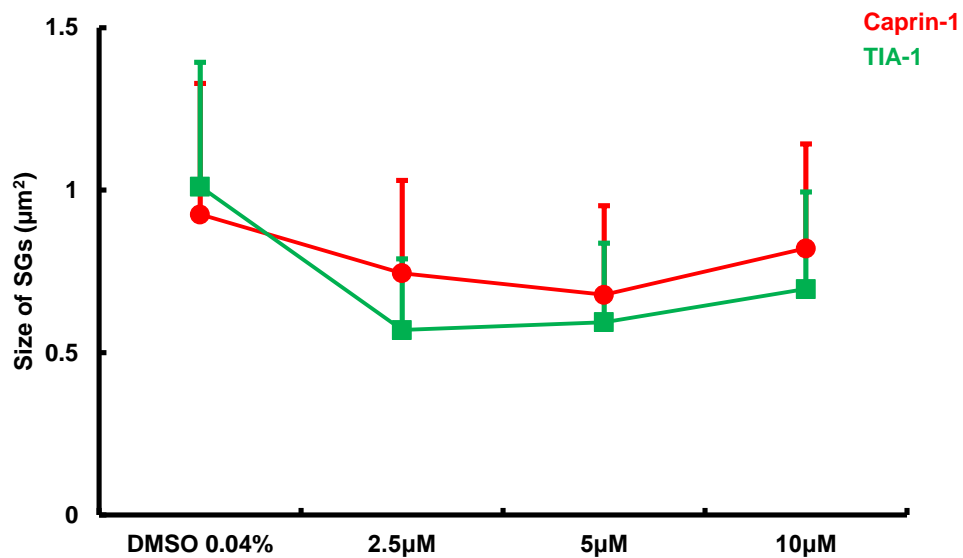


Figure 3.12 – Dose-dependent effect of pp242 on the number and size of SGs upon arsenite stress. OC-2 cells were incubated at 33°C for 24h with different concentrations of pp242 and DMSO as a control prior to 0.5mM sodium arsenite exposure for 1h. (A) Average number of SGs per cell. (B) Average size of SGs (μm²). The values represented here were obtained from 3 separate experiments with triplicates and represent the average of the 9 samples. One-way ANOVA followed by post-hoc Tukey test was performed and no differences were found. Error bars represent SEM.

Consistent with previous experiments, the size of SGs was not altered across different pp242 concentrations tested (Fig.3.13).

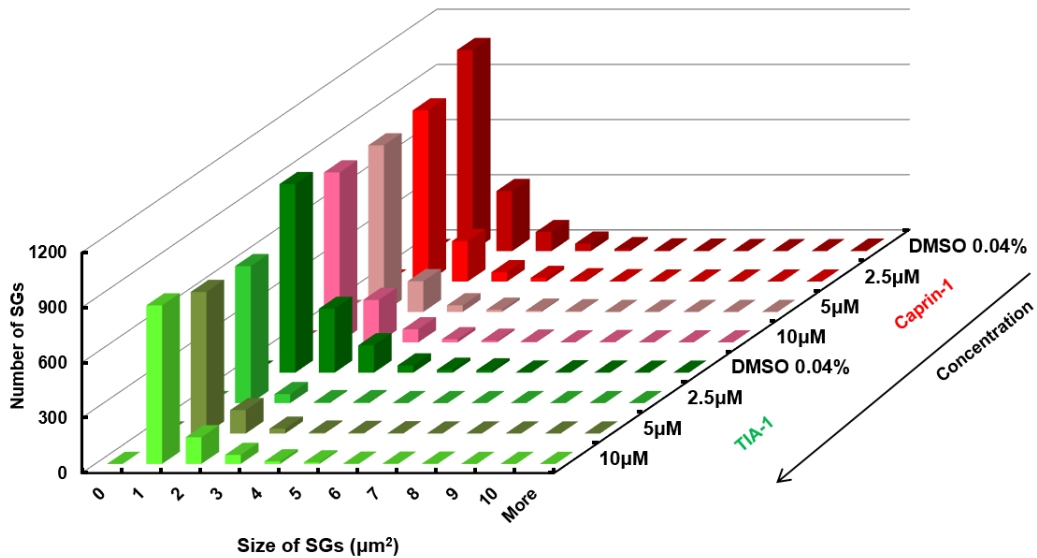


Figure 3.13 – Frequency histogram showing the distribution in size of SGs with pp242 exposure during arsenite stress. OC-2 cells were incubated with different concentrations of pp242 for 24h prior to sodium arsenite treatment. The y-axis represents the frequency of SGs, the x-axis indicates the size of SGs (from 0-10 μm^2 and more) and the z-axis indicates the pp242 concentrations used in this study, repeated for both Caprin-1 and TIA-1. The values represented here are the total frequency of SGs obtained from 9 samples.

Taken together, these experiments show that pp242 effectively reduces the number of SGs generated by heat shock stress, by 72 and 74% of controls for Caprin-1 and TIA-1, respectively, without affecting the size of SGs. However, pp242 fails to reduce the number of SGs produced by sodium arsenite stress.

3.2.3.3. ISRIB significantly reduces SG formation in OC-2 cells

Since the SG-inhibitor previously tested, pp242, only reduced SG formation under heat shock conditions and failed to reduce SGs formed as a consequence of arsenite stress, a different compound, ISRIB, was tested. ISRIB is a recently synthesised chemical that activates eIF2B and reduces eIF2 phosphorylation (Sidrauski et al. 2015), acting downstream of the stress sensor kinases and promoting protein translation (inhibition of SG formation). When compared to pp242 that acts favouring the interaction of eIF4E with its 4E-BP1 inhibitory factor (mTORC pathway), ISRIB action in eIF2B activation takes place downstream in the stress signalling pathway. Since optimised ISRIB concentrations were recently published in U2OS cells and ISRIB was found to inhibit the formation of SGs in 90% more cells than sodium arsenite stress alone (Sidrauski et al. 2015; Sekine et al. 2015), the assays presented here were performed following the optimised conditions published elsewhere.

RNA-immuno-FISH followed by confocal imaging was used to detect polyA⁺ mRNA at the same time as the SG-marker proteins Caprin-1 and TIA-1. Quantification of the number and size of SGs was performed as previously mentioned (section 2.19.1 in methods).

OC-2 cells were incubated with 200nM of ISRIB simultaneously with heat shock stress for 1h at 43°C, along with a heat shock treatment alone control.

After heat shock stress, Caprin-1 and TIA-1 aggregated with polyA⁺ mRNA at cytoplasmic SGs (Fig.3.14, heat shock panel, yellow arrows). In the presence of ISRIB during heat shock, it appeared that ISRIB abolished SG formation to levels seen in non-stressed cells, as observed by the distribution of Caprin-1 and TIA-1 SG-marker proteins (Fig.3.14, ISRIB + heat shock panel, white arrows). Consistent with this, polyA⁺ mRNA was distributed throughout the nucleus and the cytoplasm in the presence of ISRIB during heat shock stress, without aggregation at cytoplasmic SGs (Fig.3.14, ISRIB + heat shock panel, white arrows).

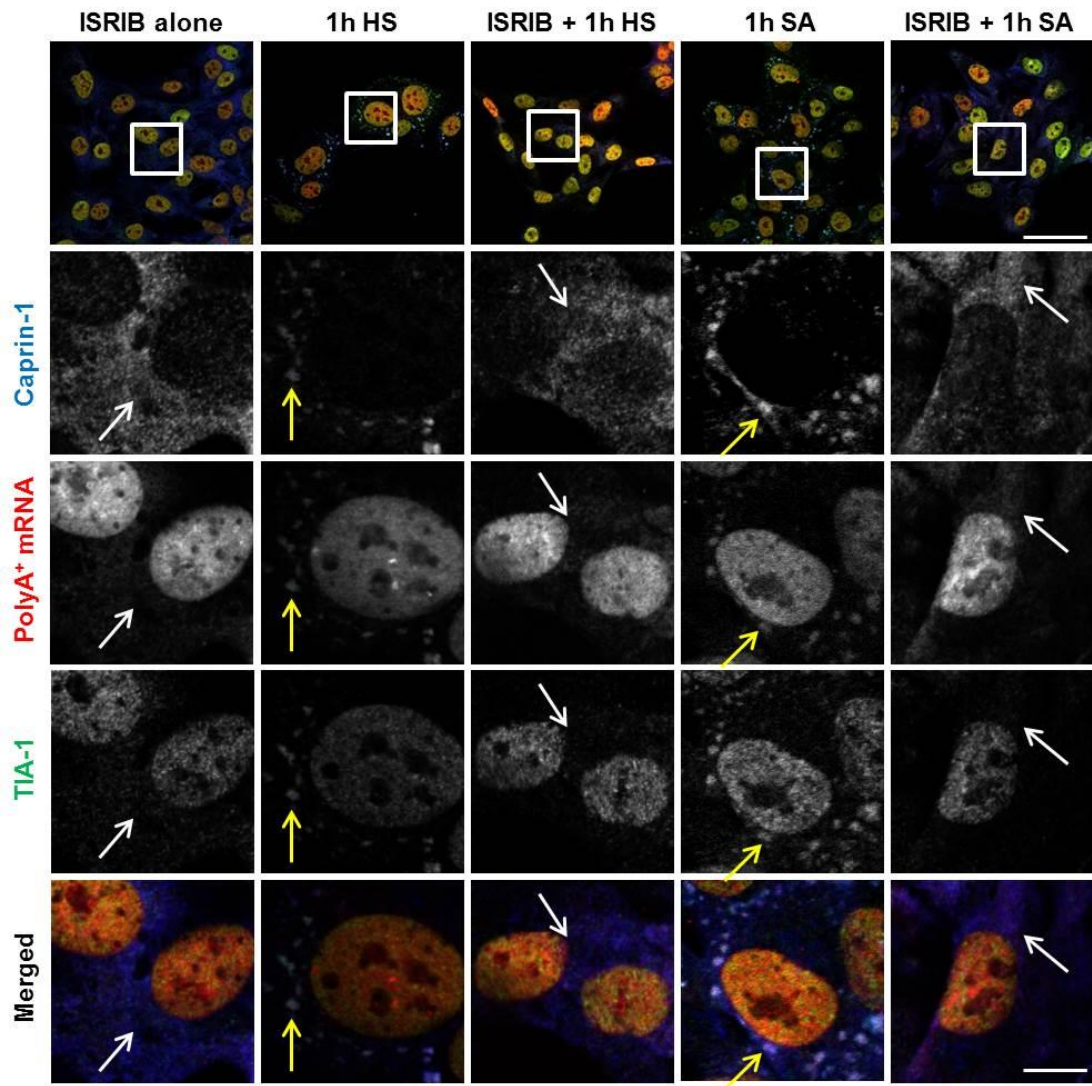


Figure 3.14 – SG formation following heat shock and arsenite stress is reduced in the presence of ISRIB. Caprin-1/TIA-1 protein distribution is shown for untreated, heat shocked and arsenite-treated samples. PolyA⁺ mRNA was detected using a Cy3-labelled probe. OC-2 cells were treated with heat shock stress (1h, 43°C) or sodium arsenite stress (1h, 0.5mM), in the absence and presence of ISRIB (200nM). Chromatin structure was assessed using DAPI staining. White arrows in untreated, ISRIB + HS and ISRIB + SA panels point to the nuclear and cytoplasmic distribution of polyA⁺ mRNA and TIA-1, not aggregating at SGs. Yellow arrows in 1h HS and 1h SA panels point to SG formation. Scale bar= 25 µm for top panel and 10 µm for boxed images.

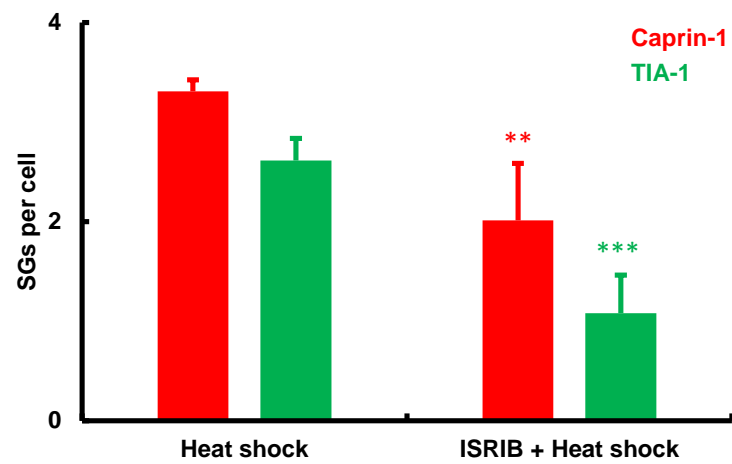
After 1h heat shock, 3.3 ± 0.1 Caprin-1 and 2.6 ± 0.2 TIA-1 positive SGs were formed on average per cell (Fig.3.15 A).

In the presence of ISRIB, these numbers were reduced to an average of 2 ± 0.5 Caprin-1 and 1 ± 0.3 TIA-1 positive SGs per cell, respectively (Fig.3.15 A). This corresponded to a significant reduction in the numbers of both Caprin-1 and TIA-1 positive SGs in the presence of ISRIB, 40 and 62%, respectively, when compared to vehicle-treated controls (Fig.3.15 A).

Regarding the size of the granules, the TIA-1 positive SGs observed in the presence of ISRIB were significantly smaller (approximately $0.5 \pm 0.3 \mu\text{m}^2$) than the TIA-1 positive SGs generated by heat shock stress alone (approximately $1.5 \pm 1.3 \mu\text{m}^2$) (Fig.3.15 B). This indicates that, for TIA-1, ISRIB not only has affected the reduction of the SG numbers, but also affected their size, upon heat shock treatment.

No significant differences at $p < 0.05$ (one-way ANOVA, post-hoc Tukey test) were found regarding the size of Caprin-1 positive SGs. No toxic effects, such as increased cell death, were observed for these conditions in the presence of ISRIB.

A



B

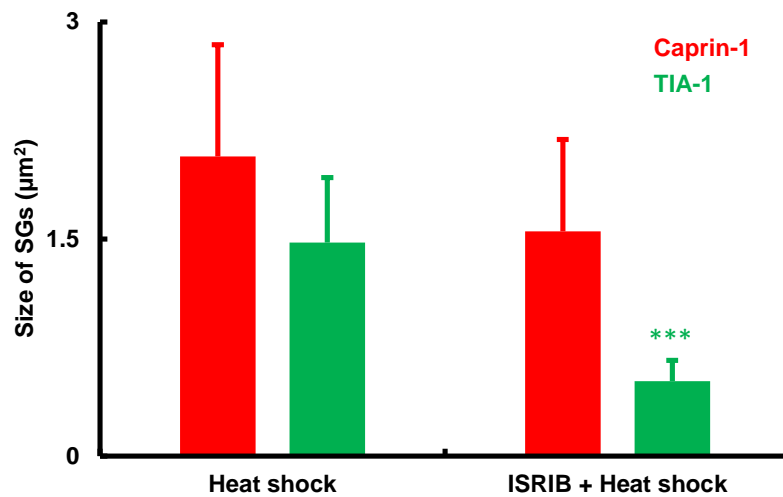


Figure 3.15 – ISRIB effects on SG number and size upon heat shock stress. OC-2 cells were incubated at 43°C for 1h in the absence (heat shock) and presence of 200nM of ISRIB (ISRIB + heat shock). (A) Average number of SGs per cell. (B) Average size of SGs (μm^2). The values represented here were obtained from 3 separate experiments with triplicates and represent the average of the 9 samples. ** $p < 0.005$; *** $p < 0.001$ (one-way ANOVA, post-hoc Tukey test). Error bars represent SEM.

ISRIB's ability to decrease SG formation was also assessed in the presence of arsenite stress. OC-2 cells were treated with 0.5mM of arsenite and 200nM of ISRIB simultaneously for 1h at 33°C. Controls without ISRIB were included (i.e. arsenite alone).

In the presence of ISRIB, there was a significant reduction on the number of SGs formed as a consequence of arsenite treatment (Fig.3.14). Qualitative data indicated polyA⁺ mRNA mostly located throughout the nucleus and the cytoplasm in the presence of ISRIB, demonstrating that polyA⁺ mRNA did not aggregate at SGs during arsenite stress when ISRIB is applied (Fig.3.14, ISRIB + arsenite panel, white arrows). Correspondingly, Caprin-1 and TIA-1 showed cellular localisations comparable to untreated samples and did not aggregate at cytoplasmic SGs when in the presence of ISRIB during arsenite treatment (Fig.3.14, ISRIB + arsenite panel, white arrows).

Sodium arsenite exposure for 1h triggered on average 10.3 ± 0.9 and 8 ± 0.9 Caprin-1 and TIA-1 positive SGs per cell, respectively (Fig.3.16 A). Quantification shows that Caprin-1 and TIA-1 positive SGs were reduced by 96 and 97%, respectively, in the presence of ISRIB when compared to arsenite treatment alone (Fig.3.16 A).

No significant changes were observed in terms of SG size for both Caprin-1 and TIA-1 positive SGs in the presence of ISRIB under arsenite conditions (Fig.3.16 B). Arsenite stress triggered the formation of Caprin-1 and TIA-1 positive SGs averaging $2.3 \pm 0.8 \mu\text{m}^2$ and $1.7 \pm 0.6 \mu\text{m}^2$ in size, respectively (Fig.3.16 B). Upon simultaneous incubation with ISRIB, the SGs observed following arsenite treatment averaged $1.9 \pm 0.8 \mu\text{m}^2$ and $1.2 \pm 0.4 \mu\text{m}^2$ in size for Caprin-1 and TIA-1, respectively (Fig.3.16 B).

No increased cell death was observed during these studies, indicating that at these conditions (1h, 200nM) ISRIB is well tolerated by the cells.

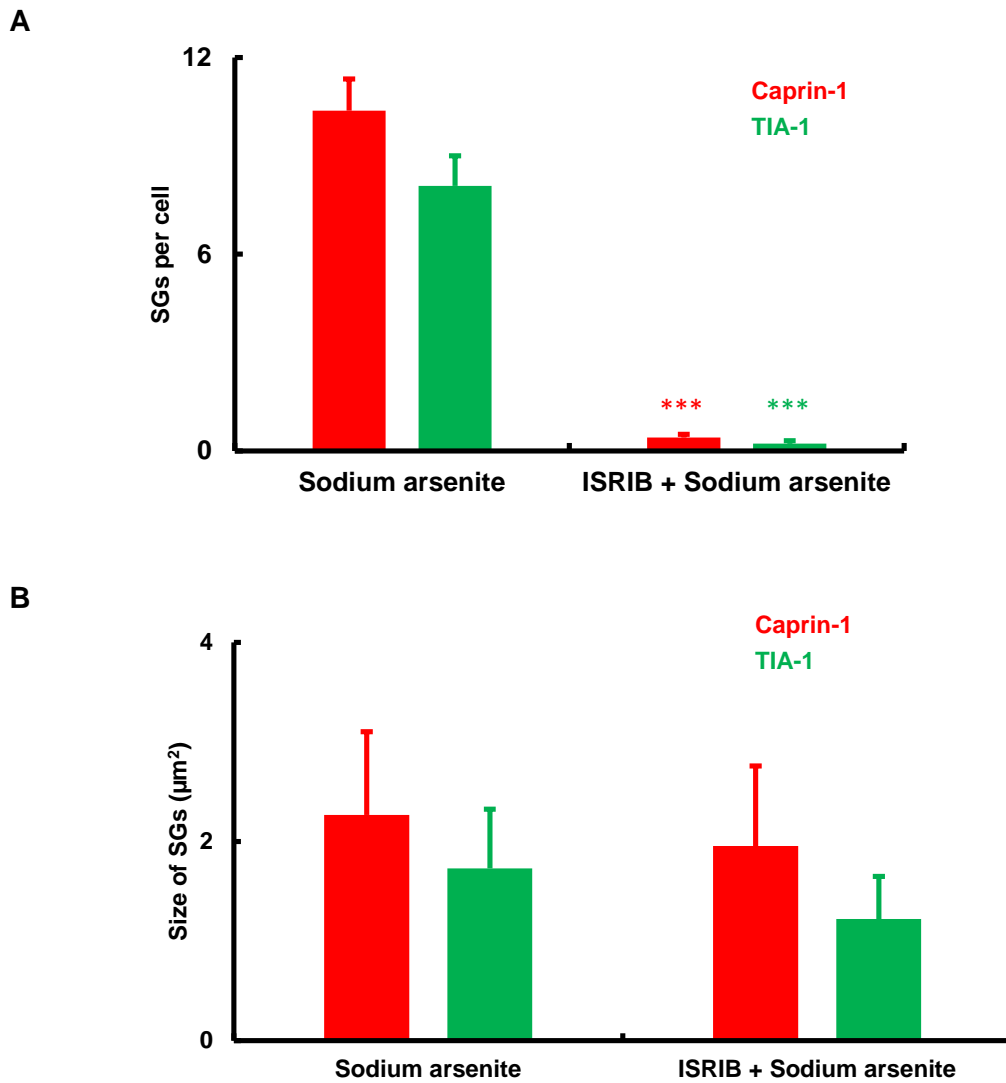


Figure 3.16 – ISRIB effects on the SG number and size upon arsenite stress. OC-2 cells were incubated at 33°C for 1h in the absence (sodium arsenite) and presence of 200nM of ISRIB (ISRIB + sodium arsenite). (A) Average number of SGs per cell. (B) Average size of SGs (μm^2). The values represented here were obtained from 3 separate experiments with triplicates and represent the average of the 9 samples. *** $p < 0.001$ (one-way ANOVA, post-hoc Tukey test). Error bars represent SEM.

As previously observed, a skewed distribution of small granules in a greater quantity and less granules of larger size, was maintained across all the concentrations tested, during ISRIB studies upon heat shock and arsenite stress (Fig.3.17).

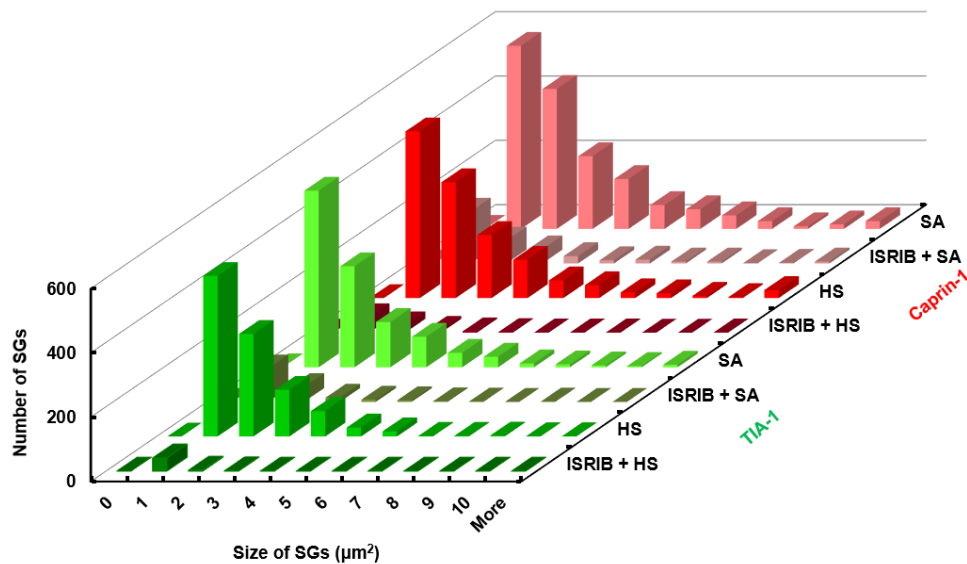


Figure 3.17 – Frequency histogram showing the distribution in size of SGs after heat shock and arsenite treatments alone and in the presence of ISRIB. OC-2 cells were incubated with 200nM of ISRIB simultaneously with heat shock (43°C) and arsenite (0.5mM) treatments. The y-axis represents the frequency of SGs, the x-axis indicates the size of SGs (from 0-10 μm² and more) and the z-axis indicates the different conditions tested, repeated for both Caprin-1 and TIA-1. The values represented here are the total frequency of SGs obtained from 9 samples.

Taken together, these results indicate that ISRIB can efficiently reduce the number of SGs upon heat shock and sodium arsenite stresses. However, when compared to pp242, ISRIB presents less reduction on the number of Caprin-1 and TIA-1 SGs during heat shock stress (72 and 74% reduction with pp242 against 40 and 62% in the presence of ISRIB, for Caprin-1 and TIA-1 positive SGs, respectively).

When used in the presence of arsenite stress, ISRIB decreases the number of SGs formed up to 96 and 97% for Caprin-1 and TIA-1, respectively, whereas pp242 failed to reduce the number of SGs upon arsenite stress.

3.2.3.4. Hydroxamate (-)-9 promotes SG formation in OC-2 cells

After developing a robust assay and demonstrating that certain compounds can reduce the number of SGs in the OC-2 cell line during stress conditions, an experiment was performed to assess whether SGs formation could be promoted in the absence of a stressor agent. Considering this, a chemical compound that can act in the stress signalling pathway in unstressed cells and produce similar effects to those caused by kinase-activator stressor agents in terms of disruption of protein translation, was chosen.

Hydroxamate (-)-9 was the chemical selected for study since this compound was previously shown to disrupt translation initiation in eukaryotes (Bordeleau et al. 2008). Hydroxamate (-)-9 is a chemical analogue of silvestrol that promotes a non-productive binding of eIF4A I and II to RNA, sequestering eIF4A from the eIF4F complex. eIF4A I and II are two RNA helicases required for the loading of the mRNA onto the 40S ribosome during the translation initiation. By disrupting the normal function of these helicases, hydroxamate (-)-9 inhibits translation initiation (Hwang et al. 2004; Bordeleau et al. 2008), thus constituting an excellent candidate to assess whether SG formation can be manipulated *in-vitro*.

The effects of hydroxamate (-)-9 in the SGs assembly were assessed in an experiment using a range of concentrations of this compound (0.001 μ M, 0.01 μ M, 0.1 μ M and 1 μ M), in which unstressed OC-2 cells were incubated for 8h. The concentrations of hydroxamate (-)-9 chosen to test were based on previous experimental conditions published elsewhere for the hydroxamate (-)-9 analogue silvestrol (Bordeleau et al. 2008). RNA-FISH combined with immunocytochemistry followed by confocal imaging was used to detect polyA⁺ mRNA at the same time as Caprin-1 and TIA-1 SG-marker proteins. Quantification of SGs in terms of number and size was performed as previously described (section 2.19.1 in methods).

Vehicle-treated control cells exhibited Caprin-1 mostly present in the cytoplasm of the cells and TIA-1 distributed throughout the nucleus and the cytoplasm, without aggregation at SGs (Fig.3.18, DMSO panel, white arrows). With increasing hydroxamate (-)-9 concentration, Caprin-1 and TIA-1 aggregated at cytoplasmic SGs (Fig.3.18, yellow arrows) that resembled those observed after exposure to heat shock or sodium arsenite stresses (see section 3.2.1 and 3.2.2).

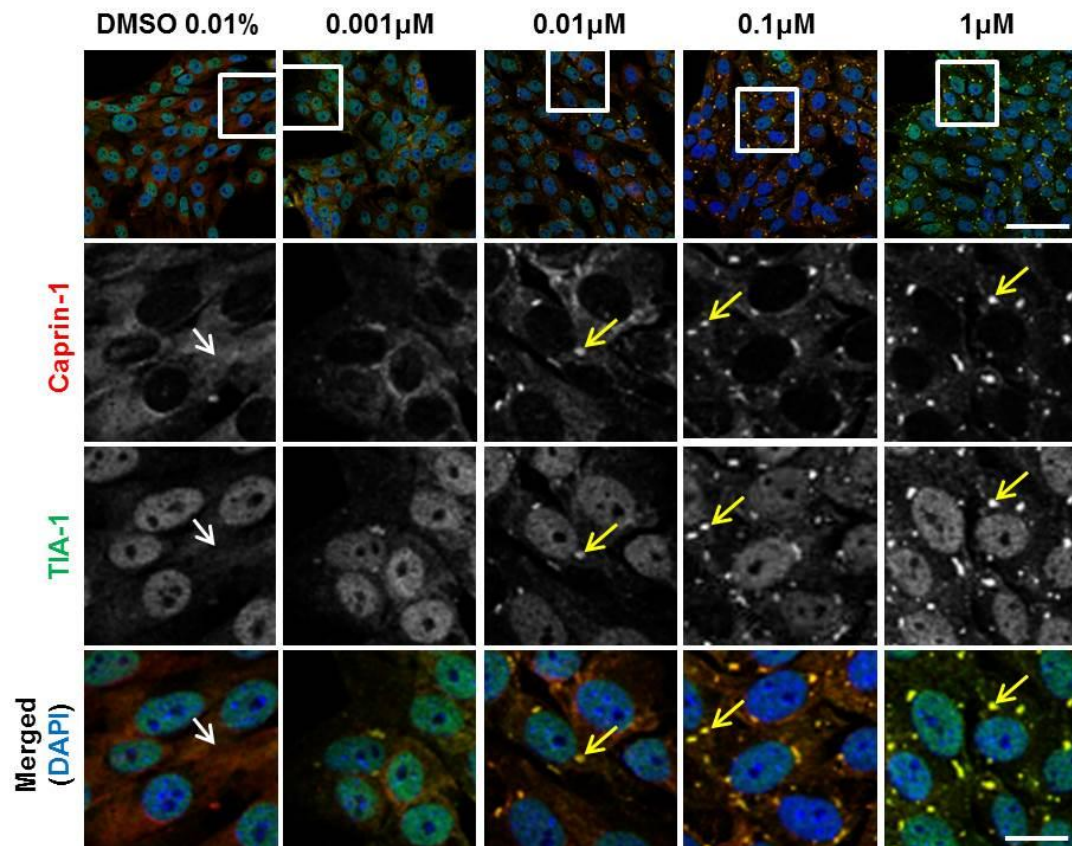


Figure 3.18 - Hydroxamate (-)-9 treatment induces the formation of SGs. Untreated OC-2 cells were incubated with a range of hydroxamate (-)-9 concentrations for 8h at 33°C. Caprin-1/TIA-1 protein distribution is shown across the different hydroxamate (-)-9 concentrations used in this study. Chromatin structure was assessed using DAPI staining. White arrows in DMSO panel point to the cytoplasmic and nuclear distribution of Caprin-1 and TIA-1, not aggregating at SGs. Yellow arrows in hydroxamate (-)-9 treatment panels point to SG formation. Scale bar= 25 μ m for top panel and 10 μ m for boxed images.

Figure 3.19 shows that, after hydroxamate (-)-9 treatment, polyA⁺ mRNA aggregates with TIA-1 (white arrows) at SGs, confirming that the pharmacologically manipulated SGs contain polyA⁺ mRNA as a component. When OC-2 cells are allowed to recover in an hydroxamate (-)-9-free medium for 14h, aggregates of polyA⁺ mRNA and TIA-1 are no longer observed in the cytoplasm of the cells (Fig.3.19, recovery panel, yellow arrows), thus confirming the reversible effects of hydroxamate (-)-9 on SG formation.

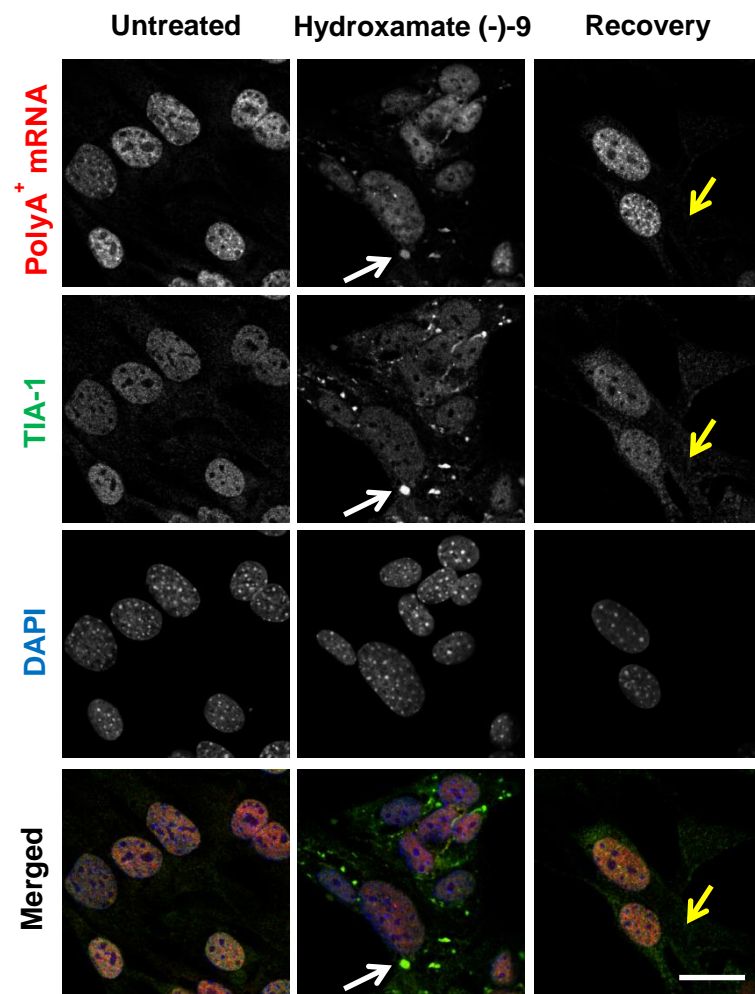


Figure 3.19 – PolyA⁺ mRNA is a component of the SGs originated by hydroxamate (-)-9 incubation. OC-2 cells were incubated for 8h with 0.1 μ M of hydroxamate (-)-9 at 33°C. PolyA⁺ mRNA was detected using a Cy3-labelled probe. The cells were allowed to recover for 14h in a hydroxamate (-)-9-free medium. Chromatin structure was assessed using DAPI staining. White arrows in hydroxamate (-)-9 treatment panels point to SG formation. Yellow arrows in recovery panel point to the nuclear and cytoplasmic distribution of polyA⁺ mRNA and TIA-1, not aggregating at SGs. Scale bar= 10 μ m for all images.

Quantification of the number of SGs revealed that 8h incubations of hydroxamate (-)-9 at a dose of 0.01 μ M and above resulted in robust and statistically significant SG formation, with average numbers per cell of 7.4 ± 1 and 4.1 ± 0.5 for Caprin-1 and TIA-1 positive SGs, respectively (Fig.3.20 A). Together with the RNA-immuno-FISH data, these results confirm the potential of hydroxamate (-)-9 to trigger SG assembly in OC-2 cells.

When treated with 0.1 μ M of hydroxamate (-)-9, Caprin-1 and TIA-1 SGs averaged $1.3 \pm 0.4 \mu\text{m}^2$ and $1.1 \pm 0.3 \mu\text{m}^2$ in size, respectively (Fig.3.20 B). No significant differences were reported as to the size of SGs amongst the different hydroxamate (-)-9 concentrations tested at $p < 0.05$ (one-way ANOVA, post-hoc Tukey test) (Fig.3.20 B).

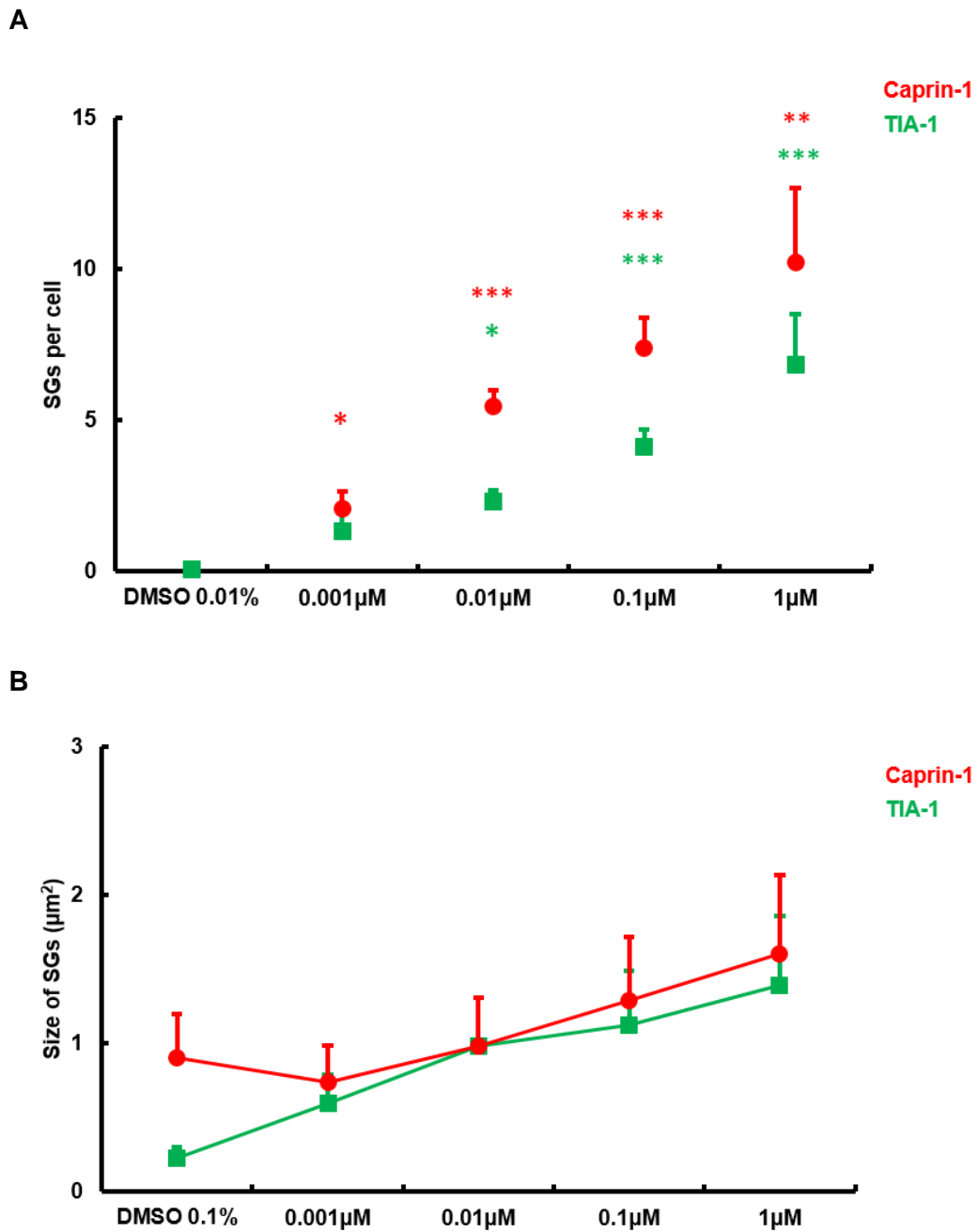


Figure 3.20 – Dose-dependent effect of hydroxamate (-)-9 in the formation of SGs. OC-2 cells were incubated at 33°C for 8h with different concentrations of hydroxamate (-)-9 and DMSO as a control. (A) Average number of SGs per cell. (B) Average size of SGs (μm^2). The values represented here were obtained from 3 separate experiments with triplicates and represent the average of the 9 samples. * $p < 0.05$; ** $p < 0.005$; *** $p < 0.001$ (one-way ANOVA, post-hoc Tukey test). Error bars represent SEM.

As observed before, the regular pattern of SGs of smaller size (between 0.2 μm^2 and 2 μm^2) and less SGs of larger size (from 2 μm^2 up to 11 μm^2) was maintained following hydroxamate (-)-9 incubations (Fig.3.21). This indicates that hydroxamate (-)-9 generates Caprin-1 and TIA-1 positive SGs that are similar in size to those produced by heat shock and sodium arsenite stresses (see sections 3.2.1 and 3.2.2).

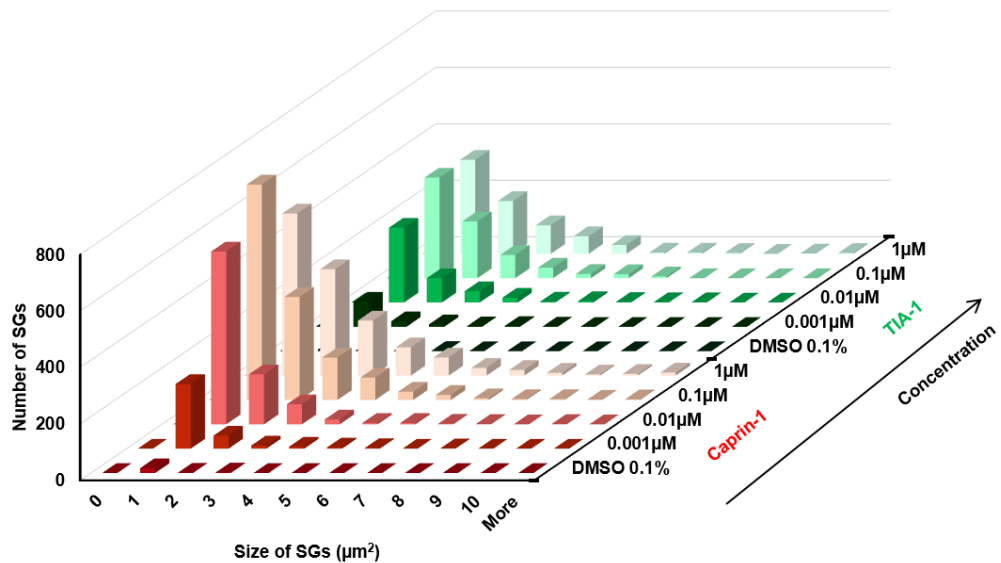


Figure 3.21 – Frequency histogram showing the distribution in size of SGs according to different hydroxamate (-)-9 concentrations. Values represent the total number of SGs observed when unstressed cells were incubated for 8h with the compound. The y-axis represents the frequency of SGs, the x-axis indicates the size of SGs (from 0-10 μm^2 and more) and the z-axis indicates the hydroxamate (-)-9 concentrations used in this study, repeated for both Caprin-1 and TIA-1. The values represented here are the total frequency of SGs obtained from 9 samples.

The time-dependence of the effect of hydroxamate (-)-9 was also tested by exposing unstressed OC-2 cells for 2h, 4h and 8h to 0.1 μ M of hydroxamate (-)-9, in order to evaluate the effect of decreasing the exposure of OC-2 cells to the compound.

Eight-hour incubation of hydroxamate (-)-9 was the only condition found to produce similar average numbers of Caprin-1 and TIA-1 positive SGs (Fig.3.22). Overall, treatment with hydroxamate (-)-9 for 8 hours generated a robust SG formation in OC-2 cells without causing additional cellular death. At 0.1 μ M for 8h, robust and statistical significant responses in terms of SG formation for both markers were observed (Fig.3.22) and so these were the experimental conditions chosen for *ex-vivo* experiments.

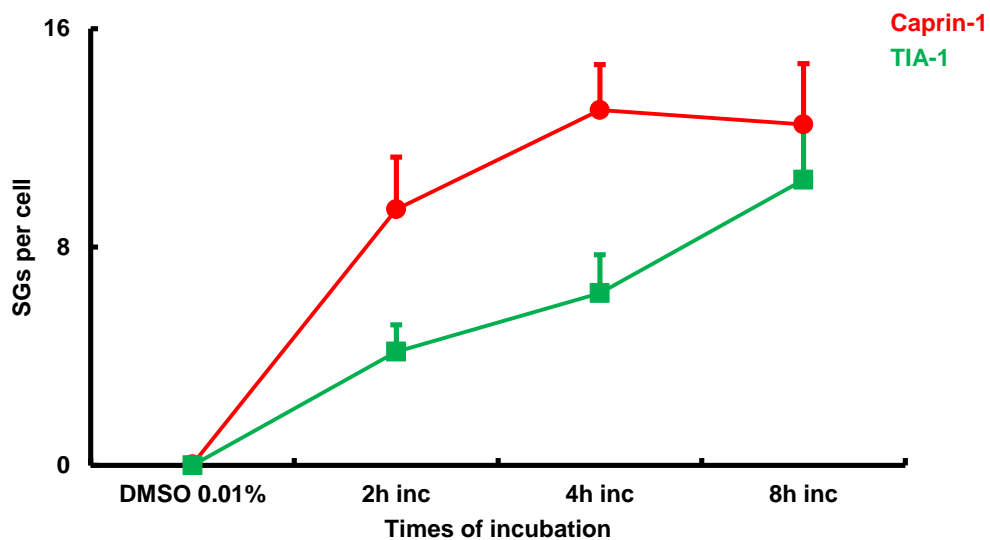


Figure 3.22 – Average number of SGs generated after different incubation periods with 0.1 μ M of hydroxamate (-)-9. OC-2 cells were incubated (inc) during 2h, 4h and 8h with 0.1 μ M of hydroxamate (-)-9. Red circles represent Caprin-1 positive SGs and green squares represent TIA-1 positive SGs. Incubation was done at 33°C in unstressed OC-2 cells. The values represented here were obtained from 3 separate triplicate experiments and represent the average of the 9 samples. One-way ANOVA followed by post-hoc Tukey test was performed and no differences were found. Error bars represent SEM.

3.2.4. Summary

The initial studies of this project aimed at understanding the regulation of SG formation in an inner ear context and to subsequently investigate whether SG formation can be manipulated, providing the basis for one of the main objectives of this thesis: understanding whether manipulation of SG formation affects hair cell survival upon ototoxic stress.

For this, OC-2 cells, an inner ear-derived cell line (Rivolta et al. 1998), were used to develop a robust assay that could identify RNA and proteins, thus confirming the nature of the SGs originated in this system. Additionally, a novel quantification method for the SG field was developed, enabling a better understanding of how different stressor agents influence the cellular response to stress in terms of SG number and size. Heat shock and sodium arsenite were chosen to stress OC-2 cells and the cellular response to those treatments was evaluated in terms of cellular localisation (RNA-immuno-FISH) and quantification of SG number and size.

Following this, different pharmacological compounds that modulate SG formation / inhibition were screened in the OC-2 cell line and their results assessed in terms of SG formation through imaging detection and quantification. Three chemical compounds were selected for study: pp242 and ISRIB to test whether SG inhibition could be performed upon stress and hydroxamate (-)-9 to test whether SG formation could be pharmacologically promoted in untreated cells.

When the different stress paradigms are compared against each other, sodium arsenite (1h, 0.5mM) was found to generate the greatest response in terms of SG formation in the OC-2 cell line (Fig.3.23). The numbers of SGs generated by arsenite treatment were significantly greater than in heat shock (1h, 43°C) for Caprin-1 and TIA-1 positive SGs (Fig.3.23).

Both pp242 and ISRIB, the two SG-inhibitors tested, significantly decreased the number of SGs triggered by heat shock stress (Fig.3.23). However, upon sodium arsenite stress conditions, only ISRIB reduced the numbers of SGs and these were statistically significant for Caprin-1 and TIA-1 (Fig.3.23).

Hydroxamate (-)-9 produced a number of SGs intermediate between heat shock and sodium arsenite (Fig.3.23).

The size of the SGs generated by the different treatments was only affected by the presence of ISRIB during heat shock stress for TIA-1, as indicated in Figure 3.24.

The general size of the SGs generated by the different treatments was found to average approximately $1\text{-}2\mu\text{m}^2$ for both Caprin-1 and TIA-1 positive SGs (Fig.3.24).

All together, these results indicate that OC-2 cells respond to heat shock and arsenite stresses by assembling SGs and that these can be detected and quantified in terms of number and size. Additionally, polyA⁺ mRNA was identified for the first time as a component of SGs formed in the OC-2 cell line, confirming the RNA nature of the aggregates found upon stress. These results here presented also confirm that SG manipulation can be performed in the OC-2 cell line. ISRIB and hydroxamate (-)-9 were screened and validated as an inhibitor and promotor of SG formation, respectively. Thus, these two manipulators constitute excellent candidates to test whether SG manipulation affects hair cell survival upon ototoxic stress. This hypothesis will be explored in Chapter 4.

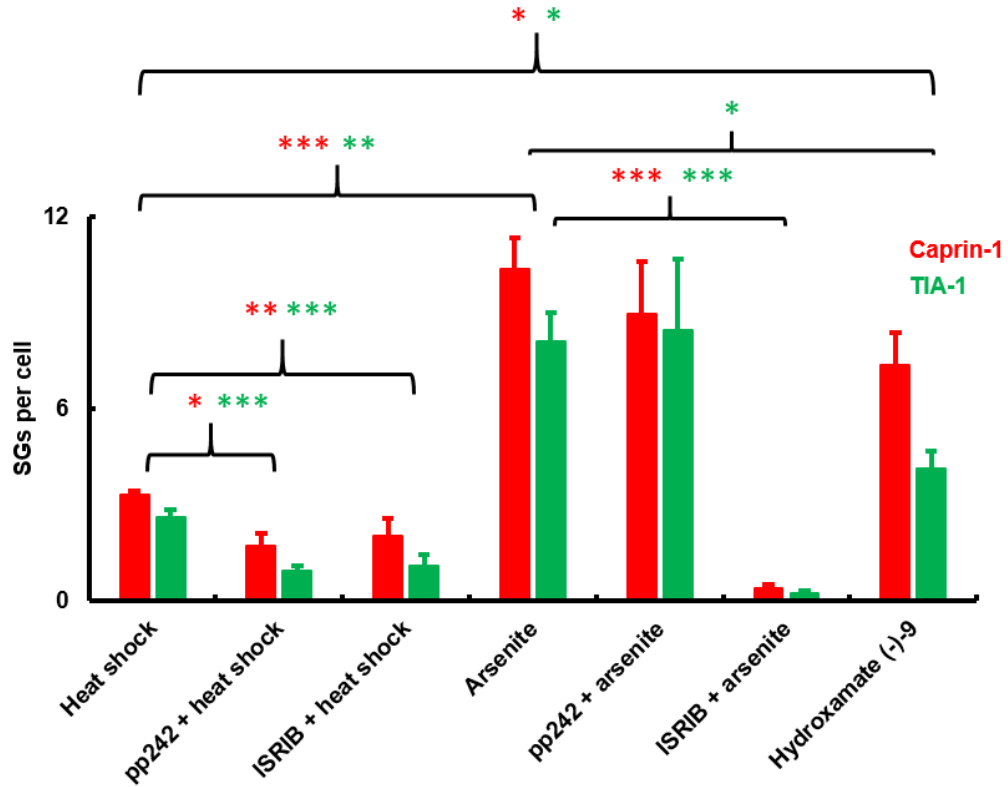


Figure 3.23 – Summary of the number of SGs generated by the different treatments in OC-2 cells. The average number of SGs per cell is represented here. Caprin-1 SGs are indicated by red bars and TIA-1 SGs indicated by green bars. Incubations were performed in OC-2 cells as follows: heat shock (1h at 43°C), sodium arsenite (1h at 0.5mM), hydroxamate (-)-9 (0.1µM for 8h), pre-incubation for 24h with 5µM of pp242 prior to either heat shock or 10µM pp242 prior to sodium arsenite stress, ISRIB 200nM simultaneously with heat shock and sodium arsenite treatments. * $p < 0.05$; ** $p < 0.005$; *** $p < 0.001$ (one-way ANOVA, post-hoc Tukey test). Error bars represent SEM (n=9 for each condition).

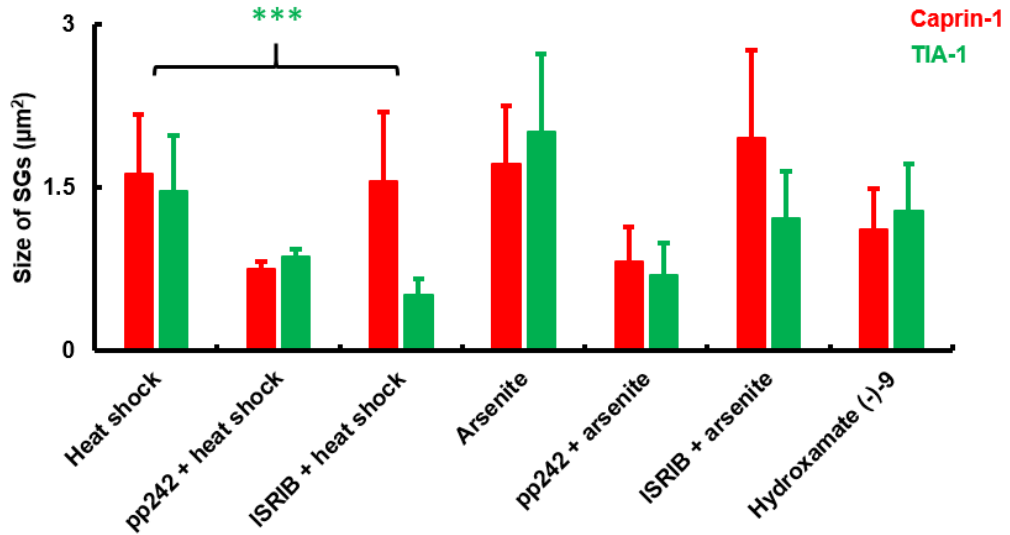


Figure 3.24 – Summary of the size of SGs generated by the different treatments in OC-2 cells. The average size of SGs per cell is represented here. Caprin-1 SGs are indicated by red bars and TIA-1 SGs indicated by green bars. Incubations were performed in OC-2 cells as follows: heat shock (1h at 43°C), sodium arsenite (1h at 0.5mM), hydroxamate (-)-9 (0.1µM for 8h), pre-incubation for 24h with 5µM of pp242 prior to either heat shock or 10µM pp242 prior to sodium arsenite stress, ISRIB 200nM simultaneously with heat shock and sodium arsenite treatments. *** $p < 0.001$ (one-way ANOVA, post-hoc Tukey test). Error bars represent SEM (n=9 for each condition).

3.3. Discussion

SGs are aggregates of mRNA molecules and proteins that are formed during stress conditions. Through dynamic sequestration of mRNA molecules by specific RNA-binding proteins, SGs are thought to be preferred sites for mRNA storage and sorting during stress (Kedersha et al. 2000; Kedersha et al. 2002). Despite their implication in the cochlea's response to ototoxic stress (Mangiardi et al. 2004; Towers et al. 2011), the mechanisms of SG assembly and regulation in the inner ear are poorly understood to date. Here, for the first time, a detailed characterisation of the SG formation in an inner ear-derived cell line is provided. Additionally, the first studies involving pharmacological manipulation of SG formation in an inner ear context are described. These are aimed at future application in mouse cochlear explants to assess the effect of manipulating SG formation on the hair cell survival upon ototoxic stress.

The initial experiments of this project were conducted in the OC-2 cell line. As previously mentioned, although OC-2 cells present experimental constraints when compared to the multicellular structure of the cochlea, they constitute a suitable inner ear-derived cell line to develop assays. Furthermore, the use of OC-2 cells enabled the optimisation of experimental conditions as well as initial screenings to test pharmacological compounds, prior to animal use.

To better understand the dynamics of SG formation, one of the most comprehensive dataset in the SG field so far was obtained as regarding their formation, components and regulation using OC-2 cells. Additionally, a novel quantification method, to determine the number and size of SGs, was developed. The use of a standard protocol for SG quantification may help to understand how different cell types respond to different stressors in terms of SG formation and, consequently, better comprehend the regulation of SG formation.

Overall consideration of the results presented here reveals that, at the conditions tested, heat shock and sodium arsenite trigger reversible SG formation in OC-2 cells, without causing increased cellular death. I demonstrated that although slightly more Caprin-1 positive SGs have been produced when compared to TIA-1 positive SGs, these two SG-markers were, in the majority of the cases, found to colocalise upon stress with polyA⁺ mRNA (Figs.3.1 and 3.4). Arsenite stress was found to trigger a greater response in terms of the number and size of the SGs assembled when compared to heat shock (Figs.3.2 A and 3.5 A), suggesting that it might

constitute a stronger stress to OC-2 cells (at least at the concentration and exposure time used here). Although sodium arsenite generated more SGs than heat shock stress in OC-2 cells, the number of SGs formed following heat shock stress was variable across different experiments (Figs.3.2 and 3.8). This can be a result of the nature of the different treatments. For heat shock stress, OC-2 cells were transferred from 33°C to 43°C and some cells may have adapted more rapidly to the heat shock condition, thus reflecting the differences observed in the number of SGs formed in different experiments. On the other hand, because sodium arsenite is a chemical added directly to the culture medium, the numbers of SGs generated following arsenite treatment were less variable.

The distribution in size of SGs was determined to be fairly regular across the different stresses and time-points tested: in general, there were more granules of smaller size (typically less than $2\mu\text{m}^2$) than granules of larger size ($>2\mu\text{m}^2$) (Figs.3.2 B and 3.5 B). The number and size of SGs formed upon these stresses are consistent with what other authors have observed before in HeLa, HEK293 and U2OS cells (Souquere et al. 2009; Zurla et al. 2011; McDonald et al. 2011; Seguin et al. 2014).

Recovery experiments showed that both heat shock- and arsenite-induced SGs disassemble over a recovery period of 4 hours (Figs.3.2 A and 3.5 A). After 4 hours, the cellular distribution of Caprin-1 and TIA-1 resembled those of untreated / unstressed cells (Figs.3.1 and 3.4). These observations confirm the reversible effects of heat shock and sodium arsenite stress on the SG formation in the OC-2 cell line.

PolyA⁺ mRNA was identified as a component of the Caprin-1 and TIA-1 SGs, for the first time in an inner ear-derived cell line, after the development of a robust assay to detect RNA to SGs (RNA-immuno-FISH). These data are consistent with reports from other studies (Kedersha et al. 1999; Kedersha & Anderson 2002; Shelkownikova et al. 2014) and suggest the presence of sequestered mRNA molecules aggregating with RNA-binding proteins during stress in the OC-2 cell line. During recovery from both heat shock and sodium arsenite stresses, polyA⁺ mRNA was detected throughout the cytoplasm and not aggregated as immediately after stress (Figs.3.1 and 3.4). These observations suggest that along with SG clearance, polyA⁺ mRNA is released from SGs and is available to resume translation.

In order to understand whether SG formation could be manipulated in the OC-2 cell line, pharmacological drugs that act on different pathways downstream of the stressor kinases were tested.

When choosing the compounds to test, many aspects were considered (e.g. possible side effects, cellular target, previous use in the SG field). One of the main concerns when choosing the chemicals to test out in these experiments was to understand where they act on the stress signalling pathways. Ideally, a compound that is used to prevent or promote SG formation should act as far downstream as possible on the stress signalling cascades, to avoid interference with other cellular pathways that may indirectly lead to cellular stress by other means. Additionally, the compounds to test need to be efficacious and safe to use and should not require long incubation periods. Moreover, when working with cellular stress pathways, selection of compounds that present reversible cellular effects is crucial, given the implication of SGs in pathological aggregates caused by persistent stress (explored in introduction section 1.13). All these features were carefully considered during the selection of the compounds to manipulate SG formation, especially considering the objective of future application in mouse cochlear explants. Priority was given to manipulators that have been used before in the SG field and demonstrated high efficacy as well as relatively short incubation periods. Correspondingly, the manipulators ultimately chosen to be used in the subsequent experiments performed in the *ex-vivo* mouse cochlea were selected by a multi-validation approach (e.g. robust efficacy on the SG reduction / promotion, no signals of increased cell death, reversible effects).

pp242, a known SG-inhibitor (Fournier et al. 2013), was used here to prevent SG formation upon heat shock and sodium arsenite stress exposure and it was found to reduce heat shock-triggered SGs by approximately 75% (Fig.3.7 A). pp242 did not seem to alter the general pattern of granule size, since more granules corresponding to a smaller size and less granules of larger size could be observed (Fig.3.7 B). pp242 failed to inhibit SGs formed as a consequence of sodium arsenite stress (Fig.3.11), demonstrating that its effects on the SG inhibition in the OC-2 cell line are specific to heat shock stress. These results diverge from a previous report on pp242 usage in HeLa cells, in which a reduction of the number of SGs by approximately 70% was achieved upon arsenite treatment (Fournier et al. 2013). Since pp242 acts by favouring eIF4E interaction with its hypophosphorylated 4E-BP1 inhibitory factor, this event seems to be crucial for protein translation to

continue during heat shock stress in the OC-2 cell line, but not during arsenite stress. An explanation for the fact that pp242 did not inhibit the formation of SGs upon sodium arsenite treatment may be related to the fact that sodium arsenite stress may inhibit PI-3K kinase. Since the PI-3K pathway was shown to be specifically inhibited under sodium arsenite stress in mouse embryonic stem cells (Ivanov et al. 2013), it can be hypothesised that the SGs formed as a consequence of sodium arsenite stress in OC-2 cells are not generated via PI-3K. Therefore, disrupting the mTORC pathway may not present any effects in terms of SG-inhibition under sodium arsenite stress conditions in the OC-2 cell line. Correspondingly, inactivation of the HRI kinase during sodium arsenite stress could be sufficient to disrupt the translation initiation and generate SGs, since this kinase has been shown to be specifically activated by arsenite stress (Lu et al. 2001; McEwen et al. 2005). These hypotheses are in agreement with the observation that upon ISRIB treatment, the SGs generated by both heat shock and arsenite stressors are inhibited (Figs.3.15 and 3.16). Since ISRIB specifically acts by activating eIF2B and reducing eIF2 phosphorylation (Sidrauski et al. 2015), its effects downstream of the sensor kinases HRI and PI-3K may explain the inhibition of SG formation under heat shock and sodium arsenite stresses. Detection of polyA⁺ mRNA corroborates the inhibitory effects of ISRIB on the SG formation, since simultaneous incubation of ISRIB with arsenite stress maintains polyA⁺ mRNA distributed throughout the nucleus and the cytoplasm, without aggregation at SGs (Fig.3.14). When compared to pp242, ISRIB decreased the number of SGs generated by both heat shock and sodium arsenite, whereas pp242 only affected the number of SGs formed upon heat shock stress. Along with the fact that no increased cellular death events were observed and that ISRIB acts downstream of pp242 in the stress signalling cascade, ISRIB was then chosen to subsequently manipulate SG formation in the *ex-vivo* mouse cochlea.

Hydroxamate (-)-9 was used in this study to promote SG formation, since this compound was previously shown to disrupt translation initiation in eukaryotes (Bordeleau et al. 2008), thus constituting an excellent candidate to assess whether SG formation can be manipulated *in-vitro* in the absence of stress. This compound triggered robust SG formation when compared to vehicle-treated controls (Figs.3.18 and 3.20) and the standard pattern of a greater number of small granules was present across all the concentrations tested (Fig.3.21). Overall, in terms of SG formation, the average number of granules produced by hydroxamate (-)-9 was intermediate between heat shock and arsenite stress. This data agrees with the

findings from other studies using U2OS and HeLa cells, in which hippuristanol and pateamine, other molecules disrupting eIF4A, effectively managed to generate SGs without other stress being applied (Zurla et al. 2011). Here, hydroxamate (-)-9 treatment also resulted in SGs containing polyA⁺ mRNA (Fig.3.19), suggesting that the effects of this compound include sequestration and triage of mRNA molecules to SGs. Moreover, during recovery from hydroxamate (-)-9 treatment, SGs could disassemble and, at the same time, polyA⁺ mRNA returned to its regular cellular distribution (Fig.3.19), demonstrating that the effects of this compound on SG formation are reversible. This observation also suggests that after recovery from hydroxamate (-)-9, polyA⁺ mRNA is released from SGs and can return to translation. These data designate hydroxamate (-)-9 as a useful pharmacological tool to manipulate SG formation, since the SGs generated by this compound resemble the granules triggered by kinase-activator stressors (e.g. heat shock and arsenite), in terms of number, size and the presence polyA⁺ mRNA in aggregation. In addition, hydroxamate (-)-9 did not cause increased cellular death and seemed to be well tolerated by the cells.

From these studies, optimum experimental conditions were set and validated for hydroxamate (-)-9 and ISRIB. These chemicals will be tested in mouse cochlear explants in order to try to understand the effect of manipulating SG formation on the hair cell survival upon ototoxic stress (Chapter 4).

4. Characterising the role of SGs during cochlear stress

4.1. Introduction

It is likely that the mammalian inner ear experiences stress permanently, whether from chemicals, drugs or as a result of exposure to environmental noise. All these factors contribute to the degradation and, ultimately, irreversible loss of hair cells (Forge & Schacht 2000; Schacht 2007; Perez & Bao 2011; Huth et al. 2011). The loss of mammalian hair cells is directly related to permanent hearing loss and deafness (Martini 2007). A better understanding of how the inner ear responds to stress may help to elucidate how hair cells are lost. The development of therapeutic strategies aimed at avoiding hair cell degradation during stress may eventually help in the prevention of hearing loss.

Aminoglycosides are a class of antibiotics used for the treatment of gram-negative bacterial infections that, despite their known side effects, are still the most commonly used antibiotics worldwide (Forge & Schacht 2000; Guthrie 2008; Audo & Warchol 2012). Aminoglycosides are thought to trigger the formation of free radicals and the activation of pro-apoptotic pathways once inside the hair cells, thus exhibiting highly ototoxic effects (Forge & Schacht 2000). Hearing loss caused by aminoglycoside exposure is associated with a permanent, bilateral high frequency pattern (Guthrie 2008).

Previous work from our laboratory in mouse cochlear explants has established that hair cells assemble SGs following aminoglycoside exposure (Towers et al. 2011), suggesting that SGs are implicated in the cochlea's response to stress.

Evidence suggests that SGs are required to allow optimal translation of stress-responsive mRNAs, thus contributing to an effective cellular response during transient stress conditions (Buchan & Parker 2009). The fact that SGs are not found during regular conditions (i.e. in unstressed cells), form transiently during cellular stress and disappear once the stress is over, have substantiated the hypothesis that the SG pathway is activated as a protective mechanism during cellular stress (Kedersha & Anderson 2002; Souquere et al. 2009). Moreover, pro-apoptotic molecules, transcription factors, stalled translation initiation complexes, amongst

others, have been reported to localise to SGs, contributing to the evidence that SGs are involved in cellular protection during stress (Kedersha et al. 1999; Kedersha et al. 2002; Tourrière et al. 2003; Kim et al. 2005; Ohn et al. 2008).

Although the formation of SGs has been generally associated with pro-survival mechanisms, dysregulation of SG formation has been linked to neurodegeneration and ageing. For instance, mutations in genes encoding proteins involved in RNA metabolism have been associated with neurological diseases (McDonald et al. 2011; Aulas et al. 2012). Aggregation of misfolded and damaged SG components has been observed as key pathological features in several diseases, such as ALS, Alzheimer's and Huntington's (Liu-Yesucevitz et al. 2011; Moreno et al. 2012; Vanderweyde et al. 2012; Ash et al. 2014). Additionally, the presence of continuous stress, characteristic of early neurodegenerative stages, may contribute to irreversible aggregation of RNA-binding proteins leading to the formation of "pathological" SGs (Ratovitski et al. 2012; Vanderweyde et al. 2012; Ash et al. 2014). Together, these different lines of evidence suggest that dysregulation of SG pathway may play a critical role in triggering neurodegeneration.

Modulation of SG formation has been tested out in neurodegeneration (Sidrauski et al. 2013; Halliday et al. 2015). Recent work has shown that suppression of those "pathological" SGs is associated with neuroprotective effects in ALS and prion-diseased mice (Kim et al. 2014; Halliday et al. 2015).

Considering all this, it seems timely to investigate the role that SG play on the hair cell's response to damage. In this chapter, the pharmacological tools previously screened (Chapter 3) are used to modulate the SG pathway during stress. Ultimately, the hypothesis explored here is whether manipulation of SG formation can promote hair cell survival during acute aminoglycoside stress.

4.2. Results

4.2.1. Cochlear cells assemble SGs in response to stress

Chapter 3 provided an initial assessment of SG formation and regulation in an inner ear-derived cell line. I developed an assay to detect RNA to SGs in OC-2 cells, therefore confirming the RNA-containing nature of the SGs formed in this system. A novel method for quantifying the number and size of SGs formed upon stress was developed. In addition, usable concentration ranges were obtained for the use of pharmacological compounds to manipulate SG assembly.

Here, mouse cochlear explants are used to investigate whether manipulation of SG formation can improve hair cell survival upon aminoglycoside toxicity. The pharmacological tools used to manipulate SG formation in the OC-2 cell line are used here and their effect is assessed in terms of hair cell survival following aminoglycoside exposure.

Initially, to understand the dynamics of SG formation in the mammalian cochlea, P3 mouse cochlear explants were used to provide a detailed description and quantification of SGs. Mouse cochlear explants were submitted to different types of stress (e.g. heat shock and arsenite) and SG formation was assessed by RNA-immuno-FISH and confocal imaging (see methods sections 2.14 and 2.16). Quantification of SGs was performed using Fiji software as detailed in methods section 2.19.2.

Mouse cochlear explants were exposed to heat shock and sodium arsenite, for 1h at 43°C and 1h at 0.5mM, respectively, following previous experimental conditions optimised in the OC-2 cell line (see sections 3.2.1 and 3.2.2). Untreated explants were kept at 37°C.

In untreated samples, polyA⁺ mRNA is detected throughout the nucleus and the cytoplasm of both hair cells and supporting cells, without aggregation at SGs (Figs.4.1 A and 4.3 A, white arrows, untreated panels), consistent with the observations in the OC-2 cell line (section 3.2.1). This is the first time that polyA⁺ mRNA is visualised in *ex-vivo* mouse cochlear cells. SG-marker protein TIA-1 is distributed throughout the nucleus and the cytoplasm of untreated cells (Figs.4.1 A and 4.3 A, white arrows, untreated panels), corroborating previous observations in OC-2 cells (section 3.2.1).

MyosinVIIa labelling hair cells in control samples (Fig.4.1, panel A, white arrowheads) reveals the highly organised organ of Corti, presenting three rows of outer hair cells and one row of inner hair cells. DAPI labels chromatin and, in untreated explants, no increased cell death was reported.

After exposure to either heat shock or sodium arsenite, cochlear cells presented SG formation in response to these stresses, as it can be seen in hair cells (Fig.4.1, panels B and C, yellow arrows) and supporting cells (Fig.4.3, panels B and C, yellow arrows).

PolyA⁺ mRNA was found to aggregate with TIA-1 at cytoplasmic SGs in both hair cells (Fig. 4.2) and supporting cells (Fig.4.4), confirming the RNA-containing nature of the granules formed upon stress in the *ex-vivo* cochlea. Following heat shock or arsenite treatments, SGs were found to be present throughout the cytoplasm of hair cells and supporting cells and occasionally around the perinuclear area (Figs.4.1 and 4.3). Figures 4.2 and 4.4 show in higher magnification SG formation inside inner hair cells and supporting cells, respectively.

The highly organised structure of the organ of Corti was maintained after either heat shock or arsenite stresses, as it can be seen by MyosinVIIa staining of the hair cells, indicating the presence of three rows of outer hair cells and one row of inner hair cells (Fig.4.1). These treatments did not cause cell death, as indicated by DAPI staining of the chromatin structure (Fig.4.1).

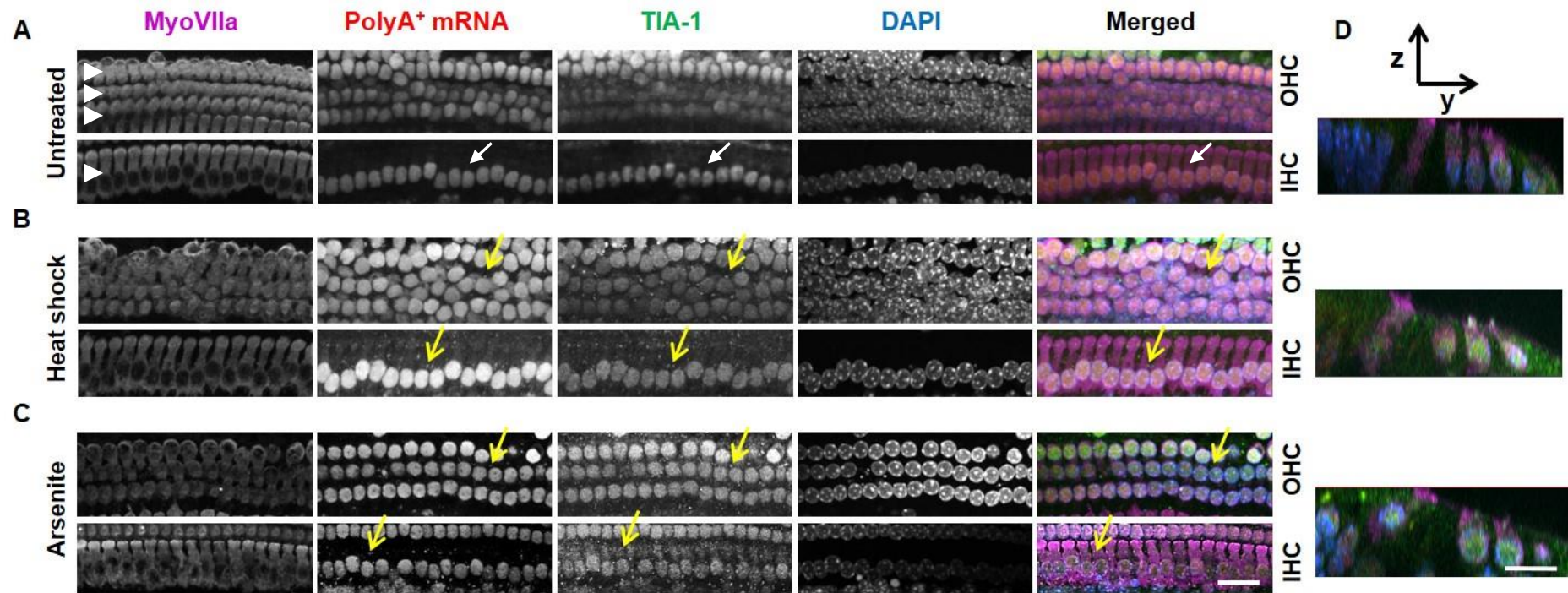


Figure 4.1 – Mouse hair cells assemble SGs in response to stress. Cochlear explant cultures from P3 mice were submitted to heat shock stress for 1h at 43°C and sodium arsenite stress for 1h at 0.5mM. (A) Untreated samples cultured at 37°C. (B) Heat shock treated samples. (C) Arsenite treated samples. (D) Z/Y single planes are shown for each condition (untreated, heat shock, arsenite). MyosinVIIa was used to mark inner and outer hair cells (IHC and OHC, respectively). In untreated samples white arrowheads mark hair cells and white arrows indicate the nuclear and cytoplasmic distribution of polyA⁺ mRNA and TIA-1, not aggregating at SGs. PolyA⁺ mRNA was detected using a Cy3-labelled probe. Yellow arrows point to SG formation following heat shock and arsenite treatments. Chromatin structure was assessed using DAPI. Images shown correspond to the middle of the basal end of the cochlear coils. Images are maximum intensity projections of confocal sub-stacks. Scale bar= 25 μm for left-hand side panels and 10 μm for right-hand side Z/Y panels.

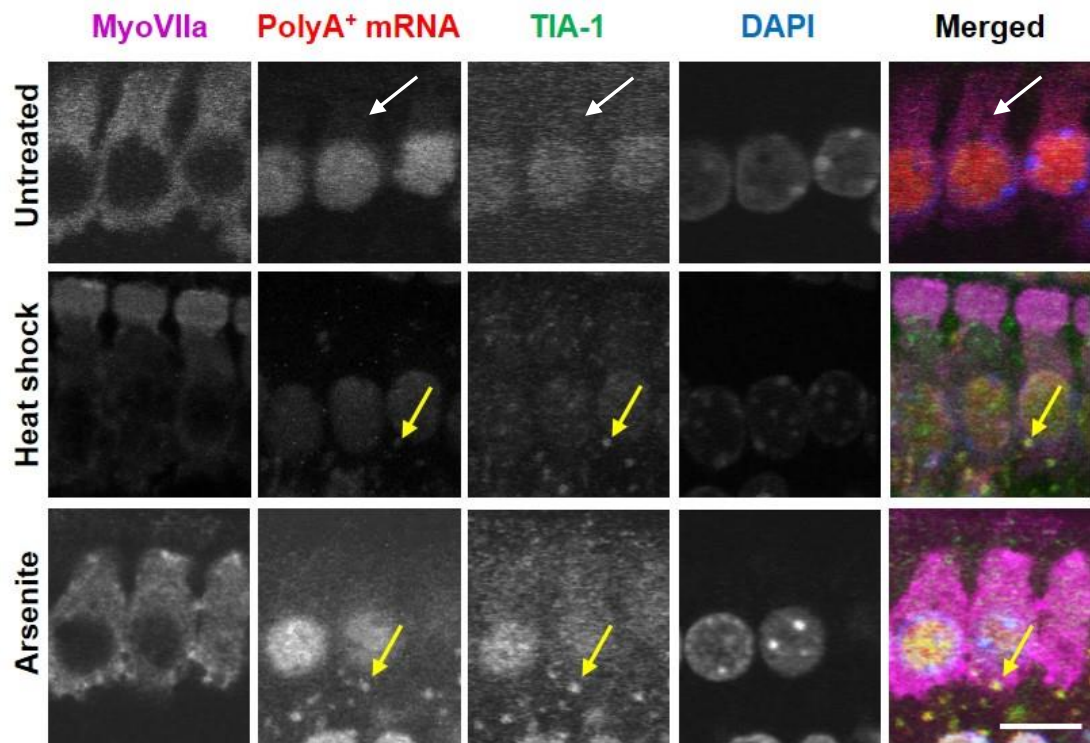


Figure 4.2 – PolyA⁺ mRNA aggregates with TIA-1 at SGs following stress in hair cells. Cochlear explant cultures from P3 mice were submitted to heat shock stress for 1h at 43°C and sodium arsenite stress for 1h at 0.5mM. Untreated samples were cultured at 37°C. White arrows point to the nuclear and cytoplasmic distribution of polyA⁺ mRNA and TIA-1, not aggregating at SGs in untreated samples. Yellow arrows point to SG formation following heat shock and arsenite stresses. MyosinVIIa was used to mark hair cells. Chromatin structure was assessed using DAPI. Images represent single stacks of confocal images. Scale bar= 10 μ m.

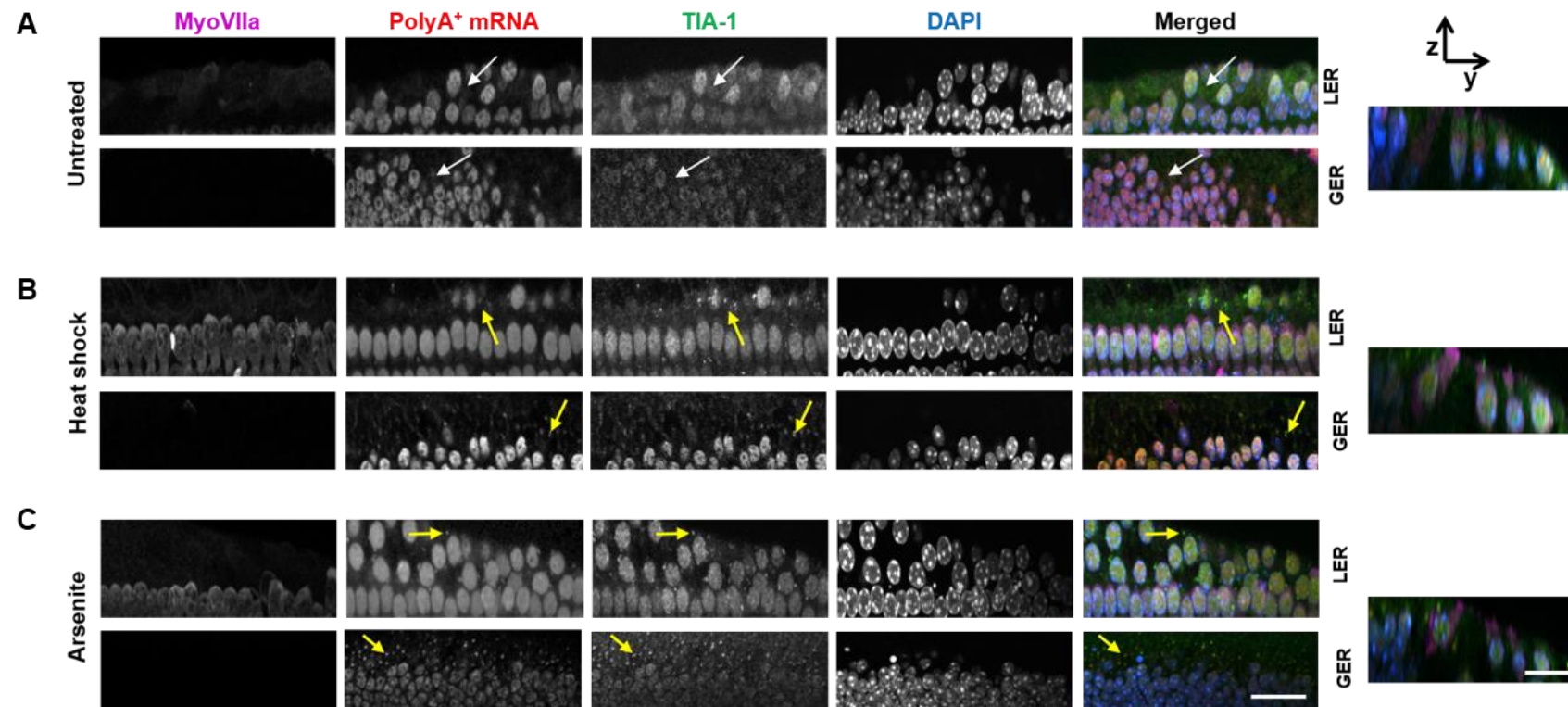


Figure 4.3 – Mouse supporting cells assemble SGs in response to stress. Cochlear explant cultures from P3 mice were submitted to heat shock stress for 1h at 43°C and sodium arsenite stress for 1h at 0.5mM. (A) Untreated samples cultured at 37°C. (B) Heat shock treated samples. (C) Arsenite treated samples. White arrows point to the nuclear and cytoplasmic distribution of polyA⁺ mRNA and TIA-1, not aggregating at SGs in untreated samples. Yellow arrows point to SG formation following heat shock and arsenite stresses. PolyA⁺ mRNA was detected using a Cy3-labelled probe. Supporting cells shown correspond to the lesser epithelial ridge (LER) and greater epithelial ridge (GER). Chromatin structure was assessed using DAPI. Images shown correspond to the middle of the basal end of the cochlear coils. Images are maximum intensity projections of confocal sub-stacks. Z/Y single planes are shown for each condition (untreated, heat shock, arsenite). Scale bar= 25 μm for left-hand side panels and 10 μm for right-hand side Z/Y panels.

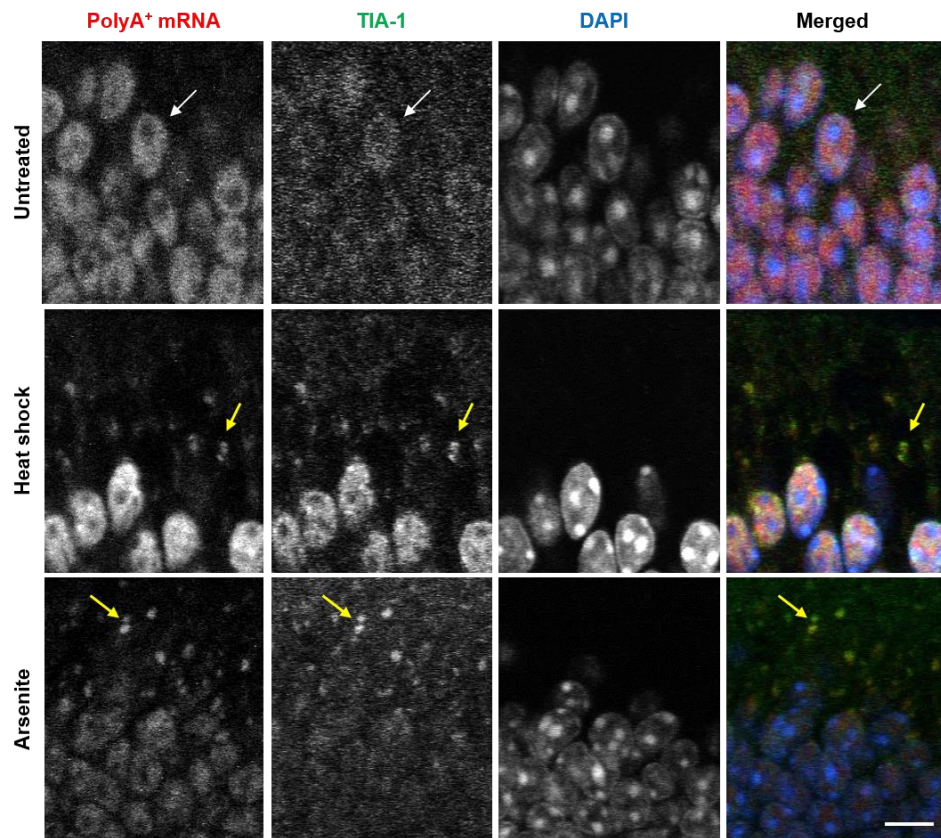


Figure 4.4 – PolyA⁺ mRNA aggregates with TIA-1 at SGs following stress in supporting cells. Cochlear explant cultures from P3 mice were submitted to heat shock stress for 1h at 43°C and sodium arsenite stress for 1h at 0.5mM. Untreated samples were cultured at 37°C. White arrows point to the nuclear and cytoplasmic distribution of polyA⁺ mRNA and TIA-1, not aggregating at SGs in untreated samples. Yellow arrows point to SG formation following heat shock and arsenite stresses. Chromatin structure was assessed using DAPI. Images represent single stacks of confocal images. Scale bar= 10 μ m.

In order to quantify SG formation in terms of number and size in the cochlear explants, the quantification protocol used in the previous section was adapted, considering the three-dimensional structure of the organ of Corti (see section 2.19.2 in methods). In brief, the multicellular structure of the organ of Corti was taken into account and MyosinVIIa signal was used to isolate the hair cells from the supporting cells. Estimated volumes for hair cells were obtained and SG quantification assessed in terms of density. Considering the polarised nature of hair cells, the hypothesis of differential SG formation in different areas of the cells was formulated. Hair cells were divided into three distinct regions: basal, middle and luminal (see methods section 2.20) and SG quantification assessed for the three different areas. When no statistical significant differences were reported amongst the different areas, the data presented below correspond to an estimation of the total number

and size of SGs per μm^3 of hair cell volume. When differences in terms of SG formation were found amongst the different hair cell regions (basal, middle, luminal), a detailed description of the number and size of SGs per μm^3 of hair cell volume in each region is shown.

The number of SGs was estimated for supporting cells considering two different areas of the epithelium: the lesser and greater epithelial ridges (see methods section 2.20). All the values shown below for hair cells and supporting cells were calculated based on approximation protocols and represent estimated values.

Quantification of the number of SGs revealed that in untreated conditions an average of 3.4×10^{-6} and $0.8 \times 10^{-3} \pm 6.6 \times 10^{-5}$ SGs were found per μm^3 of inner and outer hair cells, respectively (Fig.4.5 A and B). As regarding their size, the SGs detected in untreated conditions were found to average approximately $0.15 \mu\text{m}^2$ (Fig.4.6 A and B). In untreated supporting cells, $0.3 \times 10^{-3} \pm 0.1 \times 10^{-3}$ SGs were found per μm^3 of the lesser epithelial ridge and $1.3 \times 10^{-5} \pm 3.2 \times 10^{-6}$ SGs per μm^3 of the greater epithelial ridge (Fig.4.7 A). These averaged approximately $0.4 \mu\text{m}^2$ in size (Fig.4.7 B).

These data confirm a significant increase in the number of SGs assembled following heat shock and sodium arsenite stresses. After 1h heat shock treatment, on average $3.3 \times 10^{-3} \pm 0.2 \times 10^{-3}$ and $2.6 \times 10^{-3} \pm 0.2 \times 10^{-3}$ SGs are formed per μm^3 of inner and outer hair cells, respectively (Fig. 4.5 A and B). The SGs formed as a consequence of heat shock stress average $0.37 \mu\text{m}^2$ in size (Fig. 4.6 A and B). Supporting cells form slightly more SGs than hair cells after heat shock stress, $3.9 \times 10^{-3} \pm 0.6 \times 10^{-3}$ and $4.4 \times 10^{-3} \pm 0.4 \times 10^{-3}$ SGs per μm^3 of the lesser and greater epithelial ridges, respectively (Fig.4.7 A). The SGs formed in the supporting cells averaged approximately $0.4 \mu\text{m}^2$ in size (Fig.4.7 B).

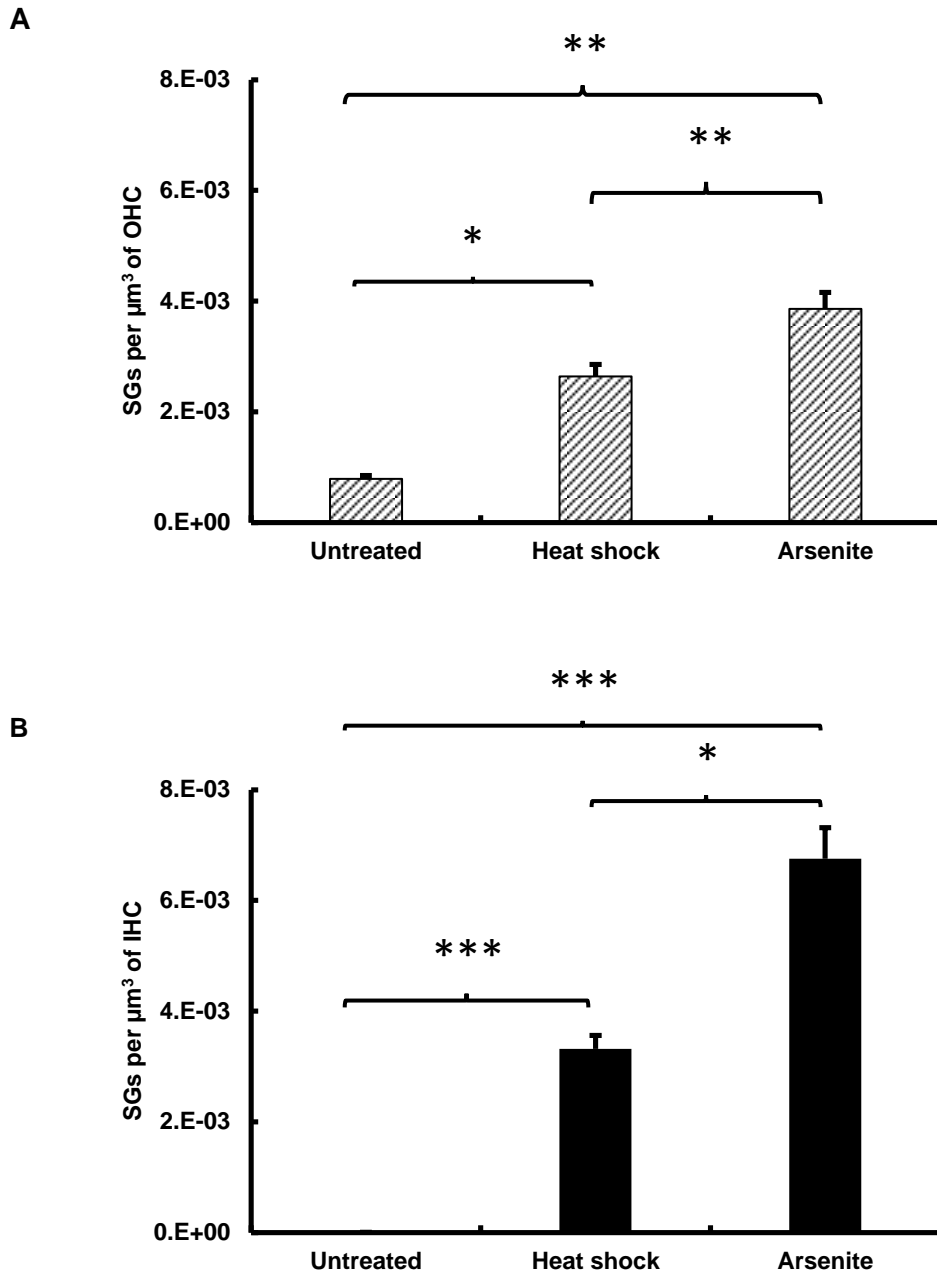


Figure 4.5 – Quantification of the number of SGs in hair cells. Average number of SGs per μm^3 of hair cell volume. (A) Outer hair cells (OHC). (B) Inner hair cells (IHC). Measurements were taken from the middle of the basal end of the cochlear coil. Black bars represent inner hair cells and striped bars represent outer hair cells. * $p < 0.05$, ** $p < 0.005$, *** $p < 0.001$ (Student's t -test against untreated condition). Error bars represent SEM ($n=4$ for each condition).

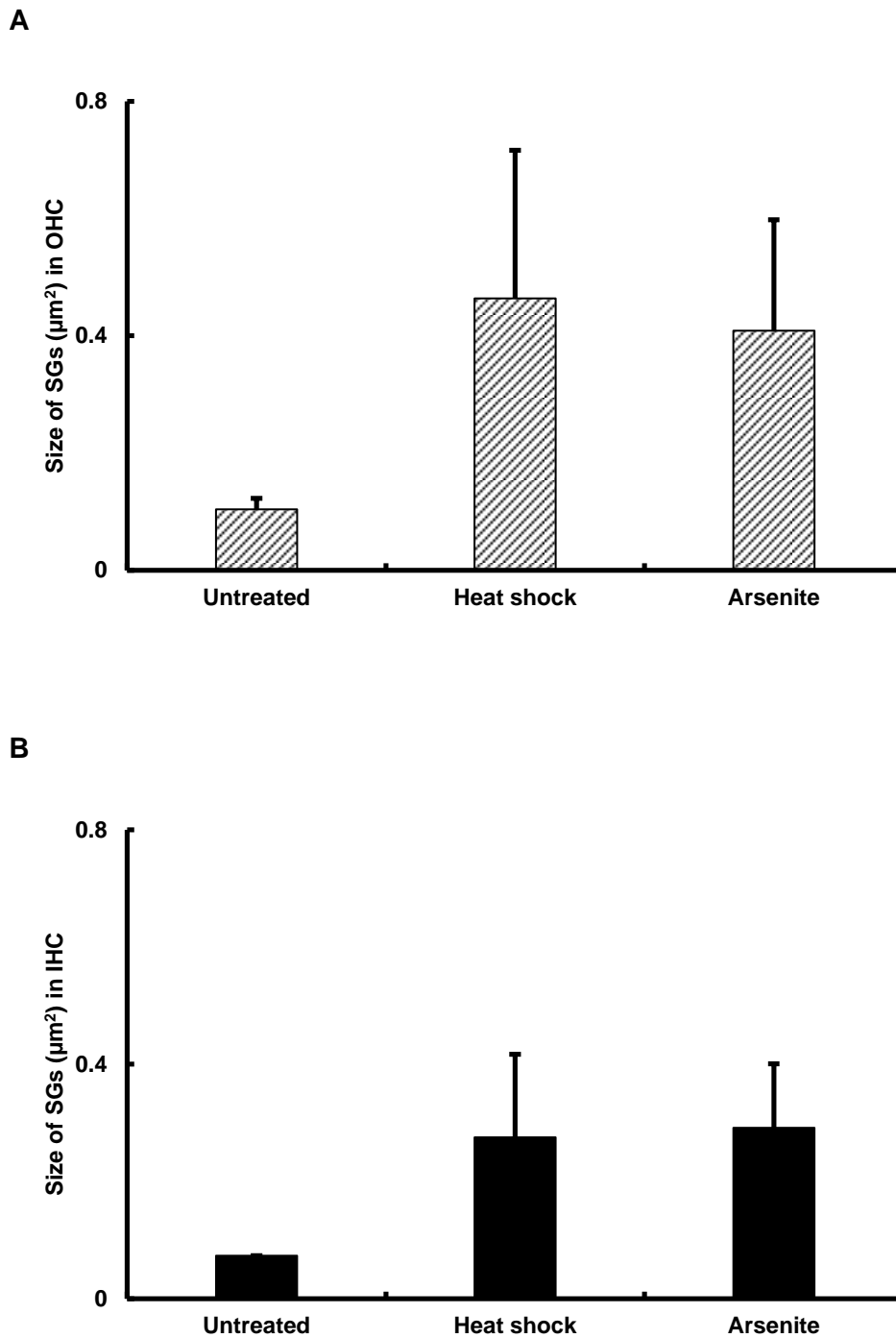
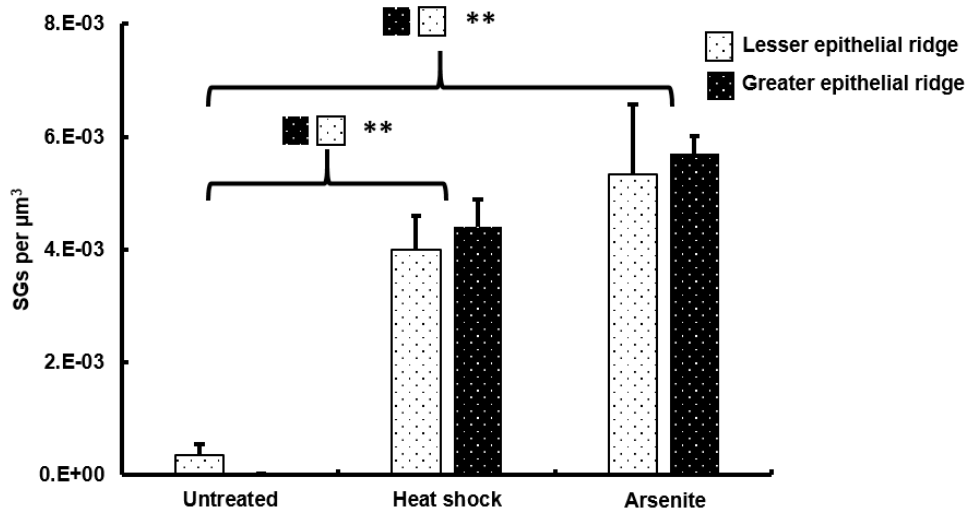


Figure 4.6 – Quantification of the size of SGs in hair cells. Average size of SGs (μm^2). (A) Outer hair cells. (B) Inner hair cells. Measurements were taken from the middle of the basal end of the cochlear coil. Black bars represent inner hair cells and striped bars represent outer hair cells. Error bars represent SEM (n=4 for each condition).

A



B

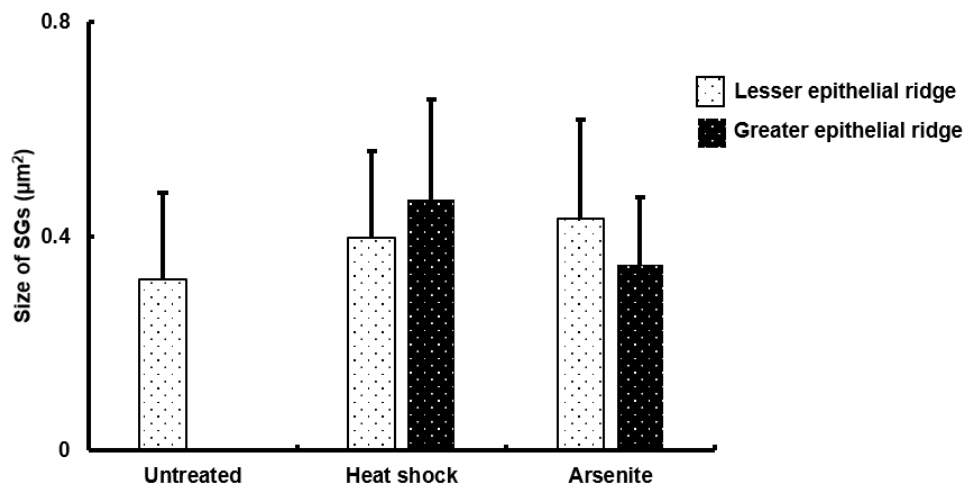


Figure 4.7 – Quantification of SGs in supporting cells. (A) Average number of SGs per μm^3 . (B) Average size of SGs (μm^2). White bars represent lesser epithelial ridge and black bars represent greater epithelial ridge. Measurements were taken from the middle of the basal end of the cochlear coil. ** $p < 0.005$ (Student's *t*-test against untreated condition). Error bars represent SEM ($n=4$ for each condition).

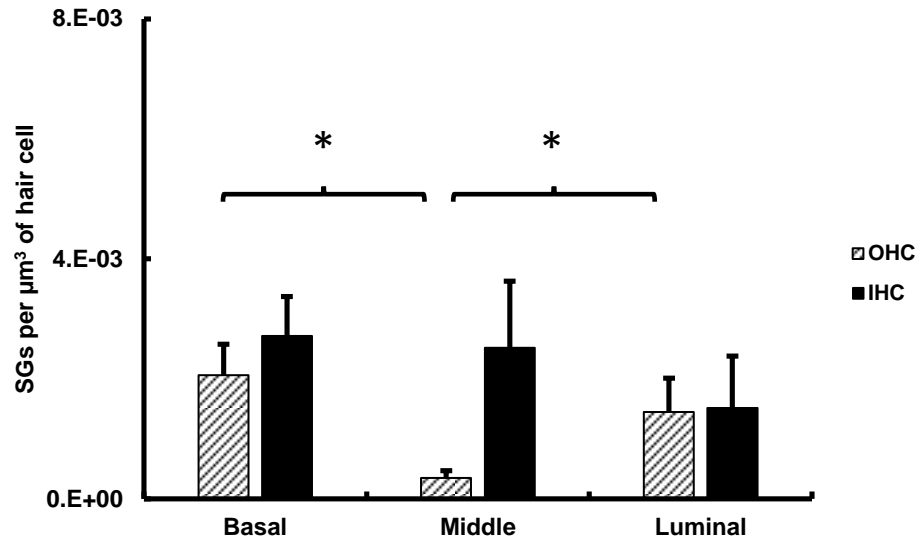
Arsenite stress generated more SGs in inner hair cells than outer hair cells ($p < 0.05$, Student's *t*-test), with an average of $6.7 \times 10^{-3} \pm 0.5 \times 10^{-3}$ and $3.8 \times 10^{-3} \pm 0.3 \times 10^{-3}$ SGs per μm^3 of inner and outer hair cells, respectively (Fig.4.5 A and B).

Quantification of these data shows that the different sub-regions of outer hair cells (basal, middle, luminal) showed differential SG formation upon arsenite stress. On average, outer hair cells generated $2.1 \times 10^{-3} \pm 0.5 \times 10^{-3}$ SGs and $1.4 \times 10^{-3} \pm 0.6 \times 10^{-3}$ SGs per μm^3 of basal and luminal cytoplasmic area, respectively (Fig.4.8 A). In fact, the lowest number of SGs generated upon arsenite treatment was found in the middle surface of the outer hair cells, with an average of $0.3 \times 10^{-3} \pm 0.1 \times 10^{-3}$ SGs formed per μm^3 of outer hair cell middle cytoplasmic area (Fig.4.8 A). This was significantly lower when compared to the basal and luminal areas, respectively ($p < 0.05$ for basal and luminal, compared to the middle region, Student's *t*-test). No differences were found regarding SG distribution in the inner hair cells (Fig.4.8 A). The arsenite-triggered SGs in hair cells were found to average approximately $0.3 \mu\text{m}^2$ in size (Fig.4.8 B) and there were no significant differences in the different cellular compartments.

Upon arsenite treatment, supporting cells presented $5.4 \times 10^{-3} \pm 1.2 \times 10^{-3}$ and $5.7 \times 10^{-3} \pm 0.3 \times 10^{-3}$ SGs per μm^3 of lesser and greater epithelial ridge, respectively (Fig.4.7 A). These averaged approximately $0.4 \mu\text{m}^2$ in size (Fig.4.7 B).

Altogether, these experiments show that mouse cochlear cells respond to heat shock and arsenite stresses by assembling SGs. Moreover, polyA⁺ mRNA was identified as a component of SGs formed in hair cells and supporting cells, confirming the RNA/protein nature of the SGs generated in cochlear cells. Additionally, detailed quantification of the number and size of SGs was performed for both hair cells and supporting cells, thus allowing a better understanding of how cochlear native cells respond to stress in terms of SG formation.

A



B

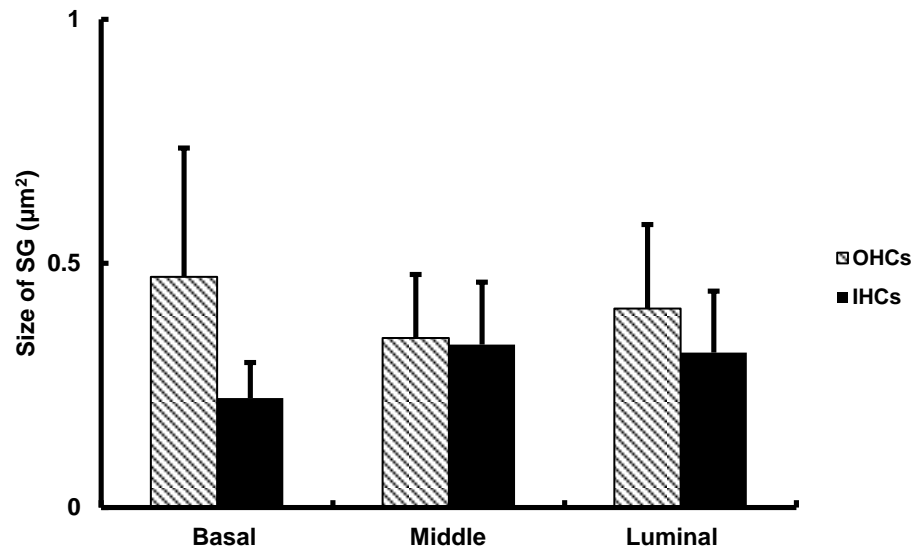


Figure 4.8 – Quantification of SGs following sodium arsenite stress in hair cells. (A) Average number of SGs per μm^3 . (B) Average size of SGs (μm^2). Arsenite treatment was performed for 1h at 0.5mM. Differences in terms of SG-numbers between the middle surface when compared to basal and luminal were significant for the outer hair cells (Student's *t*-test, * $p < 0.05$). Black bars represent inner hair cells and striped bars represent outer hair cells. Measurements were taken from the middle of the basal end of the cochlear coil. Error bars represent SEM ($n=4$ for each condition).

4.2.2. Pharmacological manipulation of SGs in mouse cochlear explants

The previous section described the first experiments performed in mouse cochlear explants, aimed at assessing SG formation in cochlear cells following different types of stress.

Here, the next experiments sought to investigate whether pharmacological manipulation of SG formation was effective in the *ex-vivo* mouse cochlea, considering the objective of using aminoglycoside stress to assess the effect on hair cell survival. For this, the pharmacological tools previously screened and validated in the OC-2 cell line (see section 3.2.3) were used.

Hydroxamate (-)-9 disrupts protein translation in eukaryotes through sequestration of eIF4A from the eIF4F translation initiation complex (Hwang et al. 2004; Bordeleau et al. 2008). In OC-2 cells, hydroxamate (-)-9 incubation resulted in SG formation, without causing cellular death (section 3.2.3.4). The number and size of SGs generated by hydroxamate (-)-9 were similar to those formed by heat shock or sodium arsenite stresses, establishing hydroxamate (-)-9 as a suitable compound to manipulate SG formation.

To test whether hydroxamate (-)-9 induces SG formation in the *ex-vivo* cochlea, mouse cochlear explants were incubated with 0.1 μ M of hydroxamate (-)-9 for 8h, following previous conditions optimised in the OC-2 cell line (section 3.2.3.4).

Hydroxamate (-)-9 treatment resulted in robust SG formation (Fig.4.9, hydroxamate (-)-9 panel, yellow arrows), in agreement with previous data obtained in OC-2 cells (section 3.2.3.4). Upon hydroxamate (-)-9 exposure, TIA-1 SG-marker protein aggregated in the cytoplasm of both hair cells and supporting cells with polyA⁺ mRNA, as shown in detail in Figures 4.10 (hair cells, hydroxamate (-)-9 panel, yellow arrows) and 4.12 (supporting cells, hydroxamate (-)-9 panel, yellow arrows). The SGs generated by hydroxamate (-)-9 treatment were found to distribute evenly throughout the cytoplasm of the cells and were found across the cytoplasm and around the perinuclear area. Figure 4.10 shows an inner hair cell at higher magnification showing a SG near the nucleus of the cell.

Hydroxamate (-)-9 treatment itself did not cause any disruption of the organ of Corti, as assessed by MyosinVIIa staining of the hair cells (Fig.4.9, hydroxamate (-)-9 panel, white arrowheads) and the F-actin filaments of the hair cell stereocilia

(Fig.4.13, yellow arrows). Following hydroxamate (-)-9 treatment, the highly organised structure of the organ of Corti was maintained with the presence of three rows of outer hair cells and one row of inner hair cells (Fig.4.9, white arrowheads). No increased cell death events were reported, as indicated by the normal DAPI staining following hydroxamate (-)-9 treatment (Fig.4.9, hydroxamate (-)-9 panel).

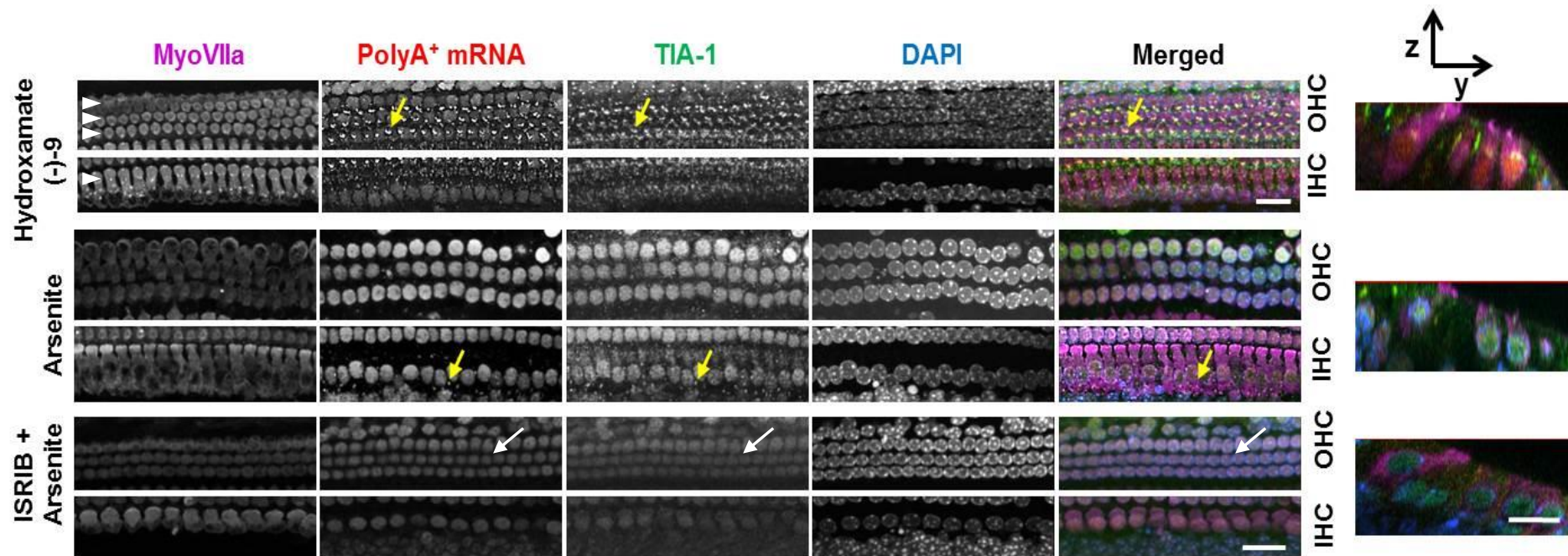


Figure 4.9 – SG formation can be manipulated in hair cells. Cochlear explant cultures from P3 mice were incubated with either 0.1 μ M of hydroxamate (-)-9 for 8h to induce SG formation and during 1h with 200nM of ISRIB in the presence of arsenite stress (1h, 0.5mM) to prevent SG formation. Arsenite treatment is shown to demonstrate SG formation. All the incubations were performed at 37°C. PolyA⁺ mRNA was detected using a Cy3-labelled probe. MyosinVIIa was used to mark inner and outer hair cells (IHC and OHC, respectively). White arrowheads in untreated samples point to hair cells. Yellow arrows point to SG formation upon hydroxamate (-)-9 or arsenite treatments. White arrows point to the nuclear and cytoplasmic distribution of polyA⁺ mRNA and TIA-1, not aggregating at SGs, upon ISRIB incubation during arsenite stress. Chromatin structure was assessed using DAPI. Images shown correspond to the middle of the basal end of the cochlear coils. Images are maximum intensity projections of confocal sub-Z-stacks. Z/Y single planes are shown for each condition (hydroxamate (-)-9, arsenite, ISRIB + arsenite). Scale bar= 25 μ m for left-hand side panels and 10 μ m for right-hand side Z/Y panels.

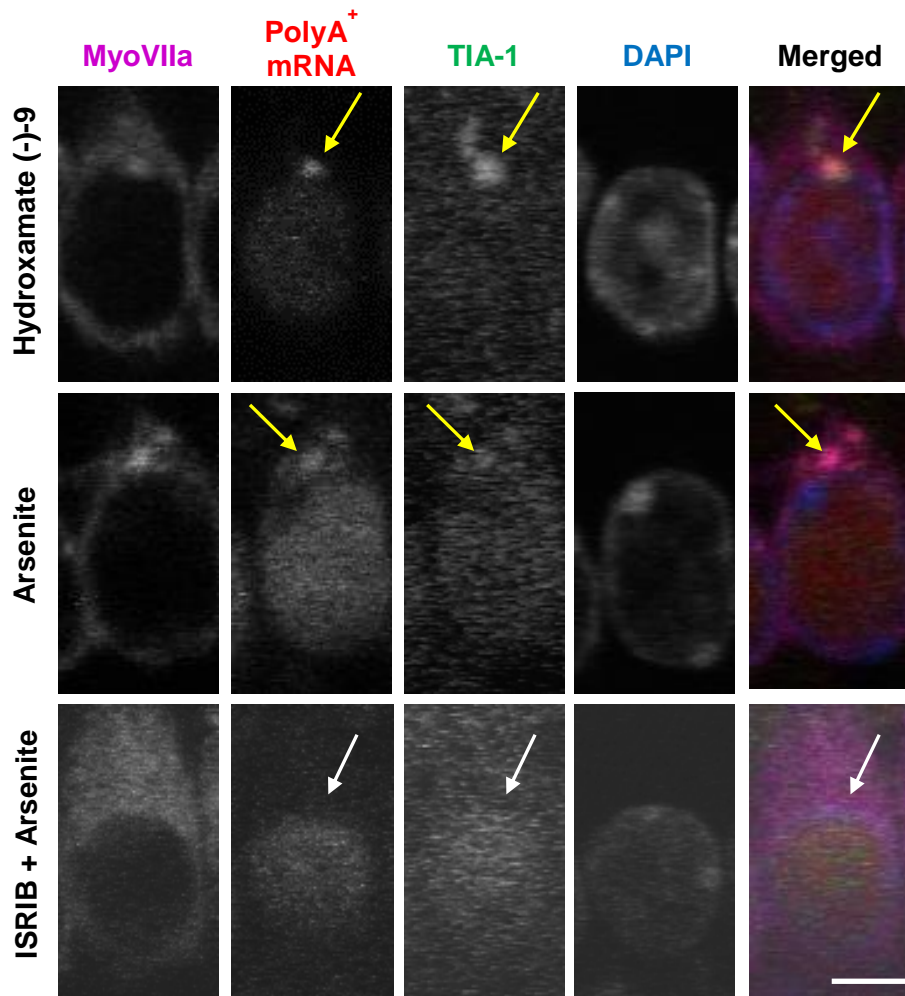


Figure 4.10 – Distribution of polyA⁺ mRNA and TIA-1 in hair cells following pharmacological manipulation of SG formation. Cochlear explant cultures from P3 mice were submitted to hydroxamate (-)-9 treatment for 8h at 37°C. ISRIB treatment (200nM) was performed in the presence of sodium arsenite stress for 1h at 0.5mM. Arsenite treatment is shown to demonstrate SG formation. MyosinVIIa was used to mark hair cells. Yellow arrows point to SG formation upon hydroxamate (-)-9 and arsenite treatments. White arrows point to the nuclear and cytoplasmic distribution of polyA⁺ mRNA and TIA-1, not aggregating at SGs, upon ISRIB incubation during arsenite stress. Chromatin structure was assessed using DAPI. Images represent single stacks of confocal images. Scale bar= 10 μ m.

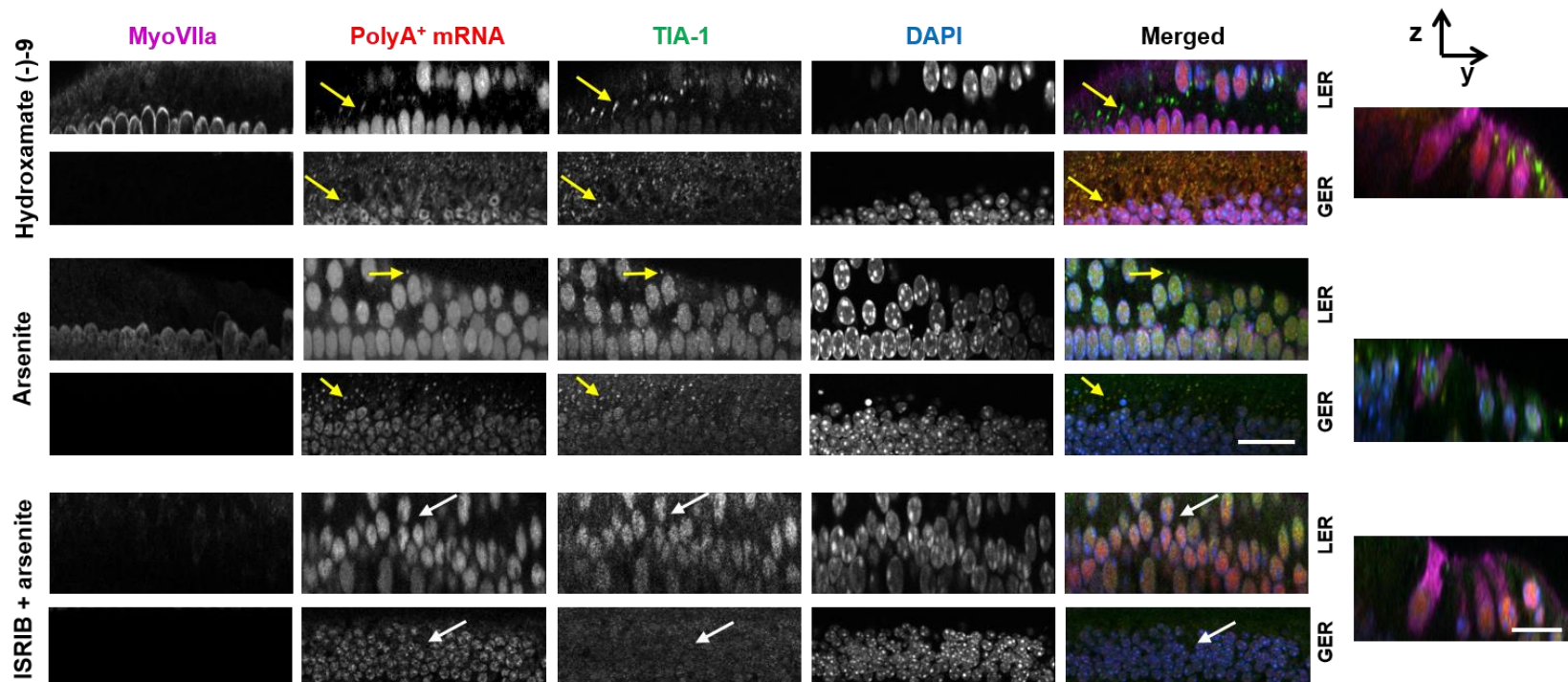


Figure 4.11 – SG formation can be manipulated in supporting cells. Cochlear explant cultures from P3 mice were incubated with either 0.1 μM of hydroxamate (-)-9 for 8h and 1h with 200nM of ISRIB in the presence of arsenite stress (1h, 0.5mM). Arsenite treatment is shown to demonstrate SG formation. All the incubations were performed at 37°C. PolyA⁺ mRNA was detected using a Cy3-labelled probe. Supporting cells are shown for the lesser epithelial ridge (LER) and greater epithelial ridge (GER). Yellow arrows point to SG formation upon hydroxamate (-)-9 and arsenite treatments. White arrows point to the nuclear and cytoplasmic distribution of polyA⁺ mRNA and TIA-1, not aggregating at SGs, upon ISRIB incubation during arsenite stress. Chromatin structure was assessed using DAPI. Images shown correspond to the middle of the basal end of the cochlear coils. Images are maximum intensity projections of confocal sub-Z-stacks. Z/Y single planes are shown for each condition (hydroxamate (-)-9, arsenite, ISRIB + arsenite). Scale bar= 25 μm for left-hand side panels and 10 μm for right-hand side Z/Y panels.

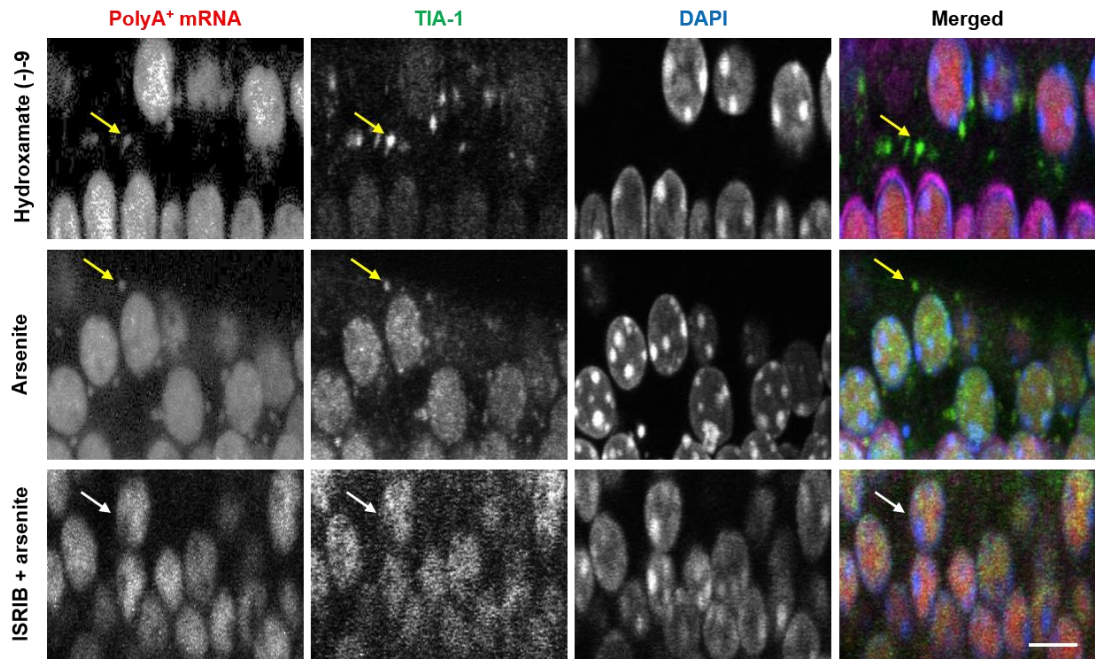


Figure 4.12 – Distribution of polyA⁺ mRNA and TIA-1 in supporting cells following pharmacological manipulation of SG formation. Cochlear explant cultures from P3 mice were submitted to hydroxamate (-)-9 treatment for 8h at 37°C. ISRIB treatment (200nM) was performed in the presence of sodium arsenite stress for 1h at 0.5mM. Arsenite treatment is shown to demonstrate SG formation. Yellow arrows point to SG formation upon hydroxamate (-)-9 and arsenite treatments. White arrows point to the nuclear and cytoplasmic distribution of polyA⁺ mRNA and TIA-1, not aggregating at SGs, upon ISRIB incubation during arsenite stress. Chromatin structure was assessed using DAPI. Images represent single stacks of confocal images. Scale bar= 10 μ m.

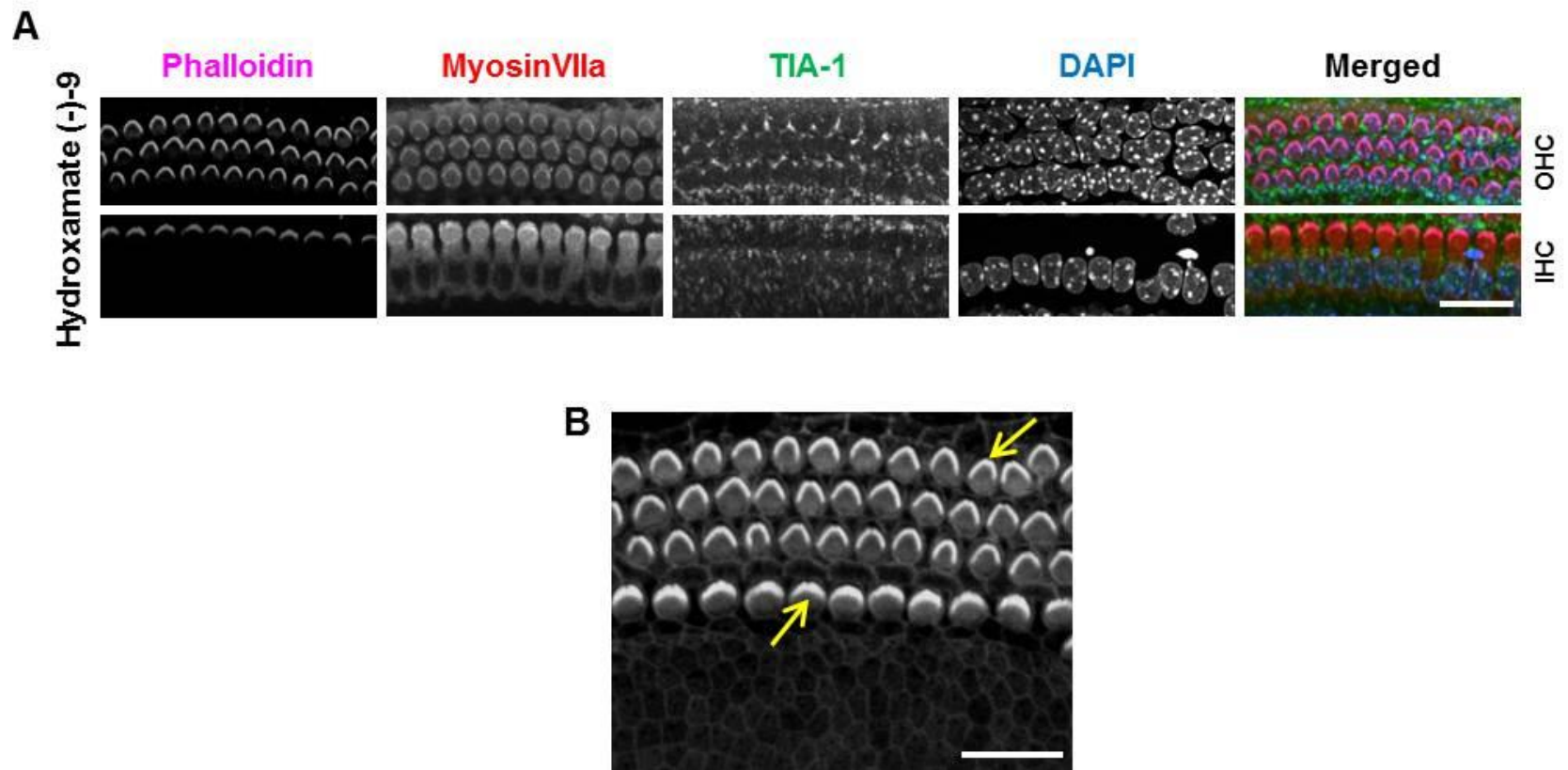


Figure 4.13 – Hydroxamate (-)-9 does not present adverse effects on the hair cell stereocilia bundles. (A) Cochlear explant cultures from P3 mice were incubated with 0.1 μ M of hydroxamate (-)-9 for 8h at 37°C. MyosinVIIa labels outer hair cells (OHC) and inner hair cells (IHC). Chromatin structure was assessed using DAPI. Images are maximum intensity projections of confocal sub-Z-stacks. (B) Maximum intensity projection of a confocal Z-stack image (35 μ m) shows filamentous actin in the hair cell bundles (yellow arrows). Images shown correspond to the middle of the basal end of the cochlear coils. Scale bar= 25 μ m.

Quantification of SG formation reveals that hydroxamate (-)-9 treatment generates more SGs in inner hair cells than in outer hair cells ($p < 0.005$, Student's *t*-test): on average, $1.2 \times 10^{-2} \pm 0.7 \times 10^{-3}$ SGs are generated per μm^3 in inner hair cells and $0.6 \times 10^{-2} \pm 0.2 \times 10^{-3}$ SGs per μm^3 in outer hair cells (Fig.4.14 A and B).

Hydroxamate (-)-9 generated SGs averaging approximately $0.6 \mu\text{m}^2$ in size in the outer hair cells, whereas the granules formed in the inner hair cells averaged approximately $0.4 \mu\text{m}^2$ in size (Fig.4.15 A and B).

Detailed quantification of SGs considering three distinct areas in hair cells (basal, middle, luminal) reveals that inner hair cells assemble more SGs per μm^3 than outer hair cells in both middle and luminal surfaces when hydroxamate (-)-9 is applied (Fig.4.16 A). No differences were reported for the basal area (Fig.4.16 A).

As regarding the supporting cells, hydroxamate (-)-9 treatment triggered the formation of $8.9 \times 10^{-3} \pm 3 \times 10^{-3}$ SGs and $9.7 \times 10^{-3} \pm 1.6 \times 10^{-3}$ SGs per μm^3 in the lesser and greater epithelial ridge supporting cells, respectively (Fig.4.17 A). The SGs generated following hydroxamate (-)-9 treatment in the supporting cells averaged $0.7 \mu\text{m}^2$ in size (Fig.4.17 B).

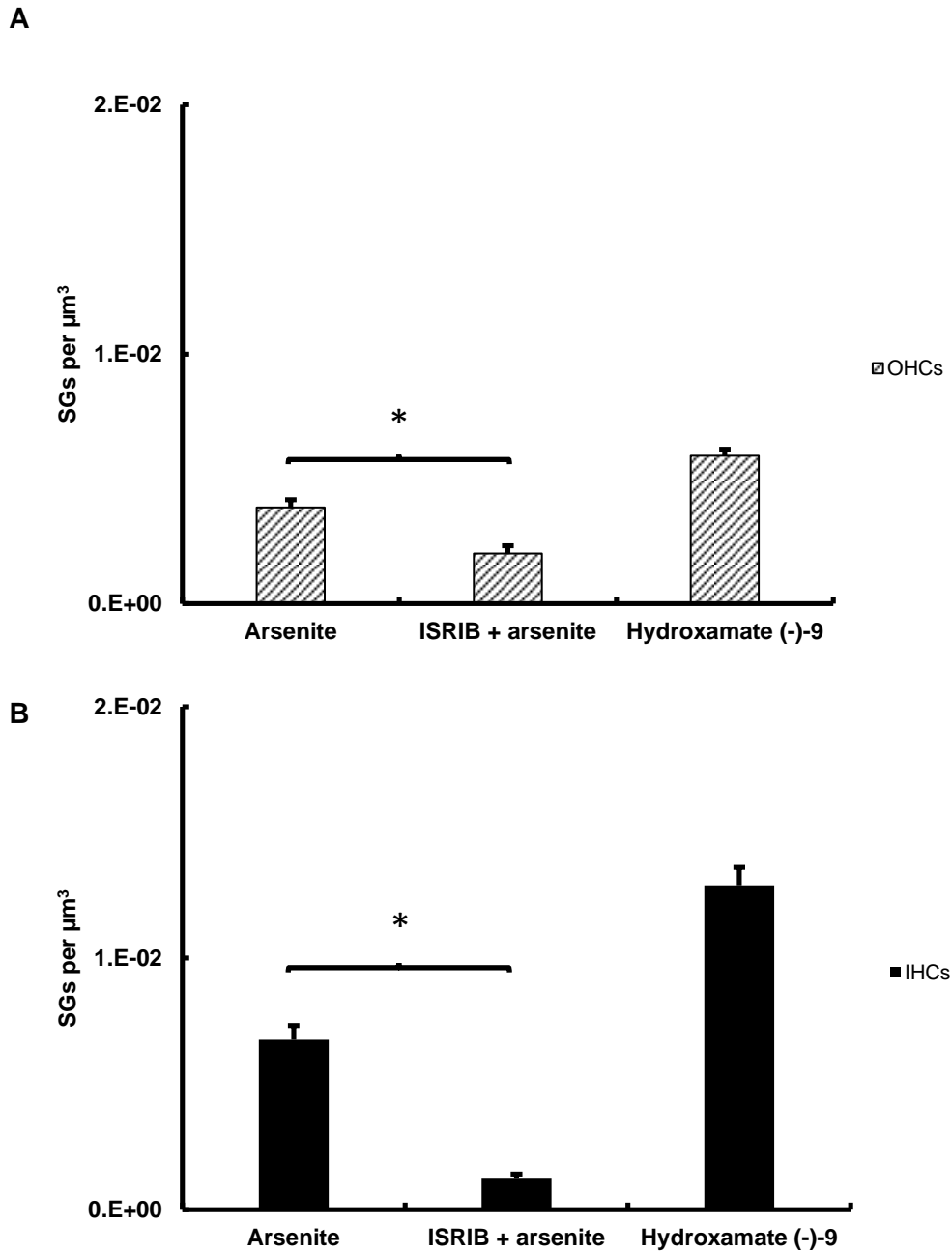


Figure 4.14 – Quantification of SGs present after ISRIB and hydroxamate (-)-9 treatments in cochlear hair cells. Average number of SGs per μm^3 of hair cell volume. (A) Outer hair cells. (B) Inner hair cells. ISRIB treatment significantly decreased the number of SGs formed upon arsenite stress (* $p < 0.05$, Student's t -test). Black bars represent inner hair cells and striped bars represent outer hair cells. Measurements were taken from the middle of the basal end of the cochlear coil. Error bars represent SEM ($n=4$ for each condition).

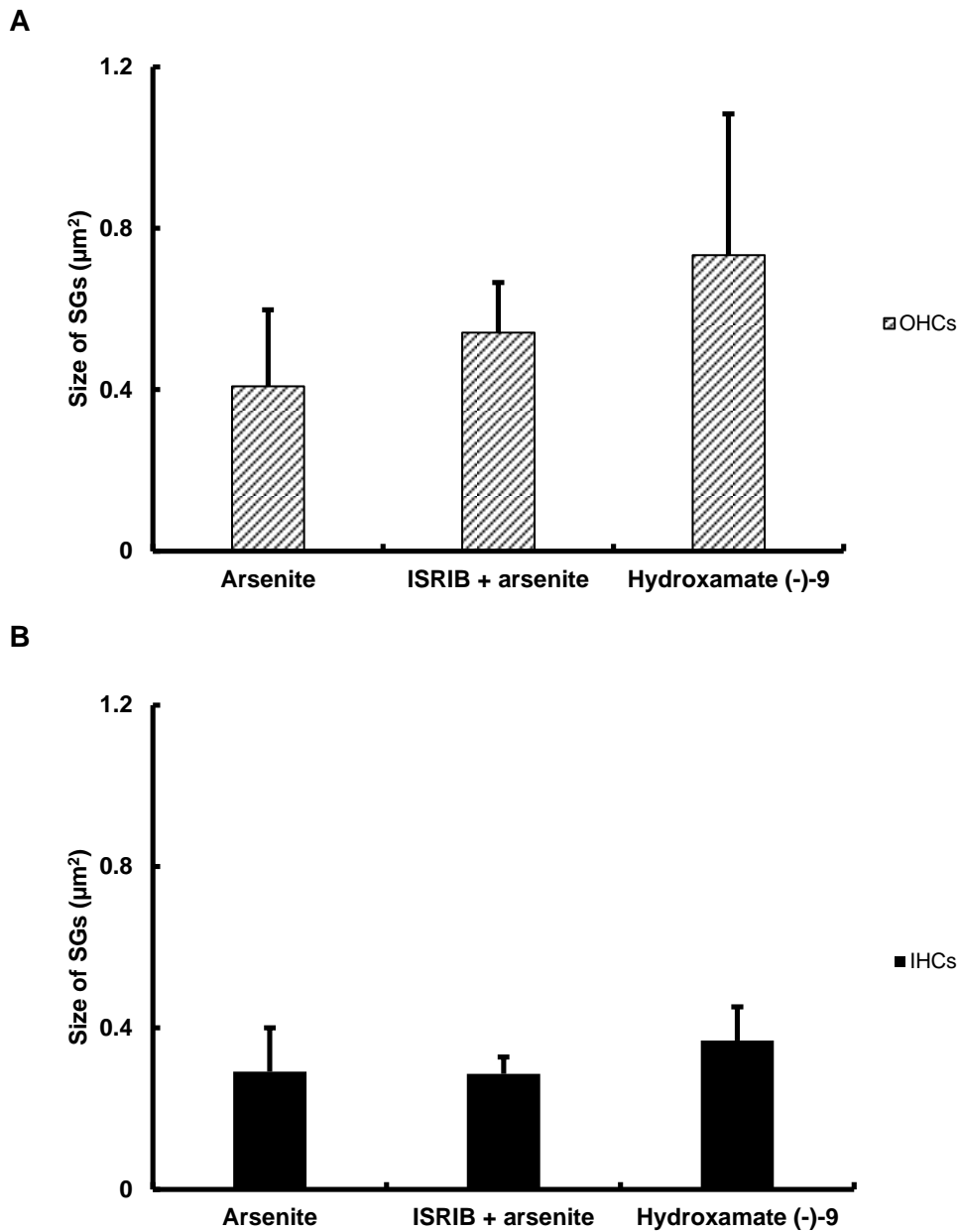
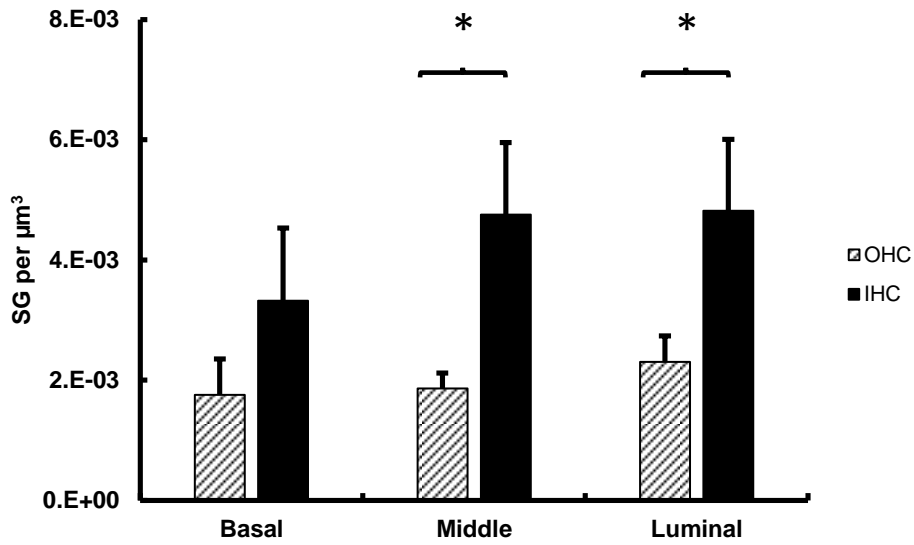


Figure 4.15 – Quantification of SG size after ISRIB and hydroxamate (-)-9 treatments in cochlear hair cells. Average size of SGs (μm^2). (A) Outer hair cells. (B) Inner hair cells. Black bars represent inner hair cells and striped bars represent outer hair cells. Measurements were taken from the middle of the basal end of the cochlear coil. Error bars represent SEM (n=4 for each condition).

A



B

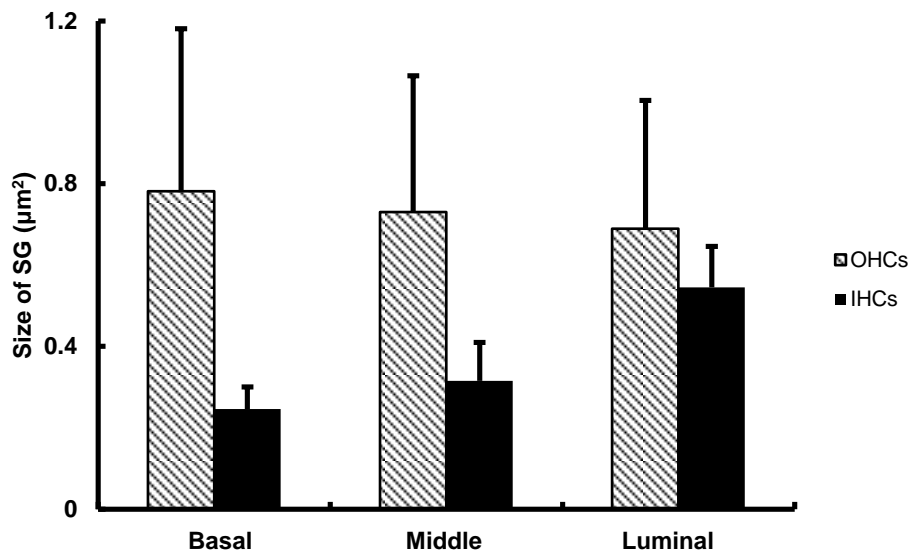


Figure 4.16 – Detailed quantification of SGs following hydroxamate (-)-9 treatment in hair cells. (A) Average number of SGs per μm^3 of hair cell volume. (B) Average size of SGs (μm^2). Hydroxamate (-)-9 incubation was performed at 37°C for 8h. The SGs formed in the inner hair cells were significantly higher in both middle and luminal surfaces (* $p < 0.05$ for both areas, Student's *t*-test) when compared to the outer hair cells. Black bars represent inner hair cells and striped bars represent outer hair cells. Measurements were taken from the middle of the basal end of the cochlear coil. Error bars represent SEM ($n=4$ for each condition).

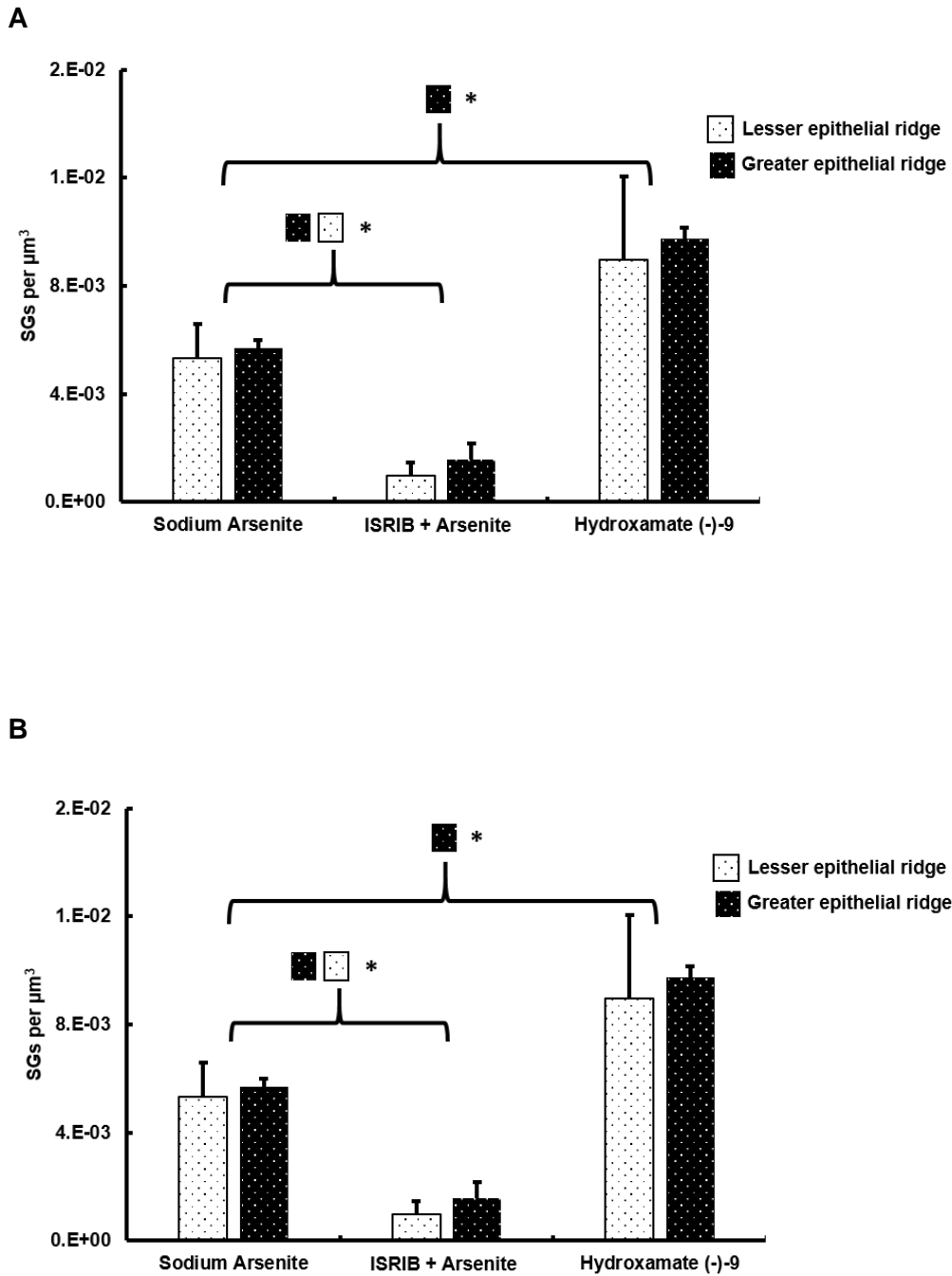


Figure 4.17 – Quantification of SGs present after ISRIB and hydroxamate (-)-9 treatments in supporting cells. (A) Average number of SGs per μm^3 . (B) Average size of SGs (μm^2). White bars represent lesser epithelial ridge and black bars represent greater epithelial ridge. The SGs formed in the greater epithelial ridge following hydroxamate (-)-9 treatment were significantly higher than the SG formed after arsenite stress (* $p < 0.05$, Student's t -test). ISRIB treatment significantly decreased the number of SGs formed following arsenite stress (* $p < 0.05$ for both areas, Student's t -test). Measurements were taken from the middle of the basal end of the cochlear coil. Error bars represent SEM ($n=4$ for each condition).

ISRIB is a newly synthesised chemical compound that activates eIF2B and reduces eIF2 phosphorylation, thus reducing SG formation when applied during stress (Sekine et al. 2015; Sidrauski et al. 2015). In OC-2 cells, ISRIB significantly reduced the number of SGs formed upon heat shock and sodium arsenite stresses without causing additional cellular death (section 3.2.3.3).

Here, to test whether SG formation could be pharmacologically inhibited in the *ex-vivo* cochlea, mouse cochlear explants were incubated with 200nM of ISRIB simultaneously with sodium arsenite stress treatment (1h, 0.5mM), following the conditions optimised in the OC-2 cell line (section 3.2.3.3).

Arsenite treatment induced SG formation in both hair cells and supporting cells (Figs.4.9 and 4.11, respectively, arsenite panels, yellow arrows), as previously shown (section 4.2.1). Upon arsenite treatment, polyA⁺ mRNA aggregated in the cytoplasm of the cells with the SG-marker protein TIA-1 (Fig.4.10 for hair cells and 4.12 for supporting cells, respectively, arsenite panels, yellow arrows).

Simultaneous incubation with ISRIB during arsenite stress resulted in a distribution of polyA⁺ mRNA and TIA-1 in hair cells and supporting cells similar to that observed in control, unstressed samples: polyA⁺ mRNA and TIA-1 distributed throughout the nucleus and cytoplasm, without aggregation at SGs (Figs. 4.10 and 4.12, for hair cells and supporting cells, respectively, ISRIB + arsenite panels, white arrows). These results suggest an effect of ISRIB on the reduction of SG formation upon arsenite stress in both hair cells and supporting cells. Figures 4.10 and 4.12 show in detail the distribution of polyA⁺ mRNA and TIA-1 in inner hair cells and supporting cells, respectively, following arsenite treatment in the presence of ISRIB (white arrows).

MyosinVIIa and DAPI data indicate that during ISRIB treatment, the organ of Corti organisation was not disrupted and no increased cellular death events were reported (Fig.4.9).

Quantification revealed that, in the presence of ISRIB during sodium arsenite treatment, on average $1.2 \times 10^{-3} \pm 0.1 \times 10^{-3}$ and $2 \times 10^{-3} \pm 0.3 \times 10^{-3}$ SGs were formed per μm^3 of inner and outer hair cells, respectively (Fig.4.14 A and B). These values correspond to a significant reduction of 82% and 48% in the number of SGs generated in inner and outer hair cells, respectively. As regarding to the size of the SGs, ISRIB treatment simultaneously with arsenite resulted in SGs averaging $0.4\mu\text{m}^2$ in size (Fig.4.14 A and B).

The supporting cells in the lesser and greater epithelial ridge formed approximately $0.9 \times 10^{-3} \pm 0.6 \times 10^{-3}$ and $1.5 \times 10^{-3} \pm 0.4 \times 10^{-3}$ SGs per μm^3 , respectively (Fig.4.17 A). When compared to the number of SGs formed upon arsenite stress alone, ISRIB incubation significantly reduced the number of SGs in 84% and 74% in the lesser and greater epithelial ridges, respectively. Consistent with previous observations, the SGs found in supporting cells averaged approximately $0.4\mu\text{m}^2$ in size (Fig.4.17 B).

Taken together, these results indicate that pharmacological manipulation of SG formation was effective in the *ex-vivo* cochlea. Since hydroxamate (-)-9 generated SG formation in both hair cells and supporting cells without causing cellular death, it could be a suitable chemical compound to evaluate the effect of promoting SG formation during ototoxicity.

ISRIB, by significantly reducing the number of SGs upon stress without causing cellular death, is also a suitable tool to evaluate the effects of inhibiting SG formation during ototoxic stress.

These two chemical compounds will be used in the next section to address the effects of manipulating SG formation on the hair cell survival during aminoglycoside stress.

4.2.3. Hydroxamate (-)-9 protects outer hair cells from aminoglycoside-induced cell death

4.2.3.1. Neomycin-induced cochlear stress

Neomycin was one of the antibiotics chosen to test out the effects of manipulating SG formation upon aminoglycoside-induced toxicity in the inner ear. The ototoxic effects of neomycin are well described, including irreversible loss of hair cells and, consequently, hearing loss (Forge & Schacht 2000; Guthrie 2008; Karasawa & Steyger 2011).

The hypothesis explored here is whether SG formation affects hair cell survival upon neomycin exposure. To test this, 0.1 μ M of hydroxamate (-)-9 (see section 4.2.2) for 14h was used to promote SG formation prior to neomycin exposure (Fig.4.18). Neomycin exposure for 6h at 1mM has been shown to cause chromatin disruption and hair cell death in cochlear explants (Towers et al. 2011). The samples were fixed immediately after neomycin exposure. Immunohistochemistry followed by confocal imaging was used to detect TIA-1 (SG-marker) and MyosinVIIa (hair cell marker) proteins. Quantification of surviving hair cells was performed as detailed in methods section 2.21.

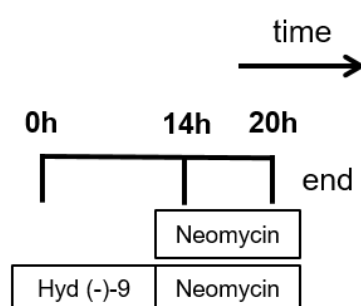


Figure 4.18 - Experimental paradigms to assess the effects of hydroxamate (-)-9 on the neomycin-induced toxicity. P3 mouse cochlear explants were submitted to 1mM neomycin incubation for 6h. Pre-incubation with 0.1 μ M hydroxamate (-)-9 for 14h prior to neomycin exposure was performed. All samples were fixed at the end of the experiment.

In untreated control samples, three rows of outer hair cells and one row of inner hair cells could be observed, along with a regular distribution of MyosinVIIa marking the hair cells across the whole cell body (Fig.4.19, untreated panel, white arrowheads). TIA-1 was located throughout the nucleus and the cytoplasm, without aggregation at SGs (Fig.4.19, untreated panel). Filamentous actin (F-actin) phalloidin was used to assess the status of the hair cell stereocilia bundles (Fig.4.19, untreated panel, white arrows).

Neomycin treatment induced the formation of SGs in hair cells (Fig.4.19, neomycin panel, yellow arrows), in agreement with previous studies from the laboratory (Towers et al. 2011). Neomycin treatment also resulted in translocation of MyosinVIIa towards the luminal surface of the cells (Fig.4.19, MyosinVIIa signal in neomycin panel). After neomycin exposure, MyosinVIIa was no longer observed across the whole hair cell body, as seen in unstressed control conditions, but highly condensed on top of the cells. This feature was repeatedly present across the different biological replicates used in this experiment and was accompanied by irregular DAPI staining, consistent with cell death (Fig.4.19, DAPI signal in neomycin panel). In addition, the pattern of F-actin expression was highly disrupted following neomycin exposure (Fig.4.19, neomycin panel, white arrows).

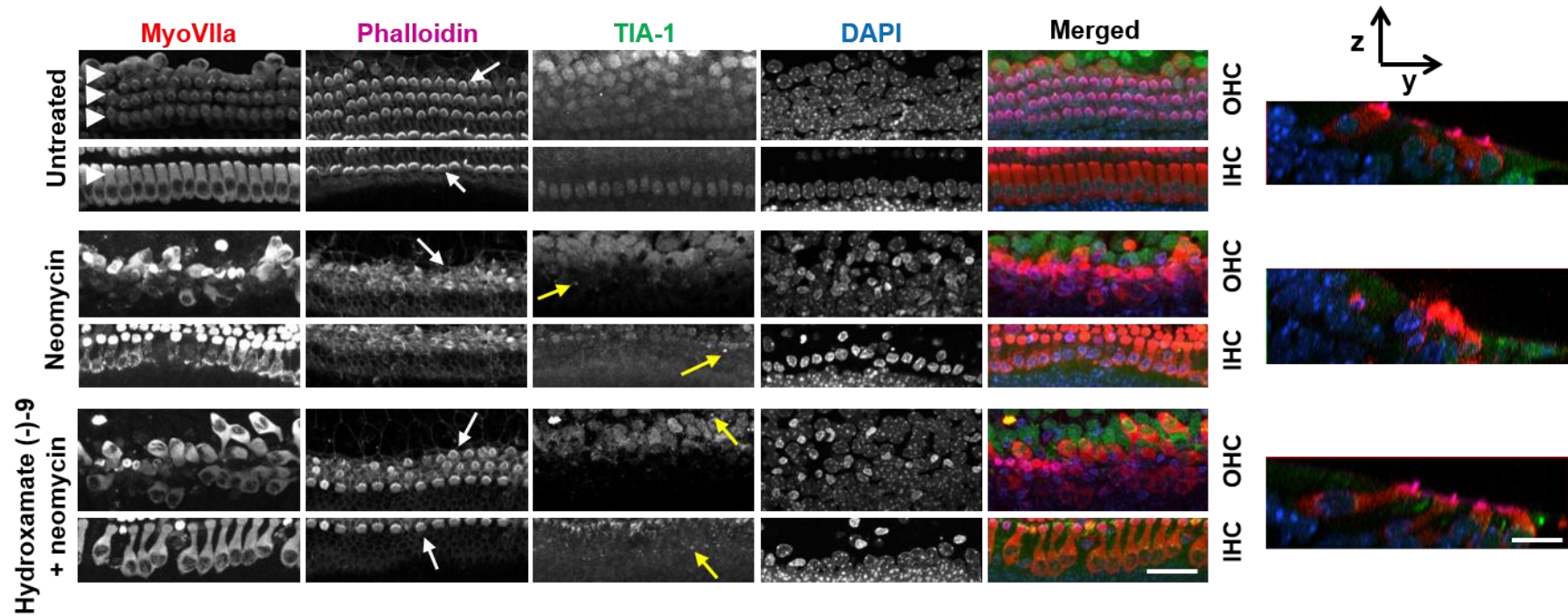


Figure 4.19 – Hydroxamate (-)-9 pre-treatment increases hair cell survival following neomycin-induced toxicity. Cochlear explant cultures from P3 mice were incubated with 0.1µM of hydroxamate (-)-9 during 14h prior to neomycin exposure for 6h at 1mM concentration. MyosinVIIa was used to mark inner hair cells (IHC) and outer hair cells (OHC). White arrowheads point to hair cells in untreated samples. Phalloidin was used to stain F-actin filaments (white arrows). Yellow arrows point to SG formation. Chromatin structure was assessed using DAPI. Images shown correspond to the middle of the basal end of the cochlear coils. Images are maximum intensity projections of confocal sub-Z-stacks. Scale bar= 25µm for left-hand side panels and 10µm for right-hand side Z/Y panels.

Under these conditions, neomycin reduced the number of inner hair cells by 40% and outer hair cells by 51%, when compared to control unstressed samples (Fig.4.20 A and B).

In order to test whether inducing SG formation prior to aminoglycoside exposure could affect hair cell survival, mouse cochlear explants were treated with 0.1 μ M of hydroxamate (-)-9 for 14h prior to neomycin exposure (1mM, 6h). Hydroxamate (-)-9 incubation resulted in an increase in the number of inner hair cells compared to the effects of neomycin alone (Fig.4.20 A). This was accompanied by maintenance of MyosinVIIa distribution across the whole hair cell body, as shown in Figure 4.19, resembling that of unstressed cells. Interestingly, the surviving hair cells presented SGs (Fig.4.19, hydroxamate (-)-9 + neomycin panel, yellow arrows). Figure 4.21 shows in higher magnification the presence of SGs in surviving inner hair cells.

Upon hydroxamate (-)-9 pre-incubation, F-actin distribution in the hair bundles seemed to be relatively normal when compared to neomycin alone treatment (Fig.4.19, hydroxamate (-)-9 + neomycin panel, white arrows).

Quantification of surviving hair cells reveals that, when hydroxamate (-)-9 was applied prior to neomycin exposure, 11 ± 0.3 inner hair cells and 23 ± 3.5 outer hair cells per 100 μ m length of the cochlea were found to survive (Fig.4.20 A and B). These values correspond to 97% and 60% survival of inner and outer hair cells, respectively, upon pre-treatment with hydroxamate (-)-9 when compared to neomycin alone. Taken together, these results indicate that hydroxamate (-)-9 treatment before neomycin exposure significantly increases the survival of inner hair cells.

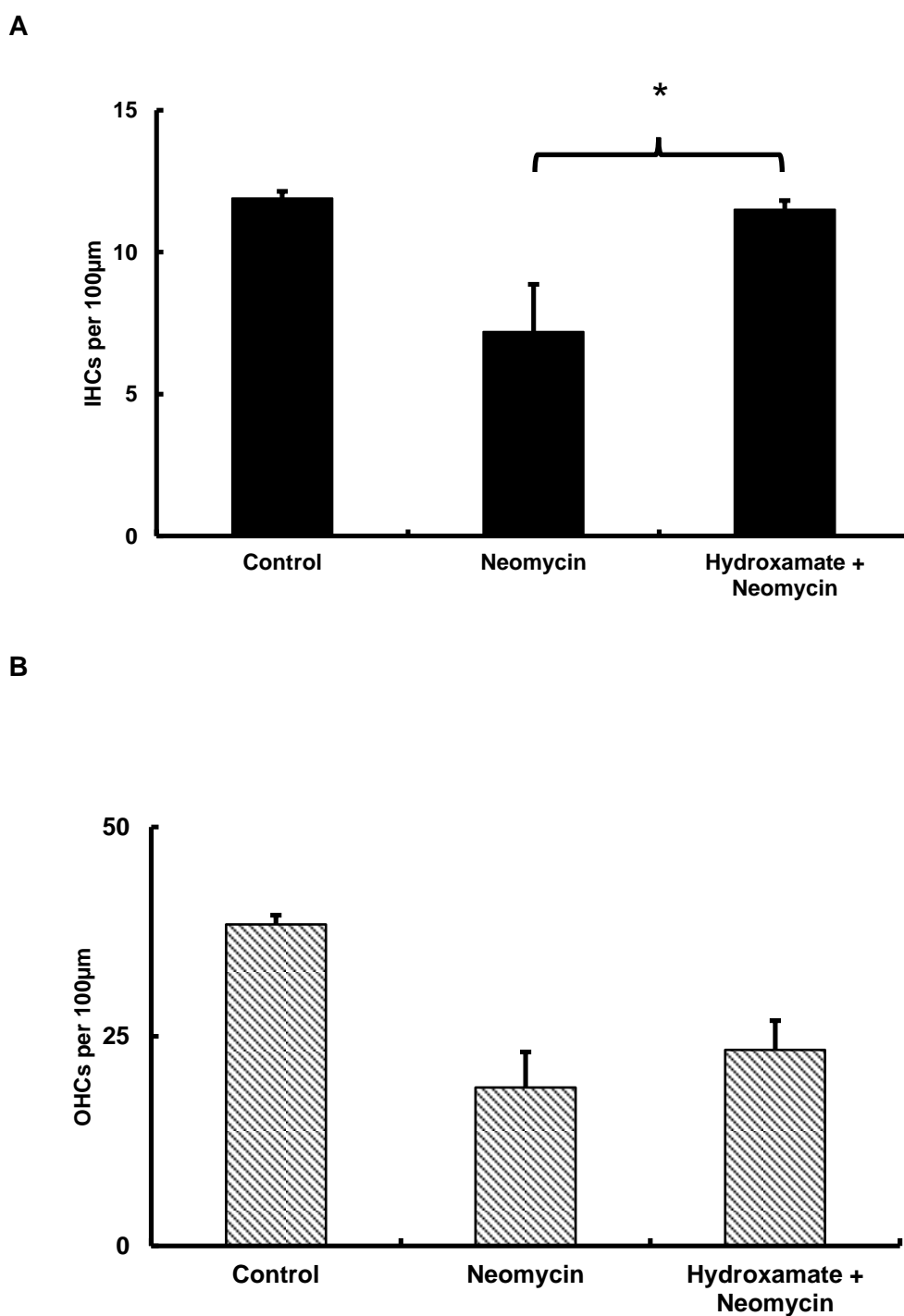


Figure 4.20 – Hydroxamate (-)-9 pre-treatment protects inner hair cells from neomycin-induced hair cell death. (A) Average number of inner hair cells per 100µm. (B) Average number of outer hair cells per 100µm. Neomycin treatment (1mM, 6h) reduced the number of IHCs and OHCs by 40% and 51%, respectively, when compared to control samples. Pre-incubation for 14h with hydroxamate (-)-9 0.1µM prior to neomycin exposure protects inner hair cells from death (* $p < 0.05$, Student's *t*-test against neomycin treatment alone). Error bars represent SEM. Replicates were used as follows: control (n=6), neomycin (n=14), hydroxamate + neomycin (n=10).

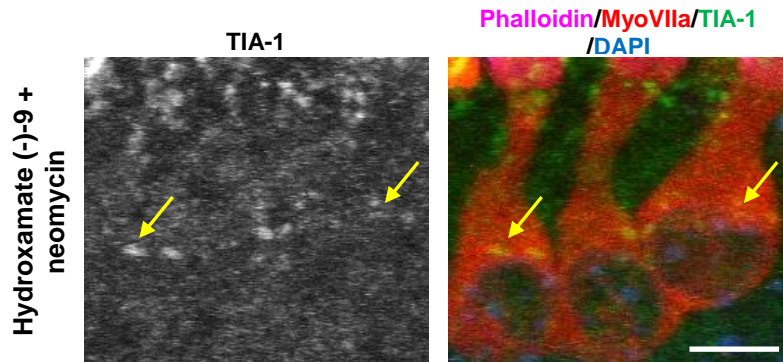


Figure 4.21 – Surviving inner hair cells reveal SG formation. Cochlear explant cultures from P3 mice were incubated with 0.1 μ M of hydroxamate (-)-9 during 14h prior to neomycin exposure for 6h at 1mM concentration. SGs are visible (arrows) in the cytoplasm of inner hair cells following treatment with hydroxamate (-)-9 prior to neomycin exposure. Images correspond to single stacks of confocal images Scale bar= 10 μ m.

In order to assess whether the effects of hydroxamate (-)-9 observed on the hair cell survival persist after neomycin exposure, mouse cochlear explants were allowed to recover from neomycin treatment for 48h in a neomycin-free medium. In this experiment, incubation with hydroxamate (-)-9 0.1 μ M was performed prior to neomycin exposure as before. In addition, the SG-inhibitor ISRIB (previously described in the section 4.2.2) was added simultaneously with neomycin and kept for 24h in a neomycin-free medium. All samples were allowed to recover for 48h in a neomycin-free medium. Quantification of hair cell survival was performed after all samples have been through the recovery period. A schematic of the experimental paradigms used is shown in Figure 4.22.

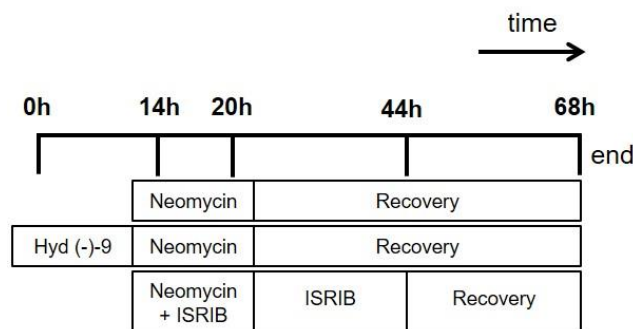


Figure 4.22 - Experimental paradigms to assess the effects of SG manipulation on the neomycin-induced toxicity. P3 mouse cochlear explants were submitted to neomycin incubation for 6h and allowed to recover for 48h. Pre-incubation with hydroxamate (-)-9 for 14h prior to neomycin exposure was performed. ISRIB was used simultaneously with neomycin and kept for 24h in a neomycin-free medium. All samples were allowed to recover for 48h in a neomycin-free medium before fixation.

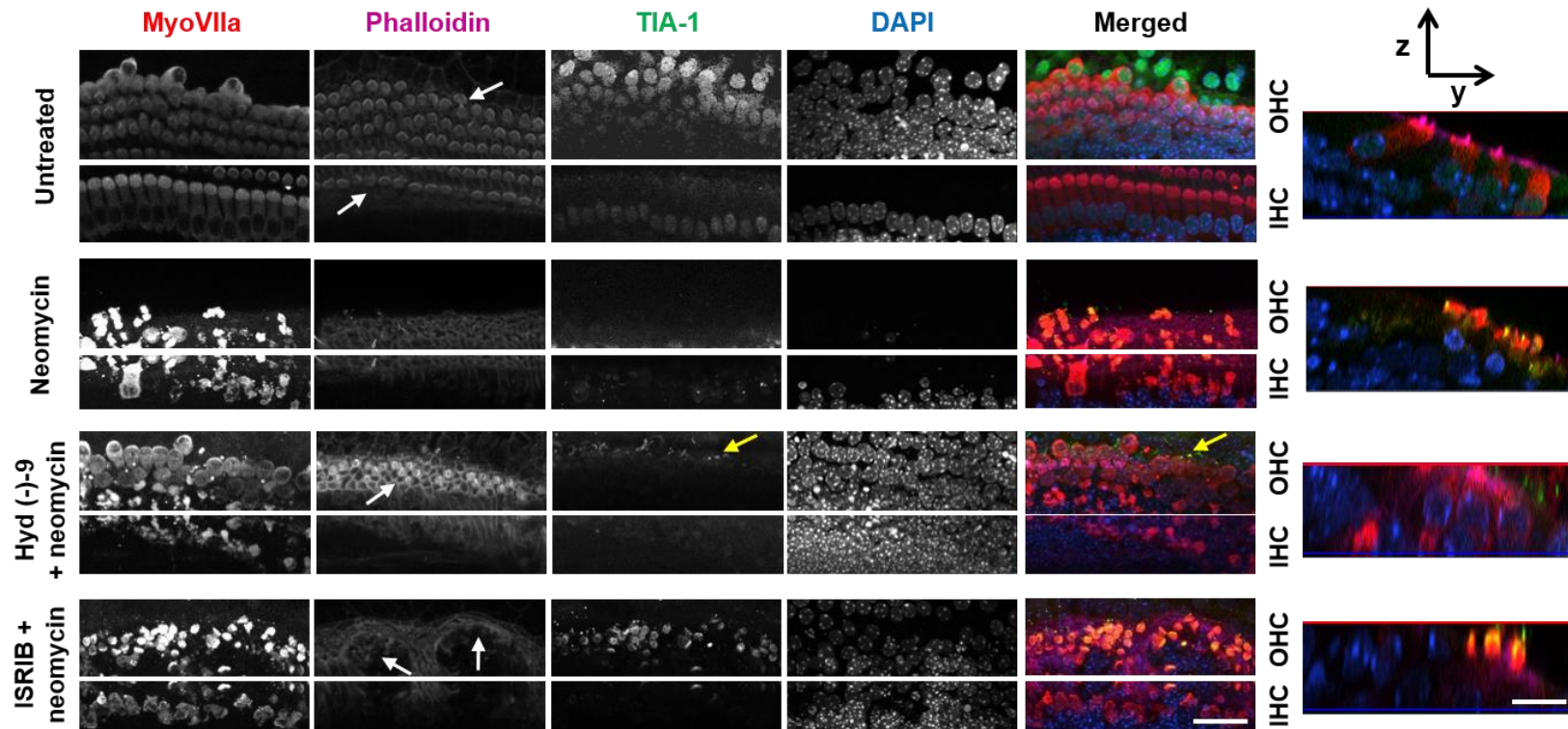


Figure 4.23 - Hydroxamate (-)-9 pre-treatment increases the number of outer hair cells after 48h recovery from neomycin-induced hair cell death. Cochlear explant cultures from P3 mice were incubated with 0.1 μ M of hydroxamate (-)-9 during 14h prior to neomycin exposure for 6h at 1mM. ISRIB 200nM was used simultaneously with neomycin incubation and kept in a neomycin-free medium for 24h. All samples were allowed to recover in a neomycin-free medium for 48h. MyosinVIIa was used to mark inner hair cells (IHC) and outer hair cells (OHC). Phalloidin stains the F-actin (white arrows). Yellow arrows point to SGs. Chromatin structure was assessed using DAPI. Images shown correspond to the middle of the basal end of the cochlear coils. Images are maximum intensity projections of confocal sub-Z-stacks. Scale bar= 25 μ m for left-hand side panels and 10 μ m for right-hand side Z/Y panels.

Untreated control samples presented three rows of outer hair cells and one row of inner hair cells, along with a regular distribution of MyosinVIIa marking the hair cells across the whole cell body (Fig.4.23, MyosinVIIa signal in untreated panel). This corresponded to an average of 12 ± 0.2 inner hair cells and 38 ± 1.1 outer hair cells present per 100 μ m length of the cochlea in control samples at the end of the experiment (Fig.4.24 A and B).

Forty-eight hours after neomycin exposure, almost no inner and outer hair cells could be detected, as indicated by the MyosinVIIa signal (Fig.4.23, neomycin panel). Quantification of the number of surviving hair cells upon neomycin treatment corroborates these observations: only 0.3 ± 0.2 inner hair cells and 2.5 ± 1.1 outer hair cells survived per 100 μ m length of the cochlea until the end of the experiment (Fig.4.24 A and B).

When assessed after 48h recovery, pre-treatment with hydroxamate (-)-9 (14h, 0.1 μ M) before neomycin exposure (6h, 1mM) resulted in an increase in the number of surviving outer hair cells, compared to neomycin treatment alone ($p < 0.005$, Student's *t*-test) (Fig.4.24 B). On average, 11 ± 2.3 outer hair cells were still present per 100 μ m length of the cochlea at the end of the experiment when hydroxamate (-)-9 was used prior to neomycin application (Fig.4.24 B). This corresponds to a protection of approximately 29% of outer hair cells by hydroxamate (-)-9 pre-treatment, as opposed to only 6% outer hair cells survival following neomycin treatment alone. As regarding the inner hair cells, only 0.2 ± 0.2 cells were found alive at the end of the experiment per 100 μ m length of the cochlea, when hydroxamate (-)-9 was used (Fig.4.24 A). These observations suggest that the protection observed in inner hair cells immediately after 6h neomycin exposure (with hydroxamate (-)-9 pre-treatment, Fig.4.20 A) did not persist over the extended time period.

Once again, under hydroxamate (-)-9 pre-treatment conditions, although some MyosinVIIa translocation towards the luminal surface of the cells could be observed in the inner hair cell region, the outer hair cells presented MyosinVIIa distributed across the whole cell body, resembling that of unstressed conditions (as well as regular chromatin structure as assessed by DAPI staining) (Fig.4.23, hydroxamate (-)-9 + neomycin panel). The effects of hydroxamate (-)-9 in the maintenance of F-actin rich hair bundles was confirmed in this experiment for the outer hair cells region, accompanied by the surviving hair cells and corroborating the data previously showed (for the samples fixed immediately after the 6h experiment)

(Fig.4.23, hydroxamate (-)-9 + neomycin panel, white arrows). Some of the surviving outer hair cells following hydroxamate (-)-9 treatment before neomycin exposure presented TIA-1-positive SG formation (Fig.4.23, hydroxamate (-)-9 + neomycin panel, yellow arrows).

Interestingly, when the SG-inhibitor ISRIB was applied, a decrease in the number of outer hair cells was observed, when compared to neomycin application alone ($p < 0.05$, Student's *t*-test) (Fig.4.24 B). This was accompanied by total disruption of the F-actin filaments (Fig.4.23, ISRIB + neomycin panel, white arrows). After 48h recovery, 24h of which was in the presence of ISRIB, MyosinVIIa was still concentrated at the apical surface of the cells and TIA-1 seemed to localise with MyosinVIIa (Fig.4.23 ISRIB + neomycin panel). These were possibly cell debris left (negative for DAPI staining), most likely corresponding to the remnant luminal part of the cells at the surface of the epithelium.

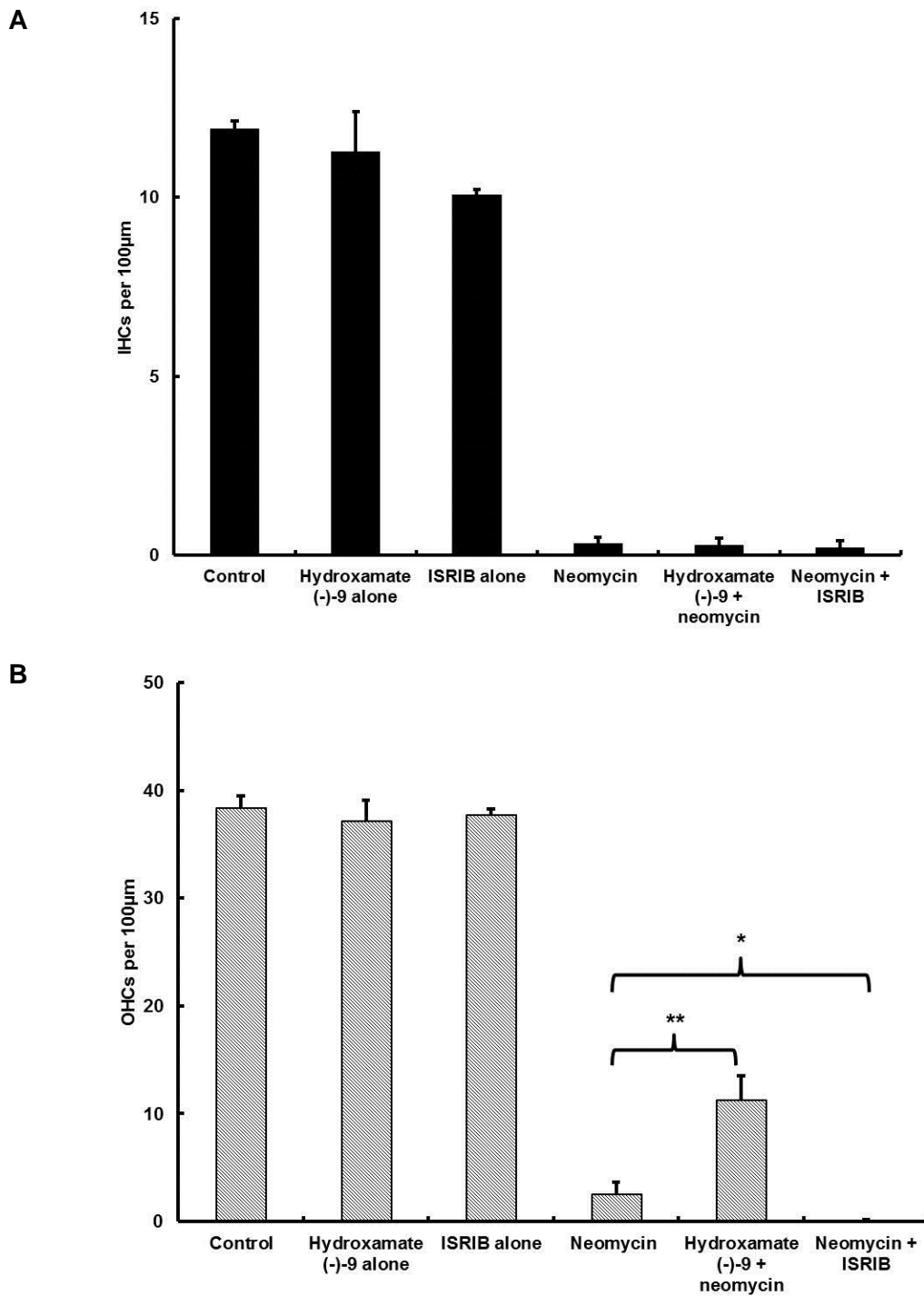


Figure 4.24 - Hydroxamate (-)-9 pre-treatment protects outer hair cells after 48h recovery from neomycin-induced hair cell death. (A) Average number of inner hair cells per 100µm. (B) Average number of outer hair cells per 100µm. Neomycin treatment (1mM, 6h) reduces the number of inner (IHC) and outer hair cells (OHC) by 97% and 94%, respectively, when compared to control samples. Pre-incubation for 14h with hydroxamate (-)-9 0.1µM prior to neomycin exposure protects outer hair cells from death (** $p < 0.005$, Student's t -test against neomycin treatment alone). In the presence of ISRIB, a significant reduction in the number of outer hair cells is observed when compared to neomycin treatment alone death (* $p < 0.05$, Student's t -test against neomycin treatment alone). Error bars represent SEM. Replicates were used as follows: control (n=6), neomycin (n=7), hydroxamate + neomycin (n=9), neomycin + ISRIB (n=4).

4.2.3.2. Sisomicin-induced cochlear stress

Since hydroxamate (-)-9 pre-treatment was found to increase the number of surviving outer hair cells upon neomycin-triggered cell death (section 4.2.3.1), I decided to test if those effects could be extended to ototoxicity caused by another aminoglycoside antibiotic.

Sisomicin is a new broad spectrum aminoglycoside related to gentamicin that has been shown to present highly ototoxic effects (Huth et al. 2015), thus constituting an appropriate choice for these experiments. Dose-response experiments using a range of sisomicin concentrations were performed in order to determine similar cell death proportions as obtained with neomycin. Sisomicin toxicity was assessed in an experiment where mouse cochlear explants were treated for 1h with sisomicin and allowed to recover in a sisomicin-free medium for 48h. Quantification of surviving hair cells was performed using FM1-43 labelling, as previously indicated (section 2.12 in methods).

Mouse cochlear explants were treated with different concentrations of sisomicin (10 μ M, 100 μ M, 200 μ M and 500 μ M) for 1h and allowed to recover for 48h in a sisomicin-free medium. The sisomicin concentrations chosen to test were based on previous studies published elsewhere (Huth et al. 2015).

Figure 4.25 shows FM1-43 labelling of hair cells, based on the reports of (Gale et al. 2001). Images were taken at the beginning of the experiment and 48h after recovery from sisomicin treatment for each of the concentrations.

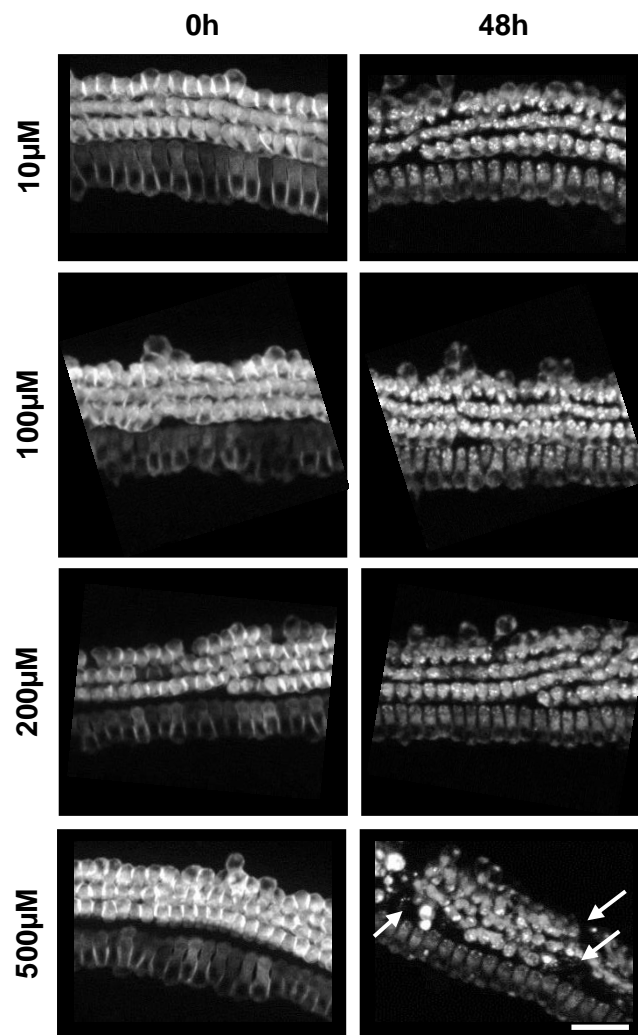


Figure 4.25 – Sisomicin-treated mouse cochlear explants. P3 mouse cochlear explants were treated with different sisomicin concentrations (10, 100, 200 and 500µM) for 1h at 37°C and allowed to recover for 48h in a sisomicin-free medium. Cultures were loaded with FM1-43 prior to sisomicin exposure and images were taken at 0h (beginning of experiment) and 48h (end of experiment). White arrows indicate hair cell loss. Representative images of each condition are shown. Images correspond to middle of the basal end of the cochlear coil and the same area was imaged at 0h and 48h time-points. Maximum intensity projections of Z-stack spinning disc images are shown. Scale bar= 25µm.

Lower doses of sisomicin did not reduce the number of inner and outer hair cells (Fig.4.26). For instance, after exposure to 200 μ M of sisomicin, an average of 90% and 85% of inner hair cells and outer hair cells have survived, respectively (Fig.4.26).

At the highest sisomicin concentration tested, 500 μ M, about 49% of inner hair cells were found to survive, whereas only 17% of the outer hair cells survived (Fig.4.26). White arrows point to hair cell loss in Figure 4.24. Considering these results, 500 μ M was the concentration chosen to induce sisomicin-triggered hair cell death.

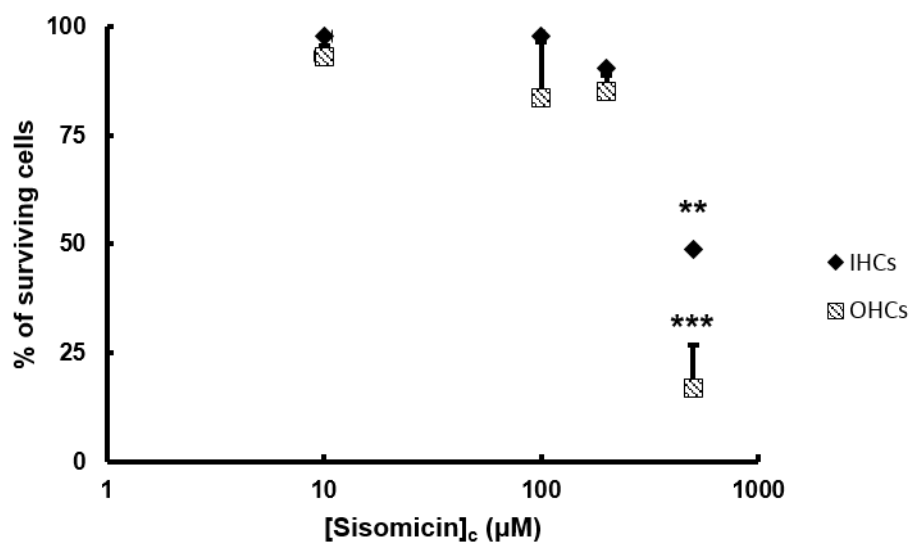


Figure 4.26 – Dose-response curve representing different sisomicin concentrations and percentage of surviving cells. P3 mouse cochlear explants were treated with different sisomicin concentrations (10, 100, 200 and 500 μ M) for 1h at 37°C and allowed to recover for 48h in a sisomicin-free medium. Hair cell counts were performed in the beginning and at the end of the experiment. Y axis represents the percentage of surviving cells found at the end of the experiment, compared to the percentage of cells present at the beginning (100%). Black diamonds represent inner hair cells (IHC) and striped squares represent outer hair cells (OHC). Student's *t*-test was performed for each condition against the lower dosage used, 10 μ M (** $p < 0.005$; *** $p < 0.001$). Error bars represent SEM. Replicates were used as follows: 10 μ M (n=4), 100 μ M (n=3), 200 μ M (n=6), 500 μ M (n=5).

To test out the effect of manipulating SG formation on sisomicin-induced hair cell death, an assay similar to the one used in section 4.2.3.1 was developed. Hydroxamate (-)-9 was used for 14h at 0.1 μ M to promote SG formation prior to sisomicin exposure (500 μ M, 1h). To inhibit SG formation, ISRIB was applied simultaneously with sisomicin and maintained post-incubation in a sisomicin-free medium for 24h. All samples were allowed to recover in a sisomicin-free medium until the end of the experiment (48h post-sisomicin application). Quantification of surviving hair cells was performed as previously described (section 2.21 in methods). Immunohistochemistry followed by confocal microscopy was used to detect TIA-1 (SG-marker) and MyosinVIIa (hair cell marker) proteins. Due to the time-course restrictions of this project and because of the available number of biological replicates, the following results are presented as preliminary data. A schematic of the experimental paradigm used is shown in Figure 4.27.

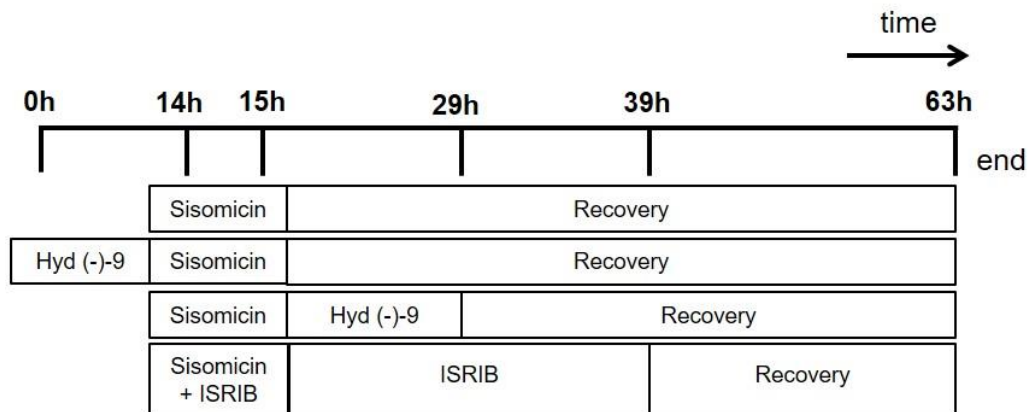


Figure 4.27 - Experimental paradigms to assess the effects of SG manipulation on the sisomicin-induced toxicity. P3 mouse cochlear explants were submitted to sisomicin treatment for 1h and allowed to recover for 48h in a sisomicin-free medium. Pre-incubation with hydroxamate (-)-9 for 14h prior to sisomicin exposure was performed. ISRIB was used simultaneously with sisomicin and kept for 24h post-sisomicin in a sisomicin-free medium. All samples were allowed to recover for 48h in a sisomicin-free medium before fixation.

Control untreated samples presented three rows of outer hair cells and one row of inner hair cells, as assessed by MyosinVIIa staining (Fig.4.28, untreated panel, white arrowheads). TIA-1 was distributed throughout the nucleus and the cytoplasm (Fig.4.28, TIA-1 signal in untreated panel), as previously observed (Fig.4.1). On average, 11 ± 0.1 inner hair cells and 37 ± 2.2 outer hair cells were present per 100 μ m length of the cochlea in control untreated samples (Fig.4.29, A and B).

Treatment with sisomicin has resulted in hair cell loss, as assessed by MyosinVIIa immunostaining (Fig.4.28, sisomicin panel). This was confirmed by quantification of the surviving hair cells: 3 ± 1.3 inner hair cells and 7 ± 2.4 outer hair cells were present at the end of the experiment per 100 μ m length of the cochlea (Fig.4.29, A and B). Sisomicin application resulted in the formation of SGs (Fig.4.28, sisomicin panel, yellow arrows). As assessed by phalloidin staining, sisomicin treatment had an effect on the disruption of the F-actin in the hair bundles, that was more pronounced in the inner hair cells region (Fig.4.28, phalloidin signal in sisomicin panel).

Pre-treatment with hydroxamate (-)-9 increased the number of surviving outer hair cells from sisomicin-induced cell death ($p < 0.05$, Student's *t*-test against sisomicin alone) (Fig.4.28, hydroxamate (-)-9 + sisomicin panel). Quantification revealed that on average 2.4 ± 1.4 inner hair cells and 20 ± 6.1 outer hair cells per 100 μ m length of the cochlea were found to survive after 48h recovery when hydroxamate (-)-9 was applied before sisomicin (Fig.4.29 A and B). Consistent with this, Figure 4.28 shows that upon hydroxamate (-)-9 treatment prior to sisomicin exposure, most of the outer hair cells were present at the end of the experiment, as assessed by MyosinVIIa staining (white arrow in MyosinVIIa panel) and DAPI staining (blue arrow in DAPI panel). Intriguingly, hydroxamate (-)-9 seemed to cause a dramatic disruption of the F-actin filaments, when compared to sisomicin alone (Fig.4.28, hydroxamate (-)-9 + sisomicin panel, red arrows).

The effect of promoting SG formation after sisomicin exposure was also assessed. In a parallel experiment, hydroxamate (-)-9 was added to the cochlear cultures for 14h subsequently to sisomicin exposure. In this case, i.e. without pre-incubation, 1.8 ± 1.6 inner hair cells and 16 ± 5.5 outer hair cells were found to be present per 100 μ m length of the cochlea at the end of the experiment (Fig.4.29 A and B). Hydroxamate (-)-9 post-incubation after sisomicin treatment did not present any significant effects on the hair cell survival ($p > 0.05$ for inner and outer hair cells, Student's *t*-test against sisomicin alone) (Fig.4.29 A and B). Consistent with

previous data, post-incubation with hydroxamate (-)-9 resulted in disruption of the stereocilia on long term hydroxamate (-)-9 exposure, as assessed by phalloidin staining (Fig.4.28, sisomicin + hydroxamate (-)-9 panel, red arrows).

ISRIB was also used in this experiment to inhibit SG formation for 24h after sisomicin exposure. When ISRIB was applied, 4 ± 1.5 inner hair cells and 11 ± 3 outer hair cells per 100 μ m length of the cochlea survived until the end of the experiment (Fig.4.29 A and B). This compound did not reveal any significant effect on the number of surviving cells when compared to sisomicin treatment alone ($p > 0.05$ for inner and outer hair cells, respectively, Student's *t*-test). The presence of ISRIB also seemed to have interfered with the F-actin in the stereocilia, as assessed by phalloidin staining (Fig.28, phalloidin signal in sisomicin + ISRIB panel).

Altogether, these experiments show that modulation of SG formation can alter the cochlea's response to acute stress, since hydroxamate (-)-9 pre-incubation has shown to protect outer hair cells from aminoglycoside-induced cell death. Moreover, ISRIB incubation decreased hair cell survival upon neomycin exposure.

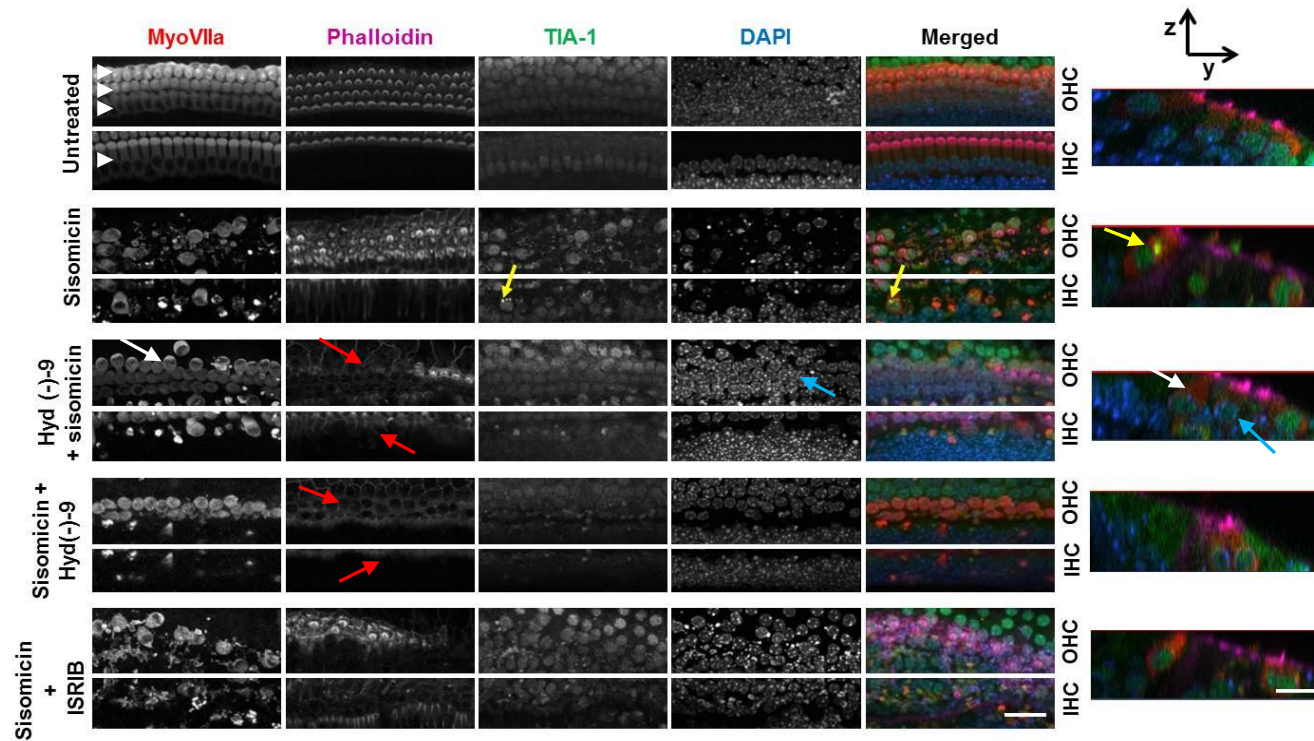


Figure 4.28 - Hydroxamate (-)-9 pre-treatment significantly protects outer hair cells after 48h recovery from sisomicin-induced hair cell death. Cochlear explant cultures from P3 mice were incubated with 0.1µM of hydroxamate (-)-9 during 14h prior to / after sisomicin exposure for 1h at 500µM concentration. ISRIB 200nM was used simultaneously with sisomicin incubation and kept in a sisomicin-free medium for 24h after sisomicin incubation. All samples were allowed to recover in a sisomicin-free medium for 48h. MyosinVIIa was used to mark the inner hair cells (IHC) and the outer hair cells (OHC). White arrowheads in untreated samples point to hair cells. White arrow indicates regular MyosinVIIa staining in hair cells. Yellow arrows point to SG formation. Phalloidin stains the F-actin filaments. Red arrows point to disruption of F-actin. Blue arrow point to healthy nucleus. Chromatin structure was assessed using DAPI. Images shown correspond to the middle of the basal end of the cochlear coils. Images are maximum intensity projections of confocal sub-Z-stacks. Scale bar= 25µm for left-hand side panels and 10µm for right-hand side Z/Y panels.

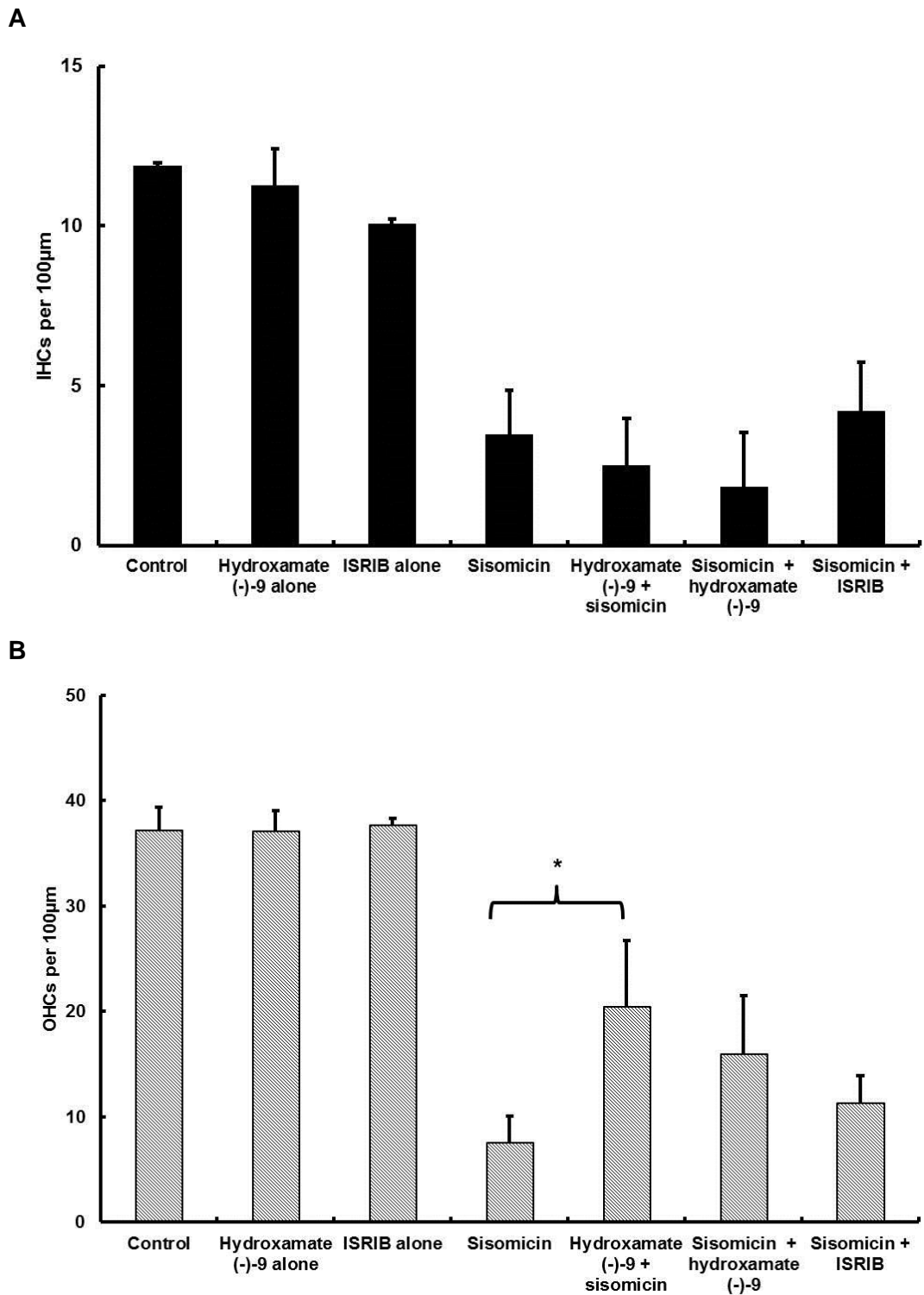


Figure 4.29 – Hydroxamate (-)-9 pre-treatment significantly protects outer hair cells after 48h recovery from sisomicin-induced hair cell death. (A) Average number of inner hair cells per 100µm. (B) Average number of inner hair cells per 100µm. P3 mouse cochlear explants were treated with 500µM of sisomicin for 1h and allowed to recover for 48h. Incubation with 0.1µM hydroxamate (-)-9 was performed for 14h prior to / after sisomicin exposure. ISRIB was added at 200nM for 24h after sisomicin treatment. All samples were allowed to recover for 48h in a sisomicin-free medium. * $p < 0.05$, Student's *t*-test. Error bars represent SEM. Replicates were used as follows: control (n=6), sisomicin (n=9), hydroxamate (-)-9 + sisomicin (n=7), sisomicin + hydroxamate (-)-9 (n=7), sisomicin + ISRIB (n=9).

4.2.4. Age-related changes in the *in-vivo* cochlea

Age-related hearing loss or presbycusis is a complex degenerative disease that represents the most common functional decline that occurs with ageing. Progressive age-related changes in the cochlea, such as degeneration of hair cells and spiral ganglion neurons, often lead to bilateral permanent hearing loss (Schuknecht 1964; Perez & Bao 2011; Lee 2013).

Given the implication of SGs in the pathophysiology of other neurodegenerative diseases, such as ALS and Alzheimer's (Aulas et al. 2012; Ash et al. 2014), and given the recent association of SGs with stress exposure in the cochlea (described in the previous sections of this chapter and in (Towers et al. 2011)), I sought to investigate SG formation in the auditory system of the C57BL/6 mouse. For this, different ages were chosen, P6, P444 and P565 and cryosections were obtained from the basal turn of the cochlea as described in section 2.13 in methods. Detection of polyA⁺ mRNA and SG-marker protein TIA-1 was performed using RNA-immuno-FISH followed by confocal imaging.

At P6, the organ of Corti presented three rows of outer hair cells and one row of inner hair cells, as assessed by MyosinVIIa immunostaining (Fig.4.30, white arrowheads). PolyA⁺ mRNA and TIA-1 were distributed throughout the nucleus and the cytoplasm of hair cells and supporting cells, without visible aggregation at SGs (Fig.4.30, white arrows).

At P444 and P565, the organ of Corti revealed signs of damage, as it can be seen by MyosinVIIa staining of the hair cells (Fig.4.30, top panel). At P565 no outer hair cells were present in the basal turn of the C57BL/6 mouse, indicating the degeneration of the cochlear hair cells with ageing (Fig.4.30, top panel).

With increased ageing, SGs were formed in both hair cells and supporting cells, as assessed by the location of polyA⁺ mRNA and TIA-1 at P444 and P565 (Figs.4.30 and 4.31, yellow arrows). Figure 4.31 show higher magnification of the inner hair cells showed in Figure 4.29. At P565, it is apparent the perinuclear location of SGs in the inner hair cell, as seen by the distribution of polyA⁺ mRNA and TIA-1 aggregates (Fig.4.31), resembling those observed following stress in the OC-2 cell line (section 3.2.1).

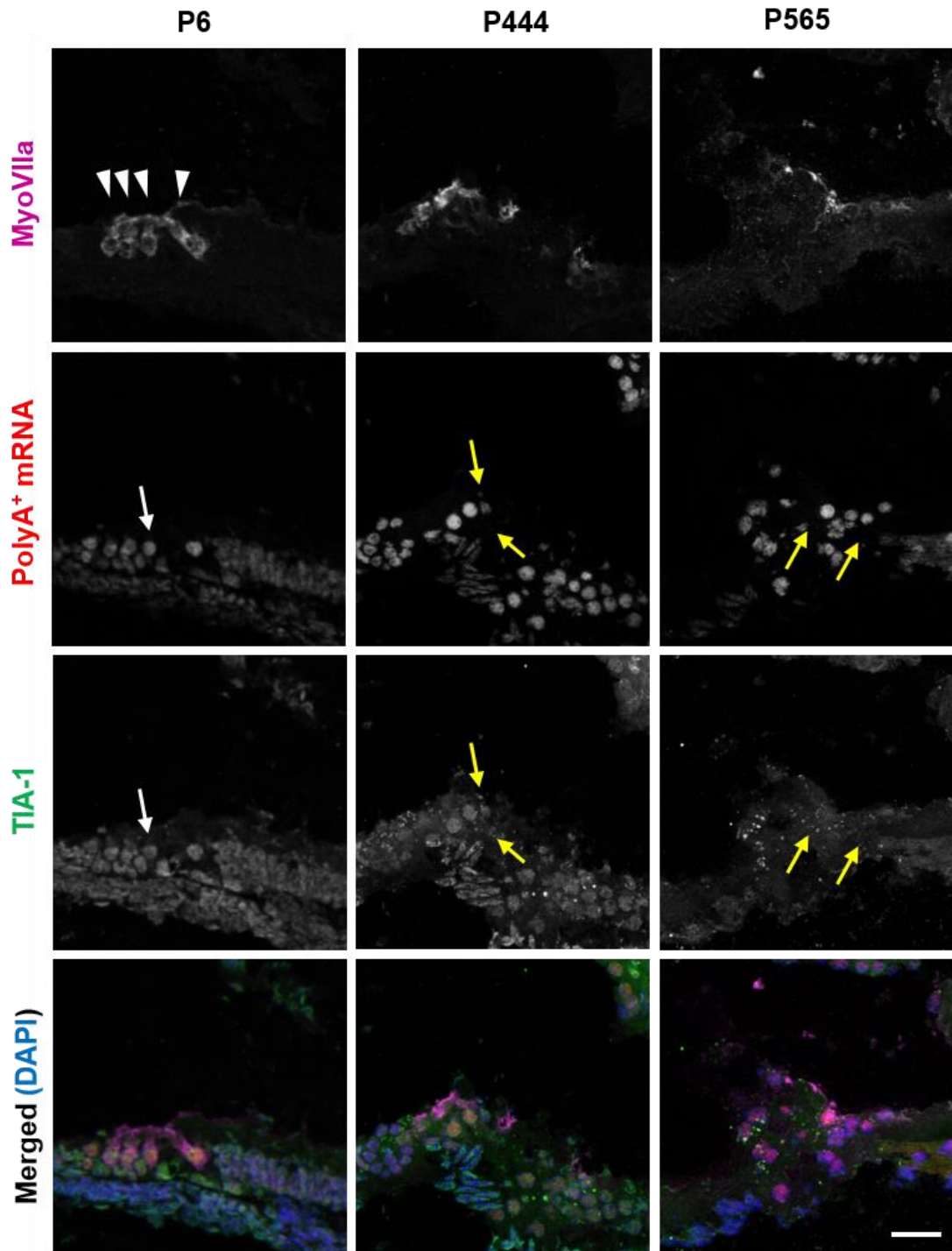


Figure 4.30 – SG formation in the aged organ of Corti. RNA-immuno-FISH was performed in cryosections of different ages from the C57BL/6 mouse strain, as indicated by postnatal (P) days. MyosinVIIa was used to label hair cells (white arrowheads in P6 sample). PolyA⁺ mRNA was detected using a Cy3-labelled probe. White arrows in P6 point to the nuclear and cytoplasmic distribution of polyA⁺ mRNA and TIA-1, not aggregating at SGs. Yellow arrows in P444 and P565 point to SGs. Merged images contain DAPI staining of the chromatin structure. Scale bar= 25µm.

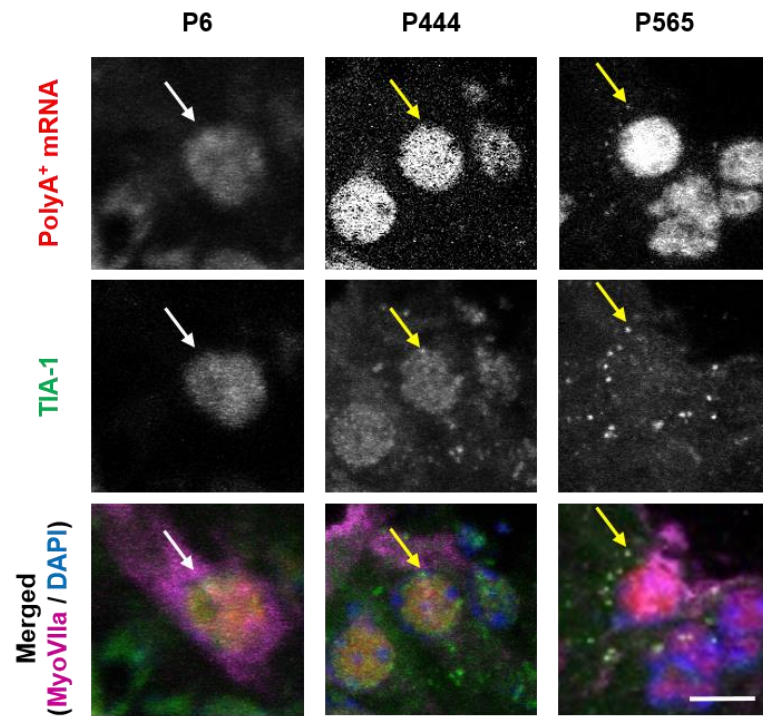


Figure 4.31 – PolyA⁺ mRNA aggregates with TIA-1 at SGs in the aged organ of Corti. RNA-immuno-FISH was performed in cryosections of different ages from the C57BL/6 mouse strain, as indicated by postnatal (P) days. MyosinVIIa was used to label hair cells. PolyA⁺ mRNA was detected using a Cy3-labelled probe. White arrows in P6 point to the nuclear and cytoplasmic distribution of polyA⁺ mRNA and TIA-1, not aggregating at SGs. Yellow arrows in P444 and P565 point to SGs. Due to its high nuclear intensity signal, polyA⁺ mRNA signal was modified through changes in brightness/contrast in order to visualise its cytoplasmic location. Merged images contain DAPI staining of the chromatin structure. Scale bar= 10µm.

SG formation was also investigated in the aged spiral ganglia. At P6 there were no SG formed in the spiral ganglion neurons, as assessed by the distribution of polyA⁺ mRNA and TIA-1 (Fig.4.32, white arrows). At P444 and P565, spiral ganglion neurons exhibited SG formation (Fig.4.32, yellow arrows). Some of the SGs formed in the aged spiral ganglion neurons also revealed to be distributed around the nucleus of the neurons, as seen by the distribution of polyA⁺ mRNA and TIA-1 at P444 and P565 (Fig.4.32, yellow arrows). Interestingly, MyosinVIIa was detected as a component of the SGs formed in the spiral ganglion neurons, as observed by its aggregation with polyA⁺ mRNA and TIA-1 at P444 and P565 (Fig.4.32, top panel).

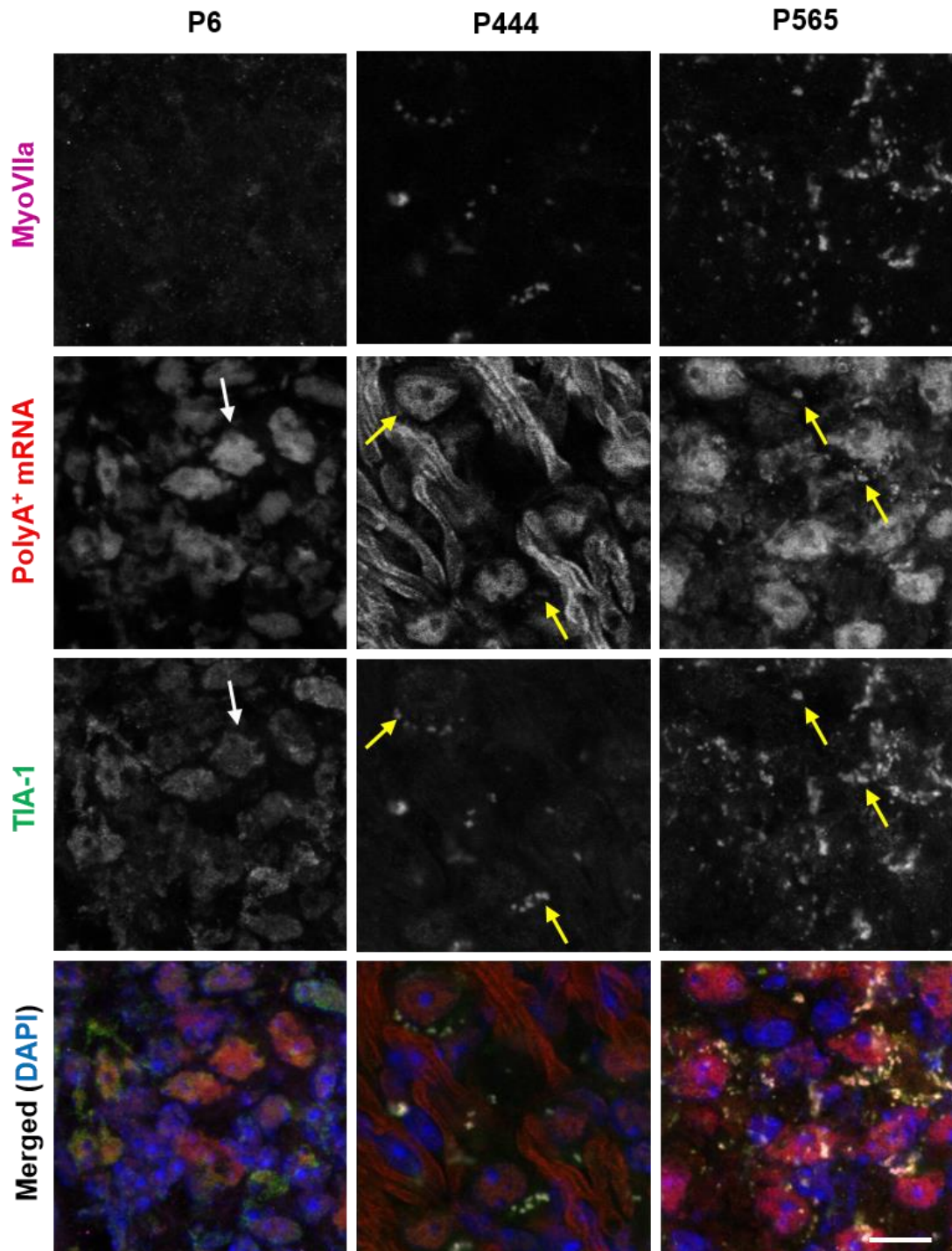


Figure 4.32 – SG formation in the aged spiral ganglia. RNA-immuno-FISH was performed in cryosections of different ages from the C57BL/6 mouse strain, as indicated by postnatal (P) days. PolyA⁺ mRNA was detected using a Cy3-labelled probe. White arrows in P6 point to the nuclear and cytoplasmic distribution of polyA⁺ mRNA and TIA-1, not aggregating at SGs. Yellow arrows in P444 and P565 point to SGs. Merged images contain DAPI staining of the chromatin structure. Scale bar = 10µm.

4.3. Discussion

Regulated mRNA/protein aggregation has been associated with cytoprotection during stress conditions (Kedersha et al. 2002; Jevtov et al. 2015; Arimoto-Matsuzaki et al. 2016). SGs have been shown to assemble within minutes of exposure to stress and, once the stress is removed, to disassemble over a period of approximately 3 hours (Souquere et al. 2009). Additionally, impairment of SG formation has been suggested to promote cell death upon stress exposure (Baguet et al. 2007; Kwon et al. 2007; Eisinger-Mathason et al. 2008; Ghisolfi et al. 2012; Arimoto-Matsuzaki et al. 2016), consistent with the hypothesis that SGs are associated with increased cell viability during transient stress conditions.

Aside from their implication in the cochlea's response to aminoglycoside-induced damage (Towers et al. 2011), little is known to date about the role of SGs during ototoxic stress. This chapter aimed at providing detailed characterisation of SG formation and regulation in the *ex-vivo* mouse organ of Corti and, subsequently, to evaluate the effect of manipulating SG formation on the hair cell survival in the aminoglycoside-damaged cochlea. In addition, SG formation as a function of ageing in the *in-vivo* C57BL/6 cochlea was analysed.

Initially, to understand how cochlear cells respond to stress in terms of SG formation, mouse cochlear explants were submitted to heat shock and arsenite stresses and SG assembly estimated through quantification of number and size. Using the RNA-immuno-FISH protocol here developed, polyA⁺ mRNA was reported to aggregate with TIA-1 for the first time in the cytoplasm of hair cells and supporting cells (Figs.4.1 and 4.3), thus confirming the potential of cochlear cells to assemble SGs as a response to stress. These results are in agreement with previous observations in the OC-2 cell line (sections 3.2.1 and 3.2.2) and suggest that most of the cytoplasmic RNA is inhibited from translation at SGs in the cochlea following stress.

Arsenite stress generated approximately twice as many SGs than heat shock in mouse cochlear explants (Figs.4.5 and 4.7), in agreement with previous results observed in OC-2 cells (section 3.2.2). Interestingly, inner hair cells assembled more SGs than outer hair cells upon arsenite stress (Fig.4.5), suggesting that inner hair cells are more sensitive to this stress than outer hair cells.

The size of the SGs generated in OC-2 cells is in agreement with other cell lines, such as HeLa or SK-N-SH cells (1-4 μm^2) (McDonald et al. 2011; Aulas et al. 2012;

Aulas et al. 2015). However, the SGs generated in the cochlear cells were generally smaller in size than those ($< 1 \mu\text{m}^2$) (Figs.4.6 and 4.7 B). This may suggest that SG assembly in cochlear native cells requires less protein aggregation than in the OC-2 cell line, or that less mRNAs are sorted to SGs in cochlear cultures. Since the work presented herein is, to my knowledge, the first to provide such a detailed description of SG formation in native tissue, the lack of other studies does not enable any comparison of these results.

To understand whether SGs could be pharmacologically manipulated in mouse cochlear explants, the pharmacological tools previously screened in OC-2 cells (section 3.2.3), were used. ISRIB, the chemical compound applied to reduce SG formation was effective (Fig.4.13). Quantification revealed that ISRIB decreased a greater number of SGs following arsenite stress in the inner hair cells compared to outer hair cells (Fig.4.13). These observations may suggest that inner hair cells are more sensitive to ISRIB effects on the stabilisation of eIF2B and, consequently, in the reduction of the number of SGs, than outer hair cells. The number of SGs reduced in the supporting cells upon ISRIB treatment was statistically significant when compared to arsenite treatment alone and did not differ between these cells in lesser and greater epithelial ridges. These results indicate that hair cells and supporting cells respond efficiently to ISRIB and, as observed by the polyA⁺ mRNA and TIA-1 distributions, suggest that polyA⁺ mRNA molecules are free from aggregation at SGs, so translation can continue during stress.

Hydroxamate (-)-9, the chemical used to promote SG formation, generated more SGs in the middle and luminal surfaces of inner hair cells, when compared to outer hair cells (Fig.4.15). These observations may suggest that inner hair cells present more sensitivity to hydroxamate (-)-9 effects on the disruption of eIF4F than outer hair cells, thus triggering a greater response in terms of SG formation. Interestingly, inner hair cells seemed to present higher sensitivity to alterations in the SG pathway than outer hair cells, as they were found to assemble more SGs following arsenite and hydroxamate (-)-9 treatments and also achieved greater reduction of SG formation upon ISRIB, when compared to outer hair cells (Figs.4.13 and 4.15, respectively).

The SGs generated by hydroxamate (-)-9 in the hair cells were on average greater in number when compared to the SGs generated by sodium arsenite (Fig.4.13). The latter finding diverges from the results in OC-2 cells, where hydroxamate (-)-9 was found to generate less SGs than sodium arsenite (section 3.2.3.4). This suggests

that hair cells may be either more sensitive to hydroxamate (-)-9 or more resistant to sodium arsenite than OC-2 cells. As regarding to the size, SGs did not vary between inner and outer hair cells, with an overall average size of approximately $0.5 \mu\text{m}^2$ (Fig.4.13). The SGs generated in the hair cells following hydroxamate (-)-9 treatment were smaller in size when compared to those found in OC-2 cells (approximately $1.2 \mu\text{m}^2$). This is in agreement with the results following kinase-inducer stressors (heat shock and arsenite), in which the SGs found in OC-2 cells were generally larger in size than those found in hair cells.

When applied alone neither ISRIB nor hydroxamate (-)-9 caused any cell death as assessed by MyosinVIIa and DAPI staining (Fig.4.9). These data indicate that both ISRIB and hydroxamate (-)-9 are well tolerated by hair cells and, consequently, constitute potential pharmacological tools to manipulate SG formation in the cochlea.

All together, these results indicate that OC-2 cells may provide a suitable inner ear-derived cell line to develop novel assays before animal use. Although OC-2 cells do not resemble hair cells morphologically, the data presented in this chapter suggest that these cells can be used when developing novel protocols, since most of the results achieved with this cell line could be replicated in mouse cochlear explants.

Two aminoglycoside antibiotics were chosen to test out the effects of manipulating SG formation following acute ototoxic insult. Neomycin reduced the number of inner and outer hair cells by 40 and 51%, respectively, when applied for 6h at 1mM. This is in agreement with previous observations (Towers et al. 2011) and expected given the known ototoxic effects of neomycin. Upon neomycin exposure, some of the surviving hair cells presented SGs (Fig.4.18). This result indicates that the cochlear hair cells respond to neomycin insult by triggering SG formation and raises the hypothesis that upon acute ototoxic stress, SG assembly may be crucial for cell survival. In support of this, in the presence of ISRIB, higher levels of cell death were observed when compared to neomycin alone treatments (Fig.4.23), suggesting that inhibiting SG formation under neomycin toxicity may help to potentiate hair cell death. This observation is in agreement with studies in other systems, such as HeLa, U2OS, MCF-7 and HT22 cell lines, in which impairment of SG assembly showed to decrease cell survival (Baguet et al. 2007; Kwon et al. 2007; Eisinger-Mathason et al. 2008; Arimoto-Matsuzaki et al. 2016) and adds evidence that SGs may be critical for an effective cellular response to stress. When hydroxamate (-)-9,

a SG promoter, was applied prior to neomycin exposure, there was an increase in the number of surviving inner hair cells compared to neomycin alone (Fig.4.19). These observations suggest that hydroxamate (-)-9 protects hair cells during neomycin stress and that induction of SGs prior to neomycin exposure may be crucial for hair cell survival.

Interestingly, although hydroxamate (-)-9 was able to protect hair cells in the short duration experiment (6h), the protective effect did not last and, at 48h recovery, inner hair cells did not survive (Fig.4.23). At the end of the 48h recovery from neomycin toxicity, only outer hair cells have survived when the explants were pre-incubated with hydroxamate (-)-9 (Fig.4.23). These results indicate that at a long-term recovery from exposure to neomycin, hydroxamate (-)-9 may be more effective in increasing the survival of outer hair cells upon neomycin exposure than inner hair cells.

Preliminary data suggests that hydroxamate (-)-9 also had an effect on the outer hair cell survival upon sisomicin exposure, since 54% of outer hair cells have survived until the end of the experiment when hydroxamate (-)-9 was applied prior to sisomicin (Fig.4.28). Taken together, these observations indicate that a pre-treatment with hydroxamate (-)-9 prior to neomycin or sisomicin exposure may protect outer hair cells from aminoglycoside-induced cell death, suggesting that hydroxamate (-)-9-triggered SG formation increases outer hair cell survival upon ototoxic stress. In fact, a subset of the surviving hair cells from either neomycin and sisomicin treatments did present SG formation (Fig.4.22 and 4.27). Furthermore, SG inhibition using ISRIB upon neomycin exposure decreased the number of surviving hair cells, thus adding additional evidence that SGs may play a key role during hair cell survival upon stress (Fig.4.23).

To my understanding, this was the first study in which manipulation of SGs has been performed during temporary stress to assess its effect on cell survival. Although a number of studies have performed pharmacological modulation of key molecules associated with the stress response, those were related to permanent, chronic stresses, characteristic of neurodegenerative pathologies. For instance, ISRIB has been shown to enhance long-term memory in mice, through decrease of eIF2 α phosphorylation and, consequently, promotion of protein translation (Sidrauski et al. 2013). Corroborating these results, ISRIB was subsequently shown to present neuroprotective effects in prion-diseased mice (Halliday et al. 2015). In addition, an inhibitor of PERK kinase named GSK2606414 was found to mitigate the

toxic effects of TDP-43 aggregation, a characteristic feature of ALS disease, through decrease of eIF2 α phosphorylation in primary neurons of rats (Kim et al. 2014). Pharmacological activation of the heat shock response has also been shown to present cytoprotective effects. Treatment with arimoclomol, a co-inducer of heat shock response, proved to efficiently delay the progression of ALS in mouse models, through activation of Hsp70 and Hsp90 chaperones (Kieran et al. 2004). In a different study, arimoclomol-mediated activation of heat shock proteins was also associated with reduced retinal degeneration in a rat model of retinitis pigmentosa (Parfitt et al. 2014). Taken together these studies relate the decrease of eIF2 α phosphorylation and/or the induction of chaperone function to cytoprotective roles during chronic protein aggregation. Consistent with this, when in the presence of chronic irreversible stress conditions, the formation of “pathological” SGs have been associated with neurodegenerative diseases (Ratovitski et al. 2012; Vanderweyde et al. 2012; Ash et al. 2014). The rationale behind those studies is that the presence of chronic stress, such as observed in ALS, for instance, combined with dysregulation of the normal SG function, contributes to the formation of chronic aggregates that eventually lead to neurodegeneration. SG formation is dependent on a reversible and highly controlled mechanism of protein aggregation. As such, dysregulation of this pathway is likely to trigger irreversible aggregation of proteins that would otherwise play significant roles in an accurate temporary stress response (Wolozin 2012). Consequently, changes in the regular cellular metabolism that lead to the presence of permanent protein aggregates may interfere in the long term with the translation of the regular pool of RNAs and contribute to irreversible and pathological post-transcriptional alterations in gene expression (Wolozin 2012). Therefore, targeting the suppression of these “pathological” SGs may perhaps constitute a realistic way to impede or reverse some effects of neurodegeneration.

Conversely, considering the evidences for the protective effects of SG formation during transient stress (Kedersha et al. 1999; Kedersha et al. 2002; Buchan et al. 2011; Arimoto-Matsuzaki et al. 2016), the hypothesis explored in this chapter was whether inducing SG formation prior to aminoglycoside exposure increases hair cell survival. The results described herein support this hypothesis since pre-incubation with hydroxamate (-)-9 increased the number of surviving outer hair cells upon neomycin and sisomicin exposure (Figs.4.23 and 4.28). Consistently, inhibition of SG formation resulted in increased hair cell death upon neomycin treatment (Fig.4.23).

It is widely recognised that aminoglycosides cause the activation of pro-apoptotic pathways once inside the hair cells, such as caspases, JNK, MAP kinases and Bcl-2 proteins, for instance (Cheng 2005; Huth et al. 2011). Given that SGs have been recently associated with inhibition of apoptosis in other systems, such as COS-7, HeLa, HT22 and U2OS cell lines through suppression of pro-apoptotic pathways (Arimoto et al. 2008; Takahashi et al. 2013; Thedieck et al. 2013; Arimoto-Matsuzaki et al. 2016), this could provide a possible explanation for the increased hair cell survival rates when hydroxamate (-)-9 was used. Nevertheless, it is yet unclear why only outer hair cells survive during a long-term recovery. A possible explanation for why only outer hair cells showed increased survival with hydroxamate (-)-9 pre-treatment following aminoglycoside exposure is that perhaps there is a critical threshold in terms of the number of SGs formed that may compromise the ability of cells to maintain essential functions. Hydroxamate (-)-9 generated almost twice more SGs in inner hair cells when compared to outer hair cells (Figs.4.13 and 4.15). Assuming this hypothesis, an excess of SGs generated by hydroxamate (-)-9 could be deleterious in a way that it could compromise the translation of essential pro-survival proteins to continue. In the same way, an “adequate” number of SGs could provide a correct balance between the translation inhibition of certain molecules during stress (e.g. pro-apoptotic factors) and the essential molecules that are needed for the cells to respond to that stress.

Another possible explanation for the greater survival of outer hair cells when compared to inner hair cells when using hydroxamate (-)-9 before aminoglycoside exposure is that inner hair cells may require higher protein translational rates than outer hair cells during stress, and so when translation initiation complexes are disrupted using hydroxamate (-)-9 the inner hair cells are negatively affected.

An additional explanation is that different cell death mechanisms may be activated in inner and outer hair cells and SGs may be more protective for certain mechanisms over others. In the experiments here presented, outer hair cells showed higher survival rates following aminoglycoside treatment than inner hair cells. This possibility diverges from data from other laboratories, since inner hair cells were generally found to be more resistant than outer hair cells (Li et al. 2002; Taylor et al. 2008; Jiang et al. 2006). However, contradictory data point to the activation of different apoptotic pathways upon aminoglycoside treatments. While some studies indicate that, following aminoglycoside exposure, outer hair cells may die from activation of caspase-dependent pathways (Taylor et al. 2008), other

studies suggest that outer hair cells die by activation of caspase-independent apoptotic pathways, such as necrosis (Jiang et al. 2006). Although the experiments presented in this thesis do not clarify the exact mechanisms of hair cell death, they suggest that inner hair cells do in fact activate alternative cell death pathways, different from those activated in outer hair cells.

Since SGs have been found to inhibit apoptosis by suppressing RACK, MTK, TRAF and JNK pathways (Kim et al. 2005; Arimoto et al. 2008), a scenario in which outer hair cells die from activation of any of these pathways following aminoglycoside treatment would help to explain the results obtained in this study when hydroxamate (-)-9 pre-incubation protected outer hair cells from death. Finally, other reasons may also explain the greater inner hair cell loss compared to outer hair cells. For instance, differences in the drugs used, along with differential rates of accumulation inside the cells may explain the differences observed in terms of hair cell death. Of course, it is also possible that the immature status of the cochlear explants could also have contributed to the observed differences.

From the experiments described in this thesis, it remains unclear whether the surviving outer hair cells are functional and whether the same effects could be replicated *in-vivo*. To clarify this, injection of hydroxamate (-)-9 and ISRIB in aminoglycoside-exposed mice could help to elucidate whether formation of SGs protects hair cell survival *in-vivo*. Assessment of hearing function through ABR recordings could determine whether these pharmacological treatments were able to protect the auditory function. Pharmacological manipulation of SG formation in the presence of other stress agents, such as noise exposure, could also provide evidence as to whether SGs are implicated on the hair cell survival upon other types of auditory stress.

Detection of SGs in the *in-vivo* aged C57BL/6 mouse demonstrated that cochlear cells assemble SGs as a function of age (Figs.4.29 and 4.31). This suggests that SGs are implicated in the response of cochlear cells to age-related changes and may be involved in degeneration of those cells. Interestingly, some of the SGs formed in the *in-vivo* hair cells and spiral ganglion neurons were reported to be present around the perinuclear area (Figs.4.29 and 4.31). This is consistent with my observations in the OC-2 cell line (sections 3.2.1 and 3.2.2) and with studies from other laboratories in HEK-293, HeLa and U2OS cells (Bosco et al. 2010; Hinton et al. 2010; Albornoz et al. 2014). Studies on the *in-vivo* amygdala and cortex in animal models of Alzheimer's disease have also reported SG formation around the

perinuclear area and that was hypothesised to relate to early onset stages of the disease (Vanderweyde et al. 2012).

Taken together, the data presented in this chapter provide further evidence that SGs are implicated in the cochlea's response to a range of different types of stress, including heat shock, oxidative stress, aminoglycoside exposure and ageing. Moreover, these support the hypothesis that SGs may be involved in the pathophysiology of neurodegeneration in the cochlea, such as observed in ALS, Alzheimer's or Huntington's disease (Liu-Yesucevitz et al. 2011; Moreno et al. 2012; Vanderweyde et al. 2012; Ash et al. 2014).

Given that manipulation of SG formation was found to alleviate the effects of aminoglycoside exposure in terms of hair cell survival, application of similar protocols in the *in-vivo* C57BL/6 mice could help to clarify whether degeneration caused with ageing could be prevented by modulation of SG pathway. Ultimately, this could help to develop novel therapeutic strategies aimed at avoiding hair cell damage, thus preventing hearing loss.

5. Investigating the role of Hsp70 in SG formation in the auditory system

5.1. Introduction

Heat shock stress causes substantial changes in the cellular organisation, including misfolding and aggregation of proteins, disruption of the cytoskeleton, fragmentation of the Golgi apparatus and endoplasmic reticulum, loss of mitochondria and lysosomes and changes in RNA splicing (Richter et al. 2010; Vogel et al. 1995; Latchman 2004). Since its discovery in 1962 (Ritossa 1962), the heat shock response has been the focus of intense research. Characterised as conservative and universal, the heat shock response is known to be common amongst bacteria, animals and plants. In addition to this, it is widely recognised that the degree of conservation extends not only to the existence of a common heat shock response in all organisms but also to a similar molecular stress response (Wu 1995; Shamovsky & Nudler 2008; Calderwood et al. 2010). This includes the expression of highly conserved proteins known as heat shock proteins, such as Hsp27, Hsp40, Hsp70 and Hsp90 (Richter et al. 2010; Latchman 2004). Despite being induced in response to heat shock, heat shock proteins have also been shown to confer resistance to other stresses, such as oxidative stress, ethanol or ischemia (Gabai & Sherman 2002). Interestingly, heat shock proteins have been reported to be present in unstressed cells. For instance, they assist in the folding of newly synthesised polypeptides and participate in the regulation of the cellular homeostasis (Mayer & Bukau 2005; Latchman 2004). The presence of heat shock proteins at basal levels in unstressed cells along with the fact that their expression dramatically increases upon stress has led to the hypothesis that pre-induction of heat shock proteins by a mild stress would confer protection to a subsequent more severe stress. This hypothesis has been widely tested in many systems, including cardiovascular disease, neurodegeneration and hearing research (Saad et al. 1995; Latchman 2001; Lee et al. 2001; Cunningham & Brandon 2006). In the inner ear, heat shock has been associated with protective effects against different types of stress. In fact, induction of heat shock prior to aminoglycoside or cisplatin treatments has shown to protect utricle hair cells from death (Cunningham & Brandon 2006; May et al. 2013; Baker et al. 2015), thus contributing to the evidence that heat shock proteins play a role in cell survival during stress.

Apart from effects in the cellular organisation previously mentioned, heat shock also interferes with the pattern of protein translation. This varies according to the type of cell and severity of stress and, while some changes correspond to an increase in the expression of some genes, others result in a general shutting down in protein synthesis following stress (Schlesinger 1994; Paschen 2003; Underhill et al. 2005).

Activation of HSF1, a transcription factor that regulates the expression of different genes encoding heat shock proteins, is one of the main effects of the heat shock response (Calderwood et al. 2010; Anckar & Sistonen 2011).

A number of mechanisms have been proposed for activation of HSF1. Upon heat shock exposure, PI-3K is activated and, in turn, activates Akt. By inhibiting GSK3, Akt promotes HSF1 activation (Chu et al. 1996; Khaleque et al. 2005). PKA also activates HSF1, through a process still unclear (Choi et al. 1991). The mTORC1 complex can also indirectly activate HSF1 after heat shock exposure by induction of Akt (Chou et al. 2012). Heat shock RNA 1 (HSR1), a non-coding RNA, and eukaryotic elongation factor 1A (eEF1A) have also been shown to be essential for HSF1 activation. Upon heat shock stress, translation shutdown and cytoskeleton collapse lead to the release of eEF1A, which is in turn free to interact with HSR1 and HSF1 and promote the heat shock response (Shamovsky et al. 2006).

Upon activation, HSF1 starts the transcription of Hsp70 mRNA (Silver & Noble 2012). Hsp70, a conserved 70 kDa class of proteins, assists in the folding, stabilisation and assembly of newly synthesised proteins. Due to its chaperone function, Hsp70 helps in the repair or degradation of denatured proteins during stress conditions (Hartl 1996; Mayer & Bukau 2005; Shaner & Morano 2007).

There is contradictory evidence regarding the association of Hsp70 with SGs: whereas Hsp70 RNA has been documented to be located outside SGs and selectively translated upon stress in different cell types (Kedersha & Anderson 2002; Tanaka et al. 2014; Ganassi et al. 2016), another study has suggested that Hsp70 is specifically recruited to SGs following heat shock stress (Hu et al. 2010). Additionally, recent research has implicated Hsp70 protein in SG clearance in yeast, *Drosophila* and HeLa cells following stress (Cherkasov et al. 2013; Walters et al. 2015; Ganassi et al. 2016). Taken together, these observations suggest that there is an association between Hsp70 and SGs, although yet poorly understood.

Herein, I question whether there is an association between the expression of Hsp70 protein and the absence of SGs during heat shock stress in the OC-2 cell line.

5.2. Results

5.2.1. Hsp70 protein expression increases during heat shock recovery and is associated with SG absence

Since recent evidence suggest that Hsp70 can protect the inner ear from stress (May et al. 2013; Baker et al. 2015), I sought to investigate whether Hsp70 might play a role in regulating SGs. If so, this might be one mechanism by which Hsp70 provides protection.

To further understand the relationship between Hsp70 and SGs, OC-2 cells were submitted to heat shock stress for 1h at 43°C and allowed to recover for 1h, 2h and 4h at 33°C (using an identical assay as detailed in section 3.2.1). Hsp70, Caprin-1 and TIA-1 protein expression was assessed using immunocytochemistry followed by confocal imaging. SG quantification was performed as previously described (section 2.19.1 in methods) and Hsp70 fluorescent intensity measured using Fiji software.

In untreated OC-2 cells the distribution of Caprin-1 was mostly cytoplasmic and TIA-1 nuclear and cytoplasmic (Fig.5.1, untreated panel). In untreated samples Hsp70 was not detected (Fig.5.1).

Heat shock stress resulted in SG formation, as it can be seen by aggregation of Caprin-1 and TIA-1 into cytoplasmic granules (Fig.5.1, white arrows). At 1h heat shock, no signal was detected for Hsp70 (Fig.5.1).

During recovery from heat shock, as expected, SGs disassembled over a period of 4h (Fig.5.1, white arrowheads). After 4h recovery, Caprin-1 was mostly distributed throughout the cytoplasm, whereas TIA-1 was distributed throughout the nucleus and the cytoplasm, without aggregation at SGs (Fig.5.1). This is in agreement with previous observations (section 3.2.1).

In a subset of cells, the intensity of Hsp70 staining increased markedly during recovery from heat shock stress (Fig.5.1, yellow arrows), consistent with increased levels of Hsp70 protein expression and absence of SGs. Hsp70 protein was mostly distributed throughout the cytoplasm and its expression appeared to increase at 2h and 4h after heat shock (Fig.5.1, yellow arrows).

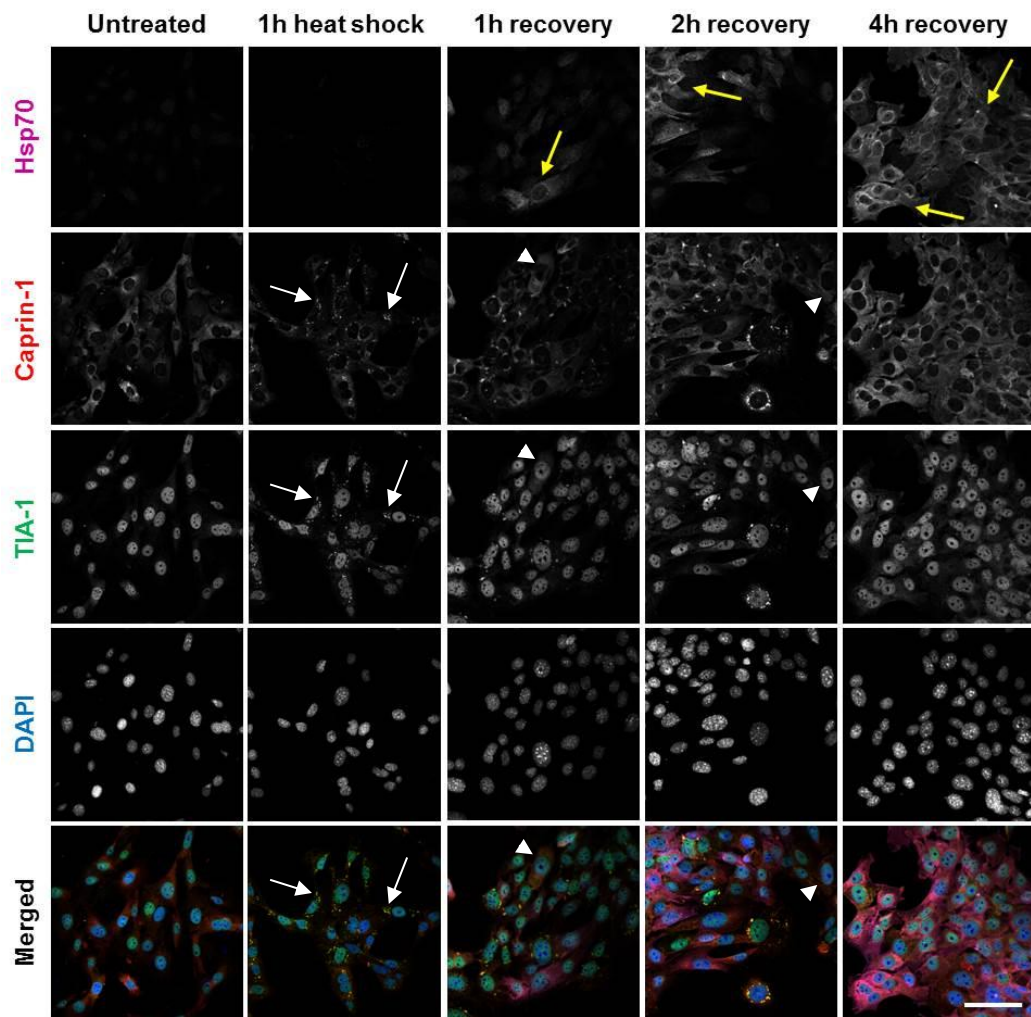


Figure 5.1 – Hsp70 protein expression increases during recovery from heat shock. OC-2 cells were treated with heat shock at 43°C for 1h and allowed to recover for 1h, 2h and 4h at 33°C. Hsp70/Caprin-1/TIA-1 protein distribution is shown. Chromatin structure was assessed using DAPI staining. Scale bar= 50µm for all images.

During recovery from heat shock (1h, 2h and 4h after heat shock), an association between Hsp70 and the absence of SGs was observed: the cells with greater numbers of Caprin-1 and TIA-1 positive SGs appeared to have lower Hsp70 expression (Fig.5.2, white arrows). Consistent with this association, the cells that presented few or no SGs during the recovery periods revealed the highest Hsp70 expression (Fig.5.2, yellow arrows).

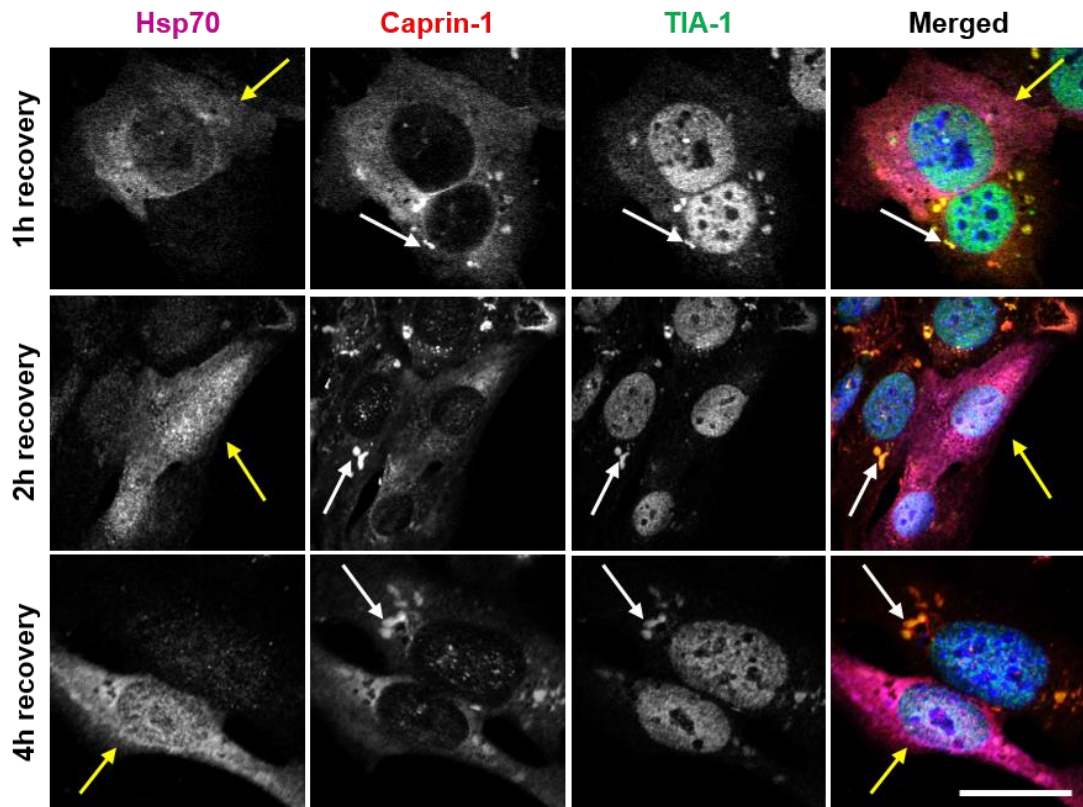


Figure 5.2 - Hsp70 protein intensity seems is correlated with the absence of SGs. Cells were stained for Hsp70/Caprin-1/TIA-1 proteins after 1h recovery, 2h recovery and 4h recovery at 33°C from 1h heat shock stress at 43°C. Chromatin structure was assessed using DAPI staining. Scale bar= 25µm for all images.

To quantify this qualitative observation, 40 cells were analysed individually (using Fiji software) by quantifying their average Hsp70 expression and the number of Caprin-1 and TIA-1 positive SGs. The cells were randomly selected (chosen by DAPI signal alone) from the four different conditions (10 cells from three different cover slips from each time-point): 1h heat shock, 1h recovery, 2h recovery and 4h recovery.

Figure 5.3 represents the changes in Hsp70 expression and the number of Caprin-1 and TIA-1 positive SGs as a function of time. The laser power, detector gain and pinhole levels used in the microscope settings were always kept consistent during the confocal imaging collection, thus enabling comparison of the intensity of the signal amongst different images. The average intensity of Hsp70 increased with the recovery periods from heat shock, at the same time that the number of Caprin-1 and TIA-1 positive SGs decreased (Fig.5.3).

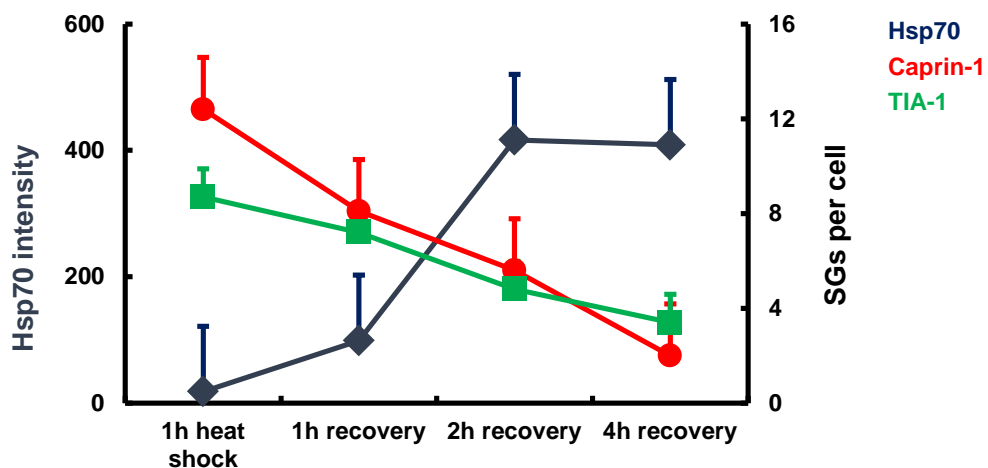


Figure 5.3 – Increased Hsp70 expression associates with SG disassembly during recovery from heat shock stress. Average intensity of Hsp70 protein (blue diamonds) and average number of Caprin-1 (red circles) and TIA-1 (green squares) SGs during heat shock stress in the OC-2 cell line. Values correspond to 1h heat shock at 43°C and different recovery periods at 33°C. Hsp70, Caprin-1 and TIA-1 measurements were randomly obtained from 40 cells, 10 per each time-point from 3 separate experiments with triplicates and represent the average of the 40 samples. Error bars represent SEM.

In Figure 5.4, the average Hsp70 intensity signal is plotted as a function of the number of SGs for each of the 40 cells. For the cells presenting between 15 and 20 SGs, Hsp70 intensity values are close to zero, which suggests that Hsp70 protein expression is reduced in the cells harbouring a high number of SGs (Fig.5.4A). In contrast, for the cells found to have less than 5 SGs, Hsp70 protein intensity can reach levels up to 1200 (Fig.5.4A), suggesting an inverse association between Hsp70 expression and SG formation and/or a positive association between Hsp70 expression and SG disassembly. When considering only the cells presenting Hsp70 intensity values up to 100, the correlation coefficient r^2 was determined as 0.5 for Caprin-1 positive SGs and 0.3 for TIA-1 positive SGs (Fig.5.4B).

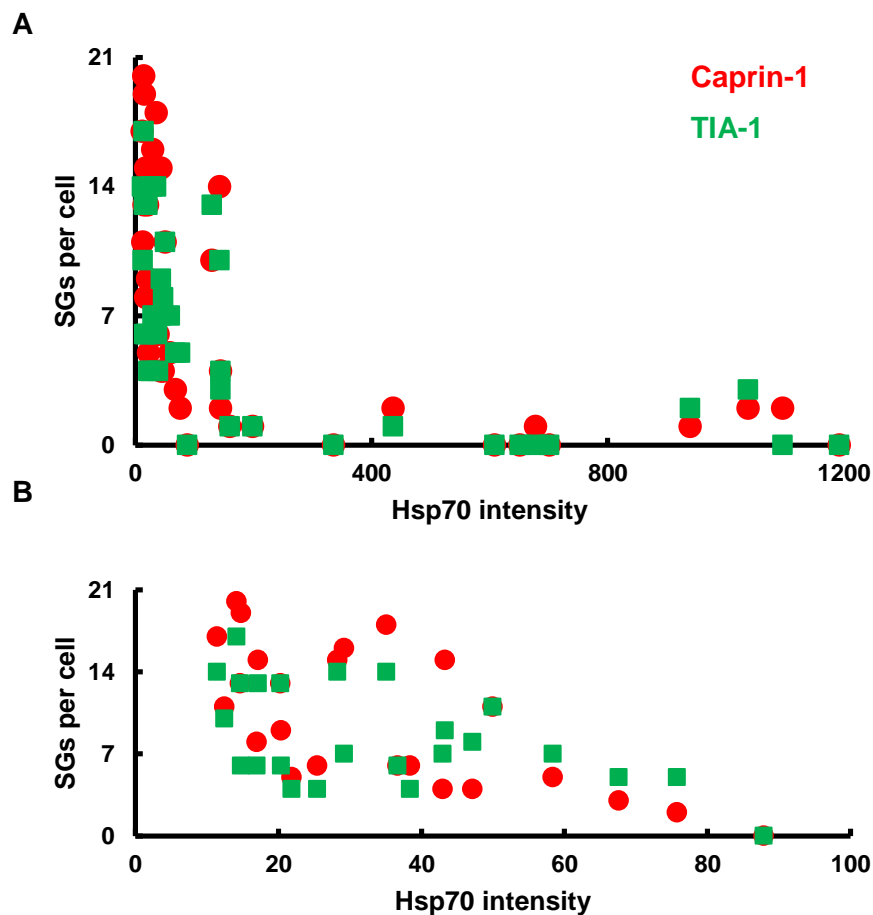


Figure 5.4 – Increased Hsp70 expression is inversely correlated with the number of SGs during heat shock stress. (A) Number of Caprin-1 and TIA-1 SGs per cell in cells containing Hsp70 intensity levels ranging from 0-1200. (B) Number of Caprin-1 and TIA-1 SGs per cell in cells containing Hsp70 intensity levels ranging from 0-100. OC-2 cells were treated for 1h with heat shock at 43°C and allowed to recover during 1h, 2h and 4h at 33°C. Values for the number of Caprin-1 (red circles) and TIA-1 (green squares) SGs, as well as Hsp70 intensity (x-axis), were obtained from 40 cells randomly selected based on DAPI staining. Ten cells were measured per each time-point and the values represented in the graphic are the sum of all the cells considered.

5.2.2. *Hsp70* gene expression increases after heat shock

After observing that Hsp70 protein expression increased in the cytoplasm of OC-2 cells during recovery from heat shock stress, *Hsp70* gene expression was analysed. qPCR was performed to evaluate *Hsp70* gene expression after 1h heat shock and the different recovery periods (1h, 2h and 4h). *Hsp70* gene expression increased after 1h heat shock stress, peaking at 2h recovery (Fig.5.5). At 4h recovery after heat shock, a substantial drop in the *Hsp70* expression levels was observed (Fig.5.5).

When compared to the time-course of Hsp70 protein expression obtained during recovery from heat shock stress (Fig.5.1), qPCR results suggest that there is a delay of approximately 1h between the activation of *Hsp70* gene expression (after 1h heat shock) and the detection of changes in protein expression.

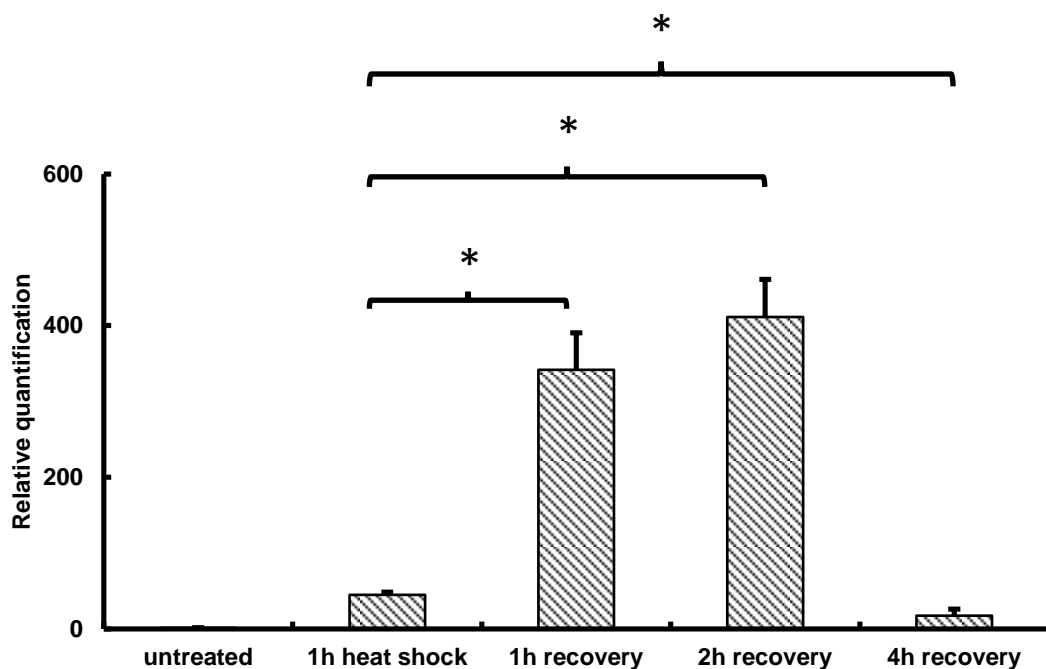


Figure 5.5 – *Hsp70* gene expression significantly increases after heat shock stress. Relative quantification under the $2^{-\Delta\Delta Ct}$ method is shown relative to untreated samples. qPCR was performed using Taqman gene expression assays using 18S RNA as the endogenous control. Data shown represents triplicate assays obtained with three different biological samples (minimum n=9). * $p < 0.05$, Student's *t*-test. Error bars represent SEM.

5.2.3. Arsenite stress does not trigger Hsp70 protein expression

Given the increase in *Hsp70* gene expression and protein intensity observed as a consequence of heat shock treatment, sodium arsenite stress was used to test if these results could also be observed under the effect of a different stressor. Hsp70, Caprin-1 and TIA-1 protein expression was assessed through immunocytochemistry followed by confocal imaging. SG quantification was performed as previously described (section 2.19.1 in methods) and Hsp70 protein intensity measured using Fiji software.

To induce stress, OC-2 cells were treated with 0.5mM of sodium arsenite for 1h and allowed to recover in an arsenite-free medium for 1h, 2h and 4h (using a similar assay as detailed in section 3.2.2).

Consistent with previous observations (section 5.2.1), untreated OC-2 cells did not reveal the presence of Hsp70 protein (Fig.5.6). No change in Hsp70 expression was observed at the end of the arsenite stress (1h) (Fig.5.6). At this time-point, SG formation was evident in the cytoplasm of the cells, as indicated by the distribution of SG-marker proteins Caprin-1 and TIA-1 (Fig.5.6, white arrows) in agreement with previous observations (see section 3.2.2).

SGs started to disassemble when the cells were allowed to recover in an arsenite-free medium (Fig.5.6, white arrowheads), as described before (section 3.2.2). Hsp70 protein was not detected during sodium arsenite stress or during the recovery time-points (Fig.5.6, top panel). The laser power, detector gain and pinhole levels used in the microscope settings were always kept consistent during the confocal imaging collection. This result suggests that Hsp70 protein is not formed under sodium arsenite stress conditions in the OC-2 cell line.

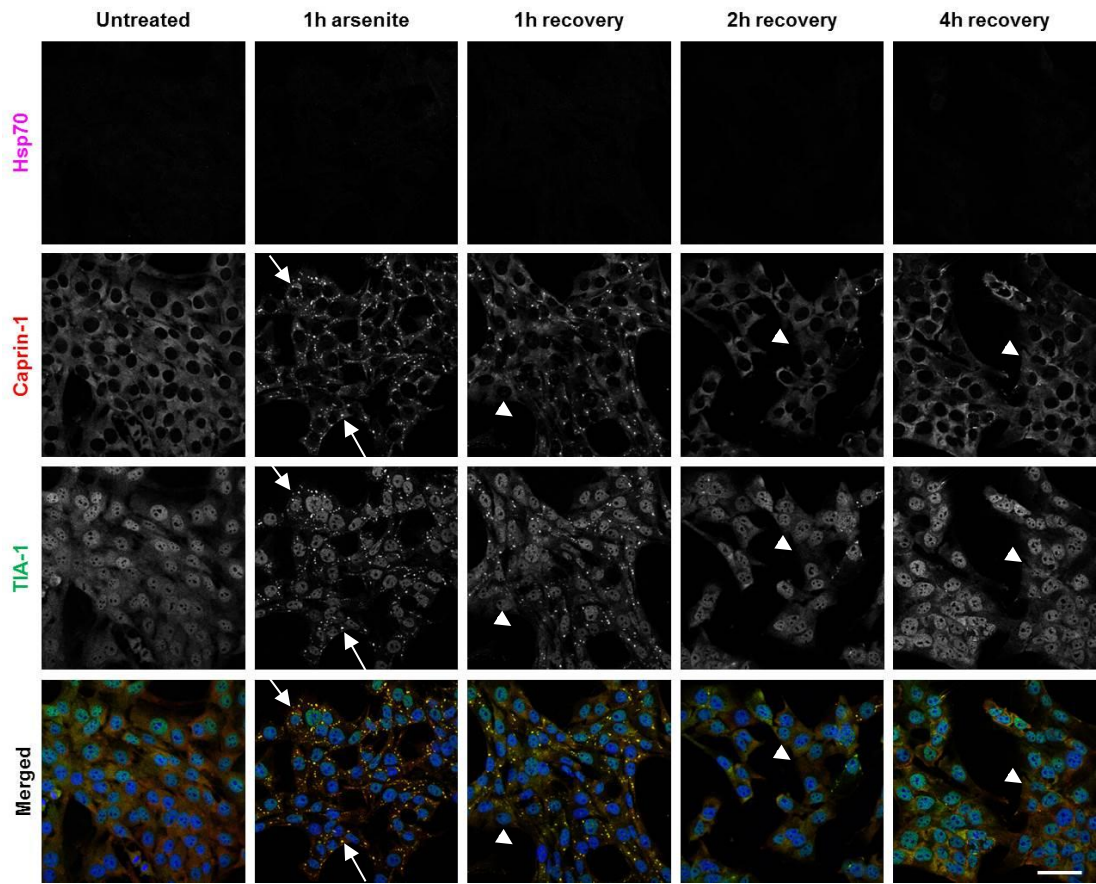


Figure 5.6 – Hsp70 protein expression does not increase during arsenite stress and subsequent recovery. OC-2 cells were treated with 0.5mM of sodium arsenite for 1h and allowed to recover in an arsenite-free medium for 1h, 2h and 4h. Hsp70/Caprin-1/TIA-1 protein distribution is shown across the time-points tested. Chromatin structure was assessed using DAPI staining. Scale bar= 50µm for all images.

5.2.4. qPCR confirms reduced *Hsp70* gene expression upon arsenite stress when compared to heat shock

To further investigate whether *Hsp70* is activated upon sodium arsenite stress exposure, qPCR was performed to evaluate the levels of *Hsp70* gene expression over the different time-points previously tested. *Hsp70* expression did increase after arsenite treatment (Fig.5.7), although the levels of activation were considerably lower and delayed than after heat shock stress (approximately 34-fold difference, Fig.5.5). *Hsp70* gene expression exhibited an increasing pattern over the 4h recovery period, peaking at 4h after arsenite treatment (Fig.5.7).

Therefore, these observations suggest that sodium arsenite treatment triggers a response in terms of *Hsp70* gene expression, although significantly reduced and shifted in time when compared to heat shock stress treatment (Fig.5.5).

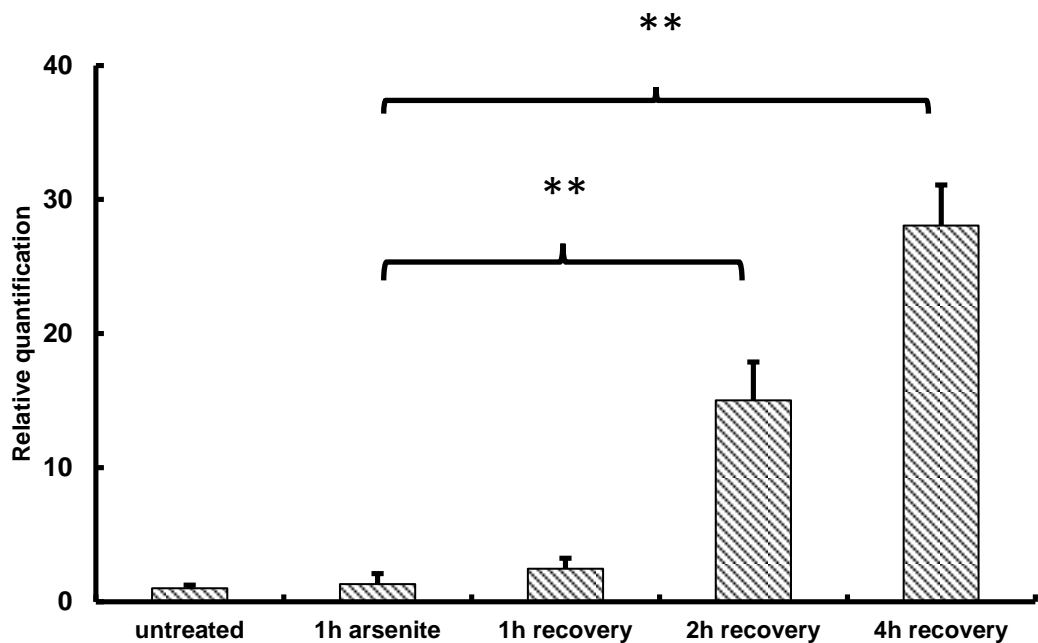


Figure 5.7 - *Hsp70* gene expression is reduced as a consequence of arsenite exposure when compared to heat shock in the OC-2 cell line. Relative quantification under the $2^{-\Delta\Delta Ct}$ method is shown relative to untreated samples. qPCR was performed using Taqman gene expression assays. 18S RNA was used as endogenous control. Data shown represents triplicate assays obtained with three different biological samples (minimum n=9). ** $p < 0.005$, Student's *t*-test. Error bars represent SEM.

5.2.5. RNA-immuno-FISH confirms the exclusion of Hsp70 RNA from SGs during stress in the OC-2 cell line

Hsp70 mRNA was initially reported to be selectively located outside SGs in HeLa cells following heat shock stress, thus being preferentially translated during stress conditions (Kedersha & Anderson 2002). These observations were later on corroborated by another study in mouse neuroblastoma cells, in which it was found that Hsp70 mRNA was specifically located outside SGs during arsenite stress (Tanaka et al. 2014). However, a different study in mouse colonic epithelial cells has suggested that Hsp70 mRNA was specifically recruited to SGs following heat shock stress (Hu et al. 2010).

Here, to clarify whether Hsp70 single mRNA is recruited to or excluded from SGs in the OC-2 cell line, RNA-immuno-FISH was performed to determine the cellular location of Hsp70 RNA during untreated, heat shock and arsenite stress conditions. RNA-immuno-FISH followed by confocal imaging was performed to detect Hsp70 RNA (after hybridisation with Stellaris probes, as indicated in methods sections 2.14 and 2.15) and TIA-1 SG-marker protein.

PolyA⁺ mRNA showed the re-localisation of most of the polyadenylated RNA to SGs after heat shock and arsenite stresses (Fig.5.8, top panel).

At the single RNA level, PTGES3 was used here as a positive control for an RNA which re-localises to SGs upon stress (Fig.5.8, middle panel), since this molecule was shown in a separate RNA immuno precipitation sequencing (RIP-seq) study from our laboratory to increase binding to SG-marker proteins Caprin-1 and TIA-1 following stress. In agreement with the RIP-seq study, PTGES3 RNA clearly re-localised after heat shock and arsenite treatments when compared to untreated conditions, and aggregated at SGs upon stress (Fig.5.8, middle panel).

In untreated cells, Hsp70 RNA was present throughout the nucleus and the cytoplasm of OC-2 cells (Fig.5.8, bottom panel). Following heat shock or arsenite stress, Hsp70 RNA did not aggregate within SGs, as assessed by comparison with TIA-1 distribution (Fig.5.8, bottom panel). In Figure 5.8, it is clear that Hsp70 RNA was detected evenly throughout the cytoplasm of the cells, without aggregation at SGs. These results are in agreement with previous observations (Kedersha & Anderson 2002; Tanaka et al. 2014) and suggest that, by being located outside SGs, Hsp70 RNA is translated during stress in the OC-2 cell line.

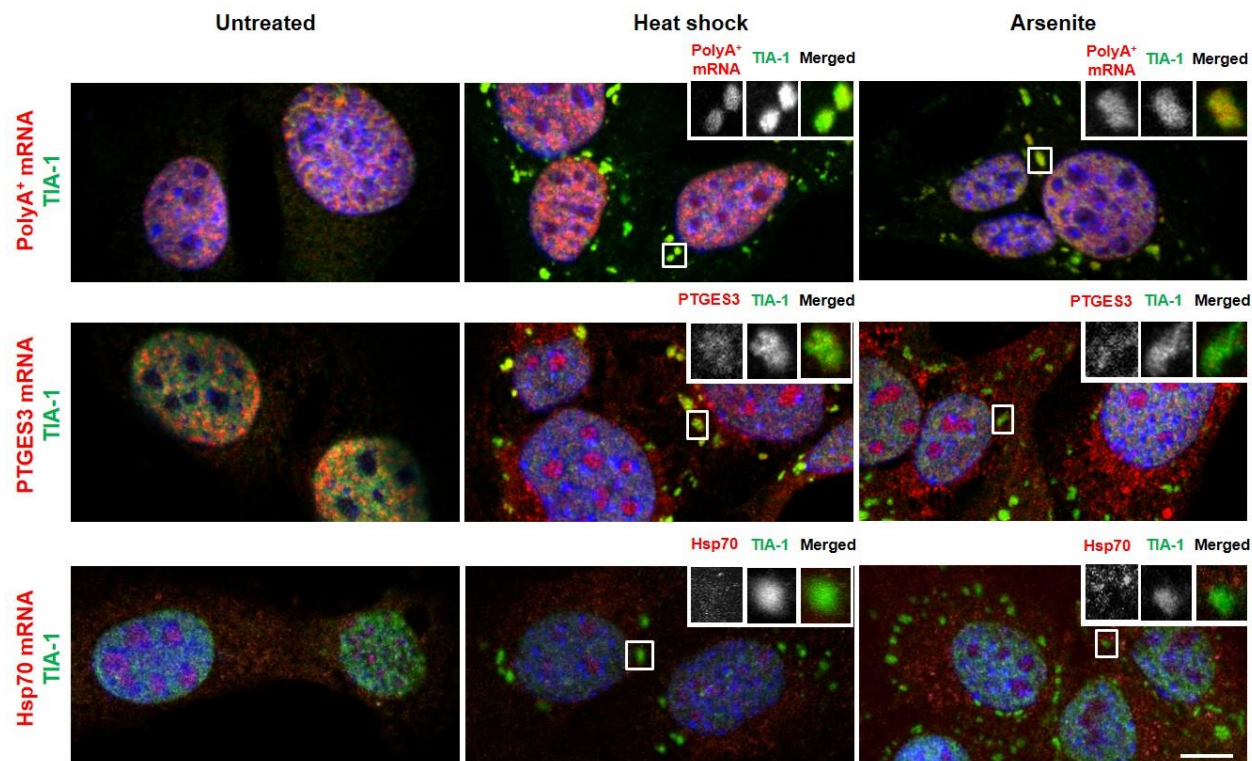


Figure 5.8 – Hsp70 mRNA is excluded from SGs during stress in the OC-2 cell line. RNA-immuno-FISH was performed for Hsp70 single mRNA (RNA FISH) followed by TIA-1 protein detection (immunostaining) to localise Hsp70 to TIA-1 positive SGs induced by heat shock and arsenite stresses. PolyA⁺ mRNA was detected using a Cy3-labelled probe. PTGES3 and Hsp70 single mRNAs were detected using a pool of Stellaris probes. Inset images show zoom in of TIA-1 positive SGs after stress treatments. Chromatin structure was assessed using DAPI staining. Scale bar= 10µm for top images and 1µm for zoomed in insets.

5.2.6. Hsp70 overexpression prior to heat shock stress impairs SG formation

Increased Hsp70 protein expression was correlated with the absence of SGs after heat shock stress (Figs.5.1 and 5.2), suggesting that Hsp70 is either inhibiting SG formation or actively participating in the disassembly of SGs during recovery from heat shock. If so, the presence of Hsp70 protein prior to stress in OC-2 cells should impair SG formation in the early stages during heat shock exposure. To test this hypothesis, Hsp70 overexpression was induced in cells using an adenovirus-mediated Hsp70 (Ad-Hsp70) construct (a kind gift from Dr Lisa Cunningham), prior to heat shock stress exposure. Hsp70, Caprin-1 and TIA-1 protein expression was assessed using immunocytochemistry followed by confocal imaging.

When OC-2 cells were incubated for 24h at 37°C with Ad-Hsp70 without any further treatment, overexpression of Hsp70 itself did not induce SGs, as assessed by Caprin-1 and TIA-1 distribution in Figure 5.9. Ad-Hsp70 positive cells showed Hsp70 and Caprin-1 presenting similar distributions, mostly throughout the cytoplasm, whereas TIA-1 was found to be present in the nucleus and cytoplasm of the cells (Fig.5.9). In Figure 5.9, yellow arrows point to an example of an Ad-Hsp70 positive cell that did not show SG formation, indicating that the adenovirus infection *per se* did not induce stress to the cells. In contrast, white arrows indicate an Ad-Hsp70 negative cell (not infected by the virus) showing SG formation (Fig.5.9).

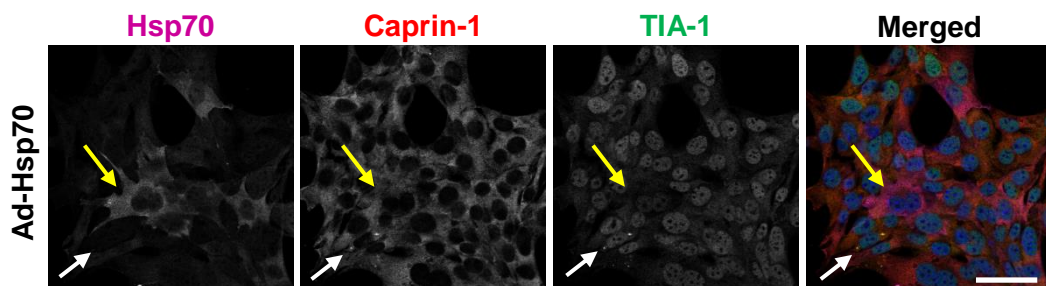


Figure 5.9 – Infection with Ad-Hsp70 does not generate SG formation in OC-2 cells. OC-2 cells were incubated for 24h at 37°C with Ad-Hsp70. Immunofluorescence is shown for Hsp70, Caprin-1 and TIA-1 proteins. Yellow arrows point to Ad-Hsp70 positive cells and white arrows point to Ad-Hsp70 negative cells (not infected by the virus). Chromatin structure was assessed by DAPI staining. Merged image includes DAPI. Scale bar= 50 μ m.

In the absence of overexpressed Hsp70, heat shock stress alone triggered the formation of Caprin-1 and TIA-1 positive SGs (Fig.5.10, heat shock panel), as previously observed (section 3.2.1). After 1h heat shock Caprin-1 and TIA-1 aggregated at cytoplasmic SGs (Fig.5.10). As observed before (section 5.2.1), at this time point (1h after heat shock) there is no detection of Hsp70 protein, since it was demonstrated that Hsp70 protein is mostly detected after 2h and 4h recovery following heat shock (Fig.5.1).

When Hsp70 was overexpressed for 24h prior to heat shock stress, there was a clear difference in terms of SG assembly: Ad-Hsp70-positive cells showed Caprin-1 mostly distributed across the cytoplasm, whereas TIA-1 was present in both nucleus and cytoplasm, without aggregation at SGs (Fig.5.10, yellow arrow, zoom in inset). In the same experiment, neighbouring cells negative for Hsp70 overexpression exhibited the expected pattern of SG formation (Fig.5.10, white arrows, boxed area), suggesting that the absence of SGs observed in the other cells was, to some extent, related to the presence of exogenous overexpressed Hsp70.

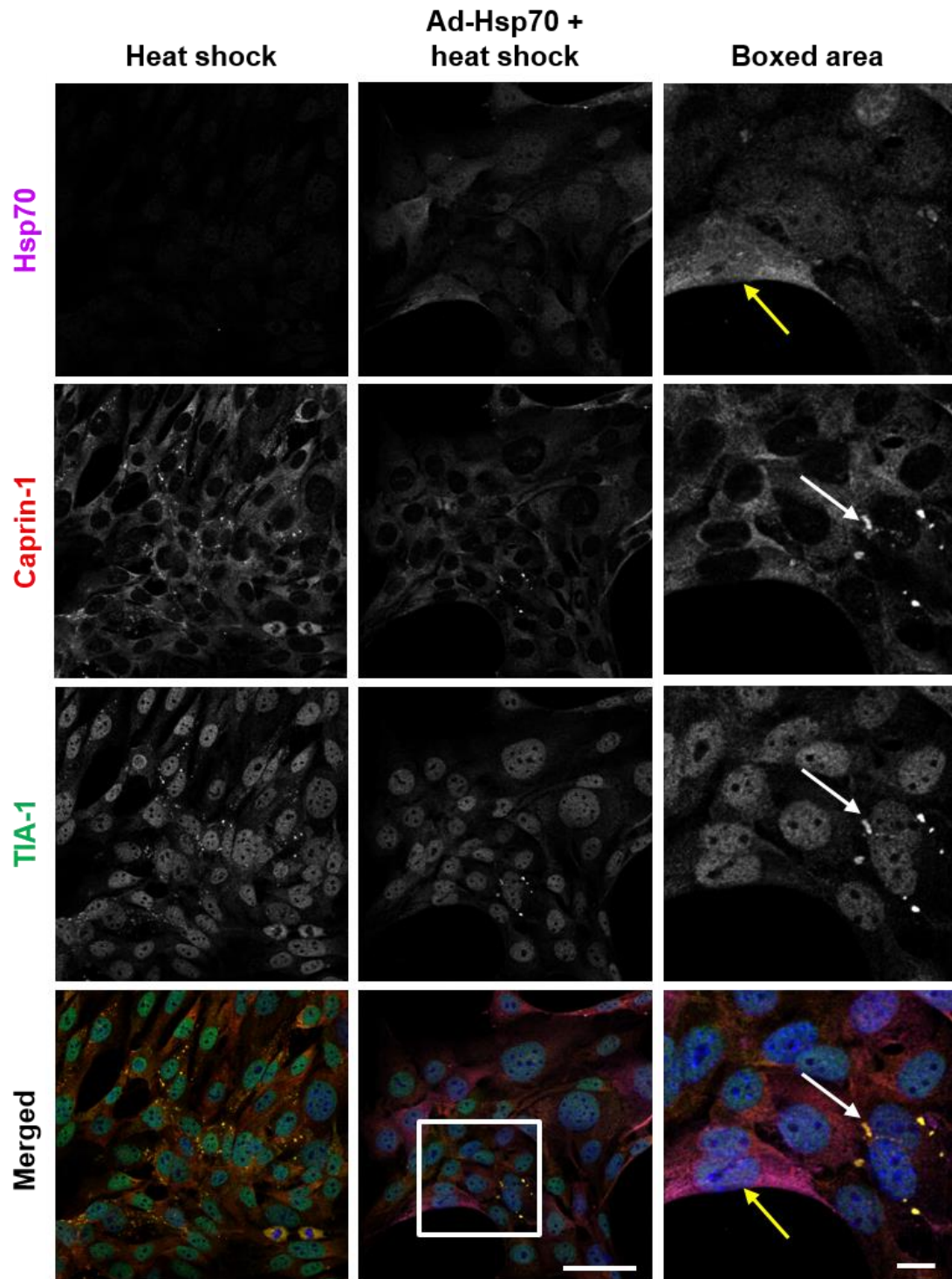


Figure 5.10 – Hsp70 overexpression inhibits SG formation under heat shock stress. Immunofluorescence data is shown for Hsp70, Caprin-1 and TIA-1 proteins. OC-2 cells were overexpressed with Ad-Hsp70 for 24h prior to heat shock stress. Boxed area show a zoomed-in region of positive Ad-Hsp70 infected cells next to Ad-Hsp70 negative cells (not infected). Chromatin structure was assessed using DAPI staining. Scale bar= 50µm for heat shock/Ad-Hsp70 + heat shock images and 10µm for zoomed-in boxed area.

Ad-Hsp70 positive cells were randomly chosen by Hsp70 and DAPI signals, and SG quantification performed as described before (section 2.19.1 in methods). Adenovirus-mediated Hsp70 overexpression significantly reduced the number of Caprin-1 and TIA-1 positive SGs by 79% and 86%, respectively, under heat shock stress conditions, when compared to heat shock alone in the absence of Hsp70 overexpression (Fig.5.11).

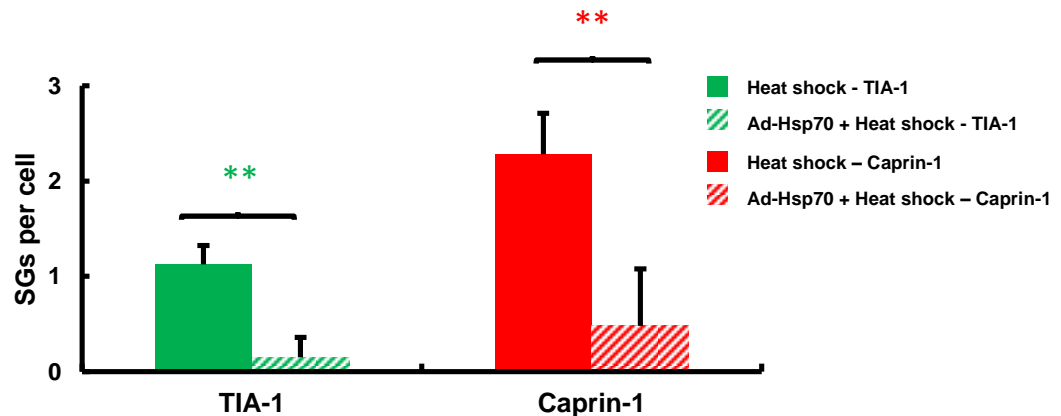


Figure 5.11 – Overexpression of Hsp70 reduces the number of SGs formed upon heat shock stress. Average number of TIA-1 and Caprin-1 SGs per cell in heat shock-treated cells (filled bars) and selected cells exposed to Ad-Hsp70 (striped bars) prior to heat shock stress exposure in the OC-2 cell line. Student's *t*-test, ** $p < 0.005$ for TIA-1 and Caprin-1, respectively, in cells overexpressing Hsp70 when compared to heat shock-treated samples. Error bars represent SEM (n=9).

Collectively, these experiments confirmed that expression of Hsp70 protein before heat shock reduced SG formation in the early stages (<1h) during heat shock stress exposure.

5.2.7. SG formation is unaffected by Hsp70 overexpression prior to arsenite stress

A reduced number of SGs was found in the presence of overexpressed Hsp70 during heat shock stress, when compared to vehicle-treated controls (Figs.5.10 and 5.11). Since arsenite stress did not trigger Hsp70 protein expression (Fig.5.6), the effect of inducing Hsp70 expression prior to arsenite exposure on the SG formation was also tested.

Arsenite stress (0.5mM for 1h) triggered the formation of SGs, as assessed by Caprin-1 and TIA-1 aggregation in the cytoplasm of the cells (Fig.5.12, arsenite panel), as previously observed (section 3.2.2).

Overexpression of Hsp70 did not affect SG formation after 1h arsenite treatment, since in Hsp70-positive cells, Caprin-1 and TIA-1 positive SGs were found, similarly as observed in non-Hsp70 expressing cells (Fig.5.12, yellow arrows, boxed area).

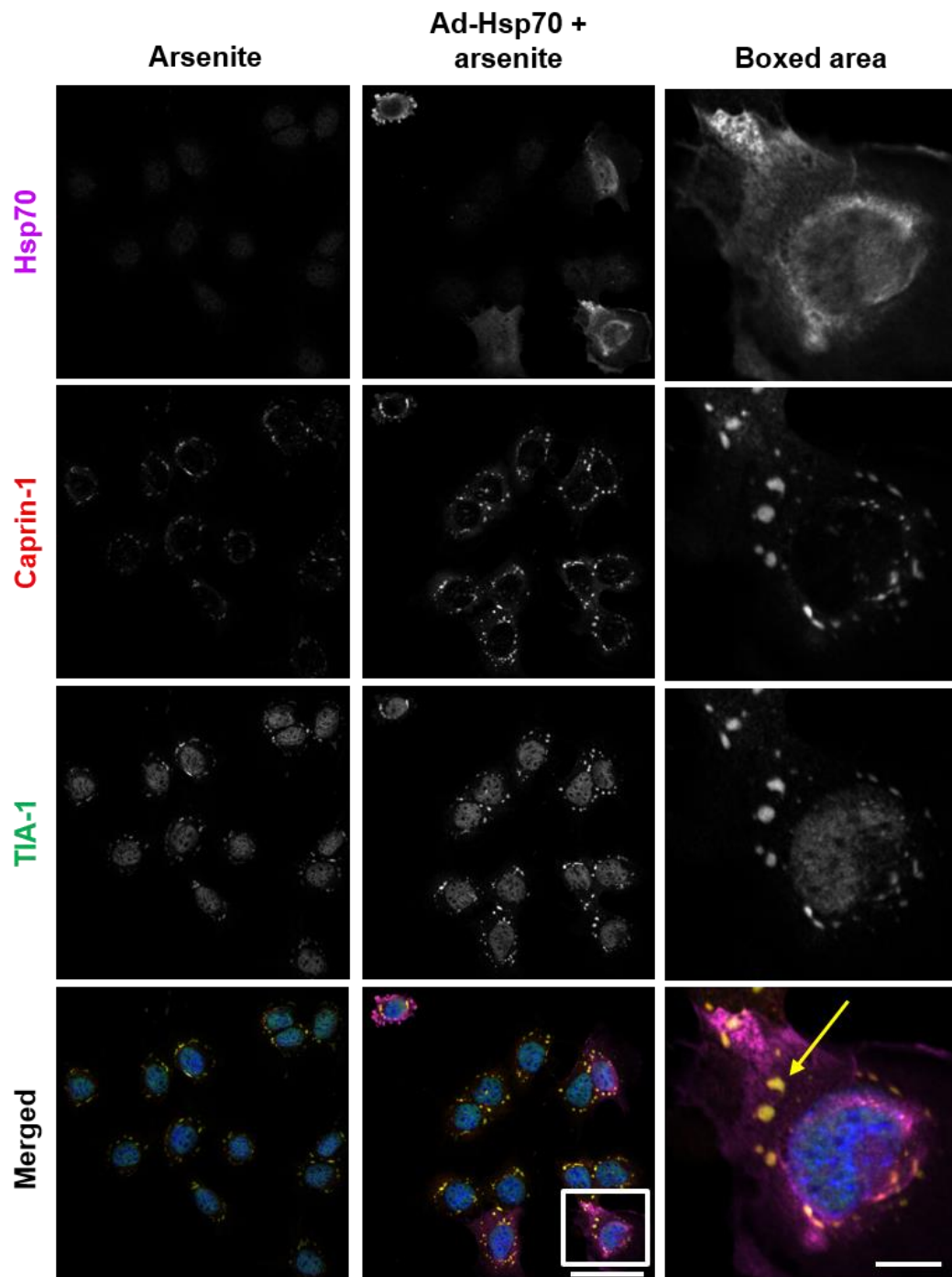


Figure 5.12 – Overexpression of Hsp70 does not reduce arsenite-induced SG formation. Immunofluorescence data is shown for Hsp70, Caprin-1 and TIA-1 proteins. Overexpression of Hsp70 was performed in OC-2 cells for 24h prior to arsenite stress. Boxed area shows a zoomed-in positive Ad-Hsp70 infected cell with Caprin-1/TIA-1 SG formation after arsenite treatment (arrow). Chromatin structure was assessed using DAPI staining. Scale bar= 50 μ m for arsenite/Ad-Hsp70 + arsenite images and 10 μ m for boxed area.

Quantification of these images confirmed that there were no significant changes in the number of SGs formed after overexpression of Hsp70 when compared to arsenite treatment alone (Fig.5.13).

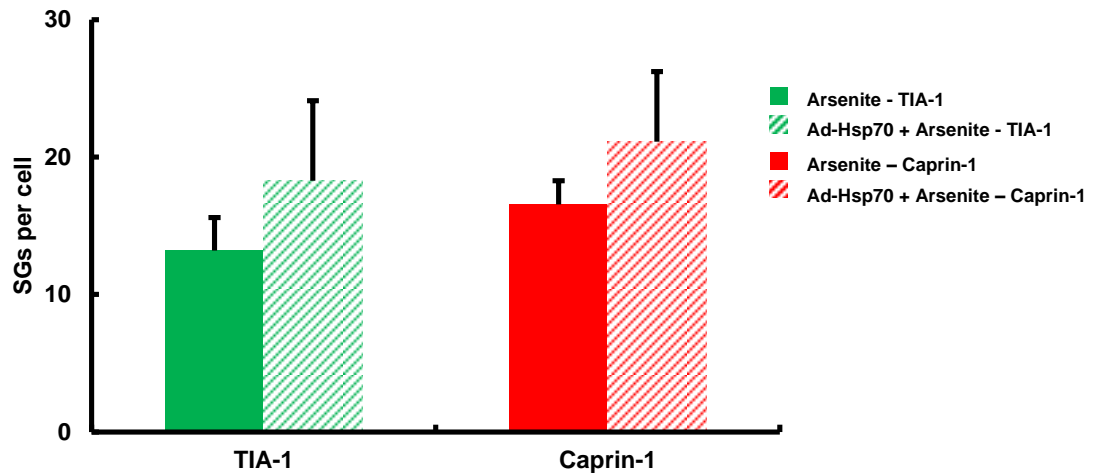


Figure 5.13 – Overexpression of Hsp70 does not affect the number of SGs formed upon arsenite stress. Average number of TIA-1 and Caprin-1 SGs per cell in arsenite-treated cells (filled bars) and selected cells exposed to Ad-Hsp70 (striped bars) prior to arsenite stress exposure in the OC-2 cell line. No differences were found. Error bars represent SEM (n=9).

Taken together, these results suggest that, in contrast to the observations during heat shock stress, under arsenite conditions, Hsp70 does not reduce or disassemble SGs in the OC-2 cell line.

5.3. Discussion

Hsp70 is a molecular chaperone involved in multiple cell protective functions (Hartl 1996; Mayer & Bukau 2005; Shaner & Morano 2007). Increased expression of Hsp70 following stress has been shown to provide cellular resistance to subsequent more severe stresses that would normally result in cell death (Mosser et al. 2000). Due to its activity during stress conditions, Hsp70 expression has been associated with SGs (Kedersha & Anderson 2002; Cherkasov et al. 2013; Walters & Parker 2015). The work described in this chapter aimed to characterise the relationship between Hsp70 and SGs using OC-2 cells.

The results presented herein suggest that there is a reciprocal relationship between Hsp70 protein expression and the absence of SGs in OC-2 cells (Figs.5.3 and 5.4). During the recovery periods from heat shock stress, most of the cells that did contain SGs presented low Hsp70 protein levels, whereas cells with high Hsp70 protein levels had fewer or no SGs present (Figs.5.1 and 5.2).

One possible explanation for the differential pattern of Hsp70 protein intensity observed amongst individual cells is that perhaps only some OC-2 cells are predisposed to a rapid HSF1 activation during heat shock stress. Thus, after heat shock, quick and robust Hsp70 expression would only occur in a subset of the cells during early recovery stages. Why only a subset of cells are predisposed to a rapid Hsp70 translation following heat shock only in some OC-2 cells is still unclear.

In these studies, neighbouring cells presented different patterns of Hsp70 protein staining as assessed by immunofluorescence during early recovery periods (Fig.5.2), with Hsp70-positive cells being adjacent to Hsp70-negative cells. This observation, along with the fact that SG formation is only observed in Hsp70-negative cells may suggest that a possible cell-to-cell communication mechanism involving the stress response activators might exist. In fact, it was recently reported that glia and glia-like supporting cells in the inner ear do actually segregate Hsp70 in the presence of heat shock stress and the secreted Hsp70 protects hair cells from neomycin-induced toxicity (May et al. 2013). May and colleagues reported that Hsp70 is not internalised by hair cells and hypothesised that Hsp70 can bind to a receptor on the hair cell surface, then triggering protective downstream signalling pathways (May et al. 2013). In other systems, Hsp70 has been shown to act at the extracellular level and to be able to bind to specific receptors on the cell surface, activating signalling pathways on the target cells (Basu et al. 2001; Delneste et al. 2002; Thériault et al. 2005; Thériault et al. 2006).

Evidence from different studies point that these receptors are likely to be scavenger receptors (Delneste et al. 2002; Thériault et al. 2005; Thériault et al. 2006).

Here, the present data suggest a causative relationship between the Hsp70 expression and the absence of SGs during recovery from heat shock (Figs.5.3 and 5.4). The latter conclusion is supported by the overexpression studies, since heat shock-induced SG formation was decreased in cells with Hsp70 overexpression (Fig.5.11).

A possible explanation for the fact that less SGs are observed in the presence of over-expressed Hsp70 is that Hsp70 may directly reduce cellular stress during heat shock, thus reducing the need for the cells to form SGs. Hsp70 presents cell protective functions, such as proofreading of protein structures, assistance and repair in protein folding and inhibition of apoptosis (Mayer & Bukau 2005). Since these are likely to directly reduce the level of cellular stress, less SGs are expected to assemble when Hsp70 is present during heat shock stress. This would be a consequence of reduced activation of the SG pathway in the presence of Hsp70, given the possible downstream effects of Hsp70 in the reduction of cellular stress.

Taken together, these data strongly suggest that there is a causative link between Hsp70 expression and SG absence during heat shock conditions. However, they do not clarify whether (i) Hsp70 expression inhibits SG formation during heat shock or whether (ii) Hsp70 promotes rapid disassembly of SGs during heat shock exposure. The first case implies that an early HSF1 activation in a subset of cells would rapidly promote Hsp70 formation in response to heat shock stress and, considering the known effects of Hsp70 as a chaperone (Mayer & Bukau 2005), due to its high availability in those cells, the cells would not have to trigger the SG pathway to respond to the stress. The second case suggests that Hsp70 would actively participate in the SG clearance from heat shock stress. The latter hypothesis would be in agreement with data from other laboratories. Recently, Hsp70 protein has been shown to play a critical role during SG disassembly in yeast, *Drosophila* and HeLa cells (Cherkasov et al. 2013; Ganassi et al. 2016). Additionally, impaired Hsp70 function in yeast has been shown to prevent the clearance/disassembly of SGs during recovery (Walters et al. 2015).

Gene expression analysis showed that *Hsp70* is activated following heat shock stress, peaking after 2h of recovery (Fig.5.5). These results are in close agreement with previous reports, in which *Hsp70* gene expression has been shown to increase after 2h recovery from heat shock stress in cultured utricles (Cunningham &

Brandon 2006). A possible synergistic effect from the different HSF1 activators upon heat shock exposure may help to explain the robust *Hsp70* gene expression activation observed following heat shock and early recovery periods. After 4h recovery, a substantial drop on the levels of *Hsp70* gene expression was observed (Fig.5.5). This data may suggest that, in the late recovery periods from heat shock, Hsp70 is no longer required by the cells. A previously described Hsp70 negative feedback mechanism (Zou et al. 1998) may help to elucidate the decrease in gene expression observed after 4h recovery from heat shock stress. The negative feedback inhibition by Hsp70 in HSF1 along with the absence of stress during the recovery period may contribute to the accentuated decrease in *Hsp70* gene expression levels after 4h recovery from heat shock. At the protein level, the strong intensity signal detected by immunostaining after 4h recovery from heat shock (Fig.5.1) is also in agreement with the qPCR data, demonstrating a shift of approximately 1h from the gene expression until the protein formation.

Although activated at substantially lower levels when compared to heat shock stress (approximately 34-fold difference), *Hsp70* gene expression did increase after arsenite stress and was shown to exhibit an increasing pattern over the 4h recovery period (Fig.5.7).

Interestingly, Hsp70 overexpression prior to arsenite stress exposure did not affect SG assembly (Figs.5.12 and 5.13). After arsenite stress, Hsp70 positive cells revealed clear SG formation, demonstrating that in the OC-2 cell line the link between Hsp70 expression and SG absence only applies following heat shock stress. From these experiments, it is still unclear how Hsp70 exclusively participates in the SG absence or clearance during heat stress conditions but not arsenite.

One possible explanation for the fact that *Hsp70* does present significantly lower activation following arsenite than heat shock stress might be that arsenite may block PI-3K kinase activation in OC-2 cells. Under sodium arsenite conditions, the protective PI-3K/AKT pathway has been shown to be inhibited mouse stem cells (Ivanov et al. 2013), activating GSK3 (Giasson et al. 2002). Active GSK3 represses HSF1, thus inhibiting *Hsp70* transcription (Wang et al. 2003; Wang et al. 2004; Zhou et al. 2004). Arsenite has also been previously shown to inhibit eIF4F and eEF1A, which in turn activate HSF1 (Shamovsky & Gershon 2004). Here, the observation of a significantly reduced *Hsp70* activation following arsenite stress along with the hypothesis that arsenite can inhibit HSF1 expression through other means may

explain the differences in the Hsp70 expression observed according to the different stressors.

In a study using mouse colonic epithelial cells, Hsp70 mRNA was shown to be specifically recruited to SGs by IFN- γ and TNF- α , inhibiting its translation following heat shock stress (Hu et al. 2009). However, data from our laboratory (Fig.5.8) and others (Kedersha & Anderson 2002; Ganassi et al. 2016) have shown Hsp70 mRNA to be selectively kept outside SGs, consistent with it being actively translated after stress and, consequently, playing an important role in cell survival. In fact, in the auditory system, heat shock and Hsp70 have been shown to protect hair cells against aminoglycoside-induced cell death. Induction of heat shock stress prior to aminoglycoside administration inhibited hair cell death in utricles from wild-type mice (Taleb et al. 2008). Consistent with this, in utricles from HSF1^{-/-} and Hsp70.1/3^{-/-} mice, heat shock stress failed to protect aminoglycoside-induced hair cell death, suggesting that HSF1 and Hsp70 are both necessary for the protective effect of heat shock observed during aminoglycoside exposure *ex-vivo* (Taleb et al. 2008). Following these results, overexpression of Hsp70 *in-vivo* inhibited aminoglycoside-induced hair cell loss, thus corroborating the results previously reported in *ex-vivo* utricles and confirming the protective effects of Hsp70 against ototoxicity *in-vivo* (Taleb et al. 2009).

From the work presented here, three hypotheses can be formulated as to how Hsp70 interferes with SG assembly upon different stressors. Firstly, to justify the differential expression of Hsp70 between different cells, one hypothesis is that HSF1 is activated only in a subset of cells, thus leading to the expression of Hsp70 and consequent SG absence only in that subset of cells. To test this hypothesis, immunofluorescence could be used to detect activated HSF1 in OC-2 cells. This would help to clarify whether HSF1 is in fact activated only in a fraction of cells and whether those cells would correspond to the Hsp70-positive cells, lacking the expression of SGs.

A second hypothesis is that Hsp70 may inhibit SG formation during heat shock stress in the OC-2 cell line. Live Hsp70 and SG imaging during heat shock stress exposure and recovery periods could help to clarify if Hsp70 acts by inhibiting SG formation or if it actively participates in an early SG clearance from heat shock stress. Earlier fixation of cells may also be considered, to analyse different time-points within 1h stress and determine the kinetics of SG formation and Hsp70 activation by measuring HSF1 activation levels.

A third hypothesis is that in the OC-2 cell line, PI-3K kinase may be only activated by heat shock and not by sodium arsenite stress, thus blocking HSF1 activation following arsenite stress. Evaluation of PI-3K, eIF2 α and eEF1A inhibitory levels after both heat shock and arsenite exposure would also help to explain this question and to elucidate which pathways are specifically activated in the OC-2 cell line during the different stressor agents. Measurements of HSF1 promoter activation could also be used to clarify whether HSF1 is activated in the OC-2 cell line following arsenite stress. This could help to explain the differences observed between *Hsp70* gene expression during the recovery periods from heat shock and arsenite treatments.

The involvement of Hsp70 during cellular stress has been extensively reported in different systems. A number of studies have described the heat shock treatment and Hsp70 as key players in cellular protection to subsequent stronger stresses. *In-vivo* protective effects of heat shock include predominantly heart and liver protection following ischemia and neuroprotection (Saad et al. 1995; Latchman 2001; Hoehn et al. 2001; Lee et al. 2001; Ahn & Jeon 2006).

Hsp70 has been the target of many studies aimed at developing therapeutic interventions. For instance, exogenous administration of Hsp70 has been shown to protect motor and sensory neurons from death after injury in mice (Tidwell et al. 2004). In neuroblastoma cells, Hsp70 was associated with the reduction of oxidative stress and apoptosis induced by the peptide isoAsp7-A β , one of the most common peptides in amyloid plaques formed during the progression of Alzheimer's disease (Yurinskaya et al. 2015). In mice models of neurodegeneration, Hsp70 administration has been shown to alleviate morphological and cognitive abnormalities characteristic of Alzheimer's pathology, by protecting spatial memory and diminishing the formation of A β peptides (Bobkova et al. 2014).

Hsp70 has also been the focus of many researchers working with mice models of ALS. Exogenous injection of Hsp70 increased lifespan, delayed symptom onset and preserved locomotor function in these mice (Gifondorwa et al. 2007). Treatment with arimoclomol, a co-inducer of heat shock proteins, has been shown to improve muscle function and motoneuron survival in later stages of ALS, thus increasing lifespan (Kieran et al. 2004; Kalmar et al. 2014). Arimoclomol was also tested in mice models of retinitis pigmentosa and, through the activation of the heat shock response and the unfolded protein response, showed to protect photoreceptor's

structure and to reduce the aggregation of rhodopsin, hence alleviating the damage caused by this pathology (Parfitt et al. 2014).

All these studies appear to converge in a common point: Hsp70 seems to constitute a plausible target for therapeutic intervention in many different neurodegenerative diseases associated with abnormal protein aggregation, motor function and cognitive disorders. Given the growing evidence that SGs may be directly involved in cell survival decisions upon acute stress and the known implications of Hsp70 in cell protection, a better understanding of the relationship between them may contribute to the development of therapeutic strategies to avoid cell death during stress conditions.

6. General discussion

This PhD thesis describes the first studies aimed at understanding the role of SGs in the inner ear. Aside from their implication in the cochlea's response to aminoglycoside damage (Towers et al. 2011), very little is known to date about the function of SGs in the auditory system.

The study of SGs is a relatively young field that has been the focus of intense research, especially after their association with neurodegeneration and viruses. Unlike other types of RNA granules, such as processing bodies, SGs are not present during physiological conditions (i.e. in unstressed cells) and only assemble upon stress exposure (Kedersha et al. 1999; Kedersha & Anderson 2007). By recruiting pro-apoptotic factors, translation initiation factors, RNA-editing enzymes, RNA-binding proteins and stalled 48S preinitiation complexes, amongst others, SGs actively reprogram mRNA metabolism in order to adapt to stress conditions and to synthesise molecules that can repair stress-induced damage (Kedersha et al. 1999; Kedersha et al. 2002; Tourrière et al. 2003; Kim et al. 2005; Gallois-Montbrun et al. 2007; Ohn et al. 2008; Papadopoulou et al. 2013; George et al. 2016). Once the stress is over, SGs disassemble and translation of the regular pool of RNAs is thought to resume (Kedersha et al. 2000; Souquere et al. 2009).

Given the previous association of SGs with cochlear stress (Towers et al. 2011) and since the mammalian inner ear is likely to be constantly exposed to stress conditions (e.g. noise, aminoglycosides, ageing), I sought to investigate the function of SGs during aminoglycoside stress. A better understanding of how the inner ear responds to stress may contribute to the development of preventative therapies that can maintain functional hair cells during stress conditions, therefore avoiding hair cell loss and, consequently, hearing loss.

In order to study SG formation and regulation in the auditory system, the first experiments of this project were developed in OC-2 cells, an inner ear-derived cell line widely used in hearing research (Rivolta et al. 1998; Rivolta & Holley 2002; Jagger et al. 2000; Clough et al. 2004; Brunetta et al. 2012). As discussed before, the mammalian organ of Corti constitutes an experimental challenge, since it is located within the temporal bone, it presents a limited number of hair cells and these do not regenerate (Martini 2007). Although OC-2 cells do not resemble hair cells morphologically and present experimental limitations when compared to the multicellular structure of the organ of Corti, they do express certain markers that

indicate their otic nature (Rivolta et al. 1998). Thus, I have developed the first assays of this project in this cell line to have an initial assessment of the dynamics of SG formation in an inner ear context. In addition, this enabled optimisation of protocols in a cell line, limiting animal usage.

A comprehensive dataset was obtained in OC-2 cells, describing the number, size and frequency of SGs formed under two different stress paradigms, heat shock and sodium arsenite. TIA-1 and Caprin-1 proteins were used to label SGs, along with detection of polyA⁺ mRNA.

Since SGs first description in mammalian cells, TIA-1 has been widely used in numerous studies as one of the main proteins to identify SGs (Kedersha et al. 1999; Souquere et al. 2009; McDonald et al. 2011; Aulas et al. 2012). Caprin-1, a known protein present in neuronal RNA granules (Shiina 2005; Shiina et al. 2010; Shiina & Tokunaga 2010), has been associated with SGs in only a few publications, especially because its association with another SG protein, G3BP1 (Solomon et al. 2007; Kolobova et al. 2009; Kunde et al. 2011). Given that recent data from our laboratory has implicated Caprin-1 in SG formation in both OC-2 cells and mouse cochlear explants (Towers et al. 2011), I have decided to further investigate Caprin-1 in SG dynamics, along with TIA-1, during heat shock and sodium arsenite stresses. Upon stress exposure, Caprin-1 and TIA-1 aggregated and colocalised at SGs (Figs.3.1 and 3.4), indicating that these two proteins participate in the regulation of SG assembly in the OC-2 cell line. When cells were allowed to recover from stress, Caprin-1 and TIA-1 gradually returned to a distribution comparable to pre-stress levels (Figs.3.1 and 3.4), consistent with SG clearance.

PolyA⁺ mRNA was here identified for the first time as a component of SGs in an inner ear-derived cell line, after the development of a robust assay that allowed localisation of RNA to SGs (RNA-immuno-FISH). A marked localisation of polyA⁺ mRNA to SGs was observed following stress (Figs.3.1 and 3.4), demonstrating that the Caprin-1/TIA-1 positive SGs identified in previous studies from the laboratory (Towers et al. 2011) do contain mRNA as a component. The recruitment of mRNA to SGs allows the confirmation of the RNA/protein nature of these aggregates and is in agreement with results from other studies in DU145 and U2OS cells, for example (Kedersha et al. 1999; Zurla et al. 2011). Moreover, this shows that polyA⁺ mRNA redistributes following stress and most of the cytoplasmic mRNA is targeted to SGs during stress conditions, suggesting that SGs may be involved in regulating the fate of RNA molecules during stress in OC-2 cells. In addition, these results indicate that

Caprin-1 and TIA-1 colocalise with polyA⁺ mRNA at SGs, confirming that these two proteins are key constituents of SGs following the activation of PKA and PI-3K (heat shock) and HRI (sodium arsenite) kinases in OC-2 cells.

The confirmation of Caprin-1 aggregation with polyA⁺ mRNA indicates that the SGs generated in OC-2 cells contain not only widely recognised SG markers, such as TIA-1, but also Caprin-1 as a main constituent. Since Caprin-1 has been shown to be mostly expressed in the brain and responsible for transport of mRNAs at the postsynaptic dendrites in the hippocampus (Shiina 2005; Shiina et al. 2010), the association of Caprin-1 with SGs in OC-2 cells suggests that the sorting of RNAs is likely to differ between OC-2 cells and other cell types and that distinct types of SGs, in terms of protein composition, are likely to be generated in different systems.

Although SGs were found to widely distribute throughout the cytoplasm of OC-2 cells following stress, a subset of SGs revealed a perinuclear distribution (Figs.3.1 and 3.4). Even though this has also been reported in other cell lines, such as HEK-293, HeLa and U2OS (Bosco et al. 2010; Hinton et al. 2010; Albornoz et al. 2014), it is not clear yet why some SGs assume a perinuclear presence following stress. A possible explanation is that perhaps those SGs may assist nascent mRNA transcripts during early exportation from the nucleus, providing a rapid triage of the early mRNAs to be translated during stress conditions.

A novel quantification method was developed during these studies that precisely quantifies the number and size of SGs formed upon stress (section 3.2.1 and 3.2.2). This is of particular interest for the SG field of research, since the use of a standard protocol could allow a comparison of how different systems respond to stress and how the different stressor agents influence SG assembly. Very few publications have attempted to quantify the number and size of SGs (Buchan et al. 2013; Arimoto-Matsuzaki et al. 2016). Using this quantification protocol, the dataset presented in this thesis is one of the most comprehensive in the SG field so far, as regarding the number, size and frequency of the SG formed upon stress.

Using this method, I determined that sodium arsenite stress triggers greater numbers of SGs in OC-2 cells than heat shock stress, although the size of SGs did not differ significantly between these two stressors (Figs.3.2 and 3.5). Although the methods for quantification of SGs published in other systems mostly refer to percentage of cells containing SGs, the number and size of SGs generated in OC-2 cells upon heat shock and arsenite stresses is consistent with what other authors have described in different cell lines, such as HeLa, HEK293 and U2OS (Souquere

et al. 2009; Zurla et al. 2011; McDonald et al. 2011; Seguin et al. 2014). This was the first time that the number of SGs was quantified per cell following different stress paradigms for three SG markers: polyA⁺ mRNA, Caprin-1 and TIA-1. In addition, recovery experiments demonstrate that both heat shock and sodium arsenite stresses have reversible effects on SG formation (Figs.3.2 and 3.5), at least at the experimental conditions used in this study. SG clearance occurs over a recovery period of approximately 4 hours in OC-2 cells after both types of stress (Figs. 3.1, 3.2, 3.4 and 3.5). This is in agreement with other studies, in which SGs disassemble when DU145, COS or HeLa cells were allowed to recover from stress (Kedersha & Anderson 2002; Kedersha et al. 2005; Souquere et al. 2009) and suggests that, once the stress is over, the translation of RNA molecules is resumed, since upon SG disassembly, polyA⁺ mRNA assumes a distribution comparable to pre-stress levels.

To investigate whether modulation of SG formation could be performed in the OC-2 cell line, different pharmacological compounds that modulate the SG pathway were used (section 3.2.3). As discussed before, when working with stress, the choice of a manipulator must be considered. One of the main concerns during this work was to choose chemicals that would act as far downstream on the SG pathway as possible, to minimise interference with other cellular pathways that, direct or indirectly, could generate additional stress to the cells. Short-term use, low toxicity and high efficacy are also desirable characteristics of a manipulator, especially when considering the objective of use in cochlear explants and, perhaps, in the *in-vivo* cochlea.

To reduce SG formation, two chemical compounds were used, pp242 and ISRIB. In OC-2 cells, pp242 decreased the number of SGs formed following heat shock exposure, but demonstrated no effect on SG formation during arsenite stress (Figs.3.8 and 3.12), whereas ISRIB significantly reduced the number of SGs formed upon both stresses (Figs.3.15 and 3.16). Since pp242 acts specifically by inactivating the mTORC pathway through hypophosphorylation of 4E-BP1, this suggests that most of the SGs generated in the OC-2 cell line following heat shock stress are produced via the mTORC pathway. Arsenite stress, on the other hand, does not seem to activate the mTORC pathway to the same extent as heat shock in OC-2 cells, since pp242 did not show any effects on the reduction of arsenite-triggered SGs. By acting further downstream in the SG pathway than pp242, ISRIB effects on the stabilisation of eIF2B and reduction of eIF2 phosphorylation (Sidrauski et al. 2015) resulted in a decrease of the number of SGs formed upon heat shock and arsenite stresses. This suggests that in OC-2 cells, the

formation of SGs under heat shock and arsenite stresses is most likely to be directly regulated by eIF2 phosphorylation.

Hydroxamate (-)-9 was used to induce SGs in OC-2 cells, since this compound acts by disrupting translation initiation, through sequestration of eIF4A from the eIF4F complex (Hwang et al. 2004; Bordeleau et al. 2008; Rodrigo et al. 2012). Incubation of untreated OC-2 cells with hydroxamate (-)-9 did result in SG formation, as assessed by RNA-immuno-FISH and quantification of SGs (Figs.3.19 and 3.20). The SGs generated by hydroxamate (-)-9 resembled those formed from heat shock and arsenite stress in terms of number, size and components. Considering this and, since both ISRIB and hydroxamate (-)-9 (i) did not increase cellular death; (ii) demonstrated high efficacy; (iii) showed reversible effects and (iv) were effectively after relatively short-term incubation period, these two chemicals were chosen to be applied to cochlear explants to assess the effect of modulating SG formation on hair cell survival during aminoglycoside stress.

Since hydroxamate (-)-9 acts by promoting SG formation, it can be hypothesised that hydroxamate (-)-9 constitutes a stressor agent to the cells *per se*. Stressor agents have been widely defined by their activation of specific stress sensor kinases that trigger downstream reactions, leading ultimately to the formation of SGs (McEwen et al. 2005; Ouyang et al. 2007; Arimoto et al. 2008). For instance, sodium arsenite activates mainly HRI kinase (Lu et al. 2001; McEwen et al. 2005), whereas heat shock activates PKA (Kiang et al. 1991; Kiang et al. 1998). As hydroxamate (-)-9 has not been reported to activate any of the stressor kinases and its analogue silvestrol has been shown to act downstream of the canonical stress response by disrupting translation initiation complexes (Bordeleau et al. 2008; Rodrigo et al. 2012), hydroxamate (-)-9 can be considered as a drug that interferes with normal protein translation leading directly to SG formation, instead of a stressor agent.

In summary, for the first time in an inner ear-derived cell line, SG formation was assessed during two different stress paradigms for three SG markers, polyA⁺ mRNA, Caprin-1 and TIA-1. These showed to colocalise at the majority of the SGs generated in OC-2 cells, suggesting that they constitute key players in the regulation of the stress response in this cell line. In addition, a novel quantification protocol determined that SGs gradually disassemble when the cells are allowed to recover, suggesting that, at the conditions used, activation of PKA and HRI kinases in OC-2 cells triggers reversible SG formation in the presence of a sub-lethal dose

of stress. Moreover, pharmacological modulation of the SG pathway successfully reduced / generated SG in an inner ear-derived cell line.

By adapting the assays developed in the OC-2 cell line, SGs were visualised and quantified in mouse cochlear explants following stress (Figs. 4.1, 4.3, 4.5 and 4.7). Ideally, assessments regarding quantification of SG formation would provide values close to absolute as possible, especially when considering the intentions of manipulating this pathway to assess cell survival. However, the three-dimensional and multicellular structure of the organ of Corti represented a major challenge during SG quantification, when compared to OC-2 cells. Consequently, the protocol developed in OC-2 cells was adapted to estimate the number of SGs formed upon stress in hair cells and supporting cells. Estimates of hair cell measurements (height, radius, nucleus size) were obtained and SG quantification performed as approximated values per unit volume (μm^3). Nevertheless, despite referring to approximation values, the data presented in this thesis constitutes the first assessment of SG quantification in cochlear cells.

The experiments presented herein demonstrate that, in addition to the recent observation of SGs in the cochlea's response to aminoglycoside treatment (Towers et al. 2011), the SG pathway is also activated following heat shock and arsenite stresses in cochlear cells (Fig.4.1). For the first time, polyA⁺ mRNA was visualised in cochlear native tissue and found to re-distribute upon stress, following the dynamics of SG formation by colocalising with TIA-1 (Figs. 4.1, 4.2, 4.3 and 4.4). This result confirms the potential of hair cells and supporting cells to assemble SGs and suggest that polyA⁺ mRNA can be triaged in native tissue following stress exposure. The confirmation that polyA⁺ mRNA is re-distributed to SGs following stress in cochlear explants suggests that cochlear cells can promote post-transcriptional changes in gene expression by regulating RNA metabolism in response to stress.

The results obtained in mouse cochlear explants show that, in a similar way to OC-2 cells, sodium arsenite generates more SGs in cochlear cells than heat shock stress (Figs.4.5 and 4.7). Generally, inner hair cells assembled more SGs than outer hair cells, suggesting that inner hair cells are more sensitive to the activation of stress-sensor kinases. SG quantification was also performed for supporting cells considering two regions of the epithelium, lesser and greater epithelial ridges, and supporting cells generally produced similar SG numbers as hair cells. Overall, the size of SGs in cochlear native cells was smaller than in OC-2 cells, suggesting that

mammalian native tissue may require less aggregation of RNA-binding proteins and polyA⁺ mRNA molecules at SGs during stress conditions than what is observed in cell lines. The lack of other studies in native tissue does not enable any comparison of these results.

So far, much of our knowledge about SG dynamics comes from studies in cell lines, such as HeLa, DU145 and COS (Kedersha et al. 1999; Kedersha et al. 2000; Kedersha et al. 2002). Cell lines provide a great system for initial studies and optimisation protocols, as they are easy to maintain and generally uniform and robust in their response to different assays. However, cell lines lack the physiological conditions of native tissue and their response in terms of SG formation, components and dynamics may not correspond to what is observed *in-vivo*. While some of the studies involving SG formation in native tissue have been performed in *Drosophila*, yeast or zebrafish (Bosco et al. 2010; Buchan et al. 2011; Gareau et al. 2013; Buchan et al. 2013; Acosta et al. 2014; Jevtov et al. 2015; Jain et al. 2016; Zampedri et al. 2016), SG dynamics in the mammalian system is still poorly understood to date. Assessments of SG formation in mammalian tissue include mostly work with rodent primary neurons or analysis of *post-mortem* human brain sections (Dormann et al. 2010; Vanderweyde et al. 2012; Ash et al. 2014; Halliday et al. 2015). To my understanding, the work here presented constitutes the first detailed assessment of SG dynamics in mammalian native tissue, which includes quantification and confirmation of RNA re-localisation to SGs following stress in mouse cochlear explants. In addition, this work also confirms that, at least at the conditions tested, despite the physiological differences between OC-2 cells and mouse cochlear explants, native cochlear cells assemble SGs following the same stress paradigms as OC-2 cells. These are similar in composition, indicating that most of the conditions optimised in the OC-2 cell line could be extrapolated to the native tissue. Moreover, validation of such protocols in mouse cochlear explants suggests that similar methodologies may be adapted to other fields of research, such as neurodegeneration, to better understand which role SGs play in different pathologies.

Using the assays developed in the OC-2 cell line, pharmacological manipulation of SG formation was successfully performed in mouse cochlear explants (section 4.2.2). This represents a major step towards understanding the implications of SG formation in the cochlea's homeostasis. The validation of such pharmacological tools implies that SGs can be manipulated to assess the effects of SG formation on the cochlea. Therefore, I sought to investigate whether manipulation of SG

formation can promote hair cell survival during aminoglycoside stress. The results obtained support this hypothesis, since pre-incubation with hydroxamate (-)-9 (SG inducer) protected outer hair cells from both neomycin- and sisomicin-induced cell death (Figs.4.23 and 4.28). Considering that hydroxamate (-)-9 acts by specifically disrupting the translation initiation (Hwang et al. 2004; Bordeleau et al. 2005; Rodrigo et al. 2012), it is not expected to present side effects on other cellular pathways given its specificity. Consequently, it can be speculated that the outer hair cell protection observed following hydroxamate (-)-9 incubation when compared to the effects of the aminoglycosides alone may be due to SG induction prior to stress exposure. This suggests that promoting changes in the RNA metabolism, such as sorting of RNA molecules and aggregation with RNA-binding proteins prior to stress exposure may confer protection to a subsequent stress treatment. This “pre-stressed” condition suggests that cells can reprogram the RNA transcripts to be translated in a way that when stress is applied, the cells are already synthesising stress-responsive molecules that can protect against stress-induced damage. In support of this hypothesis, treatment with ISRIB enhanced cellular death during neomycin exposure (Fig.4.23), suggesting that inhibition of SG formation may present additional deleterious effects during stress. This is in agreement with other studies in HeLa, U2OS, MCF-7 and HT22 cell lines, in which impairment of SG formation has been associated with cellular death (Baguet et al. 2007; Kwon et al. 2007; Eisinger-Mathason et al. 2008; Arimoto-Matsuzaki et al. 2016).

Despite the strong association between induction of SG formation and outer hair cell protection following aminoglycoside treatment, it cannot be excluded that hydroxamate (-)-9 may protect hair cells from death through other means. For instance, hydroxamates are known for their ability to form stable complexes with ferric iron (Haydon et al. 1973). The chelator activity of hydroxamates has been used in the clinic to treat iron overload caused by frequent blood transfusions (Poreddy et al. 2004). Considering that aminoglycoside ototoxicity is thought to involve the redox-capacity of a transition metal and one of the direct products of this reaction is ferric iron (as referred in introduction section 1.4), hydroxamate (-)-9 may act as an iron chelator inside the hair cells, thus neutralising the toxic effects of ferric iron. Hydroxamate (-)-9 was reported to exhibit moderate to high permeability, significantly binding by human plasma proteins (82-84% bound after 4h exposure), and excellent stability in plasma (100% remaining after 3h) (Rodrigo et al. 2012). Even though hydroxamate (-)-9 was removed before aminoglycoside incubation, since exhibits high permeability and stability, it can be assumed that hydroxamate

(-)-9 may persist inside the hair cells during sisomicin treatment (1h) or part of the neomycin treatment (6h) to function as an iron chelator.

Although hydroxamate (-)-9 pre-treatment has partially protected outer hair cells from aminoglycoside-induced death, it failed to protect inner hair cells. As previously hypothesised, this could be because hydroxamate (-)-9 generates more SGs in inner hair cells than outer hair cells. A higher number of SGs may be toxic, to some extent, since they could interfere dramatically with the triage of RNA molecules during stress, promoting the inhibition of translation to deleterious levels, or even the exchange of RNAs with processing bodies for degradation in a larger scale than needed. On the other hand, an adequate and tolerable number of SGs may provide the ideal balance between the molecules to inhibit from translation and the release of the RNAs important to be translated during stress. Experimental assays testing different concentrations and times of exposure of hydroxamate (-)-9 during aminoglycoside exposure simultaneously with SG quantification could help to determine whether there is a threshold effect in terms of SG assembly in cell protection.

Another possibility previously discussed is that upon aminoglycoside exposure, inner hair cells may trigger different cell death pathways than outer hair cells and SGs may be involved in the suppression of those pathways in outer hair cells and not in inner hair cells. Following aminoglycoside exposure, pro-apoptotic mediators such as JNK, c-Jun, c-FOS, Bcl-2 and caspases, for instance, have been shown to be activated and directly involved in aminoglycoside-triggered hair cell death (Cheng 2005; Huth et al. 2011). In addition, contradictory studies involving caspase-dependent or necrosis-triggered outer hair cell death, for instance, have been reported as a consequence of aminoglycoside exposure (Jiang et al. 2006; Taylor et al. 2008). Since SGs have been found to inhibit apoptosis by suppressing pro-apoptotic stress-responsive pathways such as RACK, MTK, TRAF and JNK (Kim et al. 2005; Arimoto et al. 2008), if outer hair cells die as a result of activation of any of these pro-apoptotic pathways, it would help to explain the results obtained herein.

Another possibility is that inner hair cells generate different SGs from outer hair cells, in terms of composition, following aminoglycoside stress. A study in DU145 and U2OS cells showed that cells can trigger different types of SGs upon sodium selenite treatment: whereas some of the SGs generated are enriched in pro-apoptotic factors such as RACK1 or HDAC6, other SGs fail to accumulate these

molecules (Fujimura 2012). A scenario in which different types of SGs are formed in inner hair cells from outer hair cells, lacking the sequestration of pro-apoptotic molecules, cannot be excluded. In this case, a failure in sequestration of pro-apoptotic molecules could promote their translation following stress, thus contributing to the observed increased cell death in inner hair cells, when compared to the outer hair cells. Identification of the molecules targeted to SGs following hydroxamate (-)-9 treatment in inner hair cells and outer hair cells would help to clarify this question and also to understand whether pro-apoptotic pathways are suppressed in outer hair cells under aminoglycoside stress. In addition, proteomic analysis of SGs generated in inner and outer hair cells could clarify whether SGs with distinct composition are formed in these cells.

The contribution of the SGs generated in supporting cells upon hydroxamate (-)-9 exposure cannot be excluded. Post-transcriptional changes in gene expression in supporting cells caused by SG assembly may lead to changes in cell-to-cell communication pathways that may trigger protective mechanisms within hair cells during aminoglycoside toxicity.

Although the results presented in this thesis suggest a protective effect of SGs upon aminoglycoside exposure on outer hair cell survival, additional experiments are needed to clarify exactly how SGs promote cell survival in the cochlea and if this can be replicated using other stresses, such as noise exposure. Future experiments could include *in-vivo* application of hydroxamate (-)-9 and ISRIB prior to / during exposure to noise or aminoglycosides in mice. ABR recordings would show whether hearing function is maintained in these animals and *post-mortem* cryosections of the inner ear or electron microscopy can be used to assess the integrity of the cochlear tissue. In addition, understanding the molecular content of SGs in the ear would help to clarify which RNAs and proteins are specifically localised to SGs, thus playing a role in alterations of gene expression at the post-transcriptional level *in-vivo*. Isolation of hair cells by fluorescence-activated cell sorting (FACS) could be performed in a mouse line expressing a transgenic fluorescent marker to monitor hair cells, for instance. Following aminoglycoside, noise exposure or even during ageing, SGs could be isolated and purified from hair cells and their proteomic content identified using mass spectrometry. The RNAs binding to SG-marker proteins, such as TIA-1 or Caprin-1 could be identified *in-vivo* using the same methodology followed by RIP-seq. The latter experiment was already performed in OC-2 cells in our laboratory to identify the transcripts showing increased binding to Caprin-1 and TIA-1 after heat shock and arsenite stress. The identification of such

SG components *in-vivo* would help to understand whether different stressor agents trigger the formation of different SGs and whether the composition of SGs is affected by the severity of the treatments. In addition, the identification of the SG components following hydroxamate (-)-9 treatment could elucidate whether this compound generates SGs similar to those formed by activation of stress kinases.

The data presented in this thesis suggest that a pre-treatment to prepare cells to a subsequent toxic exposure may protect hair cells from death. In fact, this approach has been widely tested using another type of pre-treatment condition: the induction of the heat stress response. In the inner ear, pre-induction of the heat stress response through heat shock exposure has been reported to protect utricle hair cells from cisplatin and aminoglycoside damage (Cunningham & Brandon 2006). One of the key players in the heat shock response, Hsp70, was directly associated with hair cell protection from aminoglycoside death (Taleb et al. 2008).

Considering the involvement of Hsp70 on the hair cell response to stress (Taleb et al. 2008) and the fact that Hsp70 has been recently associated with SGs (Walters et al. 2015; Ganassi et al. 2016), I investigated the relationship between Hsp70 and SGs in the OC-2 cell line following stress. *Hsp70* expression increased greatly following heat shock stress, peaking at 2h after stress exposure (Fig.5.5). This result was corroborated by immunocytochemistry, in which Hsp70 fluorescent signal was mostly detected at 2h and 4h after heat shock stress (Fig.5.1). Interestingly, Hsp70 expression was found to be higher in cells containing few or no SGs during recovery from heat shock (Fig.5.2). Conversely, cells with the greatest number of SGs during recovery presented lower Hsp70 expression, suggesting that in the OC-2 cell line there is an association between Hsp70 expression and SG absence. Overexpression assays confirmed that, in the presence of Hsp70 prior to heat shock treatment, less SGs were generated (Fig.5.11), adding additional evidence to this association. However, it remains unclear whether Hsp70 inhibits SG formation or whether Hsp70 actively promotes SG disassembly. Recent studies in yeast, *Drosophila* and HeLa cells have suggested that Hsp70 is implicated in the SG disassembly following stress (Cherkasov et al. 2013; Walters et al. 2015; Ganassi et al. 2016). Considering that overexpression of Hsp70 in OC-2 cells decreased the number of SGs after 1h of heat shock stress, an eventual participation of Hsp70 in the SG disassembly must occur within 1h and simultaneously with stress exposure. On the other hand, an inhibitory role of Hsp70 on the SG formation would suggest that, in the presence of Hsp70, OC-2 cells do not activate the SG pathway during heat shock stress. This implies that activation of the Hsp70 chaperone machinery is

enough during heat shock treatment (at the conditions tested) to promote the re-folding and stabilisation of proteins and targeting of damaged peptides to degradation.

From these experiments, it also remains unclear why only a subset of cells presents high Hsp70 expression during recovery from heat shock and not the whole population of cells. Endogenous Hsp70 formation observed following heat shock stress is most likely to be related to activation of HSF1, since HSF1 controls *Hsp70* expression (Calderwood et al. 2010; Anckar & Sistonen 2011). If this is the case, it is intriguing as to why HSF1 is activated only in a subset of OC-2 cells and not across all cells, as might be expected. To clarify this question, future experiments could include measurement of HSF1 activation in OC-2 cells, through phospho-specific antibodies for HSF1 or luciferase assays, for instance. In addition, live imaging to detect SGs and Hsp70 during heat shock exposure would help to understand whether Hsp70 formation inhibits SG formation following heat shock stress or if it actively participates in the clearance of SGs.

Interestingly, Hsp70 expression was not associated with SG inhibition or clearance following arsenite stress exposure (Fig.5.6), suggesting that this association is specific to heat shock stress conditions. With exogenous Hsp70 overexpression, OC-2 cells show SG formation after arsenite stress (Figs.5.12 and 5.13), suggesting that the Hsp70 chaperone activity is not sufficient for the stress response of OC-2 cells to arsenite treatment.

Analysis of the stress sensor kinases activated by heat shock and sodium arsenite in OC-2 cells may help to understand the differential activation of Hsp70 upon different stressor agents. Although no studies regarding the activation of stress sensor kinases or downstream pathways have been performed in this work, suggestions as to which pathways are activated following stress in the OC-2 cell line can be inferred through indirect means. Heat shock stress has been previously shown to activate PKA, PKR and PI-3K (Kiang et al. 1991; Kiang et al. 1998; Wang et al. 2003; Wang et al. 2004). The PI-3K pathway is one of the protective pathways activated by heat shock. Under unstressed conditions, active GSK3 represses HSF1 (Wang et al. 2003; Wang et al. 2004). In the presence of heat shock stress, activated PI-3K leads to Akt activation and consequent GSK3 inhibition, thus de-repressing HSF1 and promoting heat stress-specific *Hsp70* transcription (Cross et al. 1995; Pap & Cooper 1998; Hers et al. 2011; Chou et al. 2012; Moore et al. 2013). Additionally, PKA acts by directly phosphorylating GSK3, thus inhibiting its

apoptotic activity (Li et al. 2000) and ultimately contributing to HSF1 promoter activation (Choi et al. 1991). Consequently, a possible synergistic effect of PI-3K and PKA activation following stress could explain the elevated *Hsp70* expression observed in OC-2 cells following heat shock stress.

One possible mechanism by which Hsp70 is activated by heat shock stress but not by arsenite is that, in OC-2 cells, heat shock may primarily activate the PI-3K pathway and, in contrast, arsenite may act by disrupting this pathway. Inhibition of PI-3K by arsenite would lead to continuous activation of GSK3 and, consequently, repression of HSF1 and Hsp70. In fact, PI-3K pathway has been shown to be inhibited in mouse stem cells following arsenite stress (Ivanov et al. 2013). On the other hand, a specific activation of PI-3K by heat shock in OC-2 cells, would explain the robust *Hsp70* expression detected. In support of this hypothesis, pp242, one of the SG inhibitors tested in this work, only reduced the number of SGs generated by heat shock stress and failed to reduce the arsenite-triggered SGs (Figs.3.8 and 3.12). pp242, as shown before, acts by specifically disrupting the mTORC pathway, a member of the PI-3K family (Apsel et al. 2008; Feldman et al. 2009). Considering the hypothesis that PI-3K is only activated in OC-2 cells following heat shock and not arsenite, this may explain why pp242 did not reduce the number of SGs generated by arsenite stress.

These observations can also be associated with the differential number of SGs generated upon heat shock and sodium arsenite. In both OC-2 cells and cochlear explants arsenite stress resulted in more SGs than heat shock (sections 3.2.1, 3.2.2 and 4.2.1). Considering that part of the heat shock response involves the formation of Hsp70, one can hypothesise that the cells exposed to heat shock stress do not require a greatest response in terms of SG formation, given the Hsp70 chaperone activity. On the contrary, since Hsp70 activation is much lower and delayed following arsenite stress than heat shock, the cells exposed to arsenite may require a greater number of SGs to respond to stress, given the low availability of Hsp70. Another possibility is that activation of HRI kinase generates higher levels of eIF2 α phosphorylation than PI-3K, thus leading to the formation of a greater number of SGs.

The schematics in Figures 6.1, 6.2 and 6.3 summarise this hypothesis:

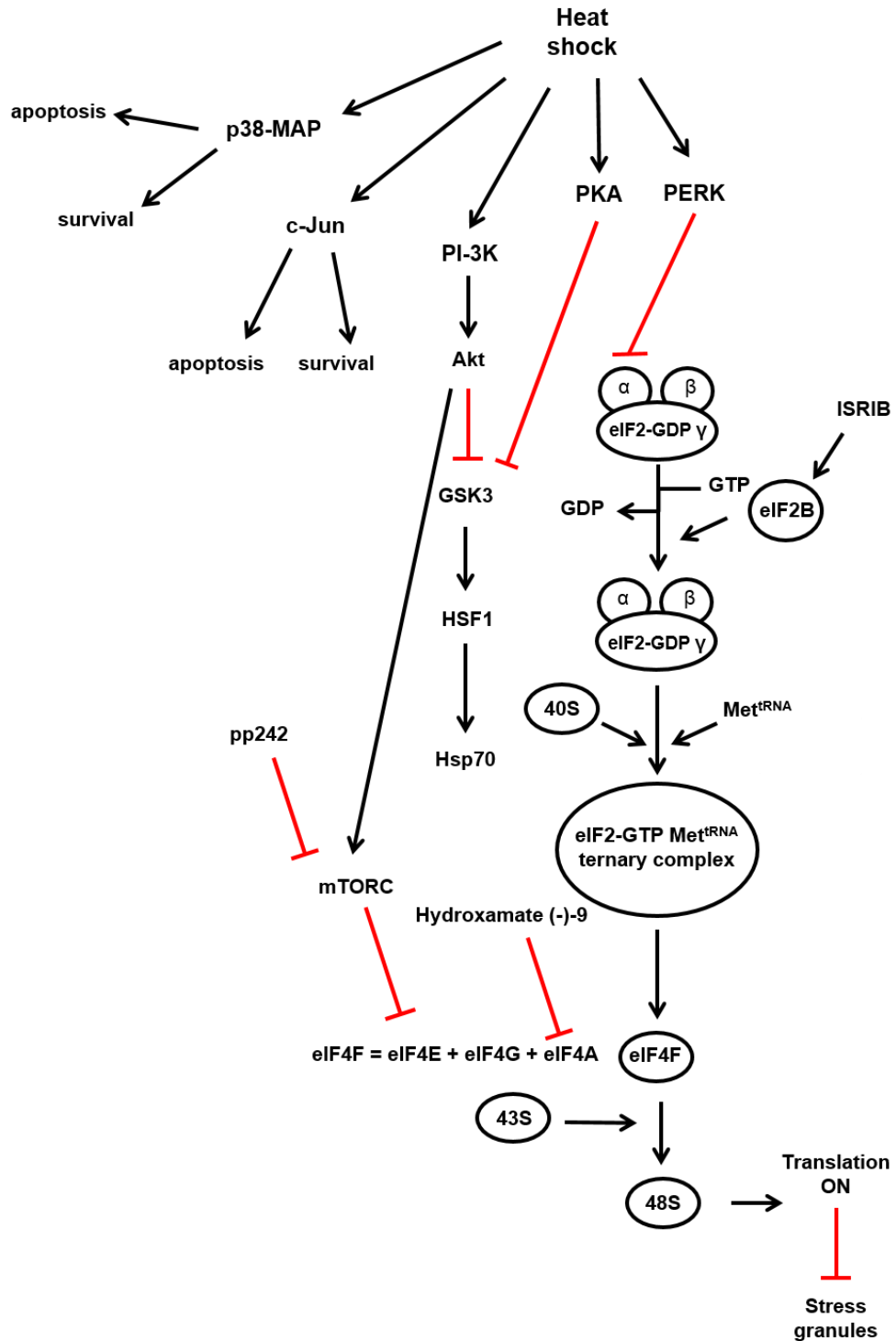


Figure 6.1 – Proposed mechanism of cell signalling pathways activated upon heat shock in OC-2 cells. Synergistic effects of PI-3K and PKA activation upon heat shock exposure contribute to repression of GSK3. When repressed, GSK3 does not inhibit HSF1, thus leading to a robust activation of Hsp70. Activated PERK kinase leads to eIF2 α phosphorylation, impairment of the assembly of eIF2-GTP-tRNA^{Met} ternary complex and, consequently, SG formation. By blocking mTORC pathway, pp242 inhibits SG assembly via PI-3K activation. By stabilising eIF2B, ISRIB reduces the effects of eIF2 α phosphorylation triggered by stress sensor kinases, contributing to the reduction of SG formation. Hydroxamate (-)-9 specifically impairs eIF4A, inhibiting the formation of eIF4F translation complex, leading to the formation of SGs. Black arrows represent activation pathways and red symbols inhibition pathways.

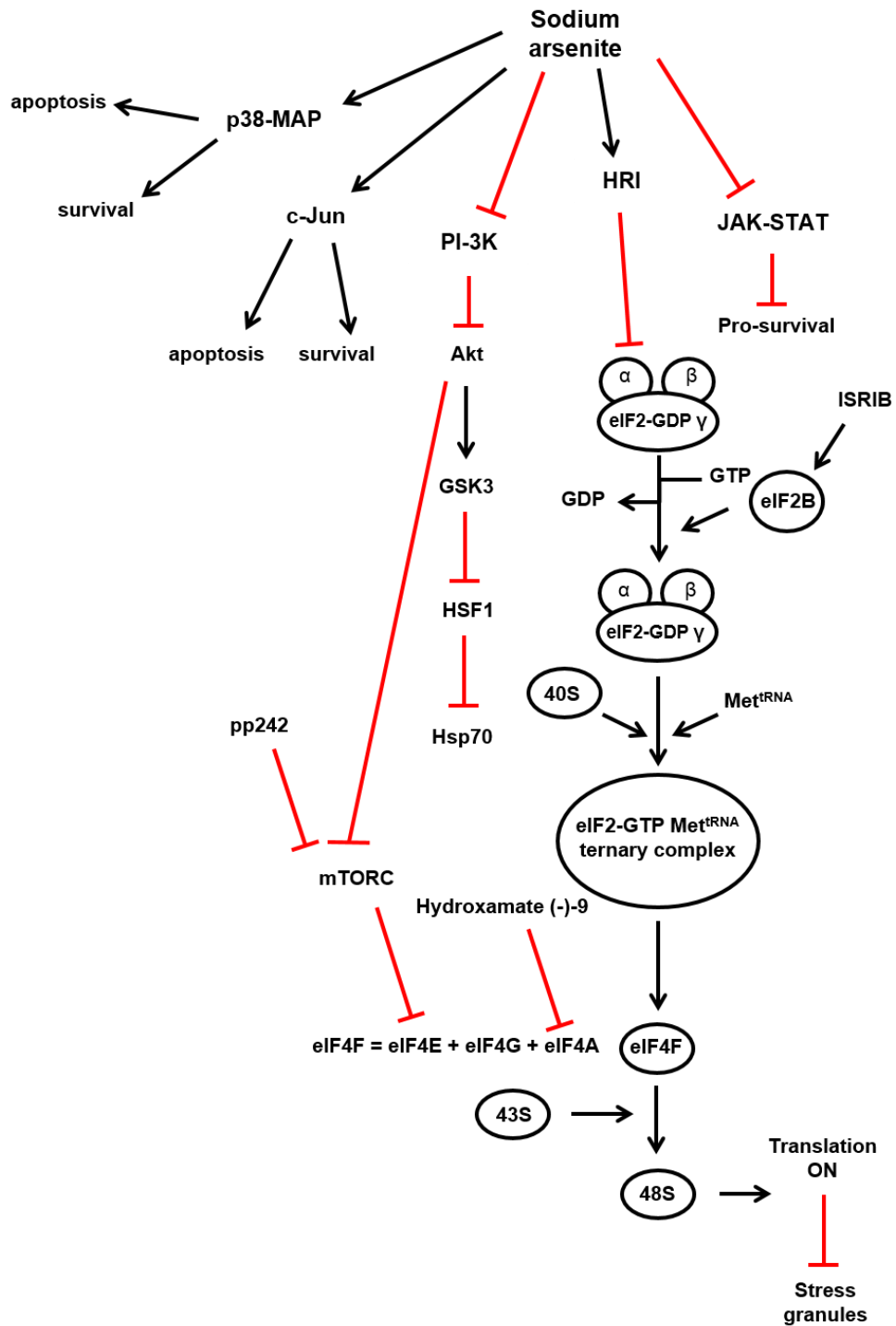


Figure 6.2 – Proposed mechanism of cell signalling pathways activated upon sodium arsenite in OC-2 cells. Arsenite activates HRI kinase that leads to eIF2 α phosphorylation, impairment of the assembly of eIF2-GTP-tRNA^{Met} ternary complex and, consequently, SG formation. PI-3K kinase is proposed to be inhibited by sodium arsenite in OC-2 cells, thus inactivating Akt. In the absence of Akt, GSK3 is active and inhibits HSF1. Inhibition of HSF1 leads to repression of Hsp70. Since PI-3K is proposed to be inhibited following arsenite stress in the OC-2 cell line, mTORC should not be involved in SG formation, so blocking this pathway using pp242 does not affect SG formation. By stabilising eIF2B, ISRIB reduces the effects of eIF2 α phosphorylation triggered by stress sensor kinases, contributing to the reduction of SG formation. Hydroxamate (-)-9 specifically impairs eIF4A, inhibiting the formation of eIF4F translation complex, leading to the formation of SGs. Black arrows represent activation pathways and red symbols inhibition pathways.

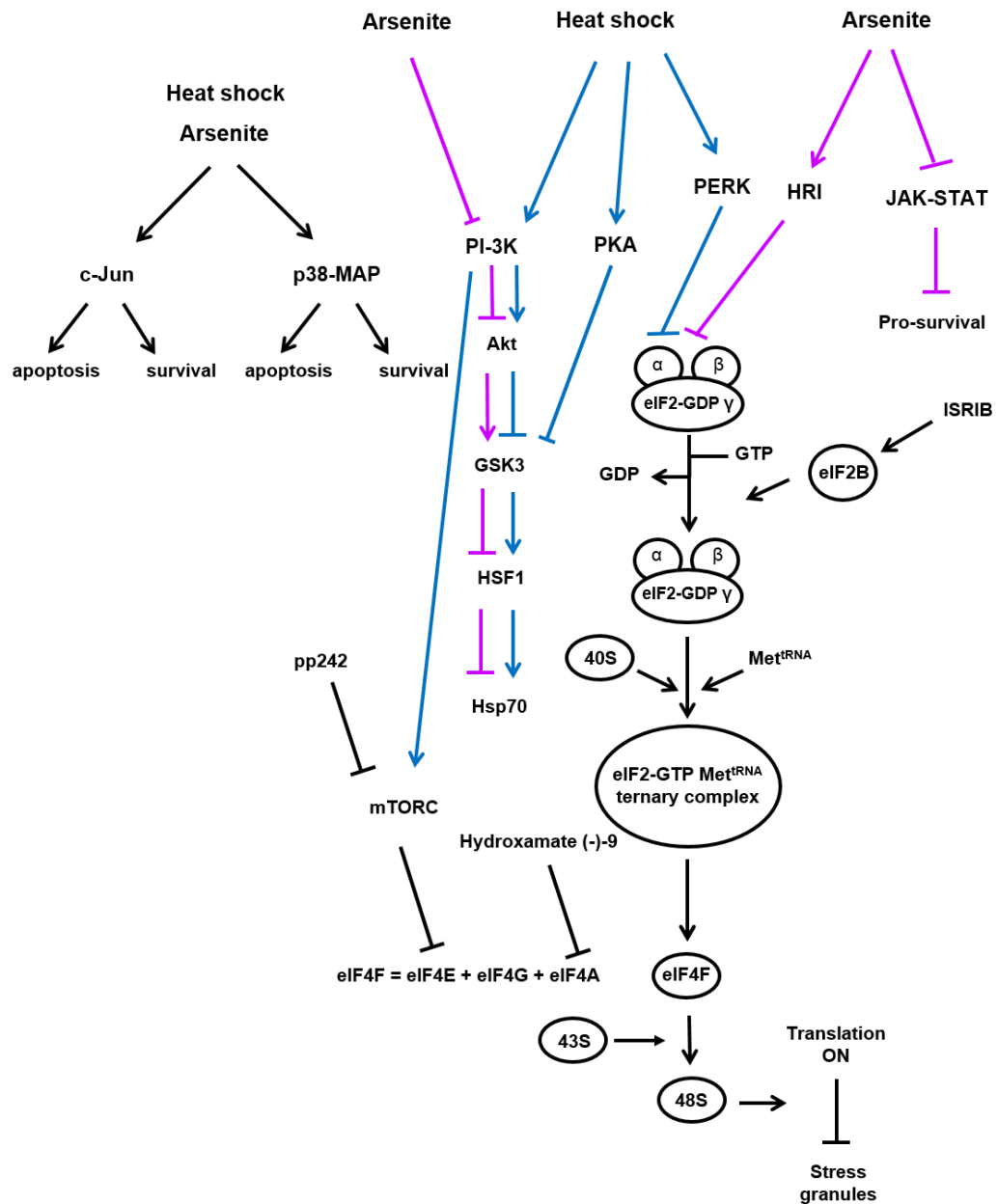


Figure 6.3 – Proposed differential pathways activated upon heat shock and arsenite stress in OC-2 cells. Activated / inhibited pathways are shown in purple for arsenite stress and in blue for heat shock stress. c-Jun and p38-MAP pathways, both activated following heat shock and arsenite stresses are shown in black. eIF2α phosphorylation is achieved following PERK activation by heat shock stress and HRI activation following arsenite treatment, leading to SG formation. Heat shock is proposed to activate PI-3K/Akt pathway, thus leading to Hsp70 protein production, whereas arsenite is suggested to specifically inhibit this pathway in OC-2 cells.

Investigation of the HSF1 promoter and of the different stress sensor kinases that are activated during heat shock and sodium arsenite stresses in OC-2 cells may help to understand which pathways are specifically triggered following exposure to these stresses and how this influences Hsp70 synthesis. Live imaging with SG-markers and Hsp70 may also help to understand the relationship between Hsp70 and SG formation.

As mentioned before, Hsp70 has been shown to protect *in-vivo* mice from aminoglycoside treatment (Taleb et al. 2009). More recently, it was demonstrated that utricular supporting cells produce Hsp70 following heat shock exposure to protect hair cells from subsequent aminoglycoside exposure (May et al. 2013). Given this, it would be interesting to evaluate the SG response of mice overexpressing Hsp70 following aminoglycoside treatment and noise exposure, for example. In addition, experiments using arimoclomol, an inducer of HSF1, may be considered *in-vivo* to determine if the SG pathway is activated in hair cells following stress or if Hsp70 is sufficient *per se* to protect hair cells from damage.

The data presented in this thesis supports the hypothesis that SGs are formed under transient stress conditions to protect cells from stress-induced death: i) SGs are generated during stress conditions and disassemble once the stress is over; ii) pharmacological induction of SG formation has been suggested to improve outer hair cell survival during aminoglycoside treatment; and iii) inhibition of SG formation was associated to increased cell death following neomycin exposure. In addition, studies involving Hsp70 and SGs indicate that almost no SGs are found in cells expressing high levels of Hsp70 protein, suggesting that if Hsp70 is providing cellular protection through its chaperone function, SGs may not be required. Furthermore, Hsp70 mRNA is suggested to be selectively excluded from SGs during stress, evidencing their role in a pro-survival RNA sorting mechanism during stress.

Despite the evidence that SG are key players promoting cell survival during transient stress (Kedersha et al. 1999; Kedersha et al. 2002; Tourrière et al. 2003; Kim et al. 2005; Ohn et al. 2008; Papadopoulou et al. 2013), recent research suggests that SGs may also be involved in neurodegeneration (Liu-Yesucevitz et al. 2011; Moreno et al. 2012; Vanderweyde et al. 2012; Ash et al. 2014). Since SG formation involves a cellular pathway that can be prone to aggregation of proteins, SG dysregulation can play a significant role on the onset of neurological disorders (Wolozin 2012). As mentioned before, SGs have been found in *post-mortem* tissue

of Alzheimer's patients (Ash et al. 2014). Additionally, mice models of ALS, Huntington's or Parkinson's disease present SG components within the pathological aggregates characteristic of these diseases (Liu-Yesucevitz et al. 2011; Vanderweyde et al. 2012; Vanderweyde et al. 2013). Moreover, the discovery of mutations in genes that lead to alterations in some SG components have provided critical evidence that dysregulation of SG formation may be directly linked with neurodegeneration (McDonald et al. 2011; Aulas et al. 2012).

In-vivo cryosections of C57BL/6 mice cochlea show that hair cells and spiral ganglion neurons assemble SGs as a function of ageing (Figs.4.29 and 4.31). Considering the hearing decline with ageing in these mice, it can be hypothesised that the presence of SGs might, to some extent, relate to the auditory phenotype of these mice. Those "pathological" SGs may be associated to the presence of a permanent stress or dysregulated with ageing and, by continuously trapping essential RNA molecules and RNA-binding proteins, may lead to neurodegeneration and ultimately, cell death. It was recently proposed that the aggregation of pathological proteins stimulates SG formation and overactive formation of SG accelerates aggregation of pathological proteins (Wolozin 2012). Future experiments to clarify this question may involve manipulation of SG formation during ageing studies (for instance, some mice would be exposed to hydroxamate (-)-9, others to ISRIB, and compared to controls), with assessments of hearing function and cellular integrity at different time-points during ageing. Understanding the mechanisms involved in the disassembly / clearance of SGs in OC-2 cells and mouse cochlear explants would also provide further evidence about regulation of SGs. For instance, autophagy have been recently associated with clearance of SGs in yeast and HeLa cells (Buchan et al. 2013; Seguin et al. 2014). Experiments involving manipulation of autophagy pathway in OC-2 cells, taking advantage of drugs already available for use (Scovassi 2013), would help to clarify if this pathway is involved in SG disassembly in the auditory system. A better knowledge of the mechanisms that regulate SG clearance may ultimately clarify whether dysregulation of SG disassembly contributes to the persistence of SGs, thus contributing to neurodegeneration. Since SGs are a relatively recent field of study, additional research will certainly help to clarify which factors cause dysfunction of SGs and how the transition from protective to pathological structures occurs.

In conclusion, the work presented in this thesis supports the hypothesis that SGs are protective structures during transient cochlear stress. The function of these structures in the inner ear has just only begun to be understood and it suggests that

regular assembly of SGs may play a significant role during stress in the auditory system. A better understanding of how the inner ear responds to stress may help in the development of preventative strategies that can impede the malfunction and degeneration of hair cells during stress, thus preventing hearing loss.

7. References

- Abernathy, C.O. et al., 1999. Arsenic: health effects, mechanisms of actions, and research issues. *Environmental health perspectives*, 107(7), pp.593–7.
- Acosta, J.R. et al., 2014. Mutant human FUS is ubiquitously mislocalized and generates persistent stress granules in primary cultured transgenic zebrafish cells. *PLoS ONE*, 9(6).
- Adeli, K., 2011. Translational control mechanisms in metabolic regulation: critical role of RNA binding proteins, microRNAs, and cytoplasmic RNA granules. *American journal of physiology. Endocrinology and metabolism*, 301(6), pp.E1051-64.
- Ahn, T.B. & Jeon, B.S., 2006. Protective role of heat shock and heat shock protein 70 in lactacystin-induced cell death both in the rat substantia nigra and PC12 cells. *Brain Res*, 1087(1), pp.159–167.
- Alberti, P.W., 2001. The anatomy and physiology of the ear and hearing. *WHO Occupational exposure to noise: evaluation, prevention and control*.
- Albornoz, A. et al., 2014. The Stress Granule Component TIA-1 Binds Tick-Borne Encephalitis Virus RNA and Is Recruited to Perinuclear Sites of Viral Replication To Inhibit Viral Translation. *Journal of virology*, 88(12), pp.6611–22.
- Altschuler, R.A. et al., 2002. Stress pathways in the rat cochlea and potential for protection from acquired deafness. *Audiology and Neuro-Otology*, 7(3), pp.152–156.
- Anckar, J. & Sistonen, L., 2011. Regulation of HSF1 function in the heat stress response: implications in aging and disease. *Annual review of biochemistry*, 80, pp.1089–115.
- Anderson, P. & Kedersha, N., 2002. Stressful initiations. *Journal of cell science*, 115(Pt 16), pp.3227–3234.
- Anderson, P. & Kedersha, N., 2006. RNA granules. *Journal of Cell Biology*, 172(6), pp.803–808.
- Anderson, P. & Kedersha, N., 2007. On Again, off Again: The SRC-3 Transcriptional Coactivator Moonlights as a Translational Corepressor. *Molecular Cell*, 25(6), pp.796–797.
- Anderson, P. & Kedersha, N., 2008. Stress granules: the Tao of RNA triage. *Trends in Biochemical Sciences*, 33(3), pp.141–150.
- Anderson, P. & Kedersha, N., 2009. RNA granules: post-transcriptional and epigenetic modulators of gene expression. *Nature reviews. Molecular cell biology*, 10(6), pp.430–436.
- Angenstein, F. et al., 2005. Proteomic characterization of messenger ribonucleoprotein complexes bound to nontranslated or translated poly(A) mRNAs in the rat cerebral cortex. *Journal of Biological Chemistry*, 280(8), pp.6496–6503.
- Antar, L.N. et al., 2005. Localization of FMRP-associated mRNA granules and requirement of microtubules for activity-dependent trafficking in hippocampal

- neurons. *Genes, Brain and Behavior*, 4(6), pp.350–359.
- Apsel, B. et al., 2008. Targeted polypharmacology: discovery of dual inhibitors of tyrosine and phosphoinositide kinases. *Nature chemical biology*, 4(11), pp.691–9.
- Aridon, P. et al., 2011. Protective role of heat shock proteins in Parkinson's disease. *Neurodegenerative Diseases*, 8(4), pp.155–168.
- Arimoto, K. et al., 2008. Formation of stress granules inhibits apoptosis by suppressing stress-responsive MAPK pathways. *Nature cell biology*, 10(11), pp.1324–32.
- Arimoto-Matsuzaki et al., 2016. TIA1 oxidation inhibits stress granule assembly and sensitizes cells to stress-induced apoptosis. *Nature communications*, 7, p.10252.
- Arrigo, P. et al., 1988. Dynamic changes in the structure and intracellular locale of the mammalian low-molecular-weight heat shock protein. *Molecular and cellular biology*, 8(12), pp.5059–5071.
- Ash, P. et al., 2014. Pathological stress granules in Alzheimer's disease. *Brain Research*, 1584, pp.52–58.
- Audo, I. & Warchol, M.E., 2012. Retinal and cochlear toxicity of drugs: new insights into mechanisms and detection. *Current opinion in neurology*, 25(1), pp.76–85.
- Aulas, A. et al., 2012. Endogenous TDP-43, but not FUS, contributes to stress granule assembly via G3BP. *Molecular Neurodegeneration*, 7(1), p.1.
- Aulas, A. et al., 2015. G3BP1 promotes stress-induced RNA granule interactions to preserve polyadenylated mRNA. *Journal of Cell Biology*, 209(1), pp.73–84.
- Baguet, A. et al., 2007. The exon-junction-complex-component metastatic lymph node 51 functions in stress-granule assembly. *Journal of cell science*, 120(Pt 16), pp.2774–84.
- Baker, T.G. et al., 2015. Heat Shock Protein-Mediated Protection Against Cisplatin-Induced Hair Cell Death. *JARO - Journal of the Association for Research in Otolaryngology*, 16(1), pp.67–80.
- Baler, R. et al., 1996. Evidence for a role of Hsp70 in the regulation of the heat shock response in mammalian cells. *Cell stress & chaperones*, 1(1), pp.33–39.
- Balzer, E. & Moss, E.G., 2007. Localization of the developmental timing regulator Lin28 to mRNP complexes, P-bodies and stress granules. *RNA biology*, 4(1), pp.16–25.
- Basu, S. et al., 2001. CD91 is a common receptor for heat shock proteins gp96, hsp90, hsp70, and calreticulin. *Immunity*, 14(3), pp.303–313.
- Beisel, K.W. et al., 2005. Development and evolution of the vestibular sensory apparatus of the mammalian ear. *Journal of vestibular research*, 15(0), pp.225–241.
- Bentmann, E. et al., 2013. Stress granules in neurodegeneration - Lessons learnt from TAR DNA binding protein of 43 kDa and fused in sarcoma. *FEBS Journal*, 280(18), pp.4348–4370.
- Bespalova, I.N. et al., 2001. Mutations in the Wolfram syndrome 1 gene (WFS1) are a common cause of low frequency sensorineural hearing loss. , 10(22),

pp.2501–2508.

- Bobkova, N. V. et al., 2014. Therapeutic effect of exogenous Hsp70 in mouse models of Alzheimer's disease. *Journal of Alzheimer's Disease*, 38(2), pp.425–435.
- Bodmer, D., 2008. Protection, regeneration and replacement of hair cells in the cochlea: Implications for the future treatment of sensorineural hearing loss. *Swiss Medical Weekly*, 138(47–48), pp.708–712.
- Bogoyevitch, M.A. et al., 2010. c-Jun N-terminal kinase (JNK) signaling: recent advances and challenges. *Biochim. Biophys. Acta*, 1804(3), pp.463–475.
- Bordeleau, M. et al., 2005. Stimulation of mammalian translation initiation factor eIF4A activity by a small molecule inhibitor of eukaryotic translation. *Proceedings of the National Academy of Sciences of the United States of America*, 102, pp.10460–10465.
- Bordeleau, M.E. et al., 2008. Therapeutic suppression of translation initiation modulates chemosensitivity in a mouse lymphoma model. *Journal of Clinical Investigation*, 118(7), pp.2651–2660.
- Borg, E. & Engström, B., 1983. Damage to sensory hairs of inner hair cells after exposure to noise in rabbits without outer hair cells. *Hearing Research*, 11(1), pp.1–6.
- Bosco, D.A. et al., 2010. Mutant FUS proteins that cause amyotrophic lateral sclerosis incorporate into stress granules. *Human Molecular Genetics*, 19(21), pp.4160–4175.
- Brehm, M.A. et al., 2007. Intracellular localization of human Ins(1,3,4,5,6)P5 2-kinase. *The Biochemical journal*, 408(3), pp.335–45.
- Brown, J.M. & Buckle, V.J., 2010. Detection of nascent RNA transcripts by fluorescence in situ hybridization. *Methods in molecular biology (Clifton, N.J.)*, 659, pp.33–50.
- Brunetta, I. et al., 2012. β 3-integrin is required for differentiation in OC-2 cells derived from mammalian embryonic inner ear. *BMC cell biology*, 13(1), p.5.
- Buchan, J.R. et al., 2008. P bodies promote stress granule assembly in *Saccharomyces cerevisiae*. *Journal of Cell Biology*, 183(3), pp.441–455.
- Buchan, J.R. & Parker, R., 2009. Eukaryotic Stress Granules : The Ins and Out of Translation. *Mol Cell*, 36(6).
- Buchan, J.R., Yoon, J.H. & Parker, R., 2011. Stress-specific composition, assembly and kinetics of stress granules in *Saccharomyces cerevisiae*. *Journal of cell science*, 124(Pt 2), pp.228–39.
- Buchan, J.R. et al., 2013. Eukaryotic stress granules are cleared by autophagy and Cdc48/VCP function. *Cell*, 153(7), pp.1461–1474.
- Calderwood, S.K. et al., 2010. Signal Transduction Pathways Leading to Heat Shock Transcription. *Signal transduction insights*, 2, pp.13–24.
- Camp, G.V., Willems, P.J. & Smith, R.J., 1997. Nonsyndromic hearing impairment: unparalleled heterogeneity. *American journal of human genetics*, 60(4), pp.758–64.
- Chalupníková, K. et al., 2008. Recruitment of the RNA helicase RHAU to stress

- granules via a unique RNA-binding domain. *Journal of Biological Chemistry*, 283(50), pp.35186–35198.
- Chen, G. & Fechter, L., 2003. The relationship between noise-induced hearing loss and hair cell loss in rats. *Hearing research*, 177(1–2), pp.81–90.
- Chen, J.J. & London, I.M., 1995. Regulation of protein synthesis by heme-regulated eIF-2 alpha kinase. *Trends in biochemical sciences*, 20(3), pp.105–108.
- Cheng, A. et al., 2005. Mechanisms of hair cell death and protection. *Curr Opin Otolaryngol Head Neck Surg*, 13(6), pp.343–348.
- Cherkasov, V. et al., 2013. Coordination of translational control and protein homeostasis during severe heat stress. *Current Biology*, 23(24), pp.2452–2462.
- Choi, H. et al., 1991. cAMP and cAMP-dependent protein kinase regulate the human heat shock protein 70 gene promoter activity. *J.Biol.Chem.*, 266(c), pp.11858–11865.
- Chou, S. et al., 2012. mTOR is essential for the proteotoxic stress response, HSF1 activation and heat shock protein synthesis. *PloS one*, 7(6), p.e39679.
- Chu, B. et al., 1996. Sequential Phosphorylation by Mitogen-activated Protein Kinase and Glycogen Synthase Kinase 3Represses Transcriptional Activation by Heat Shock Factor-1. *Journal of Biological Chemistry*, 271(48), pp.30847–30857.
- Clough, R. et al., 2004. Brn-3c (POU4F3) regulates BDNF and NT-3 promoter activity. *Biochemical and Biophysical Research Communications*, 324(1), pp.372–381.
- Coleman, L.J. et al., 2009. Combined analysis of eIF4E and 4E-binding protein expression predicts breast cancer survival and estimates eIF4E activity. *British journal of cancer*, 100(9), pp.1393–9.
- Collin, R.W.J. et al., 2008. Missense mutations in POU4F3 cause autosomal dominant hearing impairment DFNA15 and affect subcellular localization and DNA binding. *Human mutation*, 29(4), pp.545–554.
- Comis, S.D. et al., 1986. Early morphological and chemical changes induced by cisplatin in the guinea pig organ of Corti. *The Journal of laryngology and otology*, 100(12), pp.1375–1383.
- Coulthard, L.R. et al., 2009. p38MAPK: stress responses from molecular mechanisms to therapeutics. *Trends in Molecular Medicine*, 15(8), pp.369–379.
- Coyle, B. et al., 1996. Pendred syndrome (goitre and sensorineural hearing loss) maps to chromosome 7 in the region containing the nonsyndromic deafness gene DFNB4. *Nature genetics*, 12(4), pp.421–423.
- Cross, D. et al., 1995. Inhibition of glycogen synthase kinase-3 by insulin mediated by protein kinase B. *Nature*, 378(6559), pp.785–9.
- Cunningham, L. & Brandon, C., 2006. Heat shock inhibits both aminoglycoside- and cisplatin-induced sensory hair cell death. *JARO - Journal of the Association for Research in Otolaryngology*, 7(3), pp.299–307.
- Dalton, D.S. et al., 2003. The impact of hearing loss on quality of life in older adults. *The Gerontologist*, 43(5), pp.661–668.

- Dang, Y. et al., 2006. Eukaryotic initiation factor 2 α -independent pathway of stress granule induction by the natural product pateamine A. *Journal of Biological Chemistry*, 281(43), pp.32870–32878.
- Davis, J.M. et al., 1986. Effects of mild and moderate hearing impairments on language, educational and psychosocial. *Journal of speech and hearing disorders*, 51, pp.53–62.
- Dechesne, C. et al., 1992. Expression of heat shock protein, HSP72, in the guinea pig and rat cochlea after hyperthermia: immunochemical and in situ hybridization analysis. *Hearing research*, 59(2), pp.195–204.
- Delépine, M. et al., 2000. EIF2AK3, encoding translation initiation factor 2- α kinase 3, is mutated in patients with Wolcott-Rallison syndrome. *Nature genetics*, 25(4), pp.406–9.
- Delneste, Y. et al., 2002. Involvement of LOX-1 in dendritic cell-mediated antigen cross-presentation. *Immunity*, 17(3), pp.353–362.
- Dever, T.E., 2002. Gene-specific regulation by general translation factors. *Cell*, 108(4), pp.545–556.
- Dobson, C., 2003. Protein folding and misfolding. *Nature*, 426(6968), pp.884–890.
- Dormann, D. et al., 2010. ALS-associated fused in sarcoma (FUS) mutations disrupt Transportin-mediated nuclear import. *The EMBO journal*, 29(16), pp.2841–2857.
- Duncan, R. & Hershey, J., 1987. Initiation factor protein modifications and inhibition of protein synthesis. *Molecular & Cellular Biology*, 7(3), pp.1293–1295.
- Dunn, K. et al., 2011. A practical guide to evaluating colocalization in biological microscopy. *American journal of physiology. Cell physiology*, 300(4), pp.C723–42.
- Eisinger-Mathason, T. et al., 2008. Codependent functions of RSK2 and the apoptosis-promoting factor TIA-1 in stress granule assembly and cell survival. *Molecular Cell*, 31(5), pp.722–36.
- Eulalio, A. et al., 2007. P bodies: at the crossroads of post-transcriptional pathways. *Nature Reviews Molecular Cell Biology*, 8(1), pp.9–22.
- Fairfield, D.A. et al., 2005. Heat shock factor 1-deficient mice exhibit decreased recovery of hearing following noise overstimulation. *Journal of neuroscience research*, 81(4), pp.589–596.
- Fang, X. et al., 2000. Phosphorylation and inactivation of glycogen synthase kinase 3 by protein kinase A. *Proceedings of the National Academy of Sciences of the United States of America*, 97(22), pp.11960–11965.
- Farrell, P. et al., 1978. Analysis of phosphorylation of protein synthesis initiation factor eIF-2 by two-dimensional gel electrophoresis. *European journal of biochemistry / FEBS*, 89(2), pp.517–521.
- Feldman, M. et al., 2009. Active-site inhibitors of mTOR target rapamycin-resistant outputs of mTORC1 and mTORC2. *PLoS Biology*, 7(2), pp.0371–0383.
- Fettiplace, R. & Hackney, C.M., 2006. The sensory and motor roles of auditory hair cells. *Nature reviews. Neuroscience*, 7(1), pp.19–29.
- Forge, A. et al., 1999. Gap junctions and connexin expression in the inner ear.

- Novartis Foundation symposium, 219, pp.134–136.
- Forge, A. & Schacht, J., 2000. Aminoglycoside antibiotics. *Audiology and Neurotology*, 5(1), pp.3–22.
- Fournier, M. et al., 2013. Inactivation of the mTORC1-eukaryotic translation initiation factor 4E pathway alters stress granule formation. *Molecular and cellular biology*, 33, pp.2285–301.
- Francipane, M. & Lagasse, E., 2013. Selective targeting of human colon cancer stem-like cells by the mTOR inhibitor Torin-1. *Oncotarget*, 4(11), pp.1948–62.
- Fujimura, K. et al., 2009. Microscopic dissection of the process of stress granule assembly. *Biochimica et Biophysica Acta - Molecular Cell Research*, 1793(11), pp.1728–1737.
- Fujimura, K. et al., 2012. Selenite targets eIF4E-binding protein-1 to inhibit translation initiation and induce the assembly of non-canonical stress granules. *Nucleic Acids Research*, 40(16), pp.8099–8110.
- Furness, D.N., 2015. Molecular basis of hair cell loss. *Cell and Tissue Research*, 361(1), pp.387–399.
- Gabai, V. & Sherman, M., 2002. Invited review: Interplay between molecular chaperones and signaling pathways in survival of heat shock. *Journal of applied physiology*, 92(4), pp.1743–8.
- Gale, J.E. et al., 2001. FM1-43 dye behaves as a permeant blocker of the hair-cell mechanotransducer channel. *J Neurosci*, 21(18), pp.7013–7025.
- Gallois-Montbrun, S. et al., 2007. Antiviral protein APOBEC3G localizes to ribonucleoprotein complexes found in P bodies and stress granules. *Journal of virology*, 81(5), pp.2165–78.
- Ganassi, M. et al., 2016. A Surveillance Function of the HSPB8-BAG3-HSP70 Chaperone Complex Ensures Stress. *Molecular Cell*, 63(5), pp.1–15.
- Gao, B. et al., 2013. The endoplasmic reticulum stress inhibitor salubrinal inhibits the activation of autophagy and neuroprotection induced by brain ischemic preconditioning. *Acta pharmacologica Sinica*, 34(5), pp.657–66.
- Gareau, C. et al., 2013. Characterization of Fragile X Mental Retardation Protein Recruitment and Dynamics in Drosophila Stress Granules. *PLoS ONE*, 8(2).
- Gates, G.A. & Mills, J.H., 2005. Presbycusis. *Lancet*, 366(9491), pp.1111–20.
- George, C.X. et al., 2016. Editing of cellular self RNAs by adenosine deaminase ADAR1 suppresses innate immune stress responses. *Journal of Biological Chemistry*, 291(12), p.jbc.M115.709014.
- Ghisolfi, L. et al., 2012. Stress granules contribute to alpha-globin homeostasis in differentiating erythroid cells. *Biochemical and Biophysical Research Communications*, 420(4), pp.768–774.
- Giasson, B.I. et al., 2002. The environmental toxin arsenite induces tau hyperphosphorylation. *Biochemistry*, 41(51), pp.15376–15387.
- Gifondorwa, D.J. et al., 2007. Exogenous delivery of heat shock protein 70 increases lifespan in a mouse model of amyotrophic lateral sclerosis. *J Neurosci*, 27(48), pp.13173–13180.

- Gilks, N. et al., 2004. Stress granule assembly is mediated by prion-like aggregation of TIA-1. *Molecular biology of the cell*, 15(12), pp.5383–5398.
- Gingras, A., Raught, B. & Sonenberg, N., 1999. eIF4 initiation factors: effectors of mRNA recruitment to ribosomes and regulators, *Annu Rev Biochem*, pp.913–963.
- Gong, B. et al., 2013. Caprin-1 is a novel microRNA-223 target for regulating the proliferation and invasion of human breast cancer cells. *Biomedicine and Pharmacotherapy*, 67(7), pp.629–636.
- Goodier, J.L. et al., 2007. LINE-1 ORF1 protein localizes in stress granules with other RNA-binding proteins, including components of RNA interference RNA-induced silencing complex. *Molecular and cellular biology*, 27(18), pp.6469–6483.
- Gordeev, S.A. et al., 2015. mTOR kinase inhibitor pp242 causes mitophagy terminated by apoptotic cell death in E1A-Ras transformed cells. *Oncotarget*, 6(42), pp.44905–26.
- Graff, J.R. et al., 2009. eIF4E activation is commonly elevated in advanced human prostate cancers and significantly related to reduced patient survival. *Cancer Research*, 69(9), pp.3866–3873.
- Grill, B. et al., 2004. Activation/division of lymphocytes results in increased levels of cytoplasmic activation/proliferation-associated protein-1: prototype of a new family of proteins. *Journal of immunology*, 172(4), pp.2389–2400.
- Guil, S., Long, J.C. & Cáceres, J.F., 2006. hnRNP A1 relocalization to the stress granules reflects a role in the stress response. *Molecular and cellular biology*, 26(15), pp.5744–58.
- Guthrie, O.W., 2008. Aminoglycoside induced ototoxicity. *Toxicology*, 249(2–3), pp.91–96.
- Halliday, M. et al., 2015. Partial restoration of protein synthesis rates by the small molecule ISRIB prevents neurodegeneration without pancreatic toxicity. *Cell Death and Disease*, 6(3), p.e1672.
- Han, A.P. et al., 2001. Heme-regulated eIF2alpha kinase (HRI) is required for translational regulation and survival of erythroid precursors in iron deficiency. *EMBO Journal*, 20(23), pp.6909–6918.
- Harding, H.P. et al., 2000. Perk is essential for translational regulation and cell survival during the unfolded protein response. *Molecular Cell*, 5(5), pp.897–904.
- Hartl, F.U., 1996. Molecular chaperones in cellular protein folding. *Nature*, 381(6583), pp.571–579.
- Haydon, a H. et al., 1973. Hydroxamate recognition during iron transport from hydroxamate-ion chelates. *Journal of bacteriology*, 115(3), pp.912–918.
- Henderson, D. et al., 2006. The role of oxidative stress in noise-induced hearing loss. *Ear and hearing*, 27(1), pp.1–19.
- Hers, I., Vincent, E.E. & Tavar, J.M., 2011. Akt signalling in health and disease. *Cellular Signalling*, 23(10), pp.1515–1527.
- Hershey, J.W., 1991. Translational control in mammalian cells. *Annual review of biochemistry*, 60, pp.717–755.

- Hershey, J.W.B., 1989. Protein phosphorylation controls translation rates. *Journal of Biological Chemistry*, 264(35), pp.20823–20826.
- Hinton, S.D. et al., 2010. The pseudophosphatase MK-STYX interacts with G3BP and decreases stress granule formation. *The Biochemical journal*, 427(3), pp.349–57.
- Hoang, B. et al., 2012. The PP242 mammalian target of rapamycin (mTOR) inhibitor activates extracellular signal-regulated kinase (ERK) in multiple myeloma cells via a target of rapamycin complex 1 (TORC1)/eukaryotic translation initiation factor 4E (eIF-4E)/RAF pathway and activ. *The Journal of biological chemistry*, 287(26), pp.21796–805.
- Hoehn, B. et al., 2001. Overexpression of HSP72 after induction of experimental stroke protects neurons from ischemic damage. *Journal of cerebral blood flow and metabolism*, 21(11), pp.1303–1309.
- Hofmann, S. et al., 2012. Translation suppression promotes stress granule formation and cell survival in response to cold shock. *Molecular Biology of the Cell*, 23(19), pp.3786–3800.
- Hoyle, N.P. et al., 2007. Stress-dependent relocalization of translationally primed mRNPs to cytoplasmic granules that are kinetically and spatially distinct from P-bodies. *Journal of Cell Biology*, 179(1), pp.65–74.
- Hsieh, A.C. & Ruggero, D., 2010. Targeting eukaryotic translation initiation factor 4E (eIF4E) in cancer. *Clinical Cancer Research*, 16(20), pp.4914–4920.
- Hu, B.H., Henderson, D. & Nicotera, T.M., 2002. Involvement of apoptosis in progression of cochlear lesion following exposure to intense noise. *Hearing Research*, 166(1–2), pp.62–71.
- Hu, S. et al., 2009. Inflammation-induced, 3'UTR-dependent translational inhibition of Hsp70 mRNA impairs intestinal homeostasis. *American journal of physiology. Gastrointestinal and liver physiology*, 296(5), pp.G1003–G1011.
- Hu, S. et al., 2010. Stress granule formation mediates the inhibition of colonic Hsp70 translation by interferon-gamma and tumor necrosis factor-alpha. *American journal of physiology. Gastrointestinal and liver physiology*, 298(4), pp.G481-92.
- Hua, Y. & Zhou, J., 2004. Survival motor neuron protein facilitates assembly of stress granules. *FEBS Letters*, 572(1–3), pp.69–74.
- Hua Hu, B. & Henderson, D., 1997. Changes in F-actin labeling in the outer hair cell and the Deiters cell in the chinchilla cochlea following noise exposure. *Hearing Research*, 110(1–2), pp.209–218.
- Huang, T. et al., 2000. Oxidative stress-induced apoptosis of cochlear sensory cells: Otoprotective strategies. *International Journal of Developmental Neuroscience*, 18(2–3), pp.259–270.
- Huang, Y.C. et al., 2007. Expression of STAT3 and Bcl-6 oncoprotein in sodium arsenite-treated SV-40 immortalized human uroepithelial cells. *Toxicology Letters*, 173(1), pp.57–65.
- Hudspeth, A.J., 2014. Integrating the active process of hair cells with cochlear function. *Nature reviews. Neuroscience*, 15(9), pp.600–14.
- Huth, M.E., Ricci, A.J. & Cheng, A.G., 2011. Mechanisms of Aminoglycoside

- Ototoxicity and Targets of Hair Cell Protection. *International Journal of Otolaryngology*, 2011, pp.1–19.
- Huth, M.E. et al., 2015. Designer aminoglycosides prevent cochlear hair cell loss and hearing loss. *Journal of Clinical Investigation*, 125(2), pp.583–592.
- Hwang, B.Y. et al., 2004. Derivatives from *Aglaia silvestris*. *Journal of Organic Chemistry*, 69, pp.3350–3358.
- Ivanov, V.N., Wen, G. & Hei, T.K., 2013. Sodium arsenite exposure inhibits AKT and Stat3 activation, suppresses self-renewal and induces apoptotic death of embryonic stem cells. *Apoptosis*, 18(2), pp.188–200.
- Ives, D.G. et al., 1995. Characteristics and comorbidities of rural older adults with hearing impairment. *Journal of the American Geriatrics Society*, 43(7), pp.803–806.
- Jagger, D.J. et al., 2000. Calcium signalling mediated by the 9 acetylcholine receptor in a cochlear cell line from the immortomouse. *The Journal of physiology*, 527 Pt 1, pp.49–54.
- Jain, S. et al., 2016. ATPase-Modulated Stress Granules Contain a Diverse Proteome and Substructure. *Cell*, 164(3), pp.487–498.
- Jarrett, J.T. & Lansbury, P.T.J., 1993. Seeding “one-dimensional crystallization” of amyloid: a pathogenic mechanism in Alzheimer’s disease and scrapie? *Cell*, 73(6), pp.1055–1058.
- Jevtov, I. et al., 2015. TORC2 mediates the heat stress response in *Drosophila* by promoting the formation of stress granules. *J Cell Sci*, 128(14), pp.2497–2508.
- Jha, N. et al., 1992. Genotoxic effects of sodium arsenite on human cells. *Mutation research*, 284(2), pp.215–21.
- Jiang, H. et al., 2006. Caspase-independent pathways of hair cell death induced by kanamycin in vivo. *Cell death and differentiation*, 13(1), pp.20–30.
- Kaehler, C. et al., 2012. Ataxin-2-Like Is a Regulator of Stress Granules and Processing Bodies. *PLoS ONE*, 7(11), pp.1–12.
- Kalmar, B., Lu, C.-H. & Greensmith, L., 2014. The role of heat shock proteins in Amyotrophic Lateral Sclerosis: The therapeutic potential of Arimoclomol. *Pharmacology & therapeutics*, 141(1), pp.40–54.
- Karasawa, T. & Steyger, P.S., 2011. Intracellular mechanisms of aminoglycoside-induced cytotoxicity. *Integrative biology: quantitative biosciences from nano to macro*, 3(9), pp.879–86.
- Katoh, H. et al., 2013. Japanese encephalitis virus core protein inhibits stress granule formation through an interaction with Caprin-1 and facilitates viral propagation. *Journal of Virology*, 87(1), pp.489–502.
- Kedersha, N. et al., 1999. RNA-binding proteins TIA-1 and TIAR link the phosphorylation of eIF-2 alpha to the assembly of mammalian stress granules. *The Journal of Cell biology*, 147(7), pp.1431–1441.
- Kedersha, N. et al., 2000. Dynamic shuttling of TIA-1 accompanies the recruitment of mRNA to mammalian stress granules. *Journal of Cell Biology*, 151(6), pp.1257–1268.
- Kedersha, N. & Anderson, P., 2002. Stress granules: sites of mRNA triage that

- regulate mRNA stability and translatability. *Biochemical Society transactions*, 30(Pt 6), pp.963–969.
- Kedersha, N. et al., 2002. Evidence that ternary complex (eIF2-GTP-tRNA(i)(Met))-deficient preinitiation complexes are core constituents of mammalian stress granules. *Molecular biology of the cell*, 13(1), pp.195–210.
- Kedersha, N. et al., 2005. Stress granules and processing bodies are dynamically linked sites of mRNP remodeling. *Journal of Cell Biology*, 169(6), pp.871–884.
- Kedersha, N. & Anderson, P., 2007. Mammalian Stress Granules and Processing Bodies. *Methods in Enzymology*, 431(7), pp.61–81.
- Kedersha, N., Ivanov, P. & Anderson, P., 2013. Stress granules and cell signaling: More than just a passing phase? *Trends in Biochemical Sciences*, 38(10), pp.494–506.
- Kedersha, N. et al., 2016. G3BP-Caprin1-USP10 complexes mediate stress granule condensation and associate with 40S subunits. *Journal of Cell Biology*, 212(7), pp.845–860.
- Kelley, M.W., 2007. Cellular commitment and differentiation in the organ of Corti. *International Journal of Developmental Biology*, 51(6–7), pp.571–583.
- Kenneson, A., Braun, K.V.N. & Boyle, C., 2002. GJB2 (connexin 26) variants and nonsyndromic sensorineural hearing loss: A HuGE review. *Genet Med*, 4(4), pp.258–274.
- Khaleque, M.A. et al., 2005. Induction of heat shock proteins by heregulin beta1 leads to protection from apoptosis and anchorage-independent growth. *Oncogene*, 24(43), pp.6564–6573.
- Kiang, J.G., Gist, I.D. & Tsokos, G.C., 1998. Cytoprotection and regulation of heat shock proteins induced by heat shock in human breast cancer T47-D cells: role of [Ca²⁺]_i and protein kinases. *Faseb J*, 12(14), pp.1571–1579.
- Kiang, J.G., Wut, Y.Y. & Lint, M.C., 1991. Heat treatment induces an increase in intracellular cyclic AMP content in human epidermoid A-431 cells. *Biochem J*, 276, pp.683–689.
- Kieran, D. et al., 2004. Treatment with arimoclomol, a coinducer of heat shock proteins, delays disease progression in ALS mice. *Nature Medicine*, 10(4), pp.402–405.
- Kim, H.-J. et al., 2014. Therapeutic modulation of eIF2 α phosphorylation rescues TDP-43 toxicity in amyotrophic lateral sclerosis disease models. *Nature genetics*, 46(2), pp.152–60.
- Kim, J.-E. et al., 2008. Proline-Rich Transcript in Brain Protein Induces Stress Granule Formation. *Molecular and Cellular Biology*, 28(2), pp.803–813.
- Kim, W.J. et al., 2005. Sequestration of TRAF2 into Stress Granules Interrupts Tumor Necrosis Factor Signaling under Stress Conditions Sequestration of TRAF2 into Stress Granules Interrupts Tumor Necrosis Factor Signaling under Stress Conditions. *Molecular and cellular biology*, 25(6), pp.2450–2462.
- Kimball, S.R. et al., 2003. Mammalian stress granules represent sites of accumulation of stalled translation initiation complexes. *American journal of physiology. Cell physiology*, 284(2), pp.C273-84.
- Kochhar, A., Hildebrand, M.S. & Smith, R.J.H., 2007. Clinical aspects of hereditary

- hearing loss. *Genetics in medicine : official journal of the American College of Medical Genetics*, 9(7), pp.393–408.
- Kolobova, E. et al., 2009. Microtubule-dependent association of AKAP350A and CCAR1 with RNA stress granules. *Experimental Cell Research*, 315(3), pp.542–555.
- Kozak, S.L. et al., 2006. The anti-HIV-1 editing enzyme APOBEC3G binds HIV-1 RNA and messenger RNAs that shuttle between polysomes and stress granules. *Journal of Biological Chemistry*, 281(39), pp.29105–29119.
- Kraft, C. et al., 2008. Mature ribosomes are selectively degraded upon starvation by an autophagy pathway requiring the Ubp3p/Bre5p ubiquitin protease. *Nature cell biology*, 10(5), pp.602–610.
- Kramer, S. et al., 2008. Heat shock causes a decrease in polysomes and the appearance of stress granules in trypanosomes independently of eIF2(alpha) phosphorylation at Thr169. *Journal of cell science*, 121(Pt 18), pp.3002–3014.
- Kubacka, D. et al., 2013. Investigating the Consequences of eIF4E2 (4EHP) Interaction with 4E-Transporter on Its Cellular Distribution in HeLa Cells. *PLoS ONE*, 8(8), pp.1–14.
- Kunde, S.A. et al., 2011. The X-chromosome-linked intellectual disability protein PQBP1 is a component of neuronal RNA granules and regulates the appearance of stress granules. *Human Molecular Genetics*, 20(24), pp.4916–4931.
- Kurshakova, M.M. et al., 2007. SAGA and a novel Drosophila export complex anchor efficient transcription and mRNA export to NPC. *The EMBO journal*, 26(24), pp.4956–4965.
- Kwon, S., Zhang, Y. & Matthias, P., 2007. The deacetylase HDAC6 is a novel critical component of stress granules involved in the stress response. *Genes and Development*, 21(24), pp.3381–3394.
- Lagier-Tourenne, C. & Cleveland, D.W., 2009. Rethinking ALS: The FUS about TDP-43. *Cell*, 136(6), pp.1001–1004.
- Laplante, M. & Sabatini, D.M., 2009. mTOR signaling at a glance. *J Cell Sci*, 122, pp.3589–3594.
- Latchman, D.S., 2001. Heat shock proteins and cardiac protection. *Cardiovascular Research*, 51(4), pp.637–646.
- Latchman, D.S., 2004. Protective effect of heat shock proteins in the nervous system. *Current neurovascular research*, 1(1), pp.21–7.
- Lee, J.E. et al., 2001. Differential neuroprotection from human heat shock protein 70 overexpression in in vitro and in vivo models of ischemia and ischemia-like conditions. *Experimental neurology*, 170(1), pp.129–39.
- Lee, K.-Y., 2013. Pathophysiology of Age-Related Hearing Loss (Peripheral and Central). *Korean journal of audiology*, 17(2), pp.45–49.
- Legros, S. et al., 2011. The HTLV-1 Tax protein inhibits formation of stress granules by interacting with histone deacetylase 6. *Oncogene*, 30(38), pp.4050–4062.
- Leung, A.K.L., Calabrese, J.M. & Sharp, P. a, 2006. Quantitative analysis of Argonaute protein reveals microRNA-dependent localization to stress granules. *Proceedings of the National Academy of Sciences of the United States of*

- America*, 103(48), pp.18125–18130.
- Li, C.H. et al., 2010. eIF5A promotes translation elongation, polysome disassembly and stress granule assembly. *PLoS ONE*, 5(4).
- Li, M. et al., 2000. Cyclic AMP Promotes Neuronal Survival by Phosphorylation of Glycogen Synthase Kinase 3beta. *Molecular and Cellular Biology*, 20(24), pp.9356–9363.
- Li, S. et al., 2002. Hearing loss caused by progressive degeneration of cochlear hair cells in mice deficient for the Barhl1 homeobox gene. *Development*, 3532, pp.3523–3532.
- Li, W. & Chou, I.N., 1992. Effects of sodium arsenite on the cytoskeleton and cellular glutathione levels in cultured cells. *Toxicology and applied pharmacology*, 114(1), pp.132–139.
- Lin, F.R. et al., 2011. Hearing Loss and Incident Dementia. *Archives of Neurology*, 68(2), pp.214–220.
- Liu-Yesucevitz, L. et al., 2011. Local RNA Translation at the Synapse and in Disease. *Journal of Neuroscience*, 31(45), pp.16086–16093.
- Liu, X.Z. et al., 2016. Hearing loss and PRPS1 mutations : Wide spectrum of phenotypes and potential therapy. *International Journal of Audiology*, 2027(November), pp.23–28.
- Long, K., Boyce, M. & Bryant, K.F., 2005. A Selective Inhibitor of eIF2a Dephosphorylation Protects Cells from ER Stress. *Science*, 307(2005), pp.935–939.
- Lopez-Gonzalez, M.A., Delgado, F. & Lucas, M., 1999. Aminoglycosides activate oxygen metabolites production in the cochlea of mature and developing rats. *Hearing Research*, 136(1–2), pp.165–168.
- Lotan, R. et al., 2005. The RNA polymerase II subunit Rpb4p mediates decay of a specific class of mRNAs. *Genes and Development*, 19(24), pp.3004–3016.
- Low, W.K. et al., 2005. Inhibition of eukaryotic translation initiation by the marine natural product pateamine A. *Molecular Cell*, 20(5), pp.709–722.
- Lu, L., Han, A. & Chen, J., 2001. Translation Initiation Control by Heme-Regulated Eukaryotic Initiation Factor 2 alpha Kinase in Erythroid Cells under Cytoplasmic Stresses. *Mol Cell Biol*, 21(23), pp.7971–7980.
- Lukashkin, A.N., Richardson, G.P. & Russell, I.J., 2010. Multiple roles for the tectorial membrane in the active cochlea. *Hearing research*, 266(1–2), pp.26–35.
- Mahboubi, H. et al., 2013. Identification of Novel Stress Granule Components That Are Involved in Nuclear Transport. *PLoS ONE*, 8(6).
- Mangiardi, D.A. et al., 2004. Progression of hair cell ejection and molecular markers of apoptosis in the avian cochlea following gentamicin treatment. *Journal of Comparative Neurology*, 475(1), pp.1–18.
- Martini, S. and R., 2007. Genes, Hearing and Deafness: From Molecular Biology to Clinical Practice. *International Psychogeriatrics*, p.328.
- May, L.A. et al., 2013. Inner ear supporting cells protect hair cells by secreting HSP70. *Journal of Clinical Investigation*, 123(8), pp.3577–3587.

- Mayer, M.P., 2013. Hsp70 chaperone dynamics and molecular mechanism. *Trends in Biochemical Sciences*, 38(10), pp.507–514.
- Mayer, M.P. & Bukau, B., 2005. Hsp70 chaperones: Cellular functions and molecular mechanism. *Cellular and Molecular Life Sciences*, 62(6), pp.670–684.
- McDonald, K.K. et al., 2011. TAR DNA-binding protein 43 (TDP-43) regulates stress granule dynamics via differential regulation of G3BP and TIA-1. *Human Molecular Genetics*, 20(7), pp.1400–1410.
- McEwen, E. et al., 2005. Heme-regulated inhibitor kinase-mediated phosphorylation of eukaryotic translation initiation factor 2 inhibits translation, induces stress granule formation, and mediates survival upon arsenite exposure. *Journal of Biological Chemistry*, 280(17), pp.16925–16933.
- McFadden, S.L. et al., 1999. Age-related cochlear hair cell loss is enhanced in mice lacking copper/zinc superoxide dismutase. *Neurobiology of aging*, 20, pp.1–8.
- Meltser, I., Tahera, Y. & Canlon, B., 2009. Glucocorticoid receptor and mitogen-activated protein kinase activity after restraint stress and acoustic trauma. *Journal of neurotrauma*, 26(10), pp.1835–1845.
- Miller, C.L., 2011. Stress Granules and Virus Replication. *Future virology*, 6(11), pp.1329–1338.
- Molle, W.V. et al., 2002. HSP70 protects against TNF-induced lethal inflammatory shock. *Immunity*, 16(5), pp.685–695.
- Monzack, E.L. & Cunningham, L.L., 2013. Lead roles for supporting actors: Critical functions of inner ear supporting cells. *Hearing Research*, 303, pp.20–29.
- Moore, S.F. et al., 2013. Dual regulation of glycogen synthase kinase 3 (GSK3)alpha/beta by protein kinase C (PKC)alpha and Akt promotes thrombin-mediated integrin alphaIIb beta3 activation and granule secretion in platelets. *Journal of Biological Chemistry*, 288(6), pp.3918–3928.
- Moreno, J. et al., 2012. Sustained translational repression by eIF2 α -P mediates prion neurodegeneration. *Nature*, 485(7399), pp.507–511.
- Morton, N.E., 1991. Genetic epidemiology of hearing impairment. *Annals of the New York Academy of Sciences*, 630, pp.16–31.
- Moser, T. & Starr, A., 2016. Auditory neuropathy - neural and synaptic mechanisms. *Nature reviews. Neurology*, 12(3), pp.135–49.
- Mosser, D.D. et al., 1997. Role of the human heat shock protein hsp70 in protection against stress-induced apoptosis. *Molecular and cellular biology*, 17(9), pp.5317–27.
- Mosser, D.D. et al., 2000. The chaperone function of hsp70 is required for protection against stress-induced apoptosis. *Molecular and cellular biology*, 20(19), pp.7146–59.
- Mukherjea, D. et al., 2008. Short interfering RNA against transient receptor potential vanilloid 1 attenuates cisplatin-induced hearing loss in the rat. *The Journal of neuroscience : the official journal of the Society for Neuroscience*, 28(49), pp.13056–13065.
- Murai, N. et al., 2008. Activation of JNK in the inner ear following impulse noise exposure. *Journal of neurotrauma*, 25(1), pp.72–77.

- Myers, M.W. et al., 1992. Expression of the major mammalian stress protein in the rat cochlea following transient ischemia. *The Laryngoscope*, 102(9), pp.981–987.
- Nadezhdina, E.S. et al., 2010. Microtubules govern stress granule mobility and dynamics. *Biochimica et Biophysica Acta - Molecular Cell Research*, 1803(3), pp.361–371.
- Nelson, E. V et al., 2016. Ebola virus does not induce stress granule formation during infection and sequesters stress granule proteins within viral inclusions. *Journal of virology*, 90(16), pp.7268–84.
- Nicotera, T.M., Hu, B.H. & Henderson, D., 2003. The Caspase Pathway in Noise-Induced Apoptosis of the Chinchilla Cochlea. *JARO - Journal of the Association for Research in Otolaryngology*, 4(4), pp.466–477.
- Nover, L., Scharf, K.D. & Neumann, D., 1989. Cytoplasmic heat shock granules are formed from precursor particles and are associated with a specific set of mRNAs. *Molecular and cellular biology*, 9(3), pp.1298–308.
- Nover, L., Scharf, K.D. & Neumann, D., 1983. Formation of cytoplasmic heat shock granules in tomato cell cultures and leaves. *Molecular and cellular biology*, 3(9), pp.1648–55.
- Ogawa, F., Kasai, M. & Akiyama, T., 2005. A functional link between Disrupted-In-Schizophrenia 1 and the eukaryotic translation initiation factor 3. *Biochemical and Biophysical Research Communications*, 338(2), pp.771–776.
- Oh, S.H. et al., 2000. Expression of heat shock protein 72 in rat cochlea with cisplatin-induced acute ototoxicity. *Acta otolaryngologica*, 120(2), pp.146–150.
- Ohlemiller K, Wright, J. & Dugan, L., 1999. Early elevation of Cochlear ROS following Noise exposure. *Audiol Neurotol*, 63110, pp.229–236.
- Ohlemiller, K. et al., 2000. Targeted mutation of the gene for cellular glutathione peroxidase (Gpx1) increases noise-induced hearing loss in mice. *Journal of the Association for Research in Otolaryngology : JARO*, 1, pp.243–254.
- Ohn, T. et al., 2008. A functional RNAi screen links O-GlcNAc modification of ribosomal proteins to stress granule and processing body assembly. *Nature cell biology*, 10(10), pp.1224–31.
- Ohshima, D. et al., 2015. Spatio-temporal Dynamics and Mechanisms of Stress Granule Assembly. *PLoS Computational Biology*, 11(6), pp.1–22.
- Ono, A. et al., 2013. Comparative effects of PP242 and rapamycin on mTOR signalling and NOTCH signalling in leukemia cells. *Anticancer Research*, 33(3), pp.809–814.
- Osborne, M.P., Comis, S.D. & Pickles, J.O., 1984. Morphology and cross-linkage of stereocilia in the guinea-pig labyrinth examined without the use of osmium as a fixative. *Cell and tissue research*, 237(1), pp.43–48.
- Ouyang, W. et al., 2007. PI-3K/Akt signal pathway plays a crucial role in arsenite-induced cell proliferation of human keratinocytes through induction of cyclin D1. *Journal of Cellular Biochemistry*, 101(4), pp.969–978.
- Pandya, A., 1993. Nonsyndromic Hearing Loss and Deafness, Mitochondrial. *Gene Reviews*. Seattle (WA).
- Pap, M. & Cooper, G.M., 1998. Role of Glycogen Synthase Kinase-3 in the Akt Cell

- Survival Pathway. *The journal of biological chemistry*, 273(24), pp.19929–19932.
- Papadopoulou, C. et al., 2013. HuR-hnRNP interactions and the effect of cellular stress. *Molecular and Cellular Biochemistry*, 372(1–2), pp.137–147.
- Parfitt, D.A. et al., 2014. The heat-shock response co-inducer arimocloamol protects against retinal degeneration in rhodopsin retinitis pigmentosa. *Cell death & disease*, 5(5), p.e1236.
- Parker, R. & Sheth, U., 2007. P Bodies and the Control of mRNA Translation and Degradation. *Molecular Cell*, 25(5), pp.635–646.
- Paschen, W., 2003. Shutdown of translation: lethal or protective? Unfolded protein response versus apoptosis. *Journal of cerebral blood flow and metabolism*, 23(7), pp.773–779.
- Peng, A.W. et al., 2011. Integrating the biophysical and molecular mechanisms of auditory hair cell mechanotransduction. *Nature communications*, 2, p.523.
- Perez, P. & Bao, J., 2011. Why do hair cells and spiral ganglion neurons in the cochlea die during aging? *Aging and disease*, 2(3), pp.231–41.
- Pickles, J.O., Comis, S.D. & Osborne, M.P., 1984. Cross-links between stereocilia in the guinea pig organ of Corti, and their possible relation to sensory transduction. *Hearing Research*, 15(2), pp.103–112.
- Poirrier, A. et al., 2010. Oxidative stress in the cochlea: an update. *Current medicinal chemistry*, 17(30), pp.3591–604.
- Poreddy, A.R. et al., 2004. Hydroxamate-based iron chelators: Combinatorial syntheses of desferrioxamine B analogues and evaluation of binding affinities. *Journal of Combinatorial Chemistry*, 6(2), pp.239–254.
- Proietti, F.A. et al., 2005. Global epidemiology of HTLV-I infection and associated diseases. *Oncogene*, 24(39), pp.6058–68.
- Raphael, Y. & Altschuler, R.A., 2003. Structure and innervation of the cochlea. *Brain Research Bulletin*, 60(5–6), pp.397–422.
- Ratovitski, T. et al., 2012. Huntingtin protein interactions altered by polyglutamine expansion as determined by quantitative proteomic analysis. *Cell Cycle*, 11(10), pp.2006–2021.
- Riccardi, S. et al., 2016. MiR-210 promotes sensory hair cell formation in the organ of Corti. *BMC genomics*, 17, p.309.
- Richardson, G.P., Lukashkin, A.N. & Russell, I.J., 2008. The tectorial membrane: one slice of a complex cochlear sandwich. *Current opinion in otolaryngology & head and neck surgery*, 16(5), pp.458–464.
- Richter, K., Haslbeck, M. & Buchner, J., 2010. The Heat Shock Response: Life on the Verge of Death. *Molecular Cell*, 40(2), pp.253–266.
- Ritossa, F., 1962. A new puffing pattern induced by temperature shock and DNP in drosophila. *Experientia*, 18(12), pp.571–573.
- Rivolta, M.N. et al., 1998. Auditory hair cell precursors immortalized from the mammalian inner ear. *Proceedings. Biological sciences / The Royal Society*, 265(1406), pp.1595–603.

- Rivolta, M.N. & Holley, M.C., 2002. Cell lines in inner ear research. *Journal of Neurobiology*, 53(2), pp.306–318.
- Rodrigo, C.M. et al., 2012. Synthesis of rocaglamide hydroxamates and related compounds as eukaryotic translation inhibitors: Synthetic and biological studies. *Journal of Medicinal Chemistry*, 55(1), pp.558–562.
- Rothé, F. et al., 2006. Identification of FUSE-binding proteins as interacting partners of TIA proteins. *Biochemical and Biophysical Research Communications*, 343(1), pp.57–68.
- Russell, D.W. et al., 1995. Association Between X-Linked Mixed Deafness and Mutations in the POU Domain Gene POU3F4. *Science*, 267, pp.2–6.
- Russell, I.J. & Sellick, P.M., 1978. Intracellular studies of hair cells in the mammalian cochlea. *The Journal of physiology*, 284, pp.261–290.
- Saad, S. et al., 1995. Protective effect of heat shock pretreatment with heat shock protein induction before hepatic warm ischemic injury caused by Pringle's maneuver. *Surgery*, 118(3), pp.510–516.
- Sabile, A.A. et al., 2013. Caprin-1, a novel Cyr61-interacting protein, promotes osteosarcoma tumor growth and lung metastasis in mice. *Biochimica et Biophysica Acta - Molecular Basis of Disease*, 1832(8), pp.1173–1182.
- Sarge, K.D., Murphy, S.P. & Morimoto, R.I., 1993. Activation of heat shock gene transcription by heat shock factor 1 involves oligomerization, acquisition of DNA-binding activity, and nuclear localization and can occur in the absence of stress. *Molecular and cellular biology*, 13(3), pp.1392–407.
- Schacht, J., 2007. Aminoglycoside antibiotics. *Pharmacology and ototoxicity for audiologists*, 506, pp.163–176.
- Schacht, J., Talaska, A.E. & Rybak, L.P., 2013. Cisplatin and Aminoglycoside Antibiotics: Hearing Loss and Its Prevention. *The Anatomical Record*, 295(11), pp.1837–1850.
- Scharf, K.D. et al., 1998. The tomato Hsf system: HsfA2 needs interaction with HsfA1 for efficient nuclear import and may be localized in cytoplasmic heat stress granules. *Mol Cell Biol*, 18(4), pp.2240–51.
- Schewe, D.M. & Aguirre-Ghiso, J.A., 2009. Inhibition of eIF2 alpha dephosphorylation maximizes bortezomib efficiency and eliminates quiescent multiple myeloma cells surviving proteasome inhibitor therapy. *Cancer Research*, 69(4), pp.1545–1552.
- Schlesinger, M.J., 1994. How the cell copes with stress and the function of heat shock proteins. *Pediatr Res*, 36(1 Pt 1), pp.1–6.
- Schuknecht, H.F., 1964. Further observations on the pathology of prebycusis. *Archives of otolaryngology (Chicago, Ill. : 1960)*, 80, pp.369–382.
- Scovassi, A.I., 2013. Manipulation of autophagy in cancer cells- an innovative strategy to fight drug resistance. *Future Med Chem*, 5(9), pp.1009–1021.
- Seguin, S.J. et al., 2014. Inhibition of autophagy, lysosome and VCP function impairs stress granule assembly. *Cell death and differentiation*, 21(12), pp.1838–51.
- Sekine, Y. et al., 2015. Stress responses. Mutations in a translation initiation factor identify the target of a memory-enhancing compound. *Science*, 348(6238),

pp.1027–30.

- Shamovsky, I. & Gershon, D., 2004. Novel regulatory factors of HSF-1 activation: Facts and perspectives regarding their involvement in the age-associated attenuation of the heat shock response. *Mechanisms of Ageing and Development*, 125(10–11 SPEC. ISS.), pp.767–775.
- Shamovsky, I. et al., 2006. RNA-mediated response to heat shock in mammalian cells. *Nature*, 440(7083), pp.556–60.
- Shamovsky, I. & Nudler, E., 2008. New insights into the mechanism of heat shock response activation. *Cellular and Molecular Life Sciences*, 65(6), pp.855–861.
- Shaner, L. & Morano, K. a., 2007. All in the family: atypical Hsp70 chaperones are conserved modulators of Hsp70 activity. *Cell stress & chaperones*, 12(1), pp.1–8.
- Shelkovichnikova, T.A. et al., 2014. Multistep process of FUS aggregation in the cell cytoplasm involves RNA-dependent and RNA-independent mechanisms. *Human molecular genetics*, 23(19), pp.5211–5226.
- Shiina, N., 2005. A Novel RNA-Binding Protein in Neuronal RNA Granules: Regulatory Machinery for Local Translation. *Journal of Neuroscience*, 25(17), pp.4420–4434.
- Shiina, N. & Tokunaga, M., 2010. RNA granule protein 140 (RNG140), a paralog of RNG105 localized to distinct RNA granules in neuronal dendrites in the adult vertebrate brain. *Journal of Biological Chemistry*, 285(31), pp.24260–24269.
- Shiina, N., Yamaguchi, K. & Tokunaga, M., 2010. RNG105 deficiency impairs the dendritic localization of mRNAs for Na⁺/K⁺ ATPase subunit isoforms and leads to the degeneration of neuronal networks. *The Journal of neuroscience : the official journal of the Society for Neuroscience*, 30(38), pp.12816–12830.
- Shnerson, A. & Pujol, R., 1981. Age-related changes in the C57BL/6J mouse cochlea. I. Physiological findings. *Brain research*, 254(1), pp.65–75.
- Sidrauski, C. et al., 2013. Pharmacological brake-release of mRNA translation enhances cognitive memory. *eLife*, 2013(2), pp.1–22.
- Sidrauski, C., Tsai, J.C., et al., 2015. Pharmacological dimerization and activation of the exchange factor eIF2B antagonizes the integrated stress response. *eLife*, 2015(4), pp.1–27.
- Sidrauski, C., McGeachy, A.M., et al., 2015. The small molecule ISRIB reverses the effects of eIF2 alpha phosphorylation on translation and stress granule assembly. *eLife*, 4, pp.1–16.
- Silver, J.T. & Noble, E.G., 2012. Regulation of survival gene hsp70. *Cell Stress and Chaperones*, 17(1), pp.1–9.
- Smith, J. a et al., 2006. Reovirus Induces and Benefits from an Integrated Cellular Stress Response. *Journal of Virology*, 80(4), pp.2019–2033.
- Smith, R.J.H. & Jones, M.-K.N., 1993. Nonsyndromic Hearing Loss and Deafness, DFNB1. *Gene Reviews*. Seattle (WA).
- Smith, R.J.H., Ranum, P.T. & Van Camp, G., 1993. Nonsyndromic Hearing Loss and Deafness, DFNA3. *Gene Reviews*. Seattle (WA).
- Snow, E.T., 1992. Metal carcinogenesis: Mechanistic implications. *Pharmacology*

and Therapeutics, 53(1), pp.31–65.

- Solomon, S. et al., 2007. Distinct structural features of caprin-1 mediate its interaction with G3BP-1 and its induction of phosphorylation of eukaryotic translation initiation factor 2 α , entry to cytoplasmic stress granules, and selective interaction with a subset of mRNAs. *Molecular and Cellular Biology*, 27(6), pp.2324–42.
- Souquere, S. et al., 2009. Unravelling the ultrastructure of stress granules and associated P-bodies in human cells. *Journal of Cell Science*, 122(Pt 20), pp.3619–3626.
- Spongr, V.P. et al., 1997. Quantitative measures of hair cell loss in CBA and C57BL/6 mice throughout their life spans. *The Journal of the Acoustical Society of America*, 101(6), pp.3546–3553.
- Staecker, H., Zheng, Q.Y. & Van De Water, T.R., 2001. Oxidative stress in aging in the C57B16/J mouse cochlea. *Acta otolaryngologica*, 121(6), pp.666–72.
- Stoecklin, G. et al., 2004. MK2-induced tristetraprolin:14-3-3 complexes prevent stress granule association and ARE-mRNA decay. *The EMBO journal*, 23(6), pp.1313–24.
- Stohr, N. et al., 2006. ZBP1 regulates mRNA stability during cellular stress. *Journal of Cell Biology*, 175(4), pp.527–534.
- Sugahara, K. et al., 2003. Heat shock transcription factor HSF1 is required for survival of sensory hair cells against acoustic overexposure. *Hearing research*, 182(1–2), pp.88–96.
- Tabuchi, K. et al., 2010. Cochlear protection from acoustic injury by inhibitors of p38 mitogen-activated protein kinase and sequestosome 1 stress protein. *Neuroscience*, 166(2), pp.665–670.
- Takahashi, M. et al., 2013. Stress Granules Inhibit Apoptosis by Reducing Reactive Oxygen Species Production. *Molecular and Cellular Biology*, 33(4), pp.815–829.
- Taleb, M. et al., 2008. Hsp70 inhibits aminoglycoside-induced hair cell death and is necessary for the protective effect of heat shock. *JARO - Journal of the Association for Research in Otolaryngology*, 9(3), pp.277–289.
- Taleb, M. et al., 2009. Hsp70 inhibits aminoglycoside-induced hearing loss and cochlear hair cell death. *Cell Stress and Chaperones*, 14(4), pp.427–437.
- Tanaka, T. et al, 2014. HSP70 mediates degradation of the p65 subunit of nuclear factor κ B to inhibit inflammatory signaling. *Science signaling*, 7(356), p.ra119.
- Tanaka, T., Ohashi, S. & Kobayashi, S., 2014. Roles of YB-1 under arsenite-induced stress: Translational activation of HSP70 mRNA and control of the number of stress granules. *Biochimica et Biophysica Acta - General Subjects*, 1840(3), pp.985–992.
- Taylor, R.R., Nevill, G. & Forge, A., 2008. Rapid hair cell loss: A mouse model for cochlear lesions. *JARO - Journal of the Association for Research in Otolaryngology*, 9(1), pp.44–64.
- Thandapani, P. et al., 2013. Defining the RGG/RG Motif. *Molecular Cell*, 50(5), pp.613–623.
- Thedieck, K. et al., 2013. Inhibition of mTORC1 by astrin and stress granules

- prevents apoptosis in cancer cells. *Cell*, 154(4), pp.859–874.
- Thériault, J.R. et al., 2005. Extracellular HSP70 binding to surface receptors present on antigen presenting cells and endothelial/epithelial cells. *FEBS Letters*, 579(9), pp.1951–1960.
- Thériault, J.R., Adachi, H. & Calderwood, S.K., 2006. Role of scavenger receptors in the binding and internalization of heat shock protein 70. *Journal of immunology*, 177(12), pp.8604–8611.
- Thomas, M.G. et al., 2009. Mammalian Staufen 1 is recruited to stress granules and impairs their assembly. *Journal of cell science*, 122(Pt 4), pp.563–73.
- Thomas, M.G. et al., 2011. RNA granules: The good, the bad and the ugly. *Cellular Signalling*, 23(2), pp.324–334.
- Thompson, A.M. & Neely, J.G., 1992. Induction of heat shock protein in interdental cells by hyperthermia. *Otolaryngology-head and neck surgery: official journal of American Academy of Otolaryngology, Head and Neck Surgery*, 107(6 Pt 1), pp.769–774.
- Tidwell, J.L., Houenou, L.J. & Tytell, M., 2004. Administration of Hsp70 in vivo inhibits motor and sensory neuron degeneration. *Cell stress & chaperones*, 9(1), pp.88–98.
- Tourrière, H. et al., 2003. The RasGAP-associated endoribonuclease G3BP assembles stress granules. *Journal of Cell Biology*, 160(6), pp.823–831.
- Towers, E.R. et al., 2011. Caprin-1 is a target of the deafness gene Pou4f3 and is recruited to stress granules in cochlear hair cells in response to ototoxic damage. *Journal of cell science*, 124(Pt 7), pp.1145–1155.
- Uhlmann, R.F. et al., 1989. Relationship of hearing impairment to dementia and cognitive dysfunction in older adults. *Journal of the American Medical Association*, 261(13), pp.1916–1919.
- Underhill, M.F. et al., 2005. eIF2 α phosphorylation, stress perception, and the shutdown of global protein synthesis in cultured CHO cells. *Biotechnology and Bioengineering*, 89(7), pp.805–814.
- Unsworth, H. et al., 2010. mRNA escape from stress granule sequestration is dictated by localization to the endoplasmic reticulum. *FASEB journal : official publication of the Federation of American Societies for Experimental Biology*, 24(9), pp.3370–80.
- Valiente-Echeverría, F. et al., 2014. eEF2 and Ras-GAP SH3 domain-binding protein (G3BP1) modulate stress granule assembly during HIV-1 infection. *Nature communications*, 5, p.4819.
- Vanderweyde, T. et al., 2012. Contrasting pathology of the stress granule proteins TIA-1 and G3BP in tauopathies. *The Journal of neuroscience : the official journal of the Society for Neuroscience*, 32(24), pp.8270–83.
- Vanderweyde, T. et al., 2013. Role of stress granules and RNA-binding proteins in neurodegeneration: A mini-review. *Gerontology*, 59(6), pp.524–533.
- Vessey, J.P. et al., 2006. Dendritic localization of the translational repressor Pumilio 2 and its contribution to dendritic stress granules. *The Journal of neuroscience : the official journal of the Society for Neuroscience*, 26(24), pp.6496–508.

- Vogel, J.L., Parsell, D.A. & Lindquist, S., 1995. Heat-shock proteins Hsp104 and Hsp70 reactivate mRNA splicing after heat inactivation. *Current Biology*, 5(3), pp.306–317.
- Volkening, K. et al., 2009. Tar DNA binding protein of 43 kDa (TDP-43), 14-3-3 proteins and copper/zinc superoxide dismutase (SOD1) interact to modulate NFL mRNA stability. Implications for altered RNA processing in amyotrophic lateral sclerosis (ALS). *Brain Research*, 1305, pp.168–182.
- Walters, R.W. et al., 2015. Differential effects of Ydj1 and Sis1 on Hsp70-mediated clearance of stress granules in *Saccharomyces cerevisiae*. *RNA*, 21(9), pp.1660–71.
- Walters, R.W. & Parker, R., 2015. Coupling of Ribostasis and Proteostasis: Hsp70 Proteins in mRNA Metabolism. *Trends in Biochemical Sciences*, 40(10), pp.552–559.
- Wang, J. et al., 2011. Cytoplasmic HuR expression correlates with angiogenesis, lymphangiogenesis, and poor outcome in lung cancer. *Medical Oncology*, 28.
- Wang, X. et al., 2003. Regulation of molecular chaperone gene transcription involves the serine phosphorylation, 14-3-3 epsilon binding, and cytoplasmic sequestration of heat shock factor 1. *Molecular and cellular biology*, 23(17), pp.6013–26.
- Wang, X. et al., 2004. Interactions between extracellular signal-regulated protein kinase 1, 14-3-3, and heat shock factor 1 during stress. *Journal of Biological Chemistry*, 279(47), pp.49460–49469.
- Wangemann, P., 2006. Supporting sensory transduction: cochlear fluid homeostasis and the endocochlear potential. *The Journal of physiology*, 576, pp.11–21.
- Waskiewicz, A.J. & Cooper, J.A., 1995. Mitogen and stress response pathways: MAP kinase cascades and phosphatase regulation in mammals and yeast. *Current Opinion in Cell Biology*, 7(6), pp.798–805.
- Weil, D. et al., 1995. Defective myosin VIIA gene responsible for Usher syndrome type 1B. *Nature*, 374(6517), pp.60–61.
- Weiss, S. et al., 2003. The DFNA15 deafness mutation affects POU4F3 protein stability, localization, and transcriptional activity. *Molecular and cellular biology*, 23(22), pp.7957–7964.
- Weissbach, R. & Scadden, a. D.J., 2012. Tudor-SN and ADAR1 are components of cytoplasmic stress granules. *RNA*, 18, pp.462–471.
- Wheeler, J., 2016. Distinct stages in stress granule assembly and disassembly. *eLife*, 5, pp.1–25.
- Wilczynska, a et al., 2005. The translational regulator CPEB1 provides a link between dcp1 bodies and stress granules. *Journal of cell science*, 118(Pt 5), pp.981–992.
- Williams, B.R., 2001. Signal integration via PKR. *Science's STKE: signal transduction knowledge environment*, 2001(89), p.re2.
- Wolozin, B., 2012. Regulated protein aggregation: stress granules and neurodegeneration. *Molecular neurodegeneration*, 7(1), p.56.
- Wu, C., 1995. Heat shock transcription factors: structure and Regulation translocation , higher order assembly , and protein degradation. *Annual Review*

of *Cell and Developmental Biology*, 11, pp.441–469.

- Wurth, L., 2012. Versatility of RNA-binding proteins in cancer. *Comparative and Functional Genomics*, 2012.
- Xiang, M. et al., 1997. Essential role of POU-domain factor Brn-3c in auditory and vestibular hair cell development. *Proceedings of the National Academy of Sciences of the United States of America*, 94(17), pp.9445–9450.
- Xiang, M. et al., 1998. Requirement for Brn-3c in maturation and survival, but not in fate determination of inner ear hair cells. *Development (Cambridge, England)*, 125(20), pp.3935–3946.
- Xing, X. et al., 2014. PP242 suppresses cell proliferation, metastasis, and angiogenesis of gastric cancer through inhibition of the PI3K/AKT/mTOR pathway. *Anti-cancer drugs*, 25(10), pp.1129–1140.
- Xu, X. et al., 2011. Hyperthermia induces the ER stress pathway. *PLoS ONE*, 6(8).
- Yaglom, J.A. et al., 1999. The function of Hsp72 in suppression of c-Jun N-terminal kinase activation can be dissociated from its role in prevention of protein damage. *Journal of Biological Chemistry*, 274(29), pp.20223–20228.
- Yang, F. et al., 2006. Polysome-bound endonuclease PMR1 is targeted to stress granules via stress-specific binding to TIA-1. *Molecular and cellular biology*, 26(23), pp.8803–13.
- Yang, W.-H. & Bloch, D.B., 2007. Probing the mRNA processing body using protein microarrays and “autoantigenomics”. *RNA*, 13(5), pp.704–12.
- Yoshida, N., Kristiansen, A. & Liberman, M.C., 1999. Heat stress and protection from permanent acoustic injury in mice. *The Journal of neuroscience : the official journal of the Society for Neuroscience*, 19(22), pp.10116–10124.
- Yurinskaya, M.M. et al., 2015. HSP70 protects human neuroblastoma cells from apoptosis and oxidative stress induced by amyloid peptide isoAsp7-A β (1–42). *Cell Death and Disease*, 6(11), p.e1977.
- Zampedri, C. et al., 2016. Zebrafish P54 RNA helicases are cytoplasmic granules residents that are required for development and stress resilience. *Biology Open*, 1, p.bio.015826.
- Zhang, Z. et al., 2016. PP242 suppresses bladder cancer cell proliferation and migration through deactivating the mammalian target of rapamycin complex 2/AKT1 signaling pathway. *Molecular medicine reports*, 13(1), pp.333–338.
- Zou, J. et al., 1998. Repression of heat shock transcription factor HSF1 activation by HSP90 (HSP90 complex) that forms a stress-sensitive complex with HSF1. *Cell*, 94(4), pp.471–480.
- Zhou, J. et al., 2004. PI3K/Akt Is Required for Heat Shock Proteins to Protect Hypoxia-inducible Factor 1 α from pVHL-independent Degradation. *Journal of Biological Chemistry*, 279(14), pp.13506–13513.
- Zhou, J. et al., 2013. Activation of lysosomal function in the course of autophagy via mTORC1 suppression and autophagosome-lysosome fusion. *Cell research*, 23(4), pp.508–23.
- Zurla, C., Lifland, A.W. & Santangelo, P.J., 2011. Characterizing mRNA interactions with RNA granules during translation initiation inhibition. *PLoS ONE*, 6(5).

